Metabolic Flux Analysis of Neural Cell Metabolism in Primary Cultures

Ana Isabel Porém Amaral

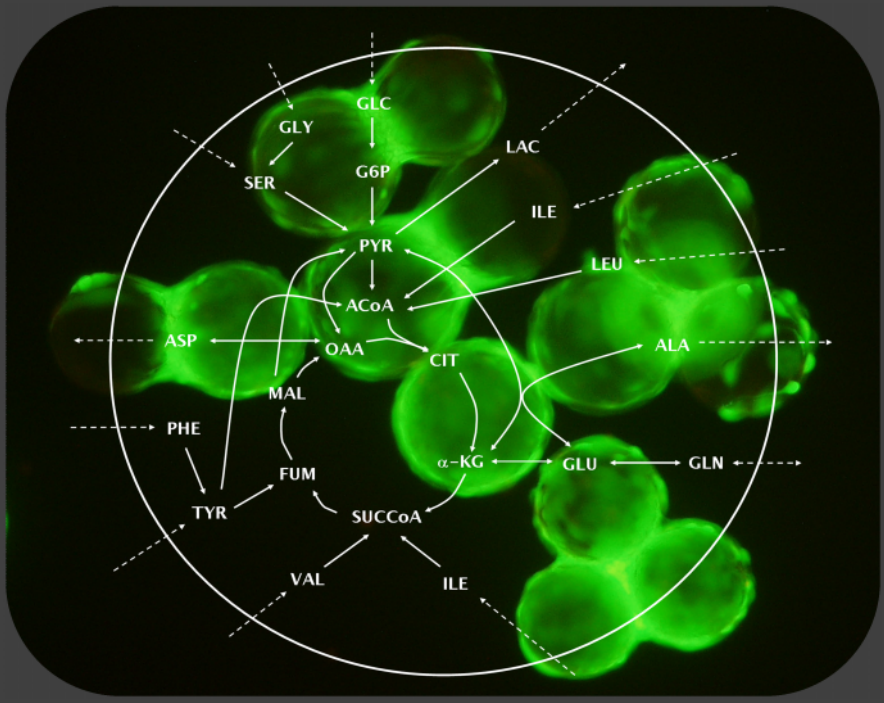

Dissertation presented to obtain the Ph.D degree in Biochemistry, Neuroscience

Instituto de Tecnologia Química e Biológica | Universidade Nova de Lisboa

Oeiras,
September 2011

INSTITUTO DE TECNOLOGIA QUÍMICA E BIOLÓGICA /UNL

Knowledge Creation

Metabolic Flux Analysis of Neural Cell Metabolism in Primary Cultures

Ana Isabel Porém Amaral

Dissertation presented to obtain the Ph.D degree in Biochemistry, Neuroscience

Instituto de Tecnologia Química e Biológica | Universidade Nova de Lisboa

Oeiras, September 2011

INSTITUTO DE TECNOLOGIA QUÍMICA E BIOLÓGICA /UNL
Knowledge Creation

Metabolic Flux Analysis of Neural Cell Metabolism in Primary Cultures

by Ana Isabel Amaral

Second Edition: October 2011

ITQB-UNL and IBET, Animal Cell Technology Unit
Instituto de Tecnologia Química e Biológica – Universidade Nova de Lisboa and
Instituto de Biologia Experimental e Tecnológica
Av. da República – EAN, 2780-157 Oeiras, Portugal
Fax: +351 21 442 11 61; Phone: +351 21 446 91 00
http://tca.itqb.unl.pt
http://www.itqb.unl.pt
http://www.ibet.pt

From left to right: Prof. Mary McKenna, Prof. Sebastian Cerdán, Prof. Ursula Sonnewald, Ana Amaral, Dr. Paula M. Alves, Prof. Helena Santos.

Supervisors

Dr Paula Marques Alves, Principal Investigator and Head of the Animal Cell Technology Unit at ITQB-UNL/IBET and Executive Director of IBET (Supervisor)

Professor Ursula Sonnewald, Full Professor and Head of the Metabolic Neuroscience Group, Department of Neuroscience, Faculty of Medicine, Norwegian University of Science and Technology (NTNU), Trondheim, Norway (co-supervisor)

Jury

Professor Mary McKenna, Full Professor at the Department of Pediatrics, University of Maryland, School of Medicine; Baltimore – Maryland, USA.

Professor Sebastian Cerdán, Full Professor and Director of the Laboratory of Imaging and Magnetic Resonance Spectrocopy (LISMAR), Instituto de Investigação Biomédica "Alberto Sols", Universidade Autónoma de Madrid;

Professor Helena Santos, Full Professor and Head of the Cell Physiology and NMR group at ITQB-UNL, Oeiras, Portugal.

Foreword

This thesis dissertation is the result of more than four years of research at the Animal Cell Technology Unit of *Instituto de Tecnologia Química e Biológica – Universidade Nova de Lisboa* and *Instituto de Biologia Experimental e Tecnológica* (Oeiras, Portugal) under the supervision of Dr. Paula M. Alves and co-supervision of Prof. Ursula Sonnewald.

This thesis aims at contributing with new metabolic flux analysis-based approaches to improve the investigation and understanding of neural cell metabolism *in vitro*, with particular emphasis on metabolic responses to pathological insults. Moreover, this thesis also contributes with a novel *in vitro* model to investigate brain ischemia.

Aos meus pais

Ao meu maninho

A todos aqueles que me inspiram

Acknowledgements

This thesis is the product of a long scientific and personal journey at the Animal Cell Technology (ACT) Unit of ITQB-UNL and IBET but also, for shorter periods, at NTNU, Norway, and MIRCen – CEA, France. It was such an enriching period full of challenges, obstacles, joyful moments, personal growth, and exchange of experiences. At this stage I can say that doing research is definitely not easy. However, it is extremely rewarding if we are able to face every challenge with a smile, enthusiasm, motivation, persistence, and hard work, until we finally achieve our goals. Nothing would have been the same without so many extraordinary people that shared this path with me and to whom I wish to acknowledge.

To my supervisor, Dr. Paula Alves, thank you for bringing me to the exciting field of neurochemistry, for your guidance, support, trust, encouragement, energy, and also for being a demanding boss when necessary. Thank you for all the opportunities that allowed me to grow both personally and as a scientist, including the visits abroad, which made total difference in the person I am today. To me, you are a role model of a successful female scientist with great personality who is able to brilliantly manage the broad and excellent ACT unit.

To my co-supervisor, Prof. Ursula Sonnewald, thank you for such a warm hosting in your lab in Trondheim, for inspiring me with your enthusiasm for research, for the encouragement and for all the support both in Norway and via *Skype* or email whenever I needed.

To Dr. Gilles Bonvento, thank you for receiving me at MIRCen – CEA, in France, for your support and guidance during my stay and during the course of our collaboration project.

To Prof. Manuel Carrondo, for your encouragement, for the example of leadership and for transmitting us that excellence, rigor, hard work and pro-activity are fundamental for success in science.

To Ana Teixeira, thank you for always being there for me, for your friendship, companionship, support, for your guidance, and for being so demanding when we wrote all our papers together. My thesis would have never been possible without your excellent skills and mentoring on MFA.

To Pedro Cruz, thank you for all the support and advice and for cheering us up with your visits at the office. I truly admire your enthusiasm for research and your example of entrepreneurship.

To Isabel Marcelino, my first scientific mentor at the ACT lab, for your encouragement, enthusiasm and joy at work, for showing me how persistence and hard work are important, and for your friendship.

To my colleagues who contributed directly to the work developed in this thesis: Sanja Martens, Vicente Bernal, Marcos Sousa, Nuno Carinhas, and Joana Tavares, thank you for your hard work and commitment and for making those long working marathons much nicer.

A special acknowledgement to my "Brain Team" colleagues Sónia, Helena, Cláudia, and Sofia, who really understand how delicate it is to work with primary brain cell cultures, for everything we shared and for all the fruitful discussions. I really enjoyed working with you and to travel with you to exciting places and conferences. And to Catarina Brito, for the support and fruitful discussions.

To all my remaining colleagues, present and former members of the Animal Cell Technology unit - this really big and wonderful "TCA" family, for everything we shared and did together, in and outside the lab. For so many great friends I will keep, you know who you are. It would be impossible to mention all of you, so I will thank you all personally! A special word to the memory of our technician and lab-manager, Nita, a true example of dedication and courage for all of us.

To my colleagues at NTNU, Norway, who made my stay in Trondheim even more special and unforgettable, in particular, my dear friends Elvar and Linn – "Tusen takk for alt". An additional acknowledgement goes to Bjørn Håkonsen and Lars Evje for their significant work contribution to this thesis.

To my colleagues at MIRCen-CEA, France, for such a nice experience, particularly, Carole Escartin, Lydie, Marion, and Marta for all the support. To Mirta and Susanne, my dear friends at "Maison du Portugal", in Paris.

To all the professors, researchers, students and friends I met in conferences and courses around the world, who inspired me and gave me that extra-motivation about my work. And to all the great people I met at this great institute ITQB who are also part of my PhD experience.

To the financial support provided by *Fundação para a Ciência a Tecnologia* (SFRH/BD/29666/2006; PTDC/BIO/69407/2006) and to the Clinigene – NoE (LSHB-CT2006-010933). I further acknowledge the Norwegian Research Council for a fellowship that allowed me to perform part of my PhD work at NTNU, Norway.

Aos meus amigos bioquímicos da FCUL, em particular, ao Filipe, Nuno, Tiago, Irina, Catarina, Ana Maria, Raquel, João, e também ao Pedro, pela amizade, por partilharem comigo a minha paixão pela ciência, e por compreenderem tão bem o que é fazer um doutoramento. Tenho a certeza que a ciência portuguesa está em boas mãos com bioquímicos como vocês.

Aos meus amigos de (quase) sempre, Pedro e João, e à Diana, por me tentarem compreender mesmo que não percebam nada de bioquímica, e por continuarem a estar aí, apesar das nossas vidas ocupadas. Vocês são a prova de que os verdadeiros amigos ficam para sempre.

À Sara, pela amizade, por todos os sorrisos e gargalhadas e tantos bons momentos partilhados.

Ao Tiago, meu grande e tão especial amigo. Obrigada por tudo aquilo que me tens dado, o carinho, a amizade, e o apoio incondicionais. Por acreditares em mim, por me inspirares, e por teres trazido "novos mundos ao meu mundo".

Às minhas imensas Amigas Vera, Ana Cristina e Ana Catarina. Por serem quem são, por me acarinharem e mimarem quando eu preciso, pela amizade e apoio incondicional. São o meu orgulho e sabem que a distância entre nós será sempre insignificante, qualquer que seja o lugar do mundo onde estejamos.

À minha família por todo o apoio e carinho e por me fazerem sentir sempre especial, principalmente, quando regresso de qualquer uma dessas tantas viagens. À minha avó "Estrudes" e à memória dos meus restantes avós, as minhas orgulhosas raízes familiares e exemplos singulares de coragem, persistência e esforço. Em especial, agradeço aos meus pais e ao meu irmão por tudo, pelo apoio, carinho, amizade, paciência infindável, estímulo e por sempre acreditarem em mim. À minha Mãe, que me mostrou que nunca devemos desistir e perseguir os nossos sonhos, por mais difíceis e impossíveis que possam parecer.

FCT Fundação para a Ciência e a Tecnologia
MINISTÉRIO DA CIÊNCIA, TECNOLOGIA E ENSINO SUPERIOR

The Research Council of Norway

Clinigene

Abstract

Brain energy metabolism results from a complex group of pathways and trafficking mechanisms between all cellular components in the brain, and importantly provides the energy for sustaining most brain functions. In recent decades, ^{13}C nuclear magnetic resonance (NMR) spectroscopy and metabolic modelling tools allowed quantifying the main cerebral metabolic fluxes *in vitro* and *in vivo*. These investigations contributed significantly to elucidate neuro-glial metabolic interactions, cerebral metabolic compartmentation and the individual contribution of neurons and astrocytes to brain energetics. However, many issues in this field remain unclear and/or under debate.

Despite the valuable amount of data generated in cell culture studies involving ^{13}C-labelled substrates and NMR spectroscopy or mass spectrometry, only a few studies have employed modelling approaches to fully explore the results obtained. Thus, the main goal of this thesis was to implement novel Metabolic Flux Analysis (MFA) methodologies combined with information provided by isotopomers of key compounds derived from the metabolism of ^{13}C-labelled precursors, allowing for a more comprehensive investigation of cell metabolism in cultured brain cells. In addition to providing a novel *in vitro* model of ischemia, this work was particularly aimed at quantifying metabolic fluxes in neurons and in astrocytes and investigating the metabolic responses of these cells to pathological conditions with high impact on human health, such as ischemia and hypoglycaemia, by analyzing the changes in the distribution of those fluxes.

Chapter 1 starts by introducing the state of the art in the field of brain energy metabolism giving particular emphasis on the current topics relevant to the studies in this thesis and on the contribution of certain techniques, such as ^{13}C-NMR spectroscopy and metabolic modelling, to the current knowledge in the field. A brief introduction on MFA methodologies and the advantages of this methodology for investigating brain cell metabolism is also provided.

The first application of MFA which aimed at investigating the effects of an ischemic episode on the metabolic fluxes of astrocytes is presented in **Chapter 2**. This work contributed, in first place, a new *in vitro* model to mimic ischemia, by cultivating rat astrocytes on Cytodex 3® microcarriers in small-scale bioreactors. The use of bioreactors technology is advantageous as it allows for a tight control and manipulation of dissolved oxygen levels, a parameter of extreme importance in these studies. By combining MFA and ^{13}C NMR spectroscopy data, we were able to characterize in detail the metabolic response of astrocytes to oxygen and glucose deprivation. The fast and transient activation of most metabolic pathways and the parallel reestablishment of intracellular ATP levels after the insult demonstrate the remarkable capacity of metabolic adaptation by these cells.

In order to explore the potential of MFA to investigate neuronal metabolism under different conditions, the work described in **Chapter 3** was aimed at characterizing the effects of glucose deprivation (mimicking brain hypoglycaemia) on neuronal metabolic fluxes. This work provided new evidence on the capacity of neurons to change their metabolism in the absence of glucose and to metabolize other substrates. The results suggest that glutamine appears to be an important neuronal fuel during and after hypoglycaemia, and that the pyruvate recycling pathway might be significant for glutamine oxidation in cerebellar neurons, both under control conditions and, even more, after hypoglycaemia. These results challenge a number of *in vitro* studies which have mainly indicated a predominant astrocytic operation of pyruvate recycling, in contrast to what had been initially reported *in vivo*.

Taking into account the complexity of cellular metabolism, and the increasing availability of techniques generating a larger amount of metabolomics data, more powerful methodologies have been recently developed. Thus, in **Chapter 4**, a new model based on the most recent version of MFA, ^{13}C isotopic transient MFA, was implemented with the aim of estimating the metabolic fluxes in cultured astrocytes in greater detail. This methodology utilizes information provided by ^{13}C-labelling time-courses of

intracellular metabolites to provide a detailed estimation of metabolic fluxes. A large number of fluxes were estimated with high accuracy, including those of parallel and reversible pathways. In particular, this work suggests that the glutamate/α-ketoglutarate exchange rate appears to be similar to the TCA cycle flux, a subject that has been highly controversial and had never been investigated *in vitro*. This work further allowed identifying and quantifying the contribution of substrates and metabolic pathways (e.g. pentose phosphate pathway and catabolism of branched-chain amino acids) to the isotopic dilution phenomenon typically observed in modelling studies both *in vitro* and *in vivo*, reinforcing their importance and the complexity of astrocytic metabolism, even under physiological conditions.

Chapter 5 describes the work performed in a collaboration project with the Molecular Imaging Research Centre – Commissariat à L'Énergie Atomique (MIRCen-CEA; France) which aimed at applying MFA to investigate the role of the glial glutamate transporters, GLAST and GLT-1, in energy metabolism. These studies are relevant not only to elucidate the role of these proteins in physiological conditions but also in the context of various neurodegenerative diseases involving glutamate excitotoxicity. Experiments were carried out with the aim of implementing a protocol to down-regulate the expression of GLAST or GLT-1 in cultured astrocytes. Lentiviral vectors carrying specific shRNA sequences as well as transfection methods (electroporation and lipofection) using plasmid DNA coding for the same sequences were tested but none was proven successful. Preliminary data suggests that the viral envelope used led to very low transduction efficiencies. Therefore, unfortunately, the main aim of this part of the work was not completed and additional studies will be required to generate a good lentiviral vector and infection protocols that will allow investigating the role of glutamate transporters in astrocytic metabolism.

Finally, **Chapter 6** provides an integrated overview and discussion of the main results of this thesis, highlighting the main findings and the contribution to current knowledge in the field and future perspectives. In summary, this thesis contributes new

knowledge on the metabolic responses of astrocytes to ischemia and of neurons to hypoglycaemia by taking advantage of the amount and specificity of the information provided by MFA methodologies. In addition, the novel modelling tools employed will be useful for in depth investigations of the responses of brain cells under physiological or pathological conditions as well as for determining the effect of drugs targeting metabolic pathways in the brain.

Resumo

O metabolismo energético cerebral resulta de uma complexidade de vias metabólicas e mecanismos que interligam os diferentes componentes celulares cerebrais, sendo extremamente importante pois fornece a energia que suporta as diversas funções do cérebro. Nas últimas décadas, estudos de espectroscopia de ressonância magnética nuclear (RMN) de ^{13}C e ferramentas de modelação metabólica permitiram quantificar os principais fluxos metabólicos cerebrais, tanto *in vitro* como *in vivo*. Estas investigações contribuíram significativamente para elucidar as interacções metabólicas entre neurónios e astrócitos, a compartimentação metabólica no cérebro e a contribuição individual de neurónios e astrócitos para o metabolismo cerebral. No entanto, existem ainda muitos aspectos controversos e/ou pouco compreendidos nesta área.

Diversos estudos *in vitro* têm permitido obter uma grande e valiosa quantidade de informação a partir do uso de compostos marcados com ^{13}C e espectroscopia de RMN e/ou espectrometria de massa. No entanto, poucos estudos utilizaram abordagens quantitativas que permitem uma caracterização mais aprofundada dos resultados obtidos. Assim, o principal objectivo desta tese foi implementar novas metodologias baseadas na Análise de Fluxos Metabólicos (AFM), em combinação com informação obtida através do uso de compostos marcados com ^{13}C e, consequentemente, investigar com maior detalhe as vias metabólicas em culturas de células de cérebro. Para além da implementação de um novo modelo *in vitro* para mimetizar isquémia cerebral, esta tese pretendeu quantificar, em particular, os fluxos metabólicos de astrócitos e neurónios e investigar as respostas metabólicas destas células a condições patológicas com grande impacto na saúde humana, como a isquémia e a hipoglicémia, analisando as alterações na distribuição desses mesmos fluxos.

O Capítulo 1 começa por introduzir o estado da arte na área do metabolismo cerebral, salientando os temas mais relevantes para os estudos desta tese e a contribuição fundamental de técnicas como a espectroscopia de RMN de ^{13}C e a modelação

metabólica para o conhecimento actual. São ainda introduzidas as metodologias de AFM e as suas vantagens no âmbito dos estudos realizados nesta tese.

No **Capítulo 2** apresenta-se o primeiro estudo de AFM que pretendeu investigar os efeitos de um insulto de isquémia cerebral nos fluxos metabólicos de astrócitos. Em primeiro lugar, este trabalho contribuiu com um novo modelo *in vitro* para mimetizar isquémia, recorrendo ao uso de bioreactores de pequena escala. Estes permitem controlar e manipular com rigor os níveis de oxigénio dissolvido no meio de cultura, um parâmetro de extrema importância neste tipo de estudos. A combinação de AFM com dados de espectroscopia de RMN de ^{13}C permitiu caracterizar detalhadamente a resposta metabólica dos astrócitos à privação simultânea de oxigénio e glucose. Em particular, salienta-se uma rápida e transiente activação de diferentes vias e o restabelecimento simultâneo dos níveis de ATP intracelulares após o insulto, demonstrando uma grande resistência e capacidade de adaptação metabólica destas células.

Com o objectivo de explorar o potencial da AFM na investigação do metabolismo neuronal em diferentes condições, o trabalho descrito no **Capítulo 3** pretendeu caracterizar os efeitos da privação da glucose (hipoglicémia) nos fluxos metabólicos de neurónios em culturas primárias. Este trabalho forneceu evidências importantes acerca da capacidade de adaptação metabólica destas células na ausência de glucose e da utilização de outros substratos. Os resultados sugerem que a glutamina é um substrato neuronal importante durante e após situações de hipoglicémia e que a via de reciclagem do piruvato será significativa para a oxidação de glutamina em neurónios, tanto em condições fisiológicas como, mais ainda, após um período de hipoglicémia. Estes resultados contradizem um largo número de estudos *in vitro* que têm apontado para uma operação predominante da via de reciclagem do piruvato em astrócitos, contrariamente ao que foi inicialmente sugerido *in vivo*.

Tendo em conta a complexidade do metabolismo celular e a crescente disponibilidade de técnicas que geram cada vez mais dados na área da metabolómica, novas e mais poderosas metodologias têm sido desenvolvidas. Assim, no **Capítulo 4**, um novo modelo baseado na versão mais recente da AFM, AFM transiente isotópica de ^{13}C, foi implementado com o objectivo estimar com maior detalhe os fluxos metabólicos de astrócitos. Um grande número de fluxos foi estimado com elevada precisão, incluindo fluxos de vias paralelas e também de vias reversíveis. Em particular, este trabalho fornece, pela primeira vez, dados obtidos *in vitro* que apoiam a hipótese de que o fluxo da reacção de inter-conversão entre glutamato e α-cetoglutarato é semelhante ao fluxo do ciclo dos ácidos tricarboxílicos (TCA), uma questão muito controversa nos estudos de modelação metabólica *in vivo*. Esta abordagem permitiu ainda identificar e quantificar a contribuição de substratos adicionais à glucose e vias metabólicas (ex. aminoácidos de cadeia ramificada e via das pentoses-fosfatadas) para as diluições isotópicas normalmente observadas nestes estudos, reforçando a sua importância e a complexidade do metabolismo destas células, mesmo em condições fisiológicas.

O **Capítulo 5** descreve o trabalho realizado num projecto de colaboração com o MIRCen-CEA (França) que teve como objectivo aplicar a AFM à investigação do papel dos dois transportadores de glutamato dos astrócitos, GLAST e GLT-1, no metabolismo energético. Estes estudos são relevantes, não só para elucidar o papel destas proteínas no metabolismo dos astrócitos em condições fisiológicas, mas também no contexto de diversas doenças neurodegenerativas que envolvem mecanismos de excitotoxicidade. Diferentes experiências foram realizadas com o objectivo de implementar um protocolo para reduzir a expressão do GLAST e GLT-1 em culturas de astrócitos. Vectores lentivirais com sequências específicas de shRNA e métodos de transfecção com DNA plasmídico para as mesmas sequências (electroporação e lipofecção) foram testados mas nenhum teve sucesso. Dados preliminares sugerem que o envelope viral utilizado terá sido a causa para a obtenção de baixas eficiências de transdução. Assim, o principal objectivo deste trabalho não foi atingido e estudos adicionais serão necessários para gerar

um bom vector lentiviral assim como protocolos de infecção que permitam investigar o papel dos transportadores de glutamato no metabolismo dos astrócitos.

Finalmente, no **Capítulo 6** é feita uma discussão integrada dos principais resultados da tese, salientando-se as principais conclusões, o contributo para o conhecimento actual e as perspectivas futuras do trabalho. Em suma, esta tese contribui com novos conhecimentos acerca das respostas metabólicas dos astrócitos a um insulto de isquémia e dos neurónios a um período de hipoglicémia, tirando partido da quantidade e especificidade da informação fornecida pelas metodologias de AFM. Estas novas ferramentas serão certamente vantajosas para investigar detalhadamente as respostas celulares a condições patológicas assim como o efeito de drogas que actuem ao nível de vias metabólicas no cérebro.

Thesis Publications

AI Amaral, AP Teixeira, S Martens, V Bernal, MFQ Sousa, PM Alves (2010) Metabolic alterations induced by ischemia in primary cultures of astrocytes: merging ^{13}C NMR spectroscopy and metabolic flux analysis J Neurochem 113(3):735-48.

AI Amaral, AP Teixeira, U Sonnewald, PM Alves (2011) "Estimation of intracellular fluxes in cerebellar neurons after hypoglycemia: importance of the pyruvate recycling pathway and glutamine oxidation" J Neurosci Res, 89 (5):700-710.

AI Amaral*, AP Teixeira*, BI Håkonsen, U Sonnewald, PM Alves (2011) "A comprehensive metabolic profile of cultured astrocytes using Isotopic Transient Metabolic Flux Analysis and ^{13}C-labelled glucose" (*equal contribution) Front Neuroenerg, **3**:5 doi 10.3389/fnene.2011.00005

Additional Publications

AI Amaral, AS Coroadinha, O-W. Merten, PM Alves (2008) "Improving retroviral vectors production: Role of carbon sources in lipid biosynthesis" J Biotechnol 138 (3-4):57-66

AS Coroadinha, L Gama-Norton, **AI Amaral**, H Hauser, PM Alves, PE Cruz (2010) "Production of Retroviral Vectors" Curr Gene Ther 1;10(6):456-73.

PE Cruz, T Rodrigues, M Carmo, D Wirth, **AI Amaral**, PM Alves, AS Coroadinha (2011) "Manufacturing of Retroviruses" In: Methods in Molecular Biology, O-W Merten and M Al-Rubeai (editors) Springer Science

Y Jin, **AI Amaral,** A McCann, L Brennan (2011) "Homocysteine levels impact directly on epigenetic reprogramming in astrocytes" Neurochem Int, 58:833-838

Abbreviations

Abbreviation	Full Form
2D	two-dimensional
3D	three-dimensional
3PG	3-phosphoglycerate
AAT	aspartate aminotransferase
AGC	aspartate-glutamate carrier
ANLS	astrocyte-neuron lactate shuttle
ATP	adenosine-3-phosphate
BBB	blood-brain barrier
BCA	bicinchoninic acid
BCAA	branched-chain amino acids
cME	cytosolic form of malic enzyme
CNS	central nervous system
DIV	days *in vitro*
DMEM	Dulbecco's modified Eagle's medium
DMF	N,N-Dimethylformamide
FAD	flavin adenine dinucleotide (oxidized form)
$FADH_2$	flavin adenine dinucleotide (reduced form)
FBA	Flux Balance Analysis
FBS	fetal bovine serum
GABA	γ-amino butyric acid
GC-MS	gas chromatrography-mass spectrometry
GDH	glutamate dehydrogenase
GFAP	glial fibrillary acidic protein
GFP	green fluorescent protein
GLUT	glucose transporter
GS	glutamine synthethase
GTP	guanosine-3-phosphate
HA	hemagglutinin

HBS	Hepes Buffered Saline
HD	Huntington's Disease
HEK	human embryonic kidney
HIF-1	hypoxia-inducible factor 1
Htt	Huntingtin
Lac/Glc	lactate production rate over glucose consumption rate
LDH	lactate dehydrogenase
MAS	malate-aspartate shuttle
MCT	monocarboxylate transporter
ME	malic enzyme
MFA	Metabolic Flux Analysis
mHtt	mutant Huntingtin
mME	mitochondrial form of malic enzyme
MRI	magnetic resonance imaging
MS	mass-spectrometry
MSNs	medium-sized spiny neurons
MSTFA	N-Methyl-N-(trimethylsilyl)trifluoroacetamide
MTBSTFA	N–Methyl-N-(t-Butyldimethylsilyl) trifluoroacetamide
NAD+	nicotinamide adenine nucleotide (oxidized)
NADH	nicotinamide adenine nucleotide (reduced)
NG2+	nerve/glial antigen 2 - positive
NGS	normal goat serum
NMR	Nuclear Magnetic Resonance
OGD	oxygen and glucose deprivation
PAG	phosphate-activated glutaminase
PBS	phosphate buffered saline
PC	pyruvate carboxylase
PDH	pyruvate dehydrogenase
Pen-Strep	Penicillin–Streptomycin
PEP	phosphoenolpyruvate
PEPCK	phosphoenolpyruvate carboxykinase

PET	Positron Emission Tomography
PFA	parafolmadehyde
PFKFB3	6-phosphofructo-2-kinase/fructose2,6-bisphosphatase, isoform 3
pO_2	partial pressure of oxygen
poly-Q	poly-glutamine
PPP	pentose phosphate pathway
RT-qPCR	Reverse Transcriptase - quantitative Polimerase Chain Reaction
SDS-PAGE	sodium dodecyl sulphate-polyacrylamide gel electrophoresis
t-BDMS-Cl	t-butyldimethylchlorosilane
TCA	Tricarboxylic acid

TABLE OF CONTENTS

Chapter 1

Introduction

CONTENTS

1 Introduction

The brain is the most complex organ in mammals. It controls most vital functions although many of the mechanisms underlying its functioning are still unknown. Moreover, it accounts for only 2% of the body weight, but receives 15% of the cardiac output (Williams and Leggett 1989) which demonstrates its high energetic demand. Cerebral metabolism is crucial to provide the energy needed in the numerous processes sustaining brain activity and, consequently, the disruption of any metabolic-related mechanism will evidently compromise brain function.

In addition to the profound metabolic alterations known to be associated with ischemic stroke and hypoglycaemia, it is currently known that many other brain pathologies, such as neurodegenerative diseases, including Huntington's, Alzheimer's and Parkinson's disease, and psychiatric disorders, like schizophrenia and depression have a metabolic component. Indeed, changes in metabolic signals detected by imaging techniques such as magnetic resonance imaging (MRI) and positron emission tomography (PET) are promising biomarkers for some of these pathologies (Andrews and Brooks 1998; Coimbra et al. 2006; Mueller et al. 2006; Liepelt et al. 2009).

Research in the last decades has shown that brain energy metabolism is very complex and compartmentalized due to the highly specialized cellular and sub-cellular localization of transporters, enzymes and metabolic pathways (reviewed by McKenna et al. 2006a). Great advances in techniques and methodologies including nuclear magnetic resonance (NMR) spectroscopy and imaging, PET, mathematical modelling, molecular biology, microscopy, genomics, proteomics and many others, largely contributed to the current knowledge in the field. However, many issues remain unclear or under intense debate. Therefore, research in this field remains an exciting task towards elucidating the mechanisms underlying brain function under physiological and pathological conditions.

This chapter summarizes the state of the art regarding research on brain energy metabolism, with a particular focus on the contribution of ^{13}C NMR spectroscopy and

metabolic modelling tools. A general overview of the metabolic alterations associated with hypoglycaemia and ischemia in the brain is also provided, as these were the pathological conditions mimicked in some studies included in this thesis.

2 The brain and its cellular populations

The brain is constituted mainly by neurons and glial cells. Although presenting distinct morphologies and specific roles, they strongly depend on close functional interactions between them and with blood vessels (Figure 1.1).

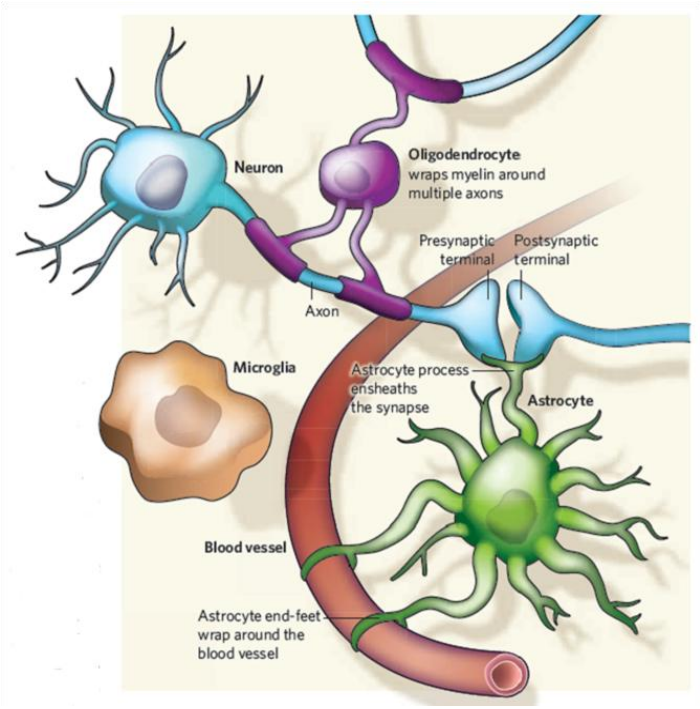

Figure 1.1 - Interactions between glial cells and neurons in the brain. Different types of glia interact with neurons and the surrounding blood vessels. Oligodendrocytes wrap myelin around axons to speed up neuronal transmission. Astrocytes extend processes that cover > 99% of the cerebrovascular surface and synapses. Microglia keep the brain under surveillance for damage or infection. Reproduced from Allen and Barres (2009) with permission of the publisher.

The blood–brain barrier (BBB), constituted mainly by endothelial cells, enzymes and transporters, physically isolates the brain and maintains the necessary extracellular

environment of the central nervous system (CNS) (Abbott et al. 2006). In addition to neurons and glia, a new class of cells called pericytes has been recently described in the brain and is thought to be important in regulating the permeability functions of the BBB (Armulik et al. 2011).

2.1 Neurons

Neurons were, for more than a century, the only studied cell type in the brain due to their unique capacity of emitting electrical signals. They are highly specialized cells and the core components of the nervous system. The number of neurons in the brain varies dramatically from species to species. It is estimated that the human brain possesses about 100 billion (10^{11}) neurons and 100 trillion (10^{14}) synapses (Williams and Herrup 1988). Neurons are electrically excitable cells which are able to process and transmit information using electrical (action potentials) and chemical (neurotransmitters) signals through a mechanism designated by synaptic transmission (Hof et al. 2004). The shape, size and neurochemistry determine their specific function. In this respect, three major classes of neurons can be considered: the inhibitory GABA (γ-amino butyric acid)ergic interneurons that make local contacts, the local excitatory spiny stellate cells in the cerebral cortex, and the excitatory glutamatergic efferent neurons, such as the cortical pyramidal neurons (Hof et al. 2004). In addition, other types of neurons localized in more specialized areas include dopaminergic, cholinergic and serotoninergic neurons. Still, and despite the heterogeneous distribution among different brain regions, more than 90% of neurons in the brain are either glutamatergic or GABAergic, according to the neurotransmitter used for their signalling process, glutamate or GABA, respectively (Hof et al. 2004). Neurotransmitters play an important role linking energy metabolism of neurons and astrocytes. This will be further elucidated later in this chapter.

2.2 Glial Cells

Despite the large number of neurons, glial cells occupy the most part of the brain volume. The proportion of glial cells to neurons varies between animals and brain

regions but seems to be correlated with the animal's size as the mouse, human and elephant brain possess approximately 65%, 90% and 97% of glial cells, respectively (Allen and Barres 2009). Their initial designation of neuroglia ("Nervenkitt") was attributed to Rudolph Virchow in the late 19th century, who described these cells as the "brain glue". They were thought to be mostly connective tissue that filled up the extracellular space and worked as chemical and physical insulators to support the diverse neuronal functions (Kimelberg 2004). Only in the beginning of the 20th century did glia finally lose their passive identity and many crucial and active functions started being attributed to these cells. In mammals, glial cells are divided into three major groups, based on their morphology, function and localization in the nervous system: (1) Schwann cells and oligodendrocytes, the myelinating cells of the peripheral and CNS, respectively (Nave and Trapp 2008); (2) microglia, the immune cells of the CNS (Hanisch and Kettenmann 2007); and (3) astrocytes, a diverse cell population with variable morphology and numerous functions, contacting essentially with all other cellular elements in the brain (Agulhon et al. 2008; Wang and Bordey 2008) (Figure 1.1). A fourth group, the nerve/glial antigen 2 - positive (NG2+) glia, has been more recently considered and includes oligodendrocyte and astrocyte progenitor cells as well as NG2+ cells that persist in the mature brain (Agulhon et al. 2008). Among the different types of glial cells, astrocytes were those studied in detail in this thesis due to their close relationship with neurons at the metabolic level, as described below.

2.2.1 Astrocytes

Astrocytes derive their name from the stellate morphology traditionally observed in histological preparations. However, they are quite heterogeneous among different brain regions, even at the transcriptome level (Bachoo et al. 2004). Astrocytes are found throughout the brain and spinal cord and, on the basis of number, surface area, and volume, are the predominant glial cell type. Protoplasmic astrocytes are the most common type of astrocytes (Agulhon et al. 2008). Individually, they occupy distinct, non-overlapping domains and their fine processes are connected to other astrocytes via gap

junctions at their boundaries (Bushong et al. 2002). More than 99% of the cerebrovascular surface is ensheathed by astrocyte processes (Haydon and Carmignoto 2006) and processes from a single astrocyte can envelop approximately 140 000 synapses, as in the CA1 region of the hippocampus (Bushong et al. 2002).

Astrocytes have, thus, the unique role of dynamic coordination of cerebral functions. They participate in the regulation of water and ionic homeostasis (Simard and Nedergaard 2004) and in the maintenance of the BBB (Hawkins and Davis 2005). Moreover, even though astrocytes do not produce action potentials, they individually respond to synaptically released neurotransmitters through elevations in intracellular Ca^{2+} levels (Agulhon et al. 2008; Schummers et al. 2008). These Ca^{2+} transients induce the release of chemical transmitters ("gliotransmitters" – ATP, glutamate and D-serine) allowing them to communicate with neurons. In this way, astrocytes control synaptic transmission in a process called tripartite-synapse, and regulate local blood flow in situations of intense neuronal activity (neurovascular-coupling mechanism) (Haydon and Carmignoto 2006; Iadecola and Nedergaard 2007; Halassa et al. 2009). Nevertheless, it is still elusive how both excitatory and inhibitory signals provided by the same glial cell act in concert to regulate neuronal function.

Finally, astrocytes play a key role in brain energy metabolism. They supply energy substrates to neurons, in a process essential for neurotransmission, and are responsible for neurotransmitter uptake and recycling, thereby preventing excitotoxicity and controlling synaptic signals (Hertz and Zielke 2004; Pellerin et al. 2007). Moreover, they synthesize the main antioxidant molecule in the brain, glutathione (Dringen and Hirrlinger 2003). The role of both astrocytes and neurons in brain energy metabolism, in physiological and pathological scenarios, is the basis for the work described in this thesis and, therefore, will be more thoroughly addressed in the subsequent sections of this chapter.

3 *In vitro* models for neuroscience research

The high degree of complexity of the brain makes it difficult to investigate specific biochemical and cellular mechanisms using *in vivo* models and, therefore, simple research models are required. As illustrated in the following sections of this chapter, cultured brain cells have been crucial to elucidate many aspects of brain energy metabolism and are still widely used to investigate a number of research questions, including mechanisms of disease.

In addition to their simplicity, *in vitro* models are advantageous compared to animal models since they possess high cellular specificity and are not influenced by the blood flow component, hormones, immune system, and temperature variations occurring *in vivo* (Meloni et al. 2001). The absence of these factors allows, for example, investigating cell-specific changes in gene/protein expression, determining the metabolic responses of a particular cell type under different conditions or determining the mechanism of action of a therapeutic agent (Meloni et al. 2001). In addition, it is easier and less expensive to perform molecular manipulations, such as antisense oligonucleotide and gene transfection experiments, in cultured cells. Also, *in vitro* models are valuable for drug-screening, enabling to select the most promising compounds to be tested *in vivo*, as well as to perform preliminary studies regarding novel research hypotheses, thereby reducing the number of animals used. This is actually a crucial aspect in current neuroscience research, due to the stricter rules and definitions of ethical impact underlying the use of animals, which need to be fully accomplished by researchers.

One of the oldest *in vitro* models to study the brain is the organotypic brain slice culture from the CNS of young rodents (reviewed by Gahwiler et al. 1997). This preparation continues to differentiate in culture and preserves a level of cellular organization that closely resembles that observed in situ. Therefore, it has been particularly used to investigate mechanisms involved in synaptic transmission. However,

it is very technically demanding and its heterogeneous composition and complexity makes it difficult to investigate cell-specific mechanisms.

Some of these aspects can be overcome by the use of monotypic neural cell cultures, including both tumour-derived cell lines and primary cultures, which are simpler models regarding both culture preparation/maintenance and the cellular features reproduced. Cell lines, such as glioma or neuroblastoma cells (Bouzier et al. 1998; Rae et al. 2003), are much easier to cultivate but their immortalization properties limit their ability to model non-tumoural tissue. Dissociated primary neural cell cultures are prepared from neonatal rodent brain, are normally selectively enriched in one particular cell type and therefore are considered to represent mainly the features of that cell population (Hertz et al. 1998).

Neural cells can be cultivated in the more classical two-dimensional (2D) monolayer systems, such as tissue-culture flasks or dishes, but also immobilized in microcarriers or in gel threads (Alves et al. 1996b; Alves et al. 2000a; Sa Santos et al. 2005) and in the form of three-dimensional (3D) aggregates (Santos et al. 2007), depending on the purpose of the study. Monolayer 2D cultures have the advantage of being easily monitored and characterised using microscopy techniques. By cultivating more than one cell type (e.g. neurons and astrocytes) in the same dish, a 2D co-culture is obtained (e.g. Waagepetersen et al. 2002). However, these culture approaches are limited in respect to their spatial environment when compared to 3D aggregates. Aggregating neural cell cultures or neurospheres are able to reconstitute spontaneously a histotypic brain architecture to reproduce critical steps of brain development and to reach a high level of structural and functional maturity (reviewed by Honegger et al. 2011). Even so, in addition to being much more technically demanding, 3D cultures might have the possible drawback of nutrient and oxygen transport limitation and accumulation of toxic byproducts in the centre of aggregates with higher diameters, which might affect cell viability (Alves et al. 1996a). Both simple 2D co-cultures and 3D aggregates are

advantageous *in vitro* models to investigate metabolic interactions between different cell types since they retain some degree of complexity, including cell-cell interactions.

Biotechnological advances in suspension culture systems adequate for neural cells, namely small scale bioreactors and low shear-stress impellers, have been advantageous for the implementation of novel *in vitro* models for neuroscience research, for example, using primary cultures (e.g. Sa Santos et al. 2005) and stem cells (e.g. Serra et al. 2009). These systems are hydrodynamically well characterized, allow for a better homogeneity of the cultures, easy-sampling, and reproducibility between experiments due to the tight control of culture variables (gas-composition of the culture medium, pH, temperature, stirring rate). Oxygen and nutrient delivery to the cells is also much more efficient in stirred systems, as well as its manipulation during culture time. Therefore, they are particularly well-suited to perform pathological challenges involving the manipulation of oxygen levels, such as hypoxia (Sa Santos et al. 2005), anoxia (Sa Santos et al. 2011) or ischemia (Amaral et al. 2010). The use of bioreactors is thus advantageous when compared to the use of hypoxic incubators/chambers (e.g. Almeida et al. 2002), that do not enable the tight monitoring of oxygen levels.

Finally, although neural cell cultures have been mainly of rodent origin, human-derived *in vitro* models, particularly those based on stem cells have been increasing in recent decades (reviewed by Gibbons and Dragunow 2010). These are very promising to investigate cellular, molecular or biochemical mechanisms of human cells in physiology and disease. While it is important to acknowledge that pre-clinical *in vivo* studies in rodents and primates will always be required to validate findings obtained *in vitro*, before their translation to humans, all the advances in *in vitro* neural cell models and culture systems will certainly continue to make them excellent and privileged models for many research purposes in future decades.

4 Brain Energy Metabolism: Nutrients and Metabolic Pathways

4.1 Glucose - the main cerebral energy fuel

Energy consuming processes in the adult brain account for ~25% of the total body glucose utilization and for ~20% of the total oxygen consumed (Magistretti 2004). However, glucose is not the main energy substrate in all stages of brain development. In fact, a transitory switch occurs from a combination of glucose, monocarboxylates, including lactate, and ketone bodies, such as acetoacetate and ß-hydroxybutyrate in the postnatal period to a predominance of glucose as main fuel in the mature brain (Nehlig 1997; Vannucci and Simpson 2003). The uptake of metabolic substrates from the blood into the brain is mediated by specific facilitative transporter proteins in endothelial cells of the BBB and in brain cells. It is the differential developmental expression of glucose and monocarboxylate transporters (GLUTs and MCTs, respectively) that determines the maturational increase in glucose utilization (Rafiki et al. 2003; Vannucci and Simpson 2003).

Average cerebral concentrations of glucose range between 0.8–2.3 mM as estimated using several techniques and show a linear correlation with blood glucose levels (Gruetter et al. 1998a; Dienel and Cruz 2004; Barros et al. 2007). Although approximately 96% of endothelial cells are covered by astrocytic end feet, experimental evidence has shown that approximately equal proportions of glucose are taken up by neurons and astrocytes (Nehlig et al. 2004), even though this is still a matter of debate. As shown by autoradiography and PET, the rate of glucose consumption differs between brain regions, with higher values in grey matter, and also varies with time, with active areas capturing glucose more avidly (Raichle and Mintun 2006). Although it is established that oxidative metabolism predominates, as indicated by the cerebral respiratory coefficient (CO_2 production/O_2 consumption) of 0.97 (Clarke and Sokoloff 1999), the exact contribution of neurons and astrocytes to this process also remains under debate. Moreover, it is known that lactate levels in the brain increase during

activation (e.g. Dienel and Cruz 2008) and that both cell types are able to oxidize lactate (Zielke et al. 2009). These issues have provided additional sources of discussion with regard to the main substrate supporting neuronal and astrocytic metabolic activity under activation and will be further addressed below.

4.1.1 Glucose metabolism in the brain

Cerebral glucose metabolism is similar to that in other tissues but, in the particular case of the brain, it is almost entirely oxidized to CO_2 and water via glycolysis, the tricarboxylic acid (TCA) cycle and the associated oxidative phosphorylation (Magistretti 2004). Under certain conditions, and depending on the cell type, glucose can be additionally metabolized in the pentose phosphate pathway (PPP) to a significant extent (Dringen et al. 2007). Finally, glucose can eventually be stored in astrocytes in the form of glycogen, the main cerebral energy store (Brown and Ransom 2007). These pathways are generally described in Figures 1.2 and 1.3 and below.

4.1.1.1 Glycolysis, TCA cycle and Oxidative Phosphorylation

Glycolysis is the pathway responsible for the initial steps of glucose metabolism as it enters the brain, and it converts glucose into two molecules of pyruvate (Figure 1.2). Glycolytic activity is thought to be much higher in astrocytes than in neurons (to be addressed below). This pathway generates a net amount of two ATP molecules. Four ATP molecules are formed in the two last steps leading to pyruvate formation, the reactions catalyzed by phosphoglycerate kinase (EC 2.7.2.3) and pyruvate kinase (EC 2.7.1.40), whereas two ATPs are consumed to phosphorylate glucose to glucose-6-phosphate (by hexokinase; EC 2.7.1.1) and fructose-6-phosphate to fructose-1,6-bisphosphate (by phosphofructokinase; EC 2.7.1.11), respectively (Magistretti 2004). Hexokinase and phosphofructokinase both catalyze irreversible reactions, being important regulation points in carbohydrate metabolism in the brain (McKenna et al. 2006a). This is one of the main reasons why brain cells have a reduced capacity of performing gluconeogenesis, and therefore they strongly depend on glucose supply from

the blood. Even so, some authors have provided evidence suggesting the operation of gluconeogenesis in astrocytes, which are able to produce glycogen from lactate (e.g. Dringen et al. 1993b; Schmoll et al. 1995; Bernard-Helary et al. 2002).

Anaerobic glycolysis (glucose conversion into lactate) occurs when glucose utilization is higher than oxygen consumption and, consequently, the fraction of pyruvate produced from glucose exceeds that oxidized in the TCA cycle (Magistretti 2004). This also represents one of the mechanisms allowing for the maintenance of an optimal cytoplasmic NAD^+/NADH ratio, required for a continuous glycolytic activity (other mechanisms are described in sub-section 3.1.1.4).

In order for glucose metabolism to proceed via oxidation, it is required that pyruvate formed in glycolysis is transported into the mitochondria and enters the TCA cycle. The TCA cycle involves not only the catabolism of energy-rich molecules but also provides precursors for many intermediates that are utilized in the overall cellular metabolism. Pyruvate is converted into acetyl-CoA in a reaction catalyzed by the pyruvate dehydrogenase (PDH) complex localized in the mitochondrial matrix (McKenna et al. 2006a). Acetyl-CoA cannot leave the mitochondrion because of its large size; thus the PDH complex maintains a positive flow of carbon to the cycle, controlling the rate of oxidative glucose metabolism.

The oxidation of pyruvate to CO_2 in the TCA cycle generates energy-rich molecules such as GTP, NADH and $FADH_2$. NADH and $FADH_2$ transfer electrons to oxygen in the electron transport chain, leading to the production of ATP in a process called oxidative phosphorylation. The mitochondrial NAD^+/NADH ratio constitutes one of the major regulators of the TCA cycle and its value is strongly affected by oxygen levels as a result of the electron transport/oxidative phosphorylation pathway.

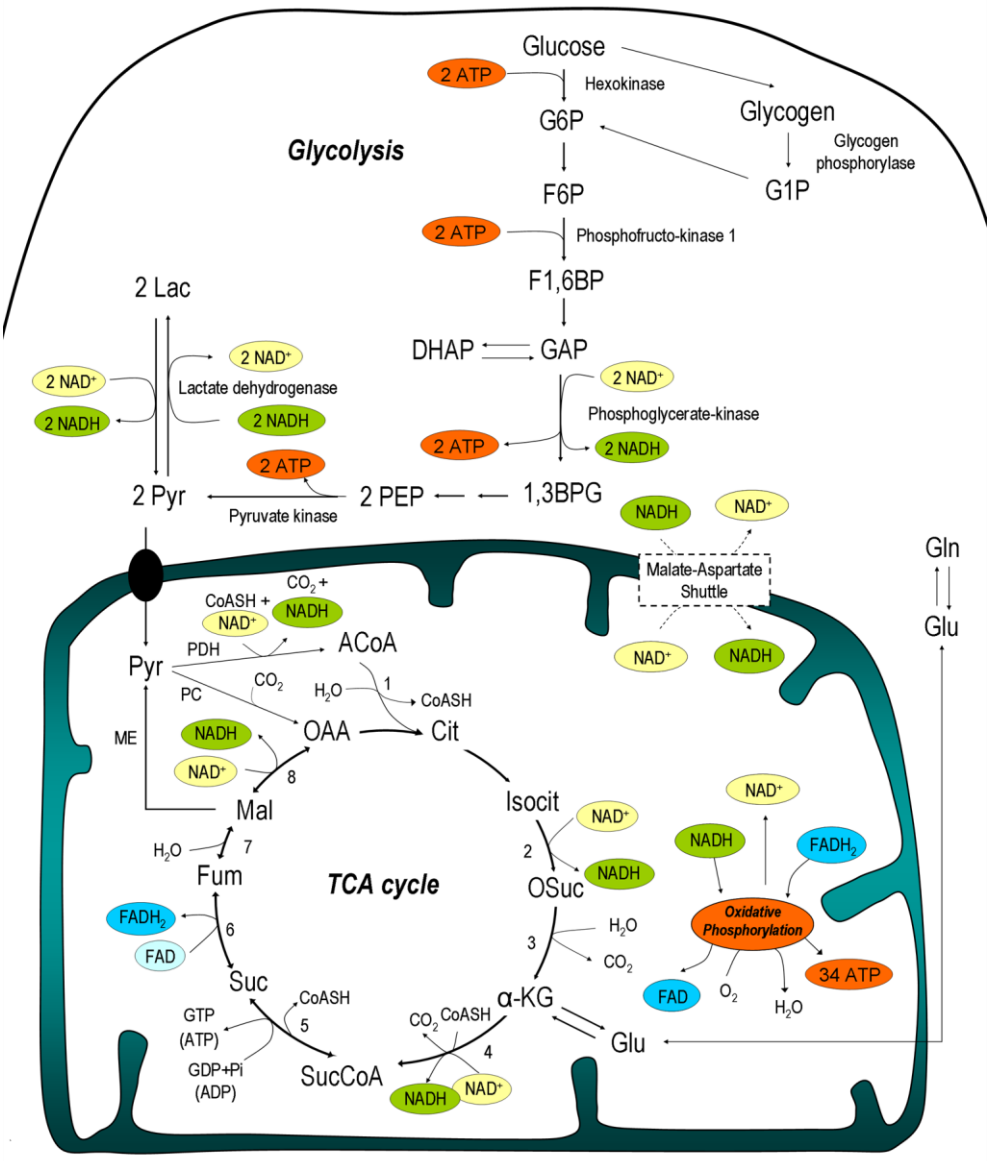

Figure 1.2 - Main reactions of glycolysis and TCA cycle. When glucose enters brain cells it is phosphorylated to glucose-6-phosphate (G6P) by hexokinase and subsequently to fructose-1,6-bisphosphate (F1,6BP) via fructose-6-phosphate (F6P) and phosphofructokinase 1, the main regulating enzyme in brain glycolysis. In one of the following steps, NADH is produced in the conversion of glyceraldehyde-3-phosphate (GAP) to 1,3-bisphosphoglycerate (1,3BPG) catalyzed by phosphoglycerate kinase. The NADH produced is either oxidized by lactate dehydrogenase, reducing pyruvate (Pyr) to lactate (Lac), or the reducing equivalent from NADH is transferred to the mitochondria, via the malate-aspartate shuttle, and oxidized in the electron transport chain as part of the oxidative phosphorylation process. In astrocytes, glucose can also be stored in the form of glycogen that is subsequently degraded into glucose-1-phosphate (G1P) and enters glycolysis via G6P. Pyruvate (Pyr) formed in glycolysis is subsequently metabolized via the tricarboxylic acid

(TCA) cycle. Pyruvate is carried into the mitochondrial matrix for oxidative decarboxylation to acetyl-CoA via the pyruvate dehydrogenase complex (PDH) or for carboxylation to oxaloacetate (OAA) via pyruvate carboxylation (PC; only in astrocytes). Acetyl-CoA (ACoA) is condensed via citrate synthase (1) to citrate (Cit), which is converted to α-ketoglutarate (α-KG) via aconitase (2) and isocitrate dehydrogenase (3). α-ketoglutarate is subsequently decarboxylated via the α-ketoglutarate dehydrogenase complex (4) to succinyl-CoA (SucCoA). Succinate (Suc) is formed from succinyl-CoA via succinyl-CoA synthase (5). Succinate dehydrogenase (6) oxidizes succinate to fumarate (Fum), which is converted into malate (Mal) via fumarase (7). Malate is then oxidized to oxaloacetate via malate dehydrogenase (8) or it can be converted to pyruvate via malic enzyme (ME). NADH and $FADH_2$ are oxidized in the electron transport chain that carries the electrons through different complexes to O_2, which is reduced to H_2O at the same time that ADP is phosphorylated into ATP, in a process called oxidative phosphorylation. Additional abbreviations: DHAP, dihydoxyacetone-phosphate, Isocit, isocitrate; OSuc, oxalosuccinate, PEP, phosphoenolpyruvate; Glu, glutamate; Gln, glutamine.

Oxidation of glucose to CO_2 provides the higher yield of ATP per glucose molecule (34 ATP) and, consequently, is fundamental to support energy-dependent brain functions. In particular, neurons require a large amount of ATP for recovery of the ion homeostasis dissipated by excitatory postsynaptic potentials (Attwell and Laughlin 2001). Therefore, it is widely accepted that these cells contribute to a major fraction of the total brain oxidative metabolism and, consequently, to cerebral ATP synthesis, even though astrocytes also significantly oxidize glucose (Hertz et al. 2007).

4.1.1.2 Pentose Phosphate Pathway (PPP)

The PPP interconverts sugar phosphates in multiple reactions divided in two branches, the oxidative and the non-oxidative branch (Figure 1.3). The oxidative part of the PPP is linked to glycolysis at the level of glucose-6-phosphate and catalyzes its conversion into ribulose-5-phosphate and CO_2. In addition, this branch is responsible for the reduction of NADP+ into NADPH, the major reducing compound. On the other hand, the non-oxidative branch interconverts pentose phosphates and phosphorylated aldoses and ketoses and is connected to glycolysis by their common intermediates glyceraldehyde-3-phosphate and fructose-6-phosphate. It also produces ribose-5-phosphates which are precursors for nucleotide synthesis (Dringen et al. 2007).

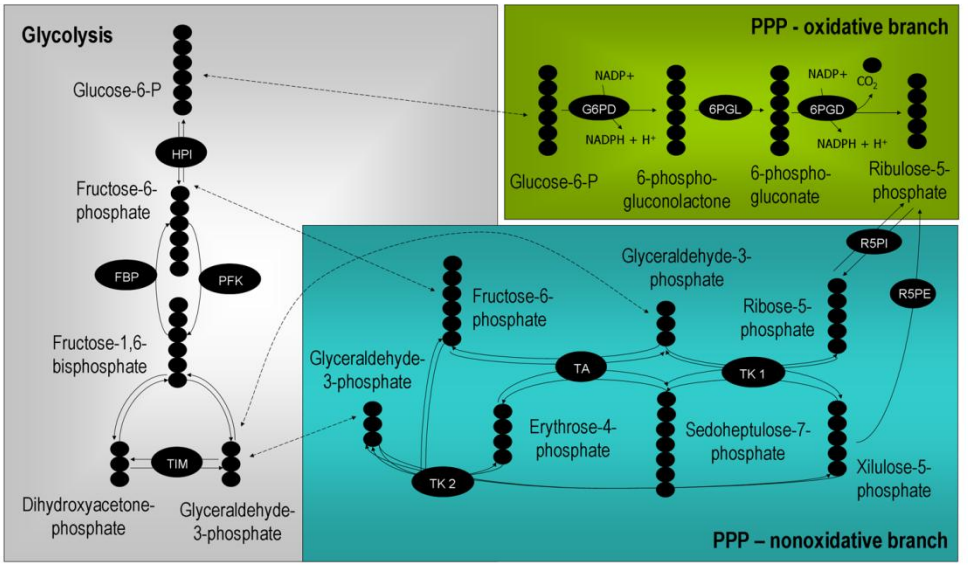

Figure 1.3 - Reactions of the PPP and their connection with glycolysis. For simplicity, only the part of glycolysis which has a link with the PPP is represented. Abbreviations: G6PD. Glucose-6-phosphate dehydrogenase; 6PGL, 6-phosphogluconolactonase; 6PGDH, 6-phosphogluconate dehydrogenase; R5PI, ribulose-5-phosphate isomerase; R5PE,ribolose-5-phosphate epimerase; TK, transketolase; TA, transaldolase; HPI, hexosephosphate isomerase; FBP, fructose-1,6-bisphosphatase; PFK, phosphofructokinase; TIM, triosephosphate isomerase.

The activity of the non-oxidative branch of the PPP in the adult brain appears to be rather low, being mainly used to support active cellular proliferation during brain development (Bilger and Nehlig 1992) or for the growth of brain tumours (Spence et al. 1997). Conversely, the oxidative branch predominates in brain cells because it provides the NADPH required for the regeneration of glutathione from its oxidized form, glutathione disulfide (GSSG) (Kletzien et al. 1994; Delgado-Esteban et al. 2000; Almeida et al. 2002). Nevertheless, the significance of the PPP in astrocytes and neurons differs.

Recent findings indicating that the glycolytic enzyme 6-phosphofructo-2-kinase/fructose2,6-bisphosphatase, isoform 3 (PFKFB3) is not active in suspensions of isolated rat cortical neurons suggested that these cells metabolize glucose mainly through the PPP (Herrero-Mendez et al. 2009). However, these results need to be confirmed in

cultured cells and *in vivo*. Different authors have shown that neurons use this pathway as a major antioxidant mechanism in the response to pro-oxidant compounds (Ben-Yoseph et al. 1996; Garcia-Nogales et al. 2003; Vaughn and Deshmukh 2008) or to stimulation of glutamate receptors (Delgado-Esteban et al. 2000). Moreover, the over-expression of PFKFB3 to redirect glucose metabolism from the PPP to glycolysis in these neurons resulted in depleted glutathione levels, apoptotic cell death and oxidative stress (Herrero-Mendez et al. 2009), confirming the extreme importance of the PPP in neurons. Even so, whether neurons use the PPP to compensate for their antioxidant fragility and, at the same time, inhibit the bioenergetically favourable glycolysis (Bolanos and Almeida 2010), remains to be elucidated *in vivo*. Despite exhibiting a high glycolytic rate and a low PPP basal activity, cultured astrocytes up-regulate this pathway under different conditions. For example, when subjected to oxidative or nitrosative stress (Ben-Yoseph et al. 1996; Garcia-Nogales et al. 1999; Bolanos and Almeida 2006), after being exposed to oxygen and glucose deprivation (Almeida et al. 2002) and when treated with amyloid beta peptides (Allaman et al. 2010). With regard to the *in vivo* context, the PPP was shown to contribute to glucose metabolism after focal brain activation in rats (Cruz et al. 2007) and was up-regulated after traumatic brain injury in humans (Dusick et al. 2007). All these findings underline the present importance attributed to the PPP in the metabolic response of brain cells to a number of pathologies in addition to its physiological significance.

4.1.1.3 Glycogen

Glucose can additionally be stored in the form of glycogen, which is predominantly located in astrocytes (Cataldo and Broadwell 1986) and present in the brain at significant levels (3-6 µmol/g tissue) (Cruz and Dienel 2002; Oz et al. 2007; Morgenthaler et al. 2008). Glycogen is degraded into glucose-1-phosphate by glycogen phosphorylase (EC 2.4.1.1) and subsequently enters glycolysis, after being converted into glucose-6-phosphate (Brown and Ransom 2007) (Figure 1.2). It is thought to be

metabolized to lactate in astrocytes and subsequently exported to fuel neurons and axons (Dringen et al. 1993a; Wender et al. 2000; Brown et al. 2004; Sickmann et al. 2005; Tekkok et al. 2005; Pellerin et al. 2007).

Based on its slow turnover under resting conditions (Oz et al. 2003; Oz et al. 2007) and rapid mobilization during an energy crisis or under hypoglycaemia (Choi et al. 2003; Oz et al. 2009), glycogen has been mainly considered an emergency fuel (Gruetter 2003; Dienel et al. 2007 and references therein). Nevertheless, its physiological role has been progressively reinforced. For instance, glycogenolysis is triggered by neuronal stimulation, when glucose alone cannot meet the high transient increase in cellular energy requirements (Swanson et al. 1992; Cruz and Dienel 2002; Brown et al. 2004; Dienel et al. 2007). Moreover, a "glycogen shunt", i.e., glucose metabolism via glycogen, is thought to operate in the brain and to contribute to lactate release during activation (Shulman et al. 2001). More recently, glycogen metabolism was shown to importantly contribute to long-term memory formation in rats through its conversion into lactate (Suzuki et al. 2011).

4.1.1.4 Cellular redox balance and shuttling of NADH

The continuous operation of glycolysis and the conversion of lactate into pyruvate via lactate dehydrogenase involve the reduction of NAD^+ into NADH (see Figure 1.2). Thus, in order to coordinate glycolytic activity with that of the TCA cycle, a low redox state (NAD^+/NADH) needs to be maintained (McKenna et al. 2000a). In addition to the reaction catalyzed by lactate dehydrogenase (LDH; EC 1.1.1.27) (Figure 1.2), this is mainly carried out by the malate-aspartate shuttle (MAS) in the brain (McKenna et al. 2006b). Because NADH cannot enter mitochondria, malate is responsible for the transfer of reducing equivalents from the cytosol into the mitochondria (Berkich et al. 2005; McKenna et al. 2006a). The MAS involves the concerted operation of important carriers [the aspartate-glutamate carrier (AGC) and the malate-α-ketoglutarate carrier] and enzymes (the cytosolic and mitochondrial isoforms of aspartate amino transferase

and malate dehydrogenase) (Palmieri et al. 2001). This shuttle additionally involves the irreversible electrogenic exchange of aspartate for glutamate and a proton via the AGC1 carrier (Aralar1), favouring the efflux of aspartate from and entry of glutamate into the mitochondria (McKenna et al. 2000a).

The real significance of the MAS in each brain cell type is not yet completely elucidated. Aralar1 and MAS activity appear to be much lower in astrocytes than in neurons (Ramos et al. 2003; Berkich et al. 2007; Xu et al. 2007) which is consistent with the enrichment of Aralar1 in neuronal mitochondria (Ramos et al. 2003; Pardo et al. 2011). Despite the presence of Aralar1 mRNA has been demonstrated in acutely isolated astrocytes from adult mice (Lovatt et al. 2007), it was recently proposed in a quite controversial study using Aralar-knockout mice that astrocytes do not seem to rely on the MAS to transfer redox equivalents to mitochondria (Pardo et al. 2011). Rather, Pardo and colleagues suggested that a neuron-to-astrocyte aspartate efflux may provide a means to transfer NADH/NAD^+ redox potential to astrocyte mitochondria (Pardo et al. 2011).

Considering the lack of strong evidence supporting the existence of the MAS in astrocytes, the operation of the glycerol-3-phosphate shuttle has alternatively been proposed to play a similar role in these cells (McKenna et al. 2000a). This shuttle is based on the concerted action of cytosolic and mitochondrial isoforms of glycerol 3-phosphate dehydrogenase, the former using NAD^+/NADH as coenzyme and the latter using FAD/$FADH_2$ for that purpose. Reducing equivalents are subsequently transferred to coenzyme Q in the respiratory chain. However, it yields less energy than the MAS due to the transport of electrons to FAD rather than NAD^+ (McKenna et al. 2006b). Nonetheless, the operation of the glycerol-3-phosphate shuttle remains controversial. Despite the evidence of glycerol-3-phosphate shuttle activity in cultured astrocytes and cerebellar neurons (Cammer et al. 1982; McKenna et al. 1993; Atlante et al. 1999), the cytosolic and mitochondrial isoforms of glycerol-3-phosphate dehydrogenase appear to be localized in glial and neuronal cells, respectively (Leveille et al. 1980; Nguyen et al. 2003).

4.1.1.5 Anaplerotic versus oxidative metabolism

Anaplerosis fuels the TCA cycle with extra carbon units required to the synthesis and release of TCA cycle intermediates (Sonnewald and Rae 2010). Pyruvate carboxylase (PC) is the main cerebral anaplerotic enzyme (Patel 1974). It is an ATP-dependent enzyme which converts pyruvate into oxaloacetate (Wallace et al. 1998). PC was shown to be primarily, if not exclusively, expressed in astrocytes *in vitro* and *in vivo* (Yu et al. 1983; Shank et al. 1985; Kaufman and Driscoll 1993; Shank et al. 1993; Cesar and Hamprecht 1995). Furthermore, using ^{13}C NMR spectroscopy in monotypic cultures of astrocytes and neurons it was shown that this pathway occurs in astrocytes and not in neurons (Sonnewald et al. 1993b; Waagepetersen et al. 2001b). Although malic enzyme or the combined action of phosphoenolpyruvate carboxykinase (PEPCK, EC 4.1.1.31) and pyruvate kinase (PK, EC 2.7.1.40) can also fix CO_2, their activity in the brain appears not to be significant (Patel 1974). Even so, Hassel and colleagues have provided some controversial evidence that neurons can carboxylate, claiming that it occurs probably via malic enzyme (Hassel 2000).

PC activity is strongly associated with the synthesis and export of glutamine both *in vivo* and *in vitro* (Gamberino et al. 1997; Gruetter et al. 2001; Waagepetersen et al. 2001a). Anaplerosis is important for neurotransmitter metabolism and ammonia detoxification as it is essential to replenish neuronal TCA cycle and neurotransmitter pools due to the continuous release of neurotransmitters (e.g. Hertz et al. 1999; Sibson et al. 2001; Oz et al. 2004; Xu et al. 2004; Zwingmann 2007). In addition, it is important to compensate for the loss of additional molecules that leave the brain, for example, lactate, which can occur via the pyruvate recycling pathway (Sonnewald et al, unpublished data).

In vivo and *in vitro* estimations of the different contributions of fluxes through PC and PDH to the synthesis of different amino acids have been based on the distinct labelling patterns derived from the metabolism of [1-^{13}C]glucose (Zwingmann and

Leibfritz 2007). However, these estimations might be limited by the appearance of the same isotopomers arising both through PC and PDH and further complicated by the equilibration of the label between oxaloacetate and fumarate due to backflow in the TCA cycle (Merle et al. 1996b, a). Therefore, the range of values reported is rather large (Table 1.1). The use of different formulas, labelled substrates, and incubation times has also contributed to this variability (see Zwingmann and Leibfritz 2007 for details). Using ^{13}C NMR spectroscopy and metabolic modelling, PC and PDH fluxes and their contribution to cerebral oxidative metabolism have been estimated *in vivo* (see subsection 5.3).

4.2 Glucose vs. Lactate supporting brain activity

Cerebral oxidative metabolism supports brain activity both under resting and activated conditions. However, glycolytic flux is up-regulated even more than the simultaneous increase in oxygen consumption upon activation (reviewed by Dienel and Cruz 2004, 2008). These changes suggest an increase in local lactate demand followed by a larger increase in local lactate production. Lactate transients and increased glucose utilization are actually the metabolic hallmarks of brain activation detected with functional brain imaging techniques (Bonvento et al. 2005). Hence, different groups have been trying to investigate the role of glucose and lactate as substrates supporting synaptic activity and, at the same time, elucidating the contribution of neurons and astrocytes to cerebral oxidative metabolism. The different theories proposed to explain these phenomena remain under a heated debate (Bonvento et al. 2005; Hertz et al. 2007; Simpson et al. 2007; Dienel and Cruz 2008; Mangia et al. 2009; Pellerin 2010). The main controversy centres around the cellular origin and fate of the lactate produced under activation.

Table 1.1 - Variability of PC/PDH ratios calculated using different ^{13}C-labelled substrates and formulas.

Labelled substrate	Formula	Comments	PC/PDH
[1-^{13}C]glucose	(C2-C3)/C4	• C2 in glutamine and glutamate are higher than C3 • Does not assume malate-fumarate equilibration	33%, 36% and 9.8% in glutamine after 15, 30 or 45 min after glucose infusion in rats (Shank et al. 1993) 58%, 41% and 0% in glutamine at 5, 15 and 30 min after glucose injection in mice (Hassel and Sonnewald 1995) Cultured astrocytes 54% in glutamine and 3% in glutamate (Merle et al. 1996a, b) 21% and 50% in glutamine in the presence or absence of glutamate, respectively (Teixeira et al. 2008)
[2-^{13}C]pyruvate [2-^{13}C]glucose	C3/C5 (Glu/Gln) C4/C1 (GABA)	• PC labels C2 or C3 whereas PDH labels C5 of glu/gln; C2 is only labelled through equilibration of the label	31% in gln, 13% in glu and 10% in GABA after 60 min glc infusion in rats (Kanamatsu and Tsukada 1999) 5.6, 13.5, 10% for glutamate, glutamine and GABA, respectively (Taylor et al. 1996) 26% in glutamine (Sibson et al. 2001)
[1,2-^{13}C]glucose		• [2,3-^{13}C]oxaloacetate, glutamate and glutamine are produced through PC	PC = 38% of the TCA cycle flux after glucose infusion in rats (Kunnecke et al. 1993)
[U-^{13}C]glucose	[2,3-$^{13}C_2$]-[2,3,4,5-$^{13}C_4$]/[4,5-$^{13}C_2$] in Glu/Gln	• Unambiguous detection of incorporation of label into metabolites due to ^{13}C-^{13}C spin-spin coupling patterns. • Some overlapping labelling patterns in glu/gln isotopomers after multiple turns of the TCA cycle might influence estimations • Confirmed the exclusive operation of PC in astrocytes (Waagepetersen et al 2001)	34% in glutamine and 16% in glutamate (Lapidot and Gopher 1994) 39% in glutamate (Qu et al. 2001)

4.2.1 The Astrocyte-Neuron Lactate Shuttle

For many years, the prevailing classical view considered glucose as the primary substrate for both neurons and astrocytes during activation and lactate, produced in the process, being removed mainly after neural activity (Chih and Roberts Jr 2003). The metabolic coupling concept involving astrocytic glycolytic activation and neuronal synaptic activity

challenged this view. The astrocyte-neuron lactate shuttle (ANLS) hypothesis, proposed by Pellerin and Magistretti, stated that glutamate, released by neurons and subsequently taken-up by astrocytes via specific transporters, would stimulate glycolysis in these cells through a mechanism mediated by the activation of the Na^+/K^+ ATPase (Pellerin and Magistretti 1994; Pellerin et al. 1998; Magistretti and Pellerin 1999). The lactate produced in astrocytic glycolysis would then be released to meet the metabolic demands of neurons (Magistretti et al. 1999). The ANLS is consistent with the strategic position of astrocytes between neurons and blood vessels, their expression of high-affinity glutamate transporters and enrichment in MCT-1 and -4 lactate transporters (Magistretti and Pellerin 1999). Supporting this concept, a 1:1 ratio between oxidative glucose consumption and astrocytic glutamate cycling was reported for the rat brain (Sibson et al. 1998; Rothman et al. 1999). Moreover, several independent groups obtained further *in vivo* (Loaiza et al. 2003; Kasischke et al. 2004; Serres et al. 2004; Caesar et al. 2008) and *in vitro* evidence (reviewed by (Bouzier-Sore et al. 2003; Pellerin et al. 2007; Barros and Deitmer 2010) that lactate supports neuronal activity using different approaches. Further recent reviews on this theory can be found in (Magistretti 2009) and (Pellerin 2010).

4.2.2 Criticisms to the ANLS and alternative theories

The ANLS theory originated an intense debate in the field and led to a number of criticisms enumerating contrasting data and claiming for insufficient experimental evidence (Chih et al. 2001; Dienel and Hertz 2001; Chih and Roberts Jr 2003; Dienel and Cruz 2003, 2004; Hertz 2004). Subsequently, the ANLS was reformulated acknowledging that astrocytic glycolysis was enhanced in response to glutamatergic activity *despite the availability of oxygen to support oxidative phosphorylation* and that lactate produced *both by neurons or astrocytes* could be used as energy fuel in neurons (Pellerin and Magistretti 2003). Furthermore, glycogenolysis was acknowledged to be a putative

additional astrocytic source of lactate to fuel intense neuronal activity (Pellerin et al. 2007).

Recent criticisms of the ANLS hypothesis have explored the significant oxidative capacity of astrocytes, the role of glucose supporting neuronal activity and the fate of lactate released during activation. Leif Hertz and colleagues emphasize that astrocytes are known to significantly oxidize glucose for energy production in addition to their high dependence on glycolysis and glycogenolysis to respond to increasing energy demands (Hertz et al. 2007). On the other hand, Bak and colleagues provided further evidence that neurons up-regulate glucose metabolism during neurotransmission, even in the presence of lactate (Bak et al. 2006b; Bak et al. 2009). Furthermore, other authors provided evidence in favour of a preferential fast transport-mediated lactate trafficking and release from the activated brain into the blood, compared to its local metabolism (Simpson et al. 2007; Contreras and Satrustegui 2009; Gandhi et al. 2009). Finally, metabolic modelling studies of glucose and lactate transport and utilization predicted that neurons should be responsible for most of glucose uptake and metabolism (Mangia et al. 2009; DiNuzzo et al. 2010). According to this hypothesis, the lactate transients observed during activation are generated by neurons, which then transfer it to astrocytes, in a totally opposite theory to the ANLS.

Despite all the results obtained *in vivo* and *in vitro*, there are still no available measurements of glucose or lactate with cellular resolution in the brain *in vivo*. Thus, it is not yet possible to describe accurately which cell type is the lactate source or the lactate fate, and whether these roles may be region-specific or affected by activity. Therefore, further data will be required to elucidate this long-lasting debate.

4.2.3 The Redox Switch/Redox Coupling Hypothesis

With a different perspective, Cerdan and colleagues proposed an alternative interpretation of the neuroglial metabolic coupling, considering the contribution of lactate-pyruvate exchange shuttles linking glycolytic and oxidative domains of

heterogeneously activated cells (Cerdan et al. 2006). The redox-coupling hypothesis is based on intracellular compartmentation of pyruvate and lactate pools observed both in neurons and astrocytes (Sonnewald et al. 1993b; Cruz et al. 2001; Waagepetersen et al. 2001a; Zwingmann et al. 2001; Schousboe et al. 2003) as well as in glioma cells (Bouzier et al. 1998). Two different pools of intracellular pyruvate were characterized; one derived from extracellular pyruvate, used mainly for lactate and alanine production and the other one derived from glucose and used primarily for oxidation (Cruz et al. 2001). This pyruvate compartmentation enables neurons and astrocytes to alternatively select between glucose and lactate, depending on their relative extracellular concentration. Herein, a redox switch using the cytosolic NAD^+/NADH ratio is proposed to modulate glycolytic flux, controlling which one of the two pyruvate pools is metabolized in the TCA cycle (Cerdan et al. 2006). This could justify that part of the lactate consumed by neurons could be transferred back to the medium as part of a lactate recycling process, which is also valid for pyruvate (Cruz et al. 2001; Zwingmann et al. 2001; Rodrigues and Cerdan 2005, 2007). The redox-switch coupling hypothesis thus suggests a reversible exchange of reducing equivalents between neurons and astrocytes, driven by the transcellular redox gradient, rather than a simple vectorial transfer of lactate from astrocytes to neurons. This hypothesis, together with the concepts of intracellular compartmentation of glutamate and monocarboxylates, is consistent with a simultaneous operation of glial and neuronal TCA cycle activity during activation (Cruz et al. 2005; Dienel and Hertz 2005).

4.3 Glutamate and glutamine metabolism

Glutamate is a central molecule in the brain as it plays multiple roles. In addition to being the major excitatory neurotransmitter (see Danbolt 2001 for references), it is the direct precursor for the inhibitory neurotransmitter GABA in neurons and of glutamine in astrocytes (Schousboe et al. 1997). Furthermore, it can be incorporated into proteins or used to synthesize glutathione (Dringen 2000), it participates in the purine nucleotide cycle and is importantly involved in intermediary metabolism, being also used as energy

substrate (Bak et al. 2006a). All these functions make glutamate homeostasis very complex. In fact, glutamate excitotoxicity is associated with many brain pathologies, including ischemia, Huntington's disease, Parkinson's disease, among others (Maragakis and Rothstein 2004). Glial glutamate transporters are thought to be involved in this process, perhaps due to altered function (including the reversal of their operation or the inability of efficiently taking up glutamate) or decreased expression levels (Danbolt 2001; Shin et al. 2005; Camacho and Massieu 2006; Faideau et al. 2010).

4.3.1 Glutamate-Glutamine cycle

The differential cellular expression of the enzymes implicated in glutamate and glutamine metabolism makes it highly compartmentalized. The exclusive astrocytic localization of the enzymes glutamine synthethase (GS) (Martinez-Hernandez et al. 1977) and PC (Yu et al. 1983; Shank et al. 1985) determines that astrocytes are the only cell type in the brain able to perform *de novo* synthesis of glutamine. In addition, phosphate-activated glutaminase (PAG), the enzyme transforming glutamine into glutamate, has a preferential neuronal expression (Kvamme et al. 2001). For this reason, neurons must rely on astrocytes through the so-called glutamate-glutamine cycle (Figure 1.4) to replenish their TCA cycle after the drain of carbon units resulting from neurotransmitter synthesis and release. This cycle has been proposed in the late 1960's based on the observation of different glutamate pools: a small pool (precursor for glutamine and attributed to the glial compartment) and a large pool with a slower turnover, attributed to the neuronal compartment (Berl et al. 1968; Clarke et al. 1970; van den Berg and Garfinkel 1971).

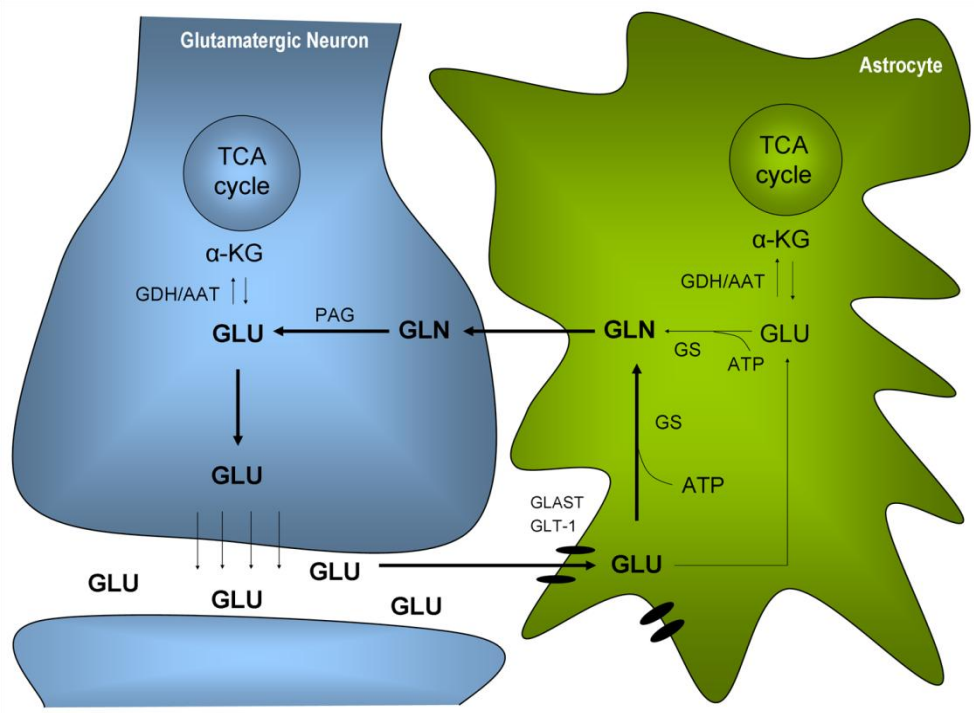

Figure 1.4 - The glutamate-glutamine cycle. After synaptic release of glutamate (GLU) by neurons, astrocytes are responsible for its uptake via specific high-affinity glutamate transporters (GLAST and GLT-1) to prevent neuronal excitotoxicity. Glutamate taken up by astrocytes is converted to glutamine (GLN) via glutamine synthetase (GS) at the expense of one ATP molecule. Glutamine is then transferred back to neurons where it is transformed into glutamate by phosphate-activated glutaminase (PAG), making it available again for neurotransmission and, this way, closing the cycle. The close association between glutamate and TCA cycle metabolism is indicated in both cells: glutamate can be additionally converted into α-ketoglutarate (α-KG) via either glutamate dehydrogenase (GDH) or aspartate amino transferase (AAT) and being subsequently oxidized.

On the other hand, GABAergic neurons are responsible for a larger fraction of their neurotransmitter reuptake compared to glutamatergic neurons (Schousboe et al. 2004). Still, a similar cycle also operates in these neurons and has quantitative significance for the replenishment of the neurotransmitter GABA pool (Sonnewald et al. 1993a). In this context, the cycle can be extended to include a glutamate-glutamine-GABA cycle (further details in Bak et al. 2006a).

The glutamate-glutamine cycle additionally generates an imbalance in ammonia homeostasis since a large amount of ammonia is produced in neurons through PAG and consumed in astrocytes for glutamine synthesis. This requires an efficient process to shuttle the excess nitrogen from neurons to astrocytes, which was, nevertheless, not taken into account in the classical proposal of the glutamate-glutamine cycle (Bak et al. 2006a; Zwingmann and Leibfritz 2007). Shuttling mechanisms involving carrier molecules such as branched chain amino acids (BCAA) (Yudkoff et al. 1994; Yudkoff 1997; Bixel et al. 2004), alanine (Waagepetersen et al. 2000; Zwingmann et al. 2000; Zwingmann et al. 2001; Rae et al. 2003) or aspartate (Bakken et al. 1997; Griffin et al. 1998; Griffin et al. 2003) are likely candidates for this role. However, the extent to which each of the proposed shuttles is coupled to the glutamate-glutamine cycle *in vivo* remains to be clarified experimentally.

4.3.2 Glutamate/Glutamine Oxidation and Pyruvate Recycling

The glutamate-glutamine cycle is not closed or stoichiometric, since glutamate and glutamine can be formed from numerous metabolites and also be additionally metabolized by neurons and astrocytes for a number of purposes, depending on the cellular needs (McKenna 2007 and references therein). The pyruvate recycling pathway (Figure 1.5) mediates the oxidation of these amino acids in order to maintain sufficient energy metabolism when substrates such as glucose or monocarboxylates are low. The carbon skeleton of glutamate has to exit the TCA cycle at the level of malate or oxaloacetate and re-enter the cycle in the form of acetyl-CoA in order to be fully oxidized (Zwingmann and Leibfritz 2007). Pyruvate recycling can occur through two general pathways, one catalyzed by the NADP-linked malic enzyme (ME, EC 1.1.1.39), which converts malate into pyruvate, and the other catalyzed by PEPCK and PK, converting oxaloacetate to phosphoenolpyruvate (PEP) and pyruvate (Cruz et al. 1998).

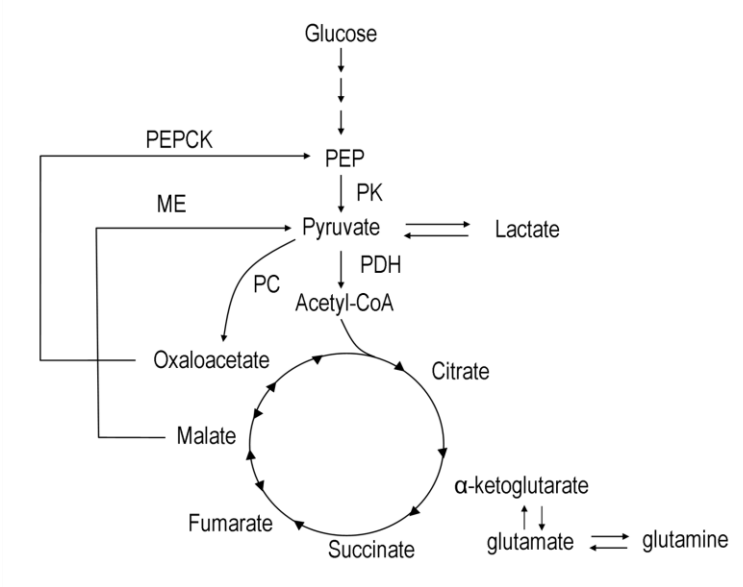

Figure 1.5 - Pathways for pyruvate recycling in brain cells. Pyruvate recycling is a major pathway for the complete oxidation of glutamine and glutamate. It is mainly mediated by malic enzyme (ME), converting malate to pyruvate. Nevertheless, it might also occur, to some extent, via the combined activities of phosphoenolpyruvate carboxykinase (PEPCK), converting oxaloacetate to phosphoenolpyruvate (PEP), and pyruvate kinase (PK), converting PEP to pyruvate. Pyruvate can then re-enter the TCA cycle via pyruvate dehydrogenase (PDH) or pyruvate carboxylase (PC; only in astrocytes).

Pyruvate recycling was known to occur in the liver due to its significant contribution to gluconeogenesis in this organ (Friedman et al. 1971). However, only in the 1990's Cerdan and colleagues provided metabolic evidence and described the localization of the enzymes required for this pathway to operate in the rat brain (Cerdan et al. 1990; Cruz et al. 1998). Although these authors used [1,2-^{13}C]acetate, a specific substrate for astrocytes, they concluded that pyruvate recycling likely occurred in neurons based on the higher amount of [4-^{13}C]glutamate compared to [4-^{13}C]glutamine as detected by ex-vivo ^{13}C NMR spectroscopy (Cerdan et al. 1990). Moreover, it was suggested that pyruvate recycling appeared to contribute with 17% of the total pyruvate metabolized via PDH in neurons (Kunnecke et al. 1993) and with approximately 30% of the acetyl-CoA entering the TCA cycle in the brain (Cerdan et al. 1990; Cruz et al. 1998; Haberg et al. 1998). However, many subsequent studies using ^{13}C-labelled acetate and/or

glucose in cultured astrocytes (Sonnewald et al. 1993b; Hassel et al. 1994; Bakken et al. 1997; Alves et al. 2000b; Waagepetersen et al. 2002) and in animal models (Hassel and Sonnewald 1995; Haberg et al. 1998; Chapa et al. 2000) provided evidence favouring a predominant operation of pyruvate recycling in astrocytes. These studies suggested that approximately 7% of the newly synthesized lactate in astrocytes was derived from this pathway and could account for 20% of the glial pool of lactate. Only more recently, glutamate and glutamine oxidation via pyruvate recycling has been reported again in cultured neurons (Olstad et al. 2007).

Finally, the cellular localization of ME, PEPCK and PK provides additional information regarding the operation of this pathway in neurons and astrocytes. In fact, mitochondrial (mME) and cytosolic (cME) ME isoforms appear to have different cellular distributions in the brain, although their relative importance to pyruvate recycling has not been clarified. Vogel et al reported relative enzyme activities of mME and cME in brain homogenates of 55% and 45%, respectively (Vogel et al. 1998). Furthermore, mME appears to be only expressed in neurons (Cruz et al. 1998; McKenna et al. 2000b) whereas cME is thought to be mainly a glial enzyme, accounting for 95% of total ME activity in astrocytes (Kurz et al. 1993; McKenna et al. 2000b; Kimmich et al. 2002). The development of mME expression mainly after synaptogenesis *in vivo* (Cruz et al. 1998) and the immature stage of neuronal primary cultures prepared from neonatal brain could justify the reduced neuronal pyruvate recycling activity observed *in vitro*. Concerning PEPCK, it is thought to contribute to pyruvate recycling mainly in astrocytes, being selectively localized in the mitochondria (Alves et al. 1995; Schmoll et al. 1995; Bakken et al. 1997; Bakken et al. 1998).

Although the significance and cellular operation of pyruvate recycling in the adult brain is still unclear, its enzymatic capacity is thought to be much higher than the measured metabolic fluxes *in vivo* (Cruz et al. 1998). This suggests that the associated enzymes might be up-regulated under pathological conditions that require oxidation of substrates other than glucose. However, cultured astrocytes subjected to glucose

deprivation or treated with iodoacetate (an inhibitor of glycolysis) did not increase the flux of [U-$^{13}C_5$]glutamate metabolism through pyruvate recycling (Bakken et al. 1998).

5 Brain Metabolism in Neuropathologies

5.1 Cerebral Ischemia and Metabolic Features

Ischemic stroke is caused by the occlusion of a major cerebral artery either by an embolus or by local thrombosis, causing severe brain damage (Dirnagl et al. 1999). It is the third leading cause of death in industrialized countries and a major cause of adult disability (Nedergaard and Dirnagl 2005). However, despite extensive research in the field, most candidate drugs have proved unsuccessful and the most effective strategy to avoid a poor outcome continues to be the fast restoration of blood supply (Rossi et al. 2007).

Ischemic brain injury results from a complex sequence of pathophysiological events that evolve over time and space (after stroke the partially perfused brain area - 'penumbra' - may progress to cell death, increasing the area of infarction - 'core' - or recover its function due to re-establishment of reperfusion by means of anti-coagulant treatment) (Dirnagl et al. 1999). The impairment of cerebral blood flow in stroke restricts the delivery of key substrates, particularly oxygen and glucose, reducing the energy required to maintain ionic gradients (Martin et al. 1994). Blood flow in the penumbral region might fall to 20% of its normal level (even lower in the core) and oxidative metabolism decreases sharply (Hertz 2008). The marked decrease in ATP synthesis favours the generation of reactive oxygen species and results in the loss of ion homeostasis across cell membranes, leading to membrane depolarization, which alters the glutamate uptake mechanisms and ultimately leads to excitotoxicity (Rossi et al. 2007).

The classical metabolic hallmarks of brain ischemia are thus the increase in the rate of anaerobic glycolysis, mainly by astrocytes, in order to deal with the fast decline in ATP supplies (Hertz 2008). Lactate accumulates to very high levels during hypoxia-

ischemia and its accompanying acidosis has been considered one of the major contributors to selective neuronal damage (Lipton 1999). On the other hand, different authors provided evidence that lactate, possibly supplied by astrocytes, can be neuroprotective after ischemia, by functioning as neuronal energy substrate during reperfusion (Schurr 2002; Berthet et al. 2009). In addition, several metabolic alterations associated with ischemia have been reported. For instance, glucose metabolism was decreased after focal cerebral ischemia in rats whereas increased oxidation of glutamate and GABA in astrocytes and of glutamine (via pyruvate recycling) in neurons was observed (Pascual et al. 1998; Thoren et al. 2006) suggesting the importance of alternative substrates in the recovery from ischemia. In fact, astrocytic metabolism was shown to be essential for neuronal survival after ischemia in rats, by providing energy substrates such as glutamine (Haberg et al. 2001; Haberg et al. 2006). Nevertheless, pyruvate carboxylation was decreased in different animal models of ischemia (Haberg et al. 2006; Richards et al. 2007). The MAS also appears to be affected in this context due to an impairment of cytosolic-mitochondrial communication (Cheeseman and Clark 1988; Lewandowski et al. 1997; Lu et al. 2008). Overall, metabolic alterations resulting from such energy failure are very complex because substrate limitations necessarily lead to profound changes in the fluxes of several pathways (reviewed by Dienel and Hertz 2005; Hertz 2008). In general, astrocytes are more resistant than neurons to ischemic damage, likely due to their higher glycolytic capacity, glycogen content, higher glutathione levels and the ability of metabolising multiple substrates, as described earlier. Their vital functions in the brain are also implicated in ischemic brain damage, although their different protective or destructive roles remain unclear (Nedergaard and Dirnagl 2005; Trendelenburg and Dirnagl 2005; Rossi et al. 2007). Therefore, ongoing research on this topic continues to further characterize metabolic alterations caused by cerebral ischemia, ultimately aiming for possible therapeutic targets.

5.2 Brain hypoglycaemia

Hypoglycaemia occurs mainly in diabetic patients receiving insulin therapy but eventually also in normal subjects due to prolonged fasting (Suh et al. 2007a). Normal glucose concentrations range between 3.9 and 7.1 mM in the blood and between 0.8 and 2.3 mM in the brain, showing a linear relationship (Gruetter et al. 1998a). When blood glucose levels fall below 2 mM, brain glucose concentration drops close to zero since blood glucose consumption exceeds transport capacity at reduced concentrations (Choi et al. 2001). Depending upon its severity, hypoglycaemia may cause irritability, impaired concentration, cognitive dysfunctions, focal neurological deficits or even seizures (Suh et al. 2007a), which highlights the importance of glucose to support brain functions.

Metabolic alterations caused by hypoglycaemia are markedly different from those typical of ischemia due to the availability of oxygen, allowing cells to eventually oxidize alternative substrates to sustain ATP production. In fact, ATP levels fall more slowly during hypoglycaemia, when compared to ischemia-like conditions (Okada and Lipton 2007). Even so, synaptic transmission is impaired well before the decline in ATP levels, even when non-glucose fuels like pyruvate or lactate are available (Okada and Lipton 2007; Suh et al. 2007a and references therein). Based on these findings, different authors suggested that the ATP produced during glycolytic glucose metabolism seems to be essential to support synaptic transmission.

Nevertheless, different substrates were shown to support brain function during or after hypoglycaemia, both *in vitro* and *in vivo*, including acetate (Criego et al. 2005), pyruvate (Suh et al. 2005; Mason et al. 2006) and glutamate and glutamine (Bakken et al. 1998; Rao et al. 2010). A significant mobilization of glycogen has also been observed under various degrees of hypoglycaemia both in humans and rats (Choi et al. 2003; Oz et al. 2009) and increased glycogen stores sustained neuronal activity under hypoglycaemia for up to 90 minutes longer than in rats with normal glycogen levels (Suh et al. 2007b). Further investigations on the metabolic adaptation of brain cells to

hypoglycaemia will not only bring new knowledge on the role of different substrates supporting brain function but will also ultimately lead to the development of better treatments for vulnerable patients.

6 Tools to Investigate Brain Metabolism

Early studies of brain metabolism have used radiolabelled tracers such as ^{14}C-labelled glucose, to investigate fluxes through different pathways (Katz and Rognstad 1967). More recently, radioactive techniques such as autoradiography and PET together with ^{14}C or ^{18}F-glucose have been used to measure regional cerebral glucose consumption (Spence et al. 1997; Nehlig et al. 2004; Thoren et al. 2006; Cruz et al. 2007). Both methods allow the determination of cerebral metabolic rates for glucose in different brain regions after appropriate modelling of the underlying tracer kinetics. However, these approaches are limited in resolution and chemical specificity, which do not make it possible to image single neural cells in the examined area, or to investigate the downstream metabolism of glucose below the phosphofructokinase step (Rodrigues and Cerdan 2007). On the other hand, imaging of NAD(P)H fluorescence transients has also been used with the aim of resolving in time the NADH balances occurring in neurons and astrocytes during glutamatergic activation (Kasischke et al. 2004). However, this technique is not cell specific and results might indicate increased oxidative or glycolytic metabolism, depending on interpretations (Kasischke et al. 2004; Brennan et al. 2006). The use of stable isotopes and the development/improvement of magnetic resonance techniques to detect them revolutionized the research in the field (Badar-Goffer et al. 1990; Cerdan et al. 1990; Shank et al. 1993). Techniques exploring the information provided by ^{13}C-labelled substrates such as ^{13}C NMR spectroscopy and mass spectrometry (MS) were those employed in this thesis and will be described in more detail below.

6.1 ^{13}C NMR spectroscopy

The use of ^{13}C-labelled compounds and magnetic resonance spectroscopy is a powerful approach to investigate brain energy metabolism both in primary cultures, brain slices and *in vivo* (reviewed by Rodrigues et al. 2009). Its main advantages rely on the low natural abundance of ^{13}C, the non-invasive character of NMR spectroscopy, in particular for *in vivo* studies, and its high chemical specificity, due to the capacity of distinguishing isotope incorporation, not only in different molecules but also in specific positions in the same molecule (^{13}C isotopomers). However, its main disadvantage is the low sensitivity when compared to other conventional metabolic techniques including mass spectrometry, radioactive counting or spectrophotometric or fluorimetric methods (Rodrigues et al. 2009).

NMR spectroscopy allows distinguishing specific nuclei surrounded by distinct chemical environments in a molecule, due to their characteristic chemical shifts. These correspond to the resonance frequencies of the different atoms, when exposed to a magnetic field, which originate the range of peaks observed in the NMR spectrum. Due to these properties, the fate of a labelled substrate can be followed directly through the different metabolic pathways of intermediary metabolism (Rodrigues et al. 2009). Figure 1.6-A illustrates the labelling patterns of [1-^{13}C]glucose in brain cells, the most commonly used substrate, as well as a typical ^{13}C NMR spectrum of a brain extract after i.v. injection of a solution containing [1-^{13}C]glucose (Figure 1.6-B). Further details about the labelling patterns of differently labelled substrates will be provided in each specific chapter of this thesis.

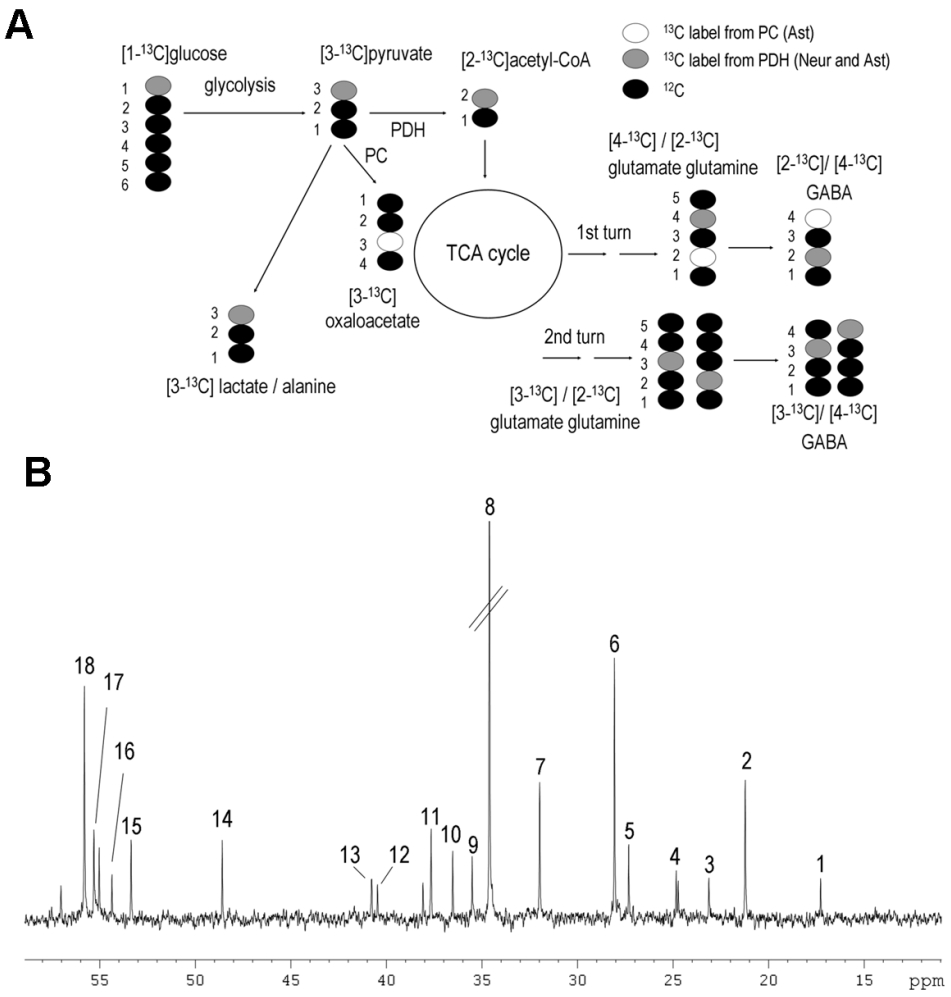

Figure 1.6 – A - Simplified scheme of labelling patterns in metabolites from [1-^{13}C]glucose in neurons and astrocytes. [1-^{13}C]glucose enters neurons and astrocytes and is transformed via glycolysis to [3-^{13}C]pyruvate. The latter can be converted to [3-^{13}C]lactate or [3-^{13}C]alanine or be transported into mitochondria to enter the TCA cycle as [2-^{13}C]acetyl-CoA, via pyruvate dehydrogenase (PDH). Condensation of [2-^{13}C]acetylCoA with unlabelled oxaloacetate will, after several steps, lead to the formation of [4-^{13}C]glutamate and glutamine and [2-^{13}C]GABA in GABAergic neurons, in the first turn of the TCA cycle. However, if the label remains in the cycle and labelled oxaloacetate condenses with labelled acetyl-CoA, [2-^{13}C]/[3-^{13}C]glutamate and glutamine and [3-^{13}C]/[4-^{13}C]GABA will be formed. In astrocytes, [3-^{13}C]pyruvate can also enter the TCA cycle via pyruvate carboxylase (PC), in the form of [3-^{13}C]oxaloacetate. After several steps, [2-^{13}C]glutamate and glutamine and [4-^{13}C]GABA will be produced. ***B – Example of a typical ^{13}C NMR spectra of a rat brain extract after i.v. injection of [1-^{13}C]glucose.*** Peak assignment: 1 – Alanine C-3, 2 - Lactate C-3, 3 – *N*-acetyl aspartate, 4 – GABA C-3, 5 – Glutamine C-3, 6 – Glutamate C-3, 7 – Glutamine C-4, 8 – Glutamate C-4, 9 – Succinate C-2/3, 10 – GABA C-2, 11 – Taurine C-2, 12 – GABA C-4, 13 – *N*-acetyl aspartate C-3, 14 – Taurine C-1, 15 – aspartate C-2, 16 - *N*-acetyl aspartate C-2, 17 – Glutamine C-2, 18 – Glutamate C-2. The NMR spectrum was gently provided by Linn Hege Nilsen (NTNU, Norway).

In the early 1990's, major technical improvements in NMR spectroscopy increased sensitivity and resolution of ^{13}C NMR spectra. Labelled glutamine and glutamate could be detected for the first time following glucose administration in the human brain (Beckmann et al. 1991; Gruetter et al. 1994). These events opened the way for numerous studies on cerebral metabolic compartmentation (Bachelard 1998; Cruz and Cerdan 1999), the determination of metabolic fluxes in live animals (Henry et al. 2002) and in humans (Gruetter et al. 1998b), and the characterization of metabolic responses related to brain activation (Patel et al. 2004) or pathological scenarios (Alves et al. 2000a), among others. Taking advantage of the fact that acetate is a glial-specific substrate (Waniewski and Martin 1998), the combined use of [1,2-^{13}C]acetate and [1-^{13}C]glucose, which originate different ^{13}C labelling patterns, importantly enabled to investigate metabolic interactions between neurons and astrocytes in multiple contexts (reviewed by Sonnewald and Kondziella 2003; Zwingmann and Leibfritz 2003). Furthermore, the indirect method [^{1}H]-observed-[^{13}C]-edited NMR spectroscopy was later developed and employed by some groups aiming to overcome the lower sensitivity when compared to direct observation of ^{13}C resonances (de Graaf et al. 2003). More recently, Rodrigues et al developed a new (^{13}C,^{2}H) NMR spectroscopy method to investigate reactions involving the fast process of hydrogen turnover by following the exchange of ^{1}H by ^{2}H in ^{13}C-labelled metabolites when metabolism occurs in media containing $^{2}H_2O$ (Rodrigues et al. 2005).

6.2 Mass Spectrometry

MS techniques have also been widely employed in several cell culture studies of brain energy metabolism and in metabolomics studies in general, due to its high sensitivity (e.g. (Yudkoff et al. 1987; Waagepetersen et al. 2001a; Olstad et al. 2007; Mishur and Rea 2011). MS identifies the isotopomer composition of a compound or sample based on the mass-to-charge (m/z) ratio of charged particles, which are generated by chemical fragmentation inside the spectrometer. In order to analyze ^{13}C or ^{15}N enrichment in amino and organic acids, samples need to be derivatized (Mawhinney et al. 1986).

Compared to ^{13}C NMR spectroscopy, MS techniques have a destructive character (the sample disintegrates during analysis), which confines its application to *in vitro* or *ex-vivo* studies. Moreover, it is less specific since the position of the label in the molecule cannot be disclosed, providing only the number of labelled atoms per molecule.

6.3 Metabolic modelling and metabolic flux estimations

Metabolic modelling of brain metabolism was first performed by van den Berg and Garfinkel more than 30 years ago, who developed multi-compartment models to elucidate apparent paradoxes of ^{14}C labelling studies using radioisotopes (van den Berg and Garfinkel 1971). More recently, advances in NMR spectroscopy combined with the use of MS and the use of ^{13}C labelled substrates allowed investigating brain metabolism based on isotopic labelling measurements and, consequently, estimating metabolic fluxes *in vitro* and *in vivo*.

6.3.1 *In vitro* and *ex-vivo* studies

In the early 90's, some authors reported the first estimations of metabolic ratios and fluxes in the brain using ^{13}C-labelled acetate and glucose (Cerdan et al. 1990; Brand et al. 1992; Lapidot and Gopher 1994). The approach used consisted in calculating isotopomer population ratios based on homonuclear ^{13}C-^{13}C spin-coupling patterns of glutamine, glutamate and GABA isotopomers detected by *ex-vivo* ^{13}C NMR spectroscopy at isotopic steady-state. In addition to demonstrating the existence of distinct metabolic compartments, these studies provided the first estimations of the relative fluxes through PDH and PC pathways in the brain. For instance, Lapidot and Gopher reported that PC accounted for 34% of glutamine synthesis and only 16% of glutamate and GABA synthesis in the rabbit brain (Lapidot and Gopher 1994).

The first metabolic modelling studies involving ^{13}C labelled substrates and NMR spectroscopy investigated the TCA cycle flux in perfused hearts or tissue extracts, based on glutamate fractional enrichment time-courses alone (Chance et al. 1983) or in

combination with isotopomer information (Malloy et al. 1987, 1988). In the latter study the flux through the anaplerotic pathway was also measured. Fluxes were estimated by fitting the experimental data (^{13}C enrichment in C2, C3 and C4 of glutamate under metabolic and isotopic steady-state) using an equation that described the different isotopomer contributions as a function of the parameters to be determined. The model developed by Malloy and colleagues considered only one metabolic compartment (the heart) and was tentatively applied to estimate fluxes in primary cultures of cerebellar astrocytes or neurons - homogeneous (one compartment) systems - by analyzing glutamate isotopomers in neurons and of glutamine in astrocytes (Martin et al. 1993). Their main results were: (i) PC flux appeared to account for 15% of glial TCA cycle, (ii) cerebellar neurons presented higher PPP activity compared to astrocytes, and (iii) used glucose as main energy source, whereas (iv) astrocytes metabolized a large amount of additional sources, as indicated by a significantly lower acetyl-CoA enrichment compared to that of lactate C3 (Martin et al. 1993). However, the original model (which assumed equal C2 and C3 enrichments) appeared to be unsuitable for analyzing the enrichment in different glutamine isotopomers after [1-^{13}C]glucose metabolism, due to PC activity. Thus, Merle et al performed some improvements (Merle et al. 1996b) and were able to additionally determine an oxaloacetate-malate backflow of 39 % in astrocytes and of 100 % in granule cells (Merle et al. 1996a). More recent developments of this model include isotopomer analysis of complex metabolic pathways including substrate oxidation, multiple pyruvate cycles and gluconeogenesis (Sherry et al. 2004).

6.3.2 *In vivo* ^{13}C metabolic modelling

In vivo metabolic models were first based in one compartment and estimated the cerebral TCA cycle flux and the glutamate-α-ketoglutarate exchange rate, Vx, based on the fitting of glutamate ^{13}C time-courses after [1-^{13}C]glucose infusion (Mason et al. 1992; Mason et al. 1995; Henry et al. 2002). Since most of the glutamate is located in neurons, these models mainly reflected the neuronal TCA cycle. The possibility of following also glutamine enrichment signals allowed the development of the two-compartment

(neurons and astrocytes) models to additionally estimate the glutamate-glutamine cycle flux (Sibson et al. 1998). Initially, these models did not include a full astrocytic compartment but they were soon expanded, enabling the separate estimation of neuronal and glial TCA cycle, pyruvate carboxylation and glutamate-glutamine cycle flux (e.g. Gruetter et al. 1998b; Shen et al. 1999; Gruetter et al. 2001). Figure 1.7 illustrates the structure of one- and two- compartment models.

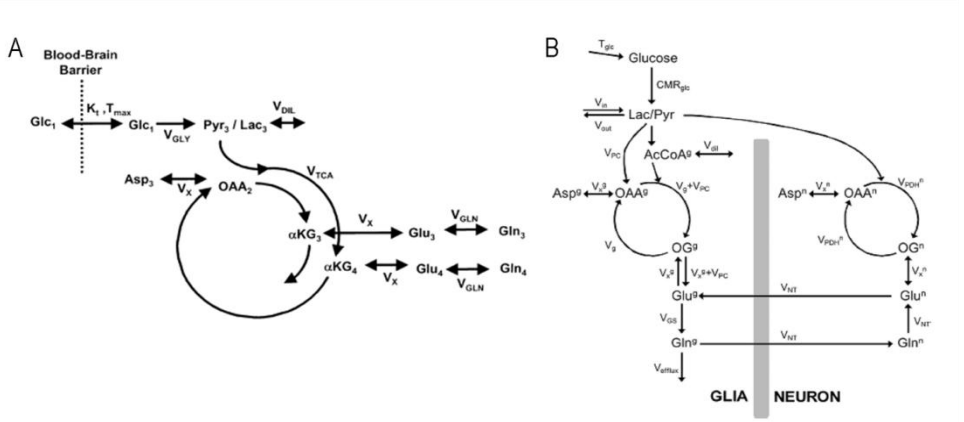

Figure 1.7 - A – One compartment model of brain metabolism describing the flow of ^{13}C label from [1-^{13}C]glucose into glutamate. Glc, glucose; Pyr, pyruvate; Lac, lactate; aKG, a-ketoglutarate; Glu, glutamate; Gln, glutamine; OAA, oxaloacetate; Asp, aspartate; V_{GLY} , rate of glycolysis; V_{DIL} , rate of exchange between labelled and unlabelled lactate; V_{TCA}, rate of TCA cycle; Vx, rate of exchange between a-ketoglutarate and glutamate; V_{GLN}, rate of exchange between glutamate and glutamine. Numbers in subscript indicate the position of the labelled carbons in each metabolite. Figure taken from Henry et al (2002) with permission from the publisher. ***B - Model of compartmentalized brain metabolism describing the flow of ^{13}C label from glucose into different metabolites of neurons and astrocytes.*** This two-compartment model includes glial (V_g) and neuronal (V^n_{PDH}) TCA cycle, glial anaplerosis (V_{PC}), apparent glutamatergic neurotransmission (i.e., glutamate–glutamine cycle; V_{NT}) and 2-oxoglutarate (OG)-glutamate (GLU) exchange in both compartments (V_X^g and V_X^n). The model additionally accounts for sources of label dilution in lactate (Lac), due to exchange with extra-cerebral lactate (V_{out}/V_{in}), and in the glial compartment at the level of acetyl-CoA (AcCoA) by glial specific substrates (V_{dil}) and due to efflux glutamine loss from the metabolic system (V_{efflux}). CMR_{glc}, cerebral metabolic rate of glucose; T_{glc}, glucose transport from blood. Figure taken from Duarte et al (2011) with permission from the authors, according to Frontiers Copyright statement.

Aiming at more accurate estimations, models were improved by including additional fluxes (e.g. V_{dil}, V_{ex} and V_{in}/V_{out}) to account for isotopic dilution in glutamine and lactate due to exchange with unlabelled metabolites in the blood (Oz et al. 2004; Shen et al. 2009). Even more complex models have been proposed (three-compartments -

astrocytes, glutamatergic and GABAergic neurons) to measure also the GABA-glutamine cycle (Patel et al. 2005). The major contributions and fluxes obtained in these studies are summarized in Table 1.2. Further details on the methodologies underlying *in vivo* metabolic modelling can be found in reviews by (Gruetter 2002; Mason and Rothman 2004; Henry et al. 2006; Shestov et al. 2007).

6.3.2.1 Modelling assumptions and related controversies

Flux estimations are inherently affected by assumptions made in the modelling. Of critical importance is the mitochondrial-cytosolic compartmentation of the metabolism of most amino acids and the need for their transport across the mitochondrial membrane. In the brain, the MAS is involved in the exchange between glutamate/α-ketoglutarate (Vx) and oxaloacetate/aspartate (see above). The magnitude of the Vx flux greatly influences TCA cycle flux estimations and has been under debate as it was first reported to be much higher than the TCA cycle rate (Mason et al. 1992; Mason et al. 1995), whereas other authors provided data suggesting that these fluxes were comparable (Gruetter et al. 2001; Henry et al. 2002). The main reasons for such discrepancies are related to the pool size of the metabolites, as it was observed that glutamate ^{13}C time-courses provide a more accurate estimation of PDH flux than those of aspartate (smaller pool size) (Gruetter 2002). Additional studies confirmed that the use of glutamate C4 time-courses alone is not sufficient for an accurate estimation of both V_{TCA} and Vx (Henry et al. 2002). Recently, Duarte et al (2011) reported ^{13}C enrichment time-courses of all aliphatic carbons of glutamate, glutamine and aspartate detected with high temporal resolution and sensitivity by *in vivo* ^{13}C NMR spectroscopy at 14.1T, after [1,6-^{13}C]glucose infusion in rats. These authors showed that Vx is similar to the TCA cycle flux, both in neurons and astrocytes, and that information from TCA cycle intermediates pools is not required for accurate flux estimation (Duarte et al. 2011), as previously suggested by mathematical simulations (Uffmann and Gruetter 2007).

Table 1.2 - Summary of the main cerebral metabolic fluxes (μmol $min^{-1}g^{-1}$) estimated using metabolic modelling of in vivo ^{13}C NMR data and key findings from these studies.

Flux	Rat Brain	Human Brain	Key findings/Conclusions
Total Cerebral TCA cycle flux	1.58[a] 0.46[c]; 0.53[d] 0.71[r] (α-chloralose) 0.16[d] (pentobarbital) 1.0 [d] (morphine)	0.8[e]; 0.6[f]; 0.84[i]; 0.73[b]	
Neuronal TCA cycle	1.6[a] 0.6[c]; 0.45[r] (α-chloralose) 1.16[n] (awake) 0.41[l]; 0.34[p] (pentobarbital) 0.80[o]; 1.22[p] (halothane)	0.8[e]; 0.6[f]; 0.83[g]; 0.60[h]; 0.70[i]; 0.72[q]	Neuronal TCA cycle rate increases with neuronal activity[g,h]
Glial TCA cycle	0.32[l] (pentobarbital) 0.48[n] (awake) 0.28[r] (α-chloralose)	0.10[e]; 0.15[f]; 0.14[i,j]	Glial TCA cycle is significant in the human brain[f] and accounts for 14% (human) to 38% (rat) of total oxidative metabolism[j,r]
Anaplerosis (V_{PC})	0.04[l] (pentobarbital) 0.18[n] (awake)	0.04[e,i]; 0.09[f]; 0.02[q]	- Anaplerosis via PC is significant and increases with neuronal activity[m,p] - PC contributes to 20% of the total turnover in the human TCA cycle[f] and for 6% of the glutamine synthesis in the human brain[q] and the majority of this flux is used for replacing glutamate lost due to glial oxidation[q]. - V_{PC} is 25% of glial TCA cycle rate
Glutamate-Glutamine cycle/ Glutamatergic Neurotransmission (V_{NT} or V_{cyc})	0.21[c]; 0.13[d]; 0.11[q] (α-chloralose) 0.4[d] (morphine) 0.51[n] (awake) 0[d]; 0.04[l]; 0.02[p] (pentobarbital) 0.31[o]; 0.58[p] (halothane)	0.32[e]; 0.17[f]; 0.25[h]; 0.32[i]; 0.34[q]	- The glutamate-glutamine cycle is a major metabolic pathway in the brain[c] - 30% of the glutamine transferred to the neurons may be derived from astrocytic anaplerosis[i,j]
Glutamate/α-ketoglutarate exchange (V_x)	199[a]; 0.88[q] 0.16 (glia) and 0.91 (neurons)[h]	57[b]; 0.57[f]	$V_x >> V_{TCA}$ [a,b] $V_x \approx V_{TCA}$ [f,m]
Glutamine Synthesis	0.21[c]; 0.17[d]; 0.18[q] (α-chloralose) 0.44 [d] (morphine) 0.04 (pentobarbital)[d]	0.47[b]; 0.26[f]	
Lactate Dilution	0.42 (V_{in}), 0.28 (V_{out})[r] (α-chloralose)	0.05[e]; 0.41[f]	$V_{out}>V_{in}$ - not all glucose consumed follows complete oxidation (only 78% of glucose was oxidized in the rat brain)[s]
Glutamine Efflux/Dilution		0.14[e]	This flux needs to be taken into account for a precise and accurate estimation of the glutamate-glutamine cycle flux[e,r,s]
Glial acetyl-CoA dilution	0.66[q] (α-chloralose)		This flux accounts for glial specific substrates or pathways fueling the TCA cycle (fatty acids, acetate, ketone bodies, pyruvate recycling)[s]

References: [a](Mason et al. 1992); [b](Mason et al. 1995), [c](Sibson et al. 1997); [d] (Sibson et al. 1998); [e] (Shen et al. 1999), [f] (Gruetter et al. 2001); [g] (Chen et al. 2001); [h] (Chhina et al. 2001); [i] (Bluml et al. 2002); [j] (Lebon et al. 2002); [l] (Choi et al. 2002); [m] (Henry et al. 2002); [n] (Oz et al. 2004); [o] (de Graaf et al. 2004); [p] (Patel et al. 2005); [q] (Mason et al. 2007); [r] (Shen et al. 2009); [s] (Duarte et al. 2011).

Nevertheless, strong debate still exists concerning the reliability of flux estimations using ^{13}C-labelled glucose and two-compartment models, in addition to the need for improved methods to evaluate their robustness (Shestov et al. 2007). It has been suggested that information from isotopomer analysis and the use of ^{13}C-labelled acetate should be used to complement glutamate and glutamine enrichment time-courses obtained after ^{13}C-glucose metabolism (Shestov et al. 2007; Boumezbeur et al. 2010). Moreover, isotopic dilution in glutamine due to exchange with blood or resulting from other metabolic pathways (Broer et al. 2007; Dusick et al. 2007; Boumezbeur et al. 2010) was also shown to greatly influence flux estimations and therefore should be taken into account (Shen et al. 2009; Duarte et al. 2011). Duarte et al (2011) further included a glial dilution factor at the level of acetyl-CoA, accounting for additional pathways such as pyruvate recycling.

6.3.3 Metabolic Flux Analysis

Metabolic flux analysis (MFA) is a well established technique to estimate intracellular fluxes and to determine factors influencing its distribution in biochemical networks (Varma and Palsson 1994; Lee et al. 1999). It has been widely applied in the biotechnology and metabolic engineering fields to a number of biological systems such as bacteria, yeast, mammalian cell cultures and, more recently, insect cells (Vallino and Stephanopoulos 1993; Nielsen 1998; Bernal et al. 2009; Quek et al. 2010). In this context, MFA represents a powerful tool allowing for a better understanding of cellular physiology and to consequently define strategies to improve bioprocess yields. Advances introduced by MFA include the identification and manipulation of nutrient limitations, the toxic accumulation of metabolic products, the fluxes particularly influencing cell or viral productivities, or even to characterize responses of cancer cells to a given treatment (Bonarius et al. 1996; Nadeau et al. 2000; Forbes et al. 2006; Carinhas et al. 2010). MFA has also been recently employed to estimate metabolic fluxes of cultured astrocytes (Teixeira et al. 2008) and, consequently, constitutes a promising tool in the field of

neurosciences. Recent reviews on the application of MFA to investigate eukaryotic cell metabolism can be found in Niklas et al. (2010) and Quek et al. (2010).

6.3.3.1 Classical or stoichiometric MFA

Stoichiometric MFA is the original and simpler version of this methodology that was first applied in the early 1990's (Varma and Palsson 1994). MFA estimates unknown intracellular fluxes using a mathematical model constrained by the metabolic network's stoichiometry and biochemistry and the pseudo-steady-state hypothesis (Lee et al. 1999), using a minimum number of experimental data. The pseudo-steady-state hypothesis implies that the sum of the fluxes leading to the synthesis and consumption of each metabolite is equal to zero and, consequently, intracellular metabolite pools will be constant. It is also assumed that metabolic fluxes are constant in the time-interval considered, which is usually confirmed by observing the linearity of metabolite consumption/production curves determined experimentally. It is generally accepted that the pools of most metabolites have a very high turnover, especially those participating in central metabolism. Consequently, the concentrations of the different metabolite pools rapidly adjust to new levels even after large perturbations, which makes it suitable to apply MFA and the quasi-steady-state assumption to estimate metabolic fluxes under such conditions (Lee et al. 1999). The general steps required to estimate metabolic fluxes using MFA are described in Table 1.3 (see Quek et al. 2010 for details).

The stoichiometry and biochemistry of intermediary metabolism of most organisms is quite well characterized and therefore network design is a relatively simple task. The number of reactions is usually high but can be reduced by combining reactions in linear pathways or removing those considered negligible based on literature information decreasing the number of fluxes to be estimated (Lee et al. 1999; Quek et al. 2010). Still, the number of unknown fluxes is always higher than the number of metabolites, which means that some metabolic rates need to be experimentally determined so that the model is able to solve the system.

Table 1.3 - Steps involved in the implementation and execution of a classical MFA experiment

Step	Description
Metabolic Network Design (Stoichiometric Matrix)	The stoichiometric matrix (metabolites and biochemical pathways relevant for the cell population under study) is derived from biochemistry text books or genome scale models. Mass balance equations are defined for each metabolite, by considering all fluxes leading to its production or consumption.
Measurements	- Quantification of the exo-metabolome (extracellular metabolites). - Total amounts of metabolites of interest (glucose, lactate, amino acids and others) are quantified in cell supernatant samples collected at different time-points. - Quantification of the biomass amount and composition. - Total cell number and cell size/volume. - Cell constituents (total cell protein, DNA or RNA). - Metabolite consumption or production rates are determined. Specific rates are calculated considering the average protein amount or cell number during the experiment. - If cell growth occurred during the experiment (in the case of cell lines), cell growth rate also needs to be calculated.
Data and Model Consistency	The consistency of the measurements and of the model is tested using the so-called redundancy matrix. This matrix establishes a relationship between measured fluxes and balanced metabolites with the aim of proving that there are no gross errors in experimental values (no bias in measurements or use of relative errors close to the detection limits) and in the model itself (no substrates or products have been ignored).
Flux Analysis	Model inputs: Metabolite consumption/production rates Cell growth rate, if applicable. Constraints: Matrix stoichiometry; pseudo-steady-state hypothesis Model outputs: Unknown intracellular fluxes and their error-covariance matrix

The simplicity of stoichiometric MFA reduces its power to estimate fluxes in more complex networks, particularly those of mammalian cells that, even though they lack many amino acid biosynthetic pathways, possess different cycles and anaplerotic reactions. These increase the number of fluxes that cannot be determined based only on uptake and excretion rates. The main weaknesses of stoichiometric MFA are summarized in Table 1.4 (details in Bonarius et al. 1997; Wiechert 2001).

Table 1.4 - Drawbacks of Stoichiometric MFA

Cannot resolve fluxes through: - parallel pathways, i.e. pathways that have a common product or substrate; - cyclic pathways, that are not coupled to any measurable fluxes - bidirectional/reversible reactions
Requires balancing of energy metabolites such as ATP, NADH and NADPH, which is difficult to accomplish (their mass balances are normally closed by approximation or remain unclosed in stoichiometric MFA studies)

Based on these shortcomings, the simple experimental determination of transmembrane rates from cell supernatant data is not enough to solve all unknown fluxes in such complex and underdetermined systems. A good option is to use additional information provided by ^{13}C-labelled substrates and ^{13}C isotopomer data to distinguish fluxes through parallel pathways that contribute differently to label distribution. This has been performed to estimate fluxes through PC and PDH or glycolysis and PPP in cultured astrocytes (Amaral et al. 2010). Furthermore, by including data from ^{13}C time-courses into the model, a higher specificity and sensitivity in flux estimations can be obtained. Of particular interest to this work is the isotopic transient ^{13}C MFA methodology, which is described in the next section.

6.3.3.2 Isotopic transient ^{13}C MFA

Isotopic transient or instationary ^{13}C MFA is a recent tool employed to estimate intracellular fluxes in short-time carbon-labelling experiments (Noh and Wiechert 2006). It is derived from stationary ^{13}C MFA which has been widely applied to the characterization of microbial cell cultures, and overcomes its main disadvantage: the extensive culture time required for isotopic equilibrium to be attained in intracellular metabolites [detailed information in Wiechert 2001; Zamboni et al. 2009). As in stoichiometric MFA, metabolic steady-state is also assumed but the isotopic transient state (i.e., the time period during which the ^{13}C label is being distributed by the different metabolite isotopomers until isotopic steady state is reached) in intracellular metabolites is considered. In this case, mass isotopomers are analyzed at different time points, normally using sensitive MS techniques, to follow the label incorporation immediately after incubating cells with a labelled substrate (Hofmann et al. 2008). Subsequently, ^{13}C isotopomer time-courses obtained experimentally are translated into metabolic fluxes using a mathematical model (Noh et al. 2007). Since ^{13}C isotopic transient MFA estimates metabolic fluxes based on ^{13}C-time-courses, it additionally needs to take into account metabolite pool sizes since they determine the rate at which a metabolite becomes labelled. Thus, at least some metabolite pool sizes must be measured so that the

model can correctly describe the observed ^{13}C time-courses. This approach does not allow lumping reactions in linear pathways when their metabolic intermediates have different pool sizes, which consequently increases the number of linear equations that constitute the model. Isotopic transient ^{13}C MFA models thus combine balances of the total metabolite pools and of individual isotopomers, containing full information about the transition of the labelled carbons within metabolites (Wiechert and Noh 2005; Noh et al. 2007). When comparing to the classical MFA, this new methodology overcomes its major disadvantages (Table 1.5; further details in Wiechert and Noh 2005; Noh et al. 2006).

Table 1.5 - Advantages and Disadvantages of ^{13}C Isotopic Transient MFA compared to Stoichiometric MFA

Advantages	Disadvantages
- Doesn't rely on uncertain cofactor balances - The use of the transient phase of label distribution allows to perform short-time experiments and to reduce the amount of labelled substrates needed - The measurable information increases, enabling the quantification of parallel fluxes - A high definition of the intracellular fluxes can be obtained - Can be used to estimate intracellular metabolite concentrations that are not possible to measure, although in a limited number	- Experimentally very demanding - requires a large number of measurements and sensitive and specific methods to quantify a large number of intracellular metabolites - Requires extensive computational work to solve a large number of differential equations

Even so, the existence of metabolic compartments in eukaryotic cells, which likely yield compartment-specific ^{13}C signatures, make it difficult to accurately estimate fluxes with good confidence without additional assumptions (Zamboni 2011). For example, some reactions can be removed from the model based on negligible activity or unique metabolite pools can be assumed based on hypothetical rapid equilibrium catalyzed by the continued action of transporters (Quek et al. 2010; Zamboni 2011). Despite the extensive experimental and computational work required, a few groups have already successfully used transient ^{13}C MFA both to investigate bacterial (Schaub et al. 2008; Noack et al. 2010) and mammalian cell metabolism (Maier et al. 2008; Lemons et al. 2010). Importantly, Maier et al have recently shown the power of this methodology to investigate drug action in metabolic fluxes and metabolite levels of primary hepatocytes

(Maier et al. 2009), opening the way for its application in drug screening and testing. Thus, isotopic transient ^{13}C MFA is a valuable tool to investigate the complexity of ^{13}C labelling time-courses derived from brain cell metabolism.

7 Aims and scope of the thesis

The main goal of this thesis was to investigate and characterize metabolic alterations typical of brain pathologies in cell culture models. Metabolic modelling approaches were employed to identify changes in metabolic fluxes of the main metabolic pathways of cerebral metabolism. Ischemia and hypoglycaemia were the pathological conditions chosen due to their huge impact on human health and the prevailing absence of effective therapies, particularly for ischemic stroke. In this context, as first aim of this thesis, it was implemented and characterized a novel *in vitro* model of ischemia using brain cells cultured in small scale bioreactors, allowing for a rigorous control of culture conditions. This provided a robust model to investigate metabolic responses of brain cells to ischemia *in vitro*. In addition, this thesis aimed at developing different metabolic modelling approaches, in combination with ^{13}C labelling techniques, to comprehensively characterize cellular metabolism. These methodologies can be used to include a large number of pathways involved in brain energy metabolism and consequently increase the specificity of information obtained. Such studies were missing in the field of brain metabolism and will certainly contribute with ideas that will allow to better explore metabolic information obtained in *in vitro* studies.

In **Chapter 2**, stoichiometric MFA was combined with information from ^{13}C NMR spectroscopy data aiming to characterize astrocytic metabolic responses to oxygen and glucose deprivation. Then, in **Chapter 3**, MFA was used to elucidate the metabolic consequences of hypoglycaemia in cultured cerebellar neurons. ^{13}C time-courses obtained by mass spectrometry were used to complement and reinforce MFA estimations. Subsequently, as a further step in the application of MFA tools to the study of brain energy metabolism, we integrated ^{13}C time-courses measured by gas

chromatrography-mass spectrometry (GC-MS) in an MFA model (Isotopic Transient ^{13}C MFA) to increase the specificity and sensitivity of flux estimations in astrocytes (**Chapter 4**). This was the first time that a ^{13}C isotopic transient model was applied to investigate brain cell metabolism and provided important knowledge concerning the main metabolic fluxes of astrocytes. Finally, **Chapter 5** describes the work performed in a second project which aimed to investigate the role of GLAST and GLT-1 glial glutamate transporters in astrocytic metabolism, using MFA, after down-regulating each of the transporters in cultured astrocytes. In particular, the goal was to elucidate the effects of glutamate transport via GLAST or GLT-1 at the level of metabolic fluxes of astrocytes due to their importance in the concept of metabolic coupling. This has also important implications in a number of pathologies involving glutamate excitotoxicity, such as Huntington's Disease (HD), and therefore can contribute to the understanding of the underlying pathological mechanisms.

8 References

Abbott N. J., Ronnback L. and Hansson E. (2006) Astrocyte-endothelial interactions at the blood-brain barrier. *Nat Rev Neurosci* 7, 41-53.

Agulhon C., Petravicz J., McMullen A. B., Sweger E. J., Minton S. K., Taves S. R., Casper K. B., Fiacco T. A. and McCarthy K. D. (2008) What is the role of astrocyte calcium in neurophysiology? *Neuron* 59, 932-946.

Allaman I., Gavillet M., Belanger M., Laroche T., Viertl D., Lashuel H. A. and Magistretti P. J. (2010) Amyloid-beta aggregates cause alterations of astrocytic metabolic phenotype: impact on neuronal viability. *J Neurosci* 30, 3326-3338.

Allen N. J. and Barres B. A. (2009) Neuroscience: Glia - more than just brain glue. *Nature* 457, 675-677.

Almeida A., Delgado-Esteban M., Bolanos J. P. and Medina J. M. (2002) Oxygen and glucose deprivation induces mitochondrial dysfunction and oxidative stress in neurones but not in astrocytes in primary culture. *J Neurochem* 81, 207-217.

Alves P. M., McKenna M. C. and Sonnewald U. (1995) Lactate metabolism in mouse brain astrocytes studied by [13C]NMR spectroscopy. *Neuroreport* 6, 2201-2204.

Alves P. M., Moreira J. L., Rodrigues J. M., Aunins J. G. and Carrondo M. J. (1996a) Two-dimensional versus three-dimensional culture systems: Effects on growth and productivity of BHK cells. *Biotechnol Bioeng* 52, 429-432.

Alves P. M., Fonseca L. L., Peixoto C. C., Almeida A. C., Carrondo M. J. and Santos H. (2000a) NMR studies on energy metabolism of immobilized primary neurons and astrocytes during hypoxia, ischemia and hypoglycemia. *NMR Biomed* 13, 438-448.

Alves P. M., Flogel U., Brand A., Leibfritz D., Carrondo M. J., Santos H. and Sonnewald U. (1996b) Immobilization of primary astrocytes and neurons for online monitoring of biochemical processes by NMR. *Dev Neurosci* 18 478-483.

Alves P. M., Nunes R., Zhang C., Maycock C. D., Sonnewald U., Carrondo M. J. and Santos H. (2000b) Metabolism of 3-(13)C-malate in primary cultures of mouse astrocytes. *Dev Neurosci* 22, 456-462.

Amaral A. I., Teixeira A. P., Martens S., Bernal V., Sousa M. F. and Alves P. M. (2010) Metabolic alterations induced by ischemia in primary cultures of astrocytes: merging 13C NMR spectroscopy and metabolic flux analysis. *J Neurochem* 113, 735-748.

Andrews T. C. and Brooks D. J. (1998) Advances in the understanding of early Huntington's disease using the functional imaging techniques of PET and SPET. *Mol Med Today* 4, 532-539.

Armulik A., Genove G., Mae M., Nisancioglu M. H., Wallgard E., Niaudet C., He L., Norlin J., Lindblom P., Strittmatter K., Johansson B. R. and Betsholtz C. (2011) Pericytes regulate the blood-brain barrier. *Nature* 468, 557-561.

Atlante A., Gagliardi S., Marra E., Calissano P. and Passarella S. (1999) Glutamate neurotoxicity in rat cerebellar granule cells involves cytochrome c release from mitochondria and mitochondrial shuttle impairment. *J Neurochem* 73, 237-246.

Attwell D. and Laughlin S. B. (2001) An energy budget for signaling in the grey matter of the brain. *J Cereb Blood Flow Metab* 21, 1133-1145.

Bachelard H. (1998) Landmarks in the application of 13C-magnetic resonance spectroscopy to studies of neuronal/glial relationships. *Dev Neurosci* 20, 277-288.

Bachoo R. M., Kim R. S., Ligon K. L., Maher E. A., Brennan C., Billings N., Chan S., Li C., Rowitch D. H., Wong W. H. and DePinho R. A. (2004) Molecular diversity of astrocytes with implications for neurological disorders. *Proc Natl Acad Sci U S A* 101, 8384-8389.

Badar-Goffer R. S., Bachelard H. S. and Morris P. G. (1990) Cerebral metabolism of acetate and glucose studied by 13C-n.m.r. spectroscopy. A technique for investigating metabolic compartmentation in the brain. *Biochem J* 266, 133-139.

Bak L. K., Schousboe A. and Waagepetersen H. S. (2006a) The glutamate/GABA-glutamine cycle: aspects of transport, neurotransmitter homeostasis and ammonia transfer. *J Neurochem* 98, 641-653.

Bak L. K., Schousboe A., Sonnewald U. and Waagepetersen H. S. (2006b) Glucose is necessary to maintain neurotransmitter homeostasis during synaptic activity in cultured glutamatergic neurons. *J Cereb Blood Flow Metab*.

Bak L. K., Walls A. B., Schousboe A., Ring A., Sonnewald U. and Waagepetersen H. S. (2009) Neuronal glucose but not lactate utilization is positively correlated with NMDA-induced neurotransmission and fluctuations in cytosolic Ca2+ levels. *J Neurochem* 109 Suppl 1, 87-93.

Bakken I. J., White L. R., Aasly J., Unsgard G. and Sonnewald U. (1997) Lactate formation from [U-13C]aspartate in cultured astrocytes: compartmentation of pyruvate metabolism. *Neurosci Lett* 237, 117-120.

Bakken I. J., White L. R., Unsgard G., Aasly J. and Sonnewald U. (1998) [U-13C]glutamate metabolism in astrocytes during hypoglycemia and hypoxia. *J Neurosci Res* 51, 636-645.

Barros L. F. and Deitmer J. W. (2010) Glucose and lactate supply to the synapse. *Brain Res Rev* 63, 149-159.

Barros L. F., Bittner C. X., Loaiza A. and Porras O. H. (2007) A quantitative overview of glucose dynamics in the gliovascular unit. *Glia* 55, 1222-1237.

Beckmann N., Turkalj I., Seelig J. and Keller U. (1991) 13C NMR for the assessment of human brain glucose metabolism in vivo. *Biochemistry* 30, 6362-6366.

Ben-Yoseph O., Boxer P. A. and Ross B. D. (1996) Assessment of the role of the glutathione and pentose phosphate pathways in the protection of primary cerebrocortical cultures from oxidative stress. *J Neurochem* 66, 2329-2337.

Berkich D. A., Xu Y., LaNoue K. F., Gruetter R. and Hutson S. M. (2005) Evaluation of brain mitochondrial glutamate and alpha-ketoglutarate transport under physiologic conditions. *J Neurosci Res* 79, 106-113.

Berkich D. A., Ola M. S., Cole J., Sweatt A. J., Hutson S. M. and LaNoue K. F. (2007) Mitochondrial transport proteins of the brain. *J Neurosci Res* 85, 3367-3377.

Berl S., Nicklas W. J. and Clarke D. D. (1968) Compartmentation of glutamic acid metabolism in brain slices. *J Neurochem* 15, 131-140.

Bernal V., Carinhas N., Yokomizo A. Y., Carrondo M. J. and Alves P. M. (2009) Cell density effect in the baculovirus-insect cells system: a quantitative analysis of energetic metabolism. *Biotechnol Bioeng* 104, 162-180.

Bernard-Helary K., Ardourel M., Magistretti P., Hevor T. and Cloix J. F. (2002) Stable transfection of cDNAs targeting specific steps of glycogen metabolism supports the existence of active gluconeogenesis in mouse cultured astrocytes. *Glia* 37, 379-382.

Berthet C., Lei H., Thevenet J., Gruetter R., Magistretti P. J. and Hirt L. (2009) Neuroprotective role of lactate after cerebral ischemia. *J Cereb Blood Flow Metab* 29, 1780-1789.

Bilger A. and Nehlig A. (1992) Quantitative histochemical changes in enzymes involved in energy metabolism in the rat brain during postnatal development. II. Glucose-6-phosphate dehydrogenase and beta-hydroxybutyrate dehydrogenase. *Int J Dev Neurosci* 10, 143-152.

Bixel M. G., Engelmann J., Willker W., Hamprecht B. and Leibfritz D. (2004) Metabolism of [U-(13)C]leucine in cultured astroglial cells. *Neurochem Res* 29, 2057-2067.

Bluml S., Moreno-Torres A., Shic F., Nguy C. H. and Ross B. D. (2002) Tricarboxylic acid cycle of glia in the in vivo human brain. *NMR Biomed* 15, 1-5.

Bolanos J. P. and Almeida A. (2006) Modulation of astroglial energy metabolism by nitric oxide. *Antioxid Redox Signal* 8, 955-965.

Bolanos J. P. and Almeida A. (2010) The pentose-phosphate pathway in neuronal survival against nitrosative stress. *IUBMB Life* 62, 14-18.

Bonarius H. P., Hatzimanikatis V., Meesters K. P., de Gooijer C. D., Schmid G. and Tramper J. (1996) Metabolic flux analysis of hybridoma cells in different culture media using mass balances. *Biotechnol Bioeng* 50, 299-318.

Bonarius H. P. J., Schmid G. and Tramper J. (1997) Flux analysis of underdetermined metabolic networks: the quest for the missing constraints. *Trends in Biotechnology* 15, 308-314.

Bonvento G., Herard A. S. and Voutsinos-Porche B. (2005) The astrocyte–neuron lactate shuttle: a debated but still valuable hypothesis for brain imaging. *J Cereb Blood Flow Metab* 25, 1394-1399.

Boumezbeur F., Petersen K. F., Cline G. W., Mason G. F., Behar K. L., Shulman G. I. and Rothman D. L. (2010) The contribution of blood lactate to brain energy metabolism in humans measured by dynamic 13C nuclear magnetic resonance spectroscopy. *J Neurosci* 30, 13983-13991.

Bouzier-Sore A. K., Serres S., Canioni P. and Merle M. (2003) Lactate involvement in neuron-glia metabolic interaction: (13)C-NMR spectroscopy contribution. *Biochimie* 85, 841-848.

Bouzier A. K., Voisin P., Goodwin R., Canioni P. and Merle M. (1998) Glucose and lactate metabolism in C6 glioma cells: evidence for the preferential utilization of lactate for cell oxidative metabolism. *Dev Neurosci* 20, 331-338.

Brand A., Engelmann J. and Leibfritz D. (1992) A 13C NMR study on fluxes into the TCA cycle of neuronal and glial tumor cell lines and primary cells. *Biochimie* 74, 941-948.

Brennan A. M., Connor J. A. and Shuttleworth C. W. (2006) NAD(P)H fluorescence transients after synaptic activity in brain slices: predominant role of mitochondrial function. *J Cereb Blood Flow Metab* 26, 1389-1406.

Broer S., Broer A., Hansen J. T., Bubb W. A., Balcar V. J., Nasrallah F. A., Garner B. and Rae C. (2007) Alanine metabolism, transport, and cycling in the brain. *J Neurochem* 102, 1758-1770.

Brown A. M. and Ransom B. R. (2007) Astrocyte glycogen and brain energy metabolism. *Glia* 55, 1263-1271.

Brown A. M., Baltan Tekkok S. and Ransom B. R. (2004) Energy transfer from astrocytes to axons: the role of CNS glycogen. *Neurochem Int* 45, 529-536.

Bushong E. A., Martone M. E., Jones Y. Z. and Ellisman M. H. (2002) Protoplasmic astrocytes in CA1 stratum radiatum occupy separate anatomical domains. *J Neurosci* 22, 183-192.

Caesar K., Hashemi P., Douhou A., Bonvento G., Boutelle M. G., Walls A. B. and Lauritzen M. (2008) Glutamate receptor-dependent increments in lactate, glucose and oxygen metabolism evoked in rat cerebellum in vivo. *J Physiol* 586, 1337-1349.

Camacho A. and Massieu L. (2006) Role of glutamate transporters in the clearance and release of glutamate during ischemia and its relation to neuronal death. *Arch Med Res* 37, 11-18.

Cammer W., Snyder D. S., Zimmerman T. R., Jr., Farooq M. and Norton W. T. (1982) Glycerol phosphate dehydrogenase, glucose-6-phosphate dehydrogenase, and lactate dehydrogenase: activities in oligodendrocytes, neurons, astrocytes, and myelin isolated from developing rat brains. *J Neurochem* 38, 360-367.

Carinhas N., Bernal V., Monteiro F., Carrondo M. J., Oliveira R. and Alves P. M. (2010) Improving baculovirus production at high cell density through manipulation of energy metabolism. *Metab Eng* 12, 39-52.

Cataldo A. and Broadwell R. (1986) Cytochemical identification of cerebral glycogen and glucose-6-phosphatase activity under normal and experimental conditions. I. Neurons and Glia. *J Elect Micro Tech* 3, 413-437.

Cerdan S., Kunnecke B. and Seelig J. (1990) Cerebral metabolism of [1,2-13C2]acetate as detected by in vivo and in vitro 13C NMR. *J Biol Chem* 265, 12916-12926.

Cerdan S., Rodrigues T. B., Sierra A., Benito M., Fonseca L. L., Fonseca C. P. and Garcia-Martin M. L. (2006) The redox switch/redox coupling hypothesis. *Neurochem Int* 48, 523-530.

Cesar M. and Hamprecht B. (1995) Immunocytochemical examination of neural rat and mouse primary cultures using monoclonal antibodies raised against pyruvate carboxylase. *J Neurochem* 64, 2312-2318.

Chance E. M., Seeholzer S. H., Kobayashi K. and Williamson J. R. (1983) Mathematical analysis of isotope labeling in the citric acid cycle with applications to 13C NMR studies in perfused rat hearts. *J Biol Chem* 258, 13785-13794.

Chapa F., Cruz F., Garcia-Martin M. L., Garcia-Espinosa M. A. and Cerdan S. (2000) Metabolism of (1-(13)C) glucose and (2-(13)C, 2-(2)H(3)) acetate in the neuronal and glial compartments of the adult rat brain as detected by [(13)C, (2)H] NMR spectroscopy. *Neurochem Int* 37, 217-228.

Cheeseman A. J. and Clark J. B. (1988) Influence of the malate-aspartate shuttle on oxidative metabolism in synaptosomes. *J Neurochem* 50, 1559-1565.

Chen W., Zhu X. H., Gruetter R., Seaquist E. R., Adriany G. and Ugurbil K. (2001) Study of tricarboxylic acid cycle flux changes in human visual cortex during hemifield visual stimulation using (1)H-[(13)C] MRS and fMRI. *Magn Reson Med* 45, 349-355.

Chhina N., Kuestermann E., Halliday J., Simpson L. J., Macdonald I. A., Bachelard H. S. and Morris P. G. (2001) Measurement of human tricarboxylic acid cycle rates during visual activation by (13)C magnetic resonance spectroscopy. *J Neurosci Res* 66, 737-746.

Chih C. P. and Roberts Jr E. L. (2003) Energy substrates for neurons during neural activity: a critical review of the astrocyte-neuron lactate shuttle hypothesis. *J Cereb Blood Flow Metab* 23, 1263-1281.

Chih C. P., Lipton P. and Roberts E. L., Jr. (2001) Do active cerebral neurons really use lactate rather than glucose? *Trends Neurosci* 24, 573-578.

Choi I. Y., Lei H. and Gruetter R. (2002) Effect of deep pentobarbital anesthesia on neurotransmitter metabolism in vivo: on the correlation of total glucose consumption with glutamatergic action. *J Cereb Blood Flow Metab* 22, 1343-1351.

Choi I. Y., Seaquist E. R. and Gruetter R. (2003) Effect of hypoglycemia on brain glycogen metabolism in vivo. *J Neurosci Res* 72, 25-32.

Choi I. Y., Lee S. P., Kim S. G. and Gruetter R. (2001) In vivo measurements of brain glucose transport using the reversible Michaelis-Menten model and simultaneous measurements of cerebral blood flow changes during hypoglycemia. *J Cereb Blood Flow Metab* 21, 653-663.

Clarke D. D. and Sokoloff L. (1999) Circulation and Energy Metabolism, in *Basic Neurochemistry: Molecular, Cellular and Medical Aspects,* 6th Edition Edition (Siegel G. J., Agranoff B. W., Albers R. W., Fisher S. K. and Uhler M. D., eds), pp 638-669. Lippincott Williams and Wilkins, Philadelphia.

Clarke D. D., Nicklas W. J. and Berl S. (1970) Tricarboxylic acid-cycle metabolism in brain. Effect of fluoroacetate and fluorocitrate on the labelling of glutamate, aspartate, glutamine and gamma-aminobutyrate. *Biochem J* 120, 345-351.

Coimbra A., Williams D. S. and Hostetler E. D. (2006) The role of MRI and PET/SPECT in Alzheimer's disease. *Curr Top Med Chem* 6, 629-647.

Contreras L. and Satrustegui J. (2009) Calcium signaling in brain mitochondria: interplay of malate aspartate NADH shuttle and calcium uniporter/mitochondrial dehydrogenase pathways. *J Biol Chem* 284, 7091-7099.

Criego A. B., Tkac I., Kumar A., Thomas W., Gruetter R. and Seaquist E. R. (2005) Brain glucose concentrations in patients with type 1 diabetes and hypoglycemia unawareness. *J Neurosci Res* 79, 42-47.

Cruz F. and Cerdan S. (1999) Quantitative 13C NMR studies of metabolic compartmentation in the adult mammalian brain. *NMR Biomed* 12, 451-462.

Cruz F., Scott S. R., Barroso I., Santisteban P. and Cerdan S. (1998) Ontogeny and cellular localization of the pyruvate recycling system in rat brain. *J Neurochem* 70, 2613-2619.

Cruz F., Villalba M., Garcia-Espinosa M. A., Ballesteros P., Bogonez E., Satrustegui J. and Cerdan S. (2001) Intracellular compartmentation of pyruvate in primary cultures of cortical neurons as detected by (13)C NMR spectroscopy with multiple (13)C labels. *J Neurosci Res* 66, 771-781.

Cruz N. F. and Dienel G. A. (2002) High glycogen levels in brains of rats with minimal environmental stimuli: implications for metabolic contributions of working astrocytes. *J Cereb Blood Flow Metab* 22, 1476-1489.

Cruz N. F., Ball K. K. and Dienel G. A. (2007) Functional imaging of focal brain activation in conscious rats: impact of [(14)C]glucose metabolite spreading and release. *J Neurosci Res* 85, 3254-3266.

Cruz N. F., Lasater A., Zielke H. R. and Dienel G. A. (2005) Activation of astrocytes in brain of conscious rats during acoustic stimulation: acetate utilization in working brain. *J Neurochem* 92, 934-947.

Danbolt N. C. (2001) Glutamate uptake. *Prog Neurobiol* 65, 1-105.

de Graaf R. A., Mason G. F., Patel A. B., Behar K. L. and Rothman D. L. (2003) In vivo 1H-[13C]-NMR spectroscopy of cerebral metabolism. *NMR Biomed* 16, 339-357.

de Graaf R. A., Mason G. F., Patel A. B., Rothman D. L. and Behar K. L. (2004) Regional glucose metabolism and glutamatergic neurotransmission in rat brain in vivo. *Proc Natl Acad Sci U S A* 101, 12700-12705.

Delgado-Esteban M., Almeida A. and Bolanos J. P. (2000) D-Glucose prevents glutathione oxidation and mitochondrial damage after glutamate receptor stimulation in rat cortical primary neurons. *J Neurochem* 75, 1618-1624.

Dienel G. A. and Hertz L. (2001) Glucose and lactate metabolism during brain activation. *J Neurosci Res* 66, 824-838.

Dienel G. A. and Cruz N. F. (2003) Neighborly interactions of metabolically-activated astrocytes in vivo. *Neurochem Int* 43, 339-354.

Dienel G. A. and Cruz N. F. (2004) Nutrition during brain activation: does cell-to-cell lactate shuttling contribute significantly to sweet and sour food for thought? *Neurochem Int* 45, 321-351.

Dienel G. A. and Hertz L. (2005) Astrocytic contributions to bioenergetics of cerebral ischemia. *Glia* 50, 362-388.

Dienel G. A. and Cruz N. F. (2008) Imaging brain activation: simple pictures of complex biology. *Ann N Y Acad Sci* 1147, 139-170.

Dienel G. A., Ball K. K. and Cruz N. F. (2007) A glycogen phosphorylase inhibitor selectively enhances local rates of glucose utilization in brain during sensory stimulation of conscious rats: implications for glycogen turnover. *J Neurochem* 102, 466-478.

DiNuzzo M., Mangia S., Maraviglia B. and Giove F. (2010) Changes in glucose uptake rather than lactate shuttle take center stage in subserving neuroenergetics: evidence from mathematical modeling. *J Cereb Blood Flow Metab* 30, 586-602.

Dirnagl U., Iadecola C. and Moskowitz M. A. (1999) Pathobiology of ischaemic stroke: an integrated view. *Trends Neurosci* 22, 391-397.

Dringen R. (2000) Metabolism and functions of glutathione in brain. *Prog Neurobiol* 62, 649-671.

Dringen R. and Hirrlinger J. (2003) Glutathione pathways in the brain. *Biol Chem* 384, 505-516.

Dringen R., Gebhardt R. and Hamprecht B. (1993a) Glycogen in astrocytes: possible function as lactate supply for neighboring cells. *Brain Res* 623, 208-214.

Dringen R., Schmoll D., Cesar M. and Hamprecht B. (1993b) Incorporation of radioactivity from [14C]lactate into the glycogen of cultured mouse astroglial cells. Evidence for gluconeogenesis in brain cells. *Biological chemistry Hoppe-Seyler* 374, 343-347.

Dringen R., Hoepken H. H., Minich T. and Ruedig C. (2007) Pentose Phospahte Pathway and NADPH Metabolism, in *Brain Energetics. Integration of Molecular and Cellular Processes,* 3rd edition Edition (Dienel G. and Gibson G., eds), pp 41-62. Springer, New York.

Duarte J. M. N., Lanz B. and Gruetter R. (2011) Compartmentalized cerebral metabolism of [1,6-13C]glucose determined by in vivo 13C NMR spectroscopy at 14.1 T. *Frontiers in Neuroenergetics* 3.

Dusick J. R., Glenn T. C., Lee W. N., Vespa P. M., Kelly D. F., Lee S. M., Hovda D. A. and Martin N. A. (2007) Increased pentose phosphate pathway flux after clinical traumatic brain injury: a [1,2-13C2]glucose labeling study in humans. *J Cereb Blood Flow Metab* 27, 1593-1602.

Faideau M., Kim J., Cormier K., Gilmore R., Welch M., Auregan G., Dufour N., Guillermier M., Brouillet E., Hantraye P., Deglon N., Ferrante R. J. and Bonvento G. (2010) In vivo expression of polyglutamine-expanded huntingtin by mouse striatal astrocytes impairs glutamate transport: a correlation with Huntington's disease subjects. *Hum Mol Genet* 19, 3053-3067.

Forbes N. S., Meadows A. L., Clark D. S. and Blanch H. W. (2006) Estradiol stimulates the biosynthetic pathways of breast cancer cells: detection by metabolic flux analysis. *Metab Eng* 8, 639-652.

Friedman B., Goodman E. H., Jr., Saunders H. L., Kostos V. and Weinhouse S. (1971) Estimation of pyruvate recycling during gluconeogenesis in perfused rat liver. *Metabolism* 20, 2-12.

Gahwiler B. H., Capogna M., Debanne D., McKinney R. A. and Thompson S. M. (1997) Organotypic slice cultures: a technique has come of age. *Trends Neurosci* 20, 471-477.

Gamberino W. C., Berkich D. A., Lynch C. J., Xu B. and LaNoue K. F. (1997) Role of pyruvate carboxylase in facilitation of synthesis of glutamate and glutamine in cultured astrocytes. *J Neurochem* 69, 2312-2325.

Gandhi G. K., Cruz N. F., Ball K. K. and Dienel G. A. (2009) Astrocytes are poised for lactate trafficking and release from activated brain and for supply of glucose to neurons. *J Neurochem* 111, 522-536.

Garcia-Nogales P., Almeida A. and Bolanos J. P. (2003) Peroxynitrite protects neurons against nitric oxide-mediated apoptosis. A key role for glucose-6-phosphate dehydrogenase activity in neuroprotection. *J Biol Chem* 278, 864-874.

Garcia-Nogales P., Almeida A., Fernandez E., Medina J. M. and Bolanos J. P. (1999) Induction of glucose-6-phosphate dehydrogenase by lipopolysaccharide contributes to preventing nitric oxide-mediated glutathione depletion in cultured rat astrocytes. *J Neurochem* 72, 1750-1758.

Gibbons H. M. and Dragunow M. (2010) Adult human brain cell culture for neuroscience research. *Int J Biochem Cell Biol* 42, 844-856.

Griffin J. L., Rae C., Dixon R. M., Radda G. K. and Matthews P. M. (1998) Excitatory amino acid synthesis in hypoxic brain slices: does alanine act as a substrate for glutamate production in hypoxia? *J Neurochem* 71, 2477-2486.

Griffin J. L., Keun H., Richter C., Moskau D., Rae C. and Nicholson J. K. (2003) Compartmentation of metabolism probed by [2-13C]alanine: improved 13C NMR sensitivity using a CryoProbe detects evidence of a glial metabolon. *Neurochem Int* 42, 93-99.

Gruetter R. (2002) In vivo 13C NMR studies of compartmentalized cerebral carbohydrate metabolism. *Neurochem Int* 41, 143-154.

Gruetter R. (2003) Glycogen: the forgotten cerebral energy store. *J Neurosci Res* 74, 179-183.

Gruetter R., Ugurbil K. and Seaquist E. R. (1998a) Steady-state cerebral glucose concentrations and transport in the human brain. *J Neurochem* 70, 397-408.

Gruetter R., Seaquist E. R. and Ugurbil K. (2001) A mathematical model of compartmentalized neurotransmitter metabolism in the human brain. *Am J Physiol Endocrinol Metab* 281, E100-112.

Gruetter R., Seaquist E. R., Kim S. and Ugurbil K. (1998b) Localized in vivo 13C-NMR of glutamate metabolism in the human brain: initial results at 4 tesla. *Dev Neurosci* 20, 380-388.

Gruetter R., Novotny E. J., Boulware S. D., Mason G. F., Rothman D. L., Shulman G. I., Prichard J. W. and Shulman R. G. (1994) Localized 13C NMR spectroscopy in the human brain of amino acid labeling from D-[1-13C]glucose. *J Neurochem* 63, 1377-1385.

Haberg A., Qu H. and Sonnewald U. (2006) Glutamate and GABA metabolism in transient and permanent middle cerebral artery occlusion in rat: Importance of astrocytes for neuronal survival. *Neurochem Int*.

Haberg A., Qu H., Saether O., Unsgard G., Haraldseth O. and Sonnewald U. (2001) Differences in neurotransmitter synthesis and intermediary metabolism between glutamatergic and GABAergic neurons during 4 hours of middle cerebral artery occlusion in the rat: the role of astrocytes in neuronal survival. *J Cereb Blood Flow Metab* 21, 1451-1463.

Haberg A., Qu H., Bakken I. J., Sande L. M., White L. R., Haraldseth O., Unsgard G., Aasly J. and Sonnewald U. (1998) In vitro and ex vivo 13C-NMR spectroscopy studies of pyruvate recycling in brain. *Dev Neurosci* 20, 389-398.

Halassa M. M., Florian C., Fellin T., Munoz J. R., Lee S. Y., Abel T., Haydon P. G. and Frank M. G. (2009) Astrocytic modulation of sleep homeostasis and cognitive consequences of sleep loss. *Neuron* 61, 213-219.

Hanisch U. K. and Kettenmann H. (2007) Microglia: active sensor and versatile effector cells in the normal and pathologic brain. *Nat Neurosci* 10, 1387-1394.

Hassel B. (2000) Carboxylation and anaplerosis in neurons and glia. *Mol Neurobiol* 22, 21-40.

Hassel B. and Sonnewald U. (1995) Glial formation of pyruvate and lactate from TCA cycle intermediates: implications for the inactivation of transmitter amino acids? *J Neurochem* 65, 2227-2234.

Hassel B., Sonnewald U., Unsgard G. and Fonnum F. (1994) NMR spectroscopy of cultured astrocytes: effects of glutamine and the gliotoxin fluorocitrate. *J Neurochem* 62, 2187-2194.

Hawkins B. T. and Davis T. P. (2005) The blood-brain barrier/neurovascular unit in health and disease. *Pharmacol Rev* 57, 173-185.

Haydon P. G. and Carmignoto G. (2006) Astrocyte control of synaptic transmission and neurovascular coupling. *Physiol Rev* 86, 1009-1031.

Henry P. G., Lebon V., Vaufrey F., Brouillet E., Hantraye P. and Bloch G. (2002) Decreased TCA cycle rate in the rat brain after acute 3-NP treatment measured by in vivo 1H-[13C] NMR spectroscopy. *J Neurochem* 82, 857-866.

Henry P. G., Adriany G., Deelchand D., Gruetter R., Marjanska M., Oz G., Seaquist E. R., Shestov A. and Ugurbil K. (2006) In vivo 13C NMR spectroscopy and metabolic modeling in the brain: a practical perspective. *Magn Reson Imaging* 24, 527-539.

Herrero-Mendez A., Almeida A., Fernandez E., Maestre C., Moncada S. and Bolanos J. P. (2009) The bioenergetic and antioxidant status of neurons is controlled by continuous degradation of a key glycolytic enzyme by APC/C-Cdh1. *Nat Cell Biol* 11, 747-752.

Hertz L. (2004) The astrocyte-neuron lactate shuttle: a challenge of a challenge. *J Cereb Blood Flow Metab* 24, 1241-1248.

Hertz L. (2008) Bioenergetics of cerebral ischemia: a cellular perspective. *Neuropharmacology* 55, 289-309.

Hertz L. and Zielke H. R. (2004) Astrocytic control of glutamatergic activity: astrocytes as stars of the show. *Trends Neurosci* 27, 735-743.

Hertz L., Peng L. and Dienel G. A. (2007) Energy metabolism in astrocytes: high rate of oxidative metabolism and spatiotemporal dependence on glycolysis/glycogenolysis. *J Cereb Blood Flow Metab* 27, 219-249.

Hertz L., Dringen R., Schousboe A. and Robinson S. R. (1999) Astrocytes: glutamate producers for neurons. *J Neurosci Res* 57, 417-428.

Hof P., Trapp B., de Vellis J., Claudio L. and Colman D. (2004) Cellular Components of Nervous Tissue, in *From molecules to Networks. An Introduction to Cellular and Molecular Neuroscience.* (Byrne J. and Roberts J., eds), pp 1-22. Elsevier Academic Press, San Diego, CA, USA.

Hofmann U., Maier K., Niebel A., Vacun G., Reuss M. and Mauch K. (2008) Identification of metabolic fluxes in hepatic cells from transient 13C-labeling experiments: Part I. Experimental observations. *Biotechnol Bioeng* 100, 344-354.

Honegger P., Defaux A., Monnet-Tschudi F. and Zurich M. G. (2011) Preparation, Maintenance, and Use of Serum-Free Aggregating Brain Cell Cultures. *Methods in molecular biology (Clifton, N.J* 758, 81-97.

Iadecola C. and Nedergaard M. (2007) Glial regulation of the cerebral microvasculature. *Nat Neurosci* 10, 1369-1376.

Kanamatsu T. and Tsukada Y. (1999) Effects of ammonia on the anaplerotic pathway and amino acid metabolism in the brain: an ex vivo 13C NMR spectroscopic study of rats after administering [2-13C]] glucose with or without ammonium acetate. *Brain Res* 841, 11-19.

Kasischke K. A., Vishwasrao H. D., Fisher P. J., Zipfel W. R. and Webb W. W. (2004) Neural activity triggers neuronal oxidative metabolism followed by astrocytic glycolysis. *Science* 305, 99-103.

Katz J. and Rognstad R. (1967) The labeling of pentose phosphate from glucose-14C and estimation of the rates of transaldolase, transketolase, the contribution of the pentose cycle, and ribose phosphate synthesis. *Biochemistry* 6, 2227-2247.

Kaufman E. E. and Driscoll B. F. (1993) Evidence for cooperativity between neurons and astroglia in the regulation of CO2 fixation in vitro. *Dev Neurosci* 15, 299-305.

Kimelberg H. K. (2004) The problem of astrocyte identity. *Neurochem Int* 45, 191-202.

Kimmich G. A., Roussie J. A. and Randles J. (2002) Aspartate aminotransferase isotope exchange reactions: implications for glutamate/glutamine shuttle hypothesis. *Am J Physiol Cell Physiol* 282, C1404-1413.

Kletzien R. F., Harris P. K. and Foellmi L. A. (1994) Glucose-6-phosphate dehydrogenase: a "housekeeping" enzyme subject to tissue-specific regulation by hormones, nutrients, and oxidant stress. *Faseb J* 8, 174-181.

Kunnecke B., Cerdan S. and Seelig J. (1993) Cerebral metabolism of [1,2-13C2]glucose and [U-13C4]3-hydroxybutyrate in rat brain as detected by 13C NMR spectroscopy. *NMR Biomed* 6, 264-277.

Kurz G. M., Wiesinger H. and Hamprecht B. (1993) Purification of cytosolic malic enzyme from bovine brain, generation of monoclonal antibodies, and immunocytochemical localization of the enzyme in glial cells of neural primary cultures. *J Neurochem* 60, 1467-1474.

Kvamme E., Torgner I. A. and Roberg B. (2001) Kinetics and localization of brain phosphate activated glutaminase. *J Neurosci Res* 66, 951-958.

Lapidot A. and Gopher A. (1994) Cerebral metabolic compartmentation. Estimation of glucose flux via pyruvate carboxylase/pyruvate dehydrogenase by 13C NMR isotopomer analysis of D-[U-13C]glucose metabolites. *J Biol Chem* 269, 27198-27208.

Lebon V., Petersen K. F., Cline G. W., Shen J., Mason G. F., Dufour S., Behar K. L., Shulman G. I. and Rothman D. L. (2002) Astroglial contribution to brain energy metabolism in humans revealed by 13C nuclear magnetic resonance spectroscopy: elucidation of the dominant pathway for neurotransmitter glutamate repletion and measurement of astrocytic oxidative metabolism. *J Neurosci* 22, 1523-1531.

Lee K., Berthiaume F., Stephanopoulos G. N. and Yarmush M. L. (1999) Metabolic flux analysis: a powerful tool for monitoring tissue function. *Tissue Eng* 5, 347-368.

Lemons J. M., Feng X. J., Bennett B. D., Legesse-Miller A., Johnson E. L., Raitman I., Pollina E. A., Rabitz H. A., Rabinowitz J. D. and Coller H. A. (2010) Quiescent fibroblasts exhibit high metabolic activity. *PLoS Biol* 8, e1000514.

Leveille P. J., McGinnis J. F., Maxwell D. S. and de Vellis J. (1980) Immunocytochemical localization of glycerol-3-phosphate dehydrogenase in rat oligodendrocytes. *Brain Res* 196, 287-305.

Lewandowski E. D., Yu X., LaNoue K. F., White L. T., Doumen C. and O'Donnell J. M. (1997) Altered metabolite exchange between subcellular compartments in intact postischemic rabbit hearts. *Circ Res* 81, 165-175.

Liepelt I., Reimold M., Maetzler W., Godau J., Reischl G., Gaenslen A., Herbst H. and Berg D. (2009) Cortical hypometabolism assessed by a metabolic ratio in Parkinson's disease primarily reflects cognitive deterioration-[18F]FDG-PET. *Mov Disord* 24, 1504-1511.

Lipton P. (1999) Ischemic cell death in brain neurons. *Physiol Rev* 79, 1431-1568.

Loaiza A., Porras O. H. and Barros L. F. (2003) Glutamate triggers rapid glucose transport stimulation in astrocytes as evidenced by real-time confocal microscopy. *J Neurosci* 23, 7337-7342.

Lovatt D., Sonnewald U., Waagepetersen H. S., Schousboe A., He W., Lin J. H., Han X., Takano T., Wang S., Sim F. J., Goldman S. A. and Nedergaard M. (2007) The transcriptome and metabolic gene signature of protoplasmic astrocytes in the adult murine cortex. *J Neurosci* 27, 12255-12266.

Lu M., Zhou L., Stanley W. C., Cabrera M. E., Saidel G. M. and Yu X. (2008) Role of the malate-aspartate shuttle on the metabolic response to myocardial ischemia. *J Theor Biol* 254, 466-475.

Magistretti P. (2004) Brain Energy Metabolism, in *From Molecules to Networks. An Introduction to Cellular and Molecular Neuroscience* (Byrne J. and Roberts J., eds), pp 67-90. Elsevier Academic Press, San Diego, CA, USA.

Magistretti P. J. (2009) Role of glutamate in neuron-glia metabolic coupling. *Am J Clin Nutr* 90, 875S-880S.

Magistretti P. J. and Pellerin L. (1999) Cellular mechanisms of brain energy metabolism and their relevance to functional brain imaging. *Philos Trans R Soc Lond B Biol Sci* 354, 1155-1163.

Magistretti P. J., Pellerin L., Rothman D. L. and Shulman R. G. (1999) Energy on demand. *Science* 283, 496-497.

Maier K., Hofmann U., Reuss M. and Mauch K. (2008) Identification of metabolic fluxes in hepatic cells from transient 13C-labeling experiments: Part II. Flux estimation. *Biotechnol Bioeng* 100, 355-370.

Maier K., Hofmann U., Bauer A., Niebel A., Vacun G., Reuss M. and Mauch K. (2009) Quantification of statin effects on hepatic cholesterol synthesis by transient (13)C-flux analysis. *Metab Eng* 11, 292-309.

Malloy C. R., Sherry A. D. and Jeffrey F. M. (1987) Carbon flux through citric acid cycle pathways in perfused heart by 13C NMR spectroscopy. *FEBS Lett* 212, 58-62.

Malloy C. R., Sherry A. D. and Jeffrey F. M. (1988) Evaluation of carbon flux and substrate selection through alternate pathways involving the citric acid cycle of the heart by 13C NMR spectroscopy. *J Biol Chem* 263, 6964-6971.

Mangia S., Simpson I. A., Vannucci S. J. and Carruthers A. (2009) The in vivo neuron-to-astrocyte lactate shuttle in human brain: evidence from modeling of measured lactate levels during visual stimulation. *J Neurochem* 109 Suppl 1, 55-62.

Maragakis N. J. and Rothstein J. D. (2004) Glutamate transporters: animal models to neurologic disease. *Neurobiol Dis* 15, 461-473.

Martin M., Portais J. C., Labouesse J., Canioni P. and Merle M. (1993) [1-13C]glucose metabolism in rat cerebellar granule cells and astrocytes in primary culture. Evaluation of flux parameters by 13C- and 1H-NMR spectroscopy. *Eur J Biochem* 217, 617-625.

Martin R. L., Lloyd H. G. and Cowan A. I. (1994) The early events of oxygen and glucose deprivation: setting the scene for neuronal death? *Trends Neurosci* 17, 251-257.

Martinez-Hernandez A., Bell K. P. and Norenberg M. D. (1977) Glutamine synthetase: glial localization in brain. *Science* 195, 1356-1358.

Mason G. F. and Rothman D. L. (2004) Basic principles of metabolic modeling of NMR (13)C isotopic turnover to determine rates of brain metabolism in vivo. *Metab Eng* 6, 75-84.

Mason G. F., Rothman D. L., Behar K. L. and Shulman R. G. (1992) NMR determination of the TCA cycle rate and alpha-ketoglutarate/glutamate exchange rate in rat brain. *J Cereb Blood Flow Metab* 12, 434-447.

Mason G. F., Petersen K. F., Lebon V., Rothman D. L. and Shulman G. I. (2006) Increased brain monocarboxylic acid transport and utilization in type 1 diabetes. *Diabetes* 55, 929-934.

Mason G. F., Petersen K. F., de Graaf R. A., Shulman G. I. and Rothman D. L. (2007) Measurements of the anaplerotic rate in the human cerebral cortex using 13C magnetic resonance spectroscopy and [1-13C] and [2-13C] glucose. *J Neurochem* 100, 73-86.

Mason G. F., Gruetter R., Rothman D. L., Behar K. L., Shulman R. G. and Novotny E. J. (1995) Simultaneous determination of the rates of the TCA cycle, glucose utilization, alpha-ketoglutarate/glutamate exchange, and glutamine synthesis in human brain by NMR. *J Cereb Blood Flow Metab* 15, 12-25.

Mawhinney T., Robinett R., Atalay A. and Madson M. (1986) Analysis of amino acids as their tert-butyldimethylsilyl derivatives by gas-liquid chromatography and mass spectrometry. *Journal of Chromatography*, 231-242.

McKenna M., Gruetter R., Sonnewald U., Waagepetersen H. and Schousboe A. (2006a) Energy Metabolism of the Brain, in *Basic Neurochemistry: Molecular, Cellular and Medical Aspects*, Seventh Edition (Bazan N., ed.), pp 531-557. Elsevier Academic Press, New York.

McKenna M. C. (2007) The glutamate-glutamine cycle is not stoichiometric: fates of glutamate in brain. *J Neurosci Res* 85, 3347-3358.

McKenna M. C., Stevenson J. H., Huang X. and Hopkins I. B. (2000a) Differential distribution of the enzymes glutamate dehydrogenase and aspartate aminotransferase in cortical synaptic mitochondria contributes to metabolic compartmentation in cortical synaptic terminals. *Neurochem Int* 37, 229-241.

McKenna M. C., Waagepetersen H. S., Schousboe A. and Sonnewald U. (2006b) Neuronal and astrocytic shuttle mechanisms for cytosolic-mitochondrial transfer of reducing equivalents: current evidence and pharmacological tools. *Biochem Pharmacol* 71, 399-407.

McKenna M. C., Tildon J. T., Stevenson J. H., Boatright R. and Huang S. (1993) Regulation of energy metabolism in synaptic terminals and cultured rat brain astrocytes: differences revealed using aminooxyacetate. *Dev Neurosci* 15, 320-329.

McKenna M. C., Stevenson J. H., Huang X., Tildon J. T., Zielke C. L. and Hopkins I. B. (2000b) Mitochondrial malic enzyme activity is much higher in mitochondria from cortical synaptic terminals compared with mitochondria from primary cultures of cortical neurons or cerebellar granule cells. *Neurochem Int* 36, 451-459.

Meloni B. P., Majda B. T. and Knuckey N. W. (2001) Establishment of neuronal in vitro models of ischemia in 96-well microtiter strip-plates that result in acute, progressive and delayed neuronal death. *Neuroscience* 108, 17-26.

Merle M., Martin M., Villegier A. and Canioni P. (1996a) Mathematical modelling of the citric acid cycle for the analysis of glutamine isotopomers from cerebellar astrocytes incubated with [1(-13)C]glucose. *Eur J Biochem* 239, 742-751.

Merle M., Martin M., Villegier A. and Canioni P. (1996b) [1-13C]glucose metabolism in brain cells: isotopomer analysis of glutamine from cerebellar astrocytes and glutamate from granule cells. *Dev Neurosci* 18, 460-468.

Mishur R. J. and Rea S. L. (2011) Applications of mass spectrometry to metabolomics and metabonomics: Detection of biomarkers of aging and of age-related diseases. *Mass Spectrom Rev*.

Morgenthaler F. D., van Heeswijk R. B., Xin L., Laus S., Frenkel H., Lei H. and Gruetter R. (2008) Non-invasive quantification of brain glycogen absolute concentration. *J Neurochem* 107, 1414-1423.

Mueller S. G., Schuff N. and Weiner M. W. (2006) Evaluation of treatment effects in Alzheimer's and other neurodegenerative diseases by MRI and MRS. *NMR Biomed* 19, 655-668.

Nadeau I., Sabatie J., Koehl M., Perrier M. and Kamen A. (2000) Human 293 cell metabolism in low glutamine-supplied culture: interpretation of metabolic changes through metabolic flux analysis. *Metab Eng* 2, 277-292.

Nave K. A. and Trapp B. D. (2008) Axon-glial signaling and the glial support of axon function. *Annu Rev Neurosci* 31, 535-561.

Nedergaard M. and Dirnagl U. (2005) Role of glial cells in cerebral ischemia. *Glia* 50, 281-286.

Nehlig A. (1997) Cerebral energy metabolism, glucose transport and blood flow: changes with maturation and adaptation to hypoglycaemia. *Diabetes Metab* 23, 18-29.

Nehlig A., Wittendorp-Rechenmann E. and Lam C. D. (2004) Selective uptake of [14C]2-deoxyglucose by neurons and astrocytes: high-resolution microautoradiographic imaging by cellular 14C-trajectography combined with immunohistochemistry. *J Cereb Blood Flow Metab* 24, 1004-1014.

Nguyen N. H., Brathe A. and Hassel B. (2003) Neuronal uptake and metabolism of glycerol and the neuronal expression of mitochondrial glycerol-3-phosphate dehydrogenase. *J Neurochem* 85, 831-842.

Nielsen J. (1998) Metabolic engineering: techniques for analysis of targets for genetic manipulations. *Biotechnol Bioeng* 58, 125-132.

Niklas J., Schneider K. and Heinzle E. (2010) Metabolic flux analysis in eukaryotes. *Curr Opin Biotechnol* 21, 63-69.

Noack S., Noh K., Moch M., Oldiges M. and Wiechert W. (2010) Stationary versus non-stationary (13)C-MFA: A comparison using a consistent dataset. *J Biotechnol*.

Noh K. and Wiechert W. (2006) Experimental design principles for isotopically instationary 13C labeling experiments. *Biotechnol Bioeng* 94, 234-251.

Noh K., Wahl A. and Wiechert W. (2006) Computational tools for isotopically instationary 13C labeling experiments under metabolic steady state conditions. *Metab Eng* 8, 554-577.

Noh K., Gronke K., Luo B., Takors R., Oldiges M. and Wiechert W. (2007) Metabolic flux analysis at ultra short time scale: isotopically non-stationary 13C labeling experiments. *J Biotechnol* 129, 249-267.

Okada Y. and Lipton P. (2007) Glucose, Oxidative Energy Metabolism, and Neural Function in Brain Slices—Glycolysis Plays a Key Role in Neural Activity, in *Brain Energetics. Integration of Molecular and Cellular Processes,* 3rd edition Edition (Dienel G. and Gibson G., eds), pp 17-39. Springer, New York.

Olstad E., Olsen G. M., Qu H. and Sonnewald U. (2007) Pyruvate recycling in cultured neurons from cerebellum. *J Neurosci Res*.

Oz G., Henry P. G., Seaquist E. R. and Gruetter R. (2003) Direct, noninvasive measurement of brain glycogen metabolism in humans. *Neurochem Int* 43, 323-329.

Oz G., Berkich D. A., Henry P. G., Xu Y., LaNoue K., Hutson S. M. and Gruetter R. (2004) Neuroglial metabolism in the awake rat brain: CO2 fixation increases with brain activity. *J Neurosci* 24, 11273-11279.

Oz G., Kumar A., Rao J. P., Kodl C. T., Chow L., Eberly L. E. and Seaquist E. R. (2009) Human brain glycogen metabolism during and after hypoglycemia. *Diabetes* 58, 1978-1985.

Oz G., Seaquist E. R., Kumar A., Criego A. B., Benedict L. E., Rao J. P., Henry P. G., Van De Moortele P. F. and Gruetter R. (2007) Human brain glycogen content and metabolism: implications on its role in brain energy metabolism. *Am J Physiol Endocrinol Metab* 292, E946-951.

Palmieri L., Pardo B., Lasorsa F. M., del Arco A., Kobayashi K., Iijima M., Runswick M. J., Walker J. E., Saheki T., Satrustegui J. and Palmieri F. (2001) Citrin and aralar1 are Ca(2+)-stimulated aspartate/glutamate transporters in mitochondria. *Embo J* 20, 5060-5069.

Pardo B., Rodrigues T. B., Contreras L., Garzon M., Llorente-Folch I., Kobayashi K., Saheki T., Cerdan S. and Satrustegui J. (2011) Brain glutamine synthesis requires neuronal-born aspartate as amino donor for glial glutamate formation. *J Cereb Blood Flow Metab* 31, 90-101.

Pascual J. M., Carceller F., Roda J. M. and Cerdan S. (1998) Glutamate, glutamine, and GABA as substrates for the neuronal and glial compartments after focal cerebral ischemia in rats. *Stroke* 29, 1048-1056; discussion 1056-1047.

Patel A. B., de Graaf R. A., Mason G. F., Rothman D. L., Shulman R. G. and Behar K. L. (2005) The contribution of GABA to glutamate/glutamine cycling and energy metabolism in the rat cortex in vivo. *Proc Natl Acad Sci U S A* 102, 5588-5593.

Patel A. B., de Graaf R. A., Mason G. F., Kanamatsu T., Rothman D. L., Shulman R. G. and Behar K. L. (2004) Glutamatergic neurotransmission and neuronal glucose oxidation are coupled during intense neuronal activation. *J Cereb Blood Flow Metab* 24, 972-985.

Patel M. S. (1974) The relative significance of CO2-fixing enzymes in the metabolism of rat brain. *J Neurochem* 22, 717-724.

Pellerin L. (2010) Food for thought: the importance of glucose and other energy substrates for sustaining brain function under varying levels of activity. *Diabetes Metab* 36 Suppl 3, S59-63.

Pellerin L. and Magistretti P. J. (1994) Glutamate uptake into astrocytes stimulates aerobic glycolysis: a mechanism coupling neuronal activity to glucose utilization. *Proc Natl Acad Sci U S A* 91, 10625-10629.

Pellerin L. and Magistretti P. J. (2003) Food for thought: challenging the dogmas. *J Cereb Blood Flow Metab* 23, 1282-1286.

Pellerin L., Bouzier-Sore A. K., Aubert A., Serres S., Merle M., Costalat R. and Magistretti P. J. (2007) Activity-dependent regulation of energy metabolism by astrocytes: an update. *Glia* 55, 1251-1262.

Pellerin L., Pellegri G., Bittar P. G., Charnay Y., Bouras C., Martin J. L., Stella N. and Magistretti P. J. (1998) Evidence supporting the existence of an activity-dependent astrocyte-neuron lactate shuttle. *Dev Neurosci* 20, 291-299.

Qu H., Eloqayli H., Unsgard G. and Sonnewald U. (2001) Glutamate decreases pyruvate carboxylase activity and spares glucose as energy substrate in cultured cerebellar astrocytes. *J Neurosci Res* 66, 1127-1132.

Quek L. E., Dietmair S., Kromer J. O. and Nielsen L. K. (2010) Metabolic flux analysis in mammalian cell culture. *Metab Eng* 12, 161-171.

Rae C., Hare N., Bubb W. A., McEwan S. R., Broer A., McQuillan J. A., Balcar V. J., Conigrave A. D. and Broer S. (2003) Inhibition of glutamine transport depletes glutamate and GABA neurotransmitter pools: further evidence for metabolic compartmentation. *J Neurochem* 85, 503-514.

Rafiki A., Boulland J. L., Halestrap A. P., Ottersen O. P. and Bergersen L. (2003) Highly differential expression of the monocarboxylate transporters MCT2 and MCT4 in the developing rat brain. *Neuroscience* 122, 677-688.

Raichle M. E. and Mintun M. A. (2006) Brain work and brain imaging. *Annu Rev Neurosci* 29, 449-476.

Ramos M., del Arco A., Pardo B., Martinez-Serrano A., Martinez-Morales J. R., Kobayashi K., Yasuda T., Bogonez E., Bovolenta P., Saheki T. and Satrustegui J. (2003) Developmental changes in the Ca2+-regulated mitochondrial aspartate-glutamate carrier aralar1 in brain and prominent expression in the spinal cord. *Brain Res Dev Brain Res* 143, 33-46.

Rao R., Ennis K., Long J. D., Ugurbil K., Gruetter R. and Tkac I. (2010) Neurochemical changes in the developing rat hippocampus during prolonged hypoglycemia. *J Neurochem* 114, 728-738.

Richards E. M., Fiskum G., Rosenthal R. E., Hopkins I. and McKenna M. C. (2007) Hyperoxic reperfusion after global ischemia decreases hippocampal energy metabolism. *Stroke* 38, 1578-1584.

Rodrigues T. B. and Cerdan S. (2005) A fast and sensitive 1H NMR method to measure the turnover of the H2 hydrogen of lactate. *Magn Reson Med* 54, 1014-1019.

Rodrigues T. B. and Cerdan S. (2007) The Cerebral Tricarboxylic Acid Cycles, in *Brain Energetics. Integration of Molecular and Cellular Processes,* 3rd edition Edition (Dienel G. and Gibson G., eds), pp 63-91. Springer, New York.

Rodrigues T. B., Fonseca C. P., Castro M. M., Cerdan S. and Geraldes C. F. (2009) 13C NMR tracers in neurochemistry: implications for molecular imaging. *Q J Nucl Med Mol Imaging* 53, 631-645.

Rodrigues T. B., Gray H. L., Benito M., Garrido S., Sierra A., Geraldes C. F., Ballesteros P. and Cerdan S. (2005) Futile cycling of lactate through the plasma membrane of C6 glioma cells as detected by (13C, 2H) NMR. *J Neurosci Res* 79, 119-127.

Rossi D. J., Brady J. D. and Mohr C. (2007) Astrocyte metabolism and signaling during brain ischemia. *Nat Neurosci* 10, 1377-1386.

Rothman D. L., Sibson N. R., Hyder F., Shen J., Behar K. L. and Shulman R. G. (1999) In vivo nuclear magnetic resonance spectroscopy studies of the relationship between the glutamate-glutamine neurotransmitter cycle and functional neuroenergetics. *Philos Trans R Soc Lond B Biol Sci* 354, 1165-1177.

Sa Santos S., Sonnewald U., Carrondo M. J. and Alves P. M. (2011) The role of glia in neuronal recovery following anoxia: In vitro evidence of neuronal adaptation. *Neurochem Int* 58, 665-675.

Sa Santos S., Fonseca L. L., Monteiro M. A., Carrondo M. J. and Alves P. M. (2005) Culturing primary brain astrocytes under a fully controlled environment in a novel bioreactor. *J Neurosci Res* 79, 26-32.

Santos S. S., Leite S. B., Sonnewald U., Carrondo M. J. and Alves P. M. (2007) Stirred vessel cultures of rat brain cells aggregates: characterization of major metabolic pathways and cell population dynamics. *J Neurosci Res* 85, 3386-3397.

Schaub J., Mauch K. and Reuss M. (2008) Metabolic flux analysis in Escherichia coli by integrating isotopic dynamic and isotopic stationary 13C labeling data. *Biotechnol Bioeng* 99, 1170-1185.

Schmoll D., Fuhrmann E., Gebhardt R. and Hamprecht B. (1995) Significant amounts of glycogen are synthesized from 3-carbon compounds in astroglial primary cultures from mice with participation of the mitochondrial phosphoenolpyruvate carboxykinase isoenzyme. *Eur J Biochem* 227, 308-315.

Schousboe A., Sonnewald U. and Waagepetersen H. S. (2003) Differential roles of alanine in GABAergic and glutamatergic neurons. *Neurochem Int* 43, 311-315.

Schousboe A., Sarup A., Bak L. K., Waagepetersen H. S. and Larsson O. M. (2004) Role of astrocytic transport processes in glutamatergic and GABAergic neurotransmission. *Neurochem Int* 45, 521-527.

Schousboe A., Westergaard N., Waagepetersen H. S., Larsson O. M., Bakken I. J. and Sonnewald U. (1997) Trafficking between glia and neurons of TCA cycle intermediates and related metabolites. *Glia* 21, 99-105.

Schummers J., Yu H. and Sur M. (2008) Tuned responses of astrocytes and their influence on hemodynamic signals in the visual cortex. *Science* 320, 1638-1643.

Schurr A. (2002) Lactate, glucose and energy metabolism in the ischemic brain (Review). *Int J Mol Med* 10, 131-136.

Serra M., Brito C., Costa E. M., Sousa M. F. and Alves P. M. (2009) Integrating human stem cell expansion and neuronal differentiation in bioreactors. *BMC biotechnology* 9, 82.

Serres S., Bezancon E., Franconi J. M. and Merle M. (2004) Ex vivo analysis of lactate and glucose metabolism in the rat brain under different states of depressed activity. *J Biol Chem* 279, 47881-47889.

Shank R. P., Leo G. C. and Zielke H. R. (1993) Cerebral metabolic compartmentation as revealed by nuclear magnetic resonance analysis of D-[1-13C]glucose metabolism. *J Neurochem* 61, 315-323.

Shank R. P., Bennett G. S., Freytag S. O. and Campbell G. L. (1985) Pyruvate carboxylase: an astrocyte-specific enzyme implicated in the replenishment of amino acid neurotransmitter pools. *Brain Res* 329, 364-367.

Shen J., Rothman D. L., Behar K. L. and Xu S. (2009) Determination of the glutamate-glutamine cycling flux using two-compartment dynamic metabolic modeling is sensitive to astroglial dilution. *J Cereb Blood Flow Metab* 29, 108-118.

Shen J., Petersen K. F., Behar K. L., Brown P., Nixon T. W., Mason G. F., Petroff O. A., Shulman G. I., Shulman R. G. and Rothman D. L. (1999) Determination of the rate of the glutamate/glutamine cycle in the human brain by in vivo 13C NMR. *Proc Natl Acad Sci U S A* 96, 8235-8240.

Sherry A. D., Jeffrey F. M. and Malloy C. R. (2004) Analytical solutions for (13)C isotopomer analysis of complex metabolic conditions: substrate oxidation, multiple pyruvate cycles, and gluconeogenesis. *Metab Eng* 6, 12-24.

Shestov A. A., Valette J., Ugurbil K. and Henry P. G. (2007) On the reliability of (13)C metabolic modeling with two-compartment neuronal-glial models. *J Neurosci Res* 85, 3294-3303.

Shin J. Y., Fang Z. H., Yu Z. X., Wang C. E., Li S. H. and Li X. J. (2005) Expression of mutant huntingtin in glial cells contributes to neuronal excitotoxicity. *J Cell Biol* 171, 1001-1012.

Shulman R. G., Hyder F. and Rothman D. L. (2001) Cerebral energetics and the glycogen shunt: neurochemical basis of functional imaging. *Proc Natl Acad Sci U S A* 98, 6417-6422.

Sibson N. R., Dhankhar A., Mason G. F., Behar K. L., Rothman D. L. and Shulman R. G. (1997) In vivo 13C NMR measurements of cerebral glutamine synthesis as evidence for glutamate-glutamine cycling. *Proc Natl Acad Sci U S A* 94, 2699-2704.

Sibson N. R., Dhankhar A., Mason G. F., Rothman D. L., Behar K. L. and Shulman R. G. (1998) Stoichiometric coupling of brain glucose metabolism and glutamatergic neuronal activity. *Proc Natl Acad Sci U S A* 95, 316-321.

Sibson N. R., Mason G. F., Shen J., Cline G. W., Herskovits A. Z., Wall J. E., Behar K. L., Rothman D. L. and Shulman R. G. (2001) In vivo (13)C NMR measurement of neurotransmitter glutamate cycling, anaplerosis and TCA cycle flux in rat brain during. *J Neurochem* 76, 975-989.

Sickmann H. M., Schousboe A., Fosgerau K. and Waagepetersen H. S. (2005) Compartmentation of lactate originating from glycogen and glucose in cultured astrocytes. *Neurochem Res* 30, 1295-1304.

Simard M. and Nedergaard M. (2004) The neurobiology of glia in the context of water and ion homeostasis. *Neuroscience* 129, 877-896.

Simpson I. A., Carruthers A. and Vannucci S. J. (2007) Supply and demand in cerebral energy metabolism: the role of nutrient transporters. *J Cereb Blood Flow Metab* 27, 1766-1791.

Sonnewald U. and Kondziella D. (2003) Neuronal glial interaction in different neurological diseases studied by ex vivo 13C NMR spectroscopy. *NMR Biomed* 16, 424-429.

Sonnewald U. and Rae C. (2010) Pyruvate carboxylation in different model systems studied by (13)C MRS. *Neurochem Res* 35, 1916-1921.

Sonnewald U., Westergaard N., Schousboe A., Svendsen J. S., Unsgard G. and Petersen S. B. (1993a) Direct demonstration by [13C]NMR spectroscopy that glutamine from astrocytes is a precursor for GABA synthesis in neurons. *Neurochem Int* 22, 19-29.

Sonnewald U., Westergaard N., Hassel B., Muller T. B., Unsgard G., Fonnum F., Hertz L., Schousboe A. and Petersen S. B. (1993b) NMR spectroscopic studies of 13C acetate and 13C glucose metabolism in neocortical astrocytes: evidence for mitochondrial heterogeneity. *Dev Neurosci* 15, 351-358.

Spence A. M., Graham M. M., Muzi M., Freeman S. D., Link J. M., Grierson J. R., O'Sullivan F., Stein D., Abbott G. L. and Krohn K. A. (1997) Feasibility of imaging pentose cycle glucose metabolism in gliomas with PET: studies in rat brain tumor models. *J Nucl Med* 38, 617-624.

Suh S. W., Hamby A. M. and Swanson R. A. (2007a) Hypoglycemia, brain energetics, and hypoglycemic neuronal death. *Glia* 55, 1280-1286.

Suh S. W., Aoyama K., Matsumori Y., Liu J. and Swanson R. A. (2005) Pyruvate administered after severe hypoglycemia reduces neuronal death and cognitive impairment. *Diabetes* 54, 1452-1458.

Suh S. W., Bergher J. P., Anderson C. M., Treadway J. L., Fosgerau K. and Swanson R. A. (2007b) Astrocyte glycogen sustains neuronal activity during hypoglycemia:studies with the glycogen phosphorylase inhibitor CP-316,819. *J Pharmacol Exp Ther*.

Suzuki A., Stern Sarah A., Bozdagi O., Huntley George W., Walker Ruth H., Magistretti Pierre J. and Alberini Cristina M. (2011) Astrocyte-Neuron Lactate Transport Is Required for Long-Term Memory Formation. *Cell* 144, 810-823.

Swanson R. A., Morton M. M., Sagar S. M. and Sharp F. R. (1992) Sensory stimulation induces local cerebral glycogenolysis: demonstration by autoradiography. *Neuroscience* 51, 451-461.

Taylor A., McLean M., Morris P. and Bachelard H. (1996) Approaches to studies on neuronal/glial relationships by 13C-MRS analysis. *Dev Neurosci* 18, 434-442.

Teixeira A. P., Santos S. S., Carinhas N., Oliveira R. and Alves P. M. (2008) Combining metabolic flux analysis tools and 13C NMR to estimate intracellular fluxes of cultured astrocytes. *Neurochem Int* 52, 478-486.

Tekkok S. B., Brown A. M., Westenbroek R., Pellerin L. and Ransom B. R. (2005) Transfer of glycogen-derived lactate from astrocytes to axons via specific monocarboxylate transporters supports mouse optic nerve activity. *J Neurosci Res* 81, 644-652.

Thoren A. E., Helps S. C., Nilsson M. and Sims N. R. (2006) The metabolism of C-glucose by neurons and astrocytes in brain subregions following focal cerebral ischemia in rats. *J Neurochem* 97, 968-978.

Trendelenburg G. and Dirnagl U. (2005) Neuroprotective role of astrocytes in cerebral ischemia: focus on ischemic preconditioning. *Glia* 50, 307-320.

Uffmann K. and Gruetter R. (2007) Mathematical modeling of (13)C label incorporation of the TCA cycle: the concept of composite precursor function. *J Neurosci Res* 85, 3304-3317.

Vallino J. J. and Stephanopoulos G. (1993) Metabolic flux distributions in Corynebacterium glutamicum during growth and lysine overproduction. *Biotechnol Bioeng* 41, 633-646.

van den Berg C. J. and Garfinkel D. (1971) A stimulation study of brain compartments. Metabolism of glutamate and related substances in mouse brain. *Biochem J* 123, 211-218.

Vannucci S. J. and Simpson I. A. (2003) Developmental switch in brain nutrient transporter expression in the rat. *Am J Physiol Endocrinol Metab* 285, E1127-1134.

Varma A. and Palsson B. O. (1994) Stoichiometric flux balance models quantitatively predict growth and metabolic by-product secretion in wild-type Escherichia coli W3110. *Appl Environ Microbiol* 60, 3724-3731.

Vaughn A. E. and Deshmukh M. (2008) Glucose metabolism inhibits apoptosis in neurons and cancer cells by redox inactivation of cytochrome c. *Nat Cell Biol* 10, 1477-1483.

Vogel R., Jennemann G., Seitz J., Wiesinger H. and Hamprecht B. (1998) Mitochondrial malic enzyme: purification from bovine brain, generation of an antiserum, and immunocytochemical localization in neurons of rat brain. *J Neurochem* 71, 844-852.

Waagepetersen H. S., Sonnewald U., Larsson O. M. and Schousboe A. (2000) A possible role of alanine for ammonia transfer between astrocytes and glutamatergic neurons. *J Neurochem* 75, 471-479.

Waagepetersen H. S., Sonnewald U., Larsson O. M. and Schousboe A. (2001a) Multiple compartments with different metabolic characteristics are involved in biosynthesis of intracellular and released glutamine and citrate in astrocytes. *Glia* 35, 246-252.

Waagepetersen H. S., Qu H., Schousboe A. and Sonnewald U. (2001b) Elucidation of the quantitative significance of pyruvate carboxylation in cultured cerebellar neurons and astrocytes. *J Neurosci Res* 66, 763-770.

Waagepetersen H. S., Qu H., Hertz L., Sonnewald U. and Schousboe A. (2002) Demonstration of pyruvate recycling in primary cultures of neocortical astrocytes but not in neurons. *Neurochem Res* 27, 1431-1437.

Wallace J. C., Jitrapakdee S. and Chapman-Smith A. (1998) Pyruvate carboxylase. *Int J Biochem Cell Biol* 30, 1-5.

Wang D. D. and Bordey A. (2008) The astrocyte odyssey. *Prog Neurobiol* 86, 342-367.

Waniewski R. A. and Martin D. L. (1998) Preferential utilization of acetate by astrocytes is attributable to transport. *J Neurosci* 18, 5225-5233.

Wender R., Brown A. M., Fern R., Swanson R. A., Farrell K. and Ransom B. R. (2000) Astrocytic glycogen influences axon function and survival during glucose deprivation in central white matter. *J Neurosci* 20, 6804-6810.

Wiechert W. (2001) 13C metabolic flux analysis. *Metab Eng* 3, 195-206.

Wiechert W. and Noh K. (2005) From stationary to instationary metabolic flux analysis. *Adv Biochem Eng Biotechnol* 92, 145-172.

Williams L. R. and Leggett R. W. (1989) Reference values for resting blood flow to organs of man. *Clin Phys Physiol Meas* 10, 187-217.

Williams R. W. and Herrup K. (1988) The control of neuron number. *Annu Rev Neurosci* 11, 423-453.

Xu Y., Oz G., LaNoue K. F., Keiger C. J., Berkich D. A., Gruetter R. and Hutson S. H. (2004) Whole-brain glutamate metabolism evaluated by steady-state kinetics using a double-isotope procedure: effects of gabapentin. *J Neurochem* 90, 1104-1116.

Xu Y., Ola M. S., Berkich D. A., Gardner T. W., Barber A. J., Palmieri F., Hutson S. M. and LaNoue K. F. (2007) Energy sources for glutamate neurotransmission in the retina: absence of the aspartate/glutamate carrier produces reliance on glycolysis in glia. *J Neurochem* 101, 120-131.

Yu A. C., Drejer J., Hertz L. and Schousboe A. (1983) Pyruvate carboxylase activity in primary cultures of astrocytes and neurons. *J Neurochem* 41, 1484-1487.

Yudkoff M. (1997) Brain metabolism of branched-chain amino acids. *Glia* 21, 92-98.

Yudkoff M., Nissim I. and Pleasure D. (1987) [15N]aspartate metabolism in cultured astrocytes. Studies with gas chromatography-mass spectrometry. *Biochem J* 241, 193-201.

Yudkoff M., Daikhin Y., Lin Z. P., Nissim I., Stern J. and Pleasure D. (1994) Interrelationships of leucine and glutamate metabolism in cultured astrocytes. *J Neurochem* 62, 1192-1202.

Zamboni N. (2011) 13C metabolic flux analysis in complex systems. *Curr Opin Biotechnol* 22, 103-108.

Zamboni N., Fendt S. M., Ruhl M. and Sauer U. (2009) (13)C-based metabolic flux analysis. *Nat Protoc* 4, 878-892.

Zielke H. R., Zielke C. L. and Baab P. J. (2009) Direct measurement of oxidative metabolism in the living brain by microdialysis: a review. *J Neurochem* 109 Suppl 1, 24-29.

Zwingmann C. (2007) The anaplerotic flux and ammonia detoxification in hepatic encephalopathy. *Metab Brain Dis* 22, 235-249.

Zwingmann C. and Leibfritz D. (2003) Regulation of glial metabolism studied by 13C-NMR. *NMR Biomed* 16, 370-399.

Zwingmann C. and Leibfritz D. (2007) Glial-Neuronal Shuttle Systems, in *Brain Energetics. Integration of Molecular and Cellular Processes,* 3rd edition Edition (Dienel G. and Gibson G., eds), pp 197-238. Springer, New York.

Zwingmann C., Richter-Landsberg C. and Leibfritz D. (2001) 13C isotopomer analysis of glucose and alanine metabolism reveals cytosolic pyruvate compartmentation as part of energy metabolism in astrocytes. *Glia* 34, 200-212.

Zwingmann C., Richter-Landsberg C., Brand A. and Leibfritz D. (2000) NMR spectroscopic study on the metabolic fate of [3-(13)C]alanine in astrocytes, neurons, and cocultures: implications for glia-neuron interactions in neurotransmitter metabolism. *Glia* 32, 286-303.

Chapter 2

Metabolic Flux Analysis of Cultured Astrocytes: Effects of Ischemia

Adapted from:

Metabolic alterations induced by ischemia in primary cultures of astrocytes: merging ^{13}C NMR spectroscopy and metabolic flux analysis

Ana I Amaral, Ana P Teixeira, Sanja Martens, Vicente Bernal, Marcos FQ Sousa and Paula M Alves (2010) J Neurochem 113(3):735-48

Abstract

Disruption of brain energy metabolism is the hallmark of cerebral ischemia, a major cause of death worldwide. Astrocytes play a key role in the regulation of brain metabolism and their vulnerability to ischemia has been described. Aiming to quantify the effects of an ischemic insult in astrocytic metabolism, primary cultures of astrocytes were subjected to 5 hours of oxygen and glucose deprivation in a bioreactor. Flux distributions, before and after ischemia, were estimated by metabolic flux analysis using isotopic information and the consumption/secretion rates of relevant extracellular metabolites as constraints. During ischemia and early recovery, 30% of cell death was observed; several metabolic alterations were also identified reflecting a metabolic response by the surviving cells. In the early recovery (approx. 10 h), astrocytes up-regulated glucose utilization by 30% and increased the pentose phosphate pathway and TCA cycle fluxes by 3 and 2-fold, respectively. Additionally, a 2-5 fold enhancement in branched-chain amino acids catabolism suggested the importance of anaplerotic molecules to the fast recovery of the energetic state, which was corroborated by measured cellular ATP levels. Glycolytic metabolism was predominant in the late recovery. In summary, this work demonstrates that changes in fluxes of key metabolic pathways are implicated in the recovery from ischemia in astrocytes.

CONTENTS

1 Introduction

Brain ischemia is usually a consequence of blood flow reduction below a critical threshold due to the occlusion of a major brain artery (Dirnagl et al. 1999). It is among the leading causes of death and long-term disability in humans. However, despite the prevalence and severe consequences, no treatment is available and, currently, the best strategy to prevent severe consequences is the rapid restoration of blood supply (Rossi et al. 2007). Disruption of brain energy metabolism is the hallmark of this pathology due to the restricted delivery of oxygen and glucose, which slows or stops the synthesis of ATP required to maintain ionic gradients (Dirnagl et al. 1999). Ischemic brain deals with the fast decline in ATP supplies by increasing the rate of anaerobic glycolysis, leading to lactate accumulation, and consequently to acidosis, though the detrimental or beneficial effects of lactate are still under discussion (Schurr 2002; Dienel and Hertz 2005).

Astrocytes are the most abundant cell type in the brain and play a key role in the regulation of cerebral energy metabolism (Hertz et al. 2007; Pellerin et al. 2007). They account for at least 15% of total oxidative metabolism in the human brain (Bluml et al. 2002; Lebon et al. 2002). Even though some authors proposed that astrocytic oxidative metabolism is proportional to their relative volume in the brain (Hertz et al. 2007), a modelling study based on a large set of *in vivo* ^{13}C NMR spectroscopy flux measurements suggested that neurons are responsible for at least 88% of the total oxidative ATP production, though astrocytes take up more than half of the glucose from the capillaries (Hyder et al. 2006). These findings are supported by numerous *in vitro* and *in vivo* studies on cerebral metabolism, showing that several metabolites, such as lactate, glutamine, alanine, and TCA cycle intermediates, are transferred from astrocytes to neurons, serving both as neuronal energy substrates and as neurotransmitter precursors (Riera et al. 2008). However, strong debate still exists regarding the "astrocyte-neuron lactate shuttle" hypothesis (Pellerin and Magistretti 1994; Pellerin et al. 2007) as recent studies suggested that most of the lactate released during activation is of neuronal origin (Bak et al. 2009; Contreras and Satrustegui 2009) and modelling studies reported a preferential

uptake of glucose by neurons and lactate shuttling from neurons to astrocytes (Mangia et al. 2009). In view of all these findings, it is not surprising that astrocytes also play a significant role on the bioenergetics of cerebral ischemia and, on the other hand, suffer its consequences (Hertz 2008).

Different studies have reported effects of ischemia on astrocytic metabolic fluxes. A decrease in glucose oxidation was observed after focal cerebral ischemia in rats, in a time-dependent manner, together with increased oxidative metabolism of neuronal GABA and glutamate and increased glutamine transfer to neurons (Pascual et al. 1998). In addition, other *in vivo* studies suggested a better preservation of astrocytic energy metabolism (Thoren et al. 2005; Haberg et al. 2006), when comparing to neurons, through increased acetate oxidation and conservation of glutamine synthesis. These findings corroborate the crucial role of astrocytic glutamate uptake for limiting neuronal death caused by the excitotoxic effect of glutamate (Danbolt 2001) through its metabolism to glutamine. Although strong evidence is still lacking, astrocytes may provide neurons with antioxidant substrates, such as glutathione, and it has been suggested that the lactate released by astrocytes in elevated amounts during ischemia may also serve as a neuronal fuel during recovery (Schurr 2002; Dienel and Hertz 2005). Even so, it has been found that astrocytes frequently undergo a slow ischemia-induced cell death process, mainly as a consequence of the impairment of glycolysis but also due to disruption of ionic homeostasis leading to mitochondrial calcium overload and depolarization (Swanson et al. 1997; Hertz 2008). Thus, further studies contributing to clarify the influence of ischemia in astrocytic metabolism are certainly required.

The aim of the present study was to characterize, using a quantitative approach, the alterations in astrocytic metabolic fluxes caused by an ischemic insult. Recently, our group demonstrated the suitability of MFA complemented with ^{13}C NMR spectroscopy data to investigate astrocytic metabolism in primary cultures (Teixeira et al. 2008). This methodology was extended in this work to estimate metabolic fluxes before and after subjecting astrocyte cultures to five hours of oxygen and glucose deprivation. To allow

for a tight control of culture conditions, experiments were performed in small scale bioreactors (Sá Santos et al. 2005). This culture system enables the rigorous control of pH, temperature and oxygen content in the medium, and allows for easy and non-invasive cell sampling, constituting therefore an advantageous system to cultivate brain cells and perform ischemia experiments *in vitro*. The vulnerability of astrocytes to ischemia was also investigated by assessing cell death and intracellular ATP changes, which were correlated with the metabolic results.

2 Materials and Methods

2.1 Materials

Plastic tissue culture flasks were purchased from Nunc (Roskilde, Denmark). Spinner flasks were purchased from Wheaton (Techne, NJ); fetal bovine serum (FBS), penicillin–streptomycin (Pen-Strep), and trypsin-EDTA (1x solution) were purchased from Invitrogen (Glasgow, UK). The culture media used were Dulbecco's modified Eagle's Medium (DMEM) from Invitrogen (Glasgow, UK), cat number 31885, to maintain cell cultures before the bioreactor experiments, and glucose-free DMEM from SIGMA-Aldrich (Steinheim, Germany), cat number D-5030, for experiments involving ^{13}C labeled glucose. D-[1-^{13}C] glucose (99% enriched) was purchased from Cambridge Isotope Laboratories (Andover, MA); all other chemicals were purchased from SIGMA-Aldrich (Steinheim, Germany). Non-porous microcarriers Cytodex 3® were purchased from GE-Healthcare (Amersham Biosciences, Uppsala, Sweden). Animals were purchased from Instituto de Higiene e Medicina Tropical (Lisbon, Portugal).

2.2 Primary cultures of astrocytes

Primary cultures of cortical astrocytes were obtained from 1-2-day-old rats and prepared as described previously (Richter-Landsberg and Besser 1994). Cells were cultured in DMEM containing 5 mM glucose and supplemented with Pen-Strep (100 U/ml) and 20% (v/v) FBS, gradually reducing its concentration to 10%. Cells were kept in a

humidified atmosphere with 7% CO_2 in air and 37ºC. After 3 weeks in culture, cells were transferred to spinner flasks with 125 ml culture volume, according with a protocol previously described (Sá Santos et al. 2005). Briefly, astrocytes were harvested from the T-flasks by mild trypsinisation, pelleted by centrifugation, re-suspended in a small volume of culture medium and immobilized in Cytodex3® microcarriers. Culture medium used in spinner cultures was DMEM supplemented with Pen-Strep (100 U/ml) and 10% (v/v) FBS and containing 10 mM glucose. The cell inoculum used was $0.35x10^6$ cells/ml. The spinners were maintained in an incubator with 7% CO_2 in air and 37ºC, with stirring speed gradually increasing from 60 to 100 rpm throughout culture time. The cells were allowed to grow on the surface of the microcarriers and usually after one week the carriers were confluent. Samples were taken on a daily basis to monitor metabolite consumption/production and cell growth and viability. 50% of the culture volume was exchanged by fresh medium, usually twice a week, in order to ensure glucose availability and to prevent an excessive accumulation of lactate or other "toxic" products of cell metabolism.

2.3 Bioreactors operation and ischemia experiments

Ischemia experiments were carried out in small scale bioreactors with working volume of 125 ml or 250 ml (Sartorius-AG, Goettingen, Germany; Figure 2.1). When cells were confluent on the microcarriers, they were harvested from the spinner flasks, washed with PBS and transferred to the bioreactor vessel. DMEM culture medium containing 2 mM [1-^{13}C] glucose and without glutamine, supplemented with 1% FBS and 100 U/ml pen/strep was used. The pO_2 (partial pressure of oxygen), pH and temperature were monitored with pH and oxygen electrodes (both from Mettler-Toledo, Urdorf, Switzerland) and a temperature sensor, respectively. The bioreactor was equipped with a 3 blade impeller stirrer to ensure proper agitation. These components are connected to the control unit (Biostat® Q-Plus – Sartorius AG, Goettingen, Germany) which uses the software MFCS/Win 2.1 for data acquisition and to control the referred culture parameters. pH was kept at 7.2 by injection of CO_2. pO_2 was maintained constant at

30% of air saturation via surface aeration with a mixture of N_2 and air. Temperature of 37ºC was controlled through water recirculation in the vessel jacket. Stirring was set to 100 rpm.

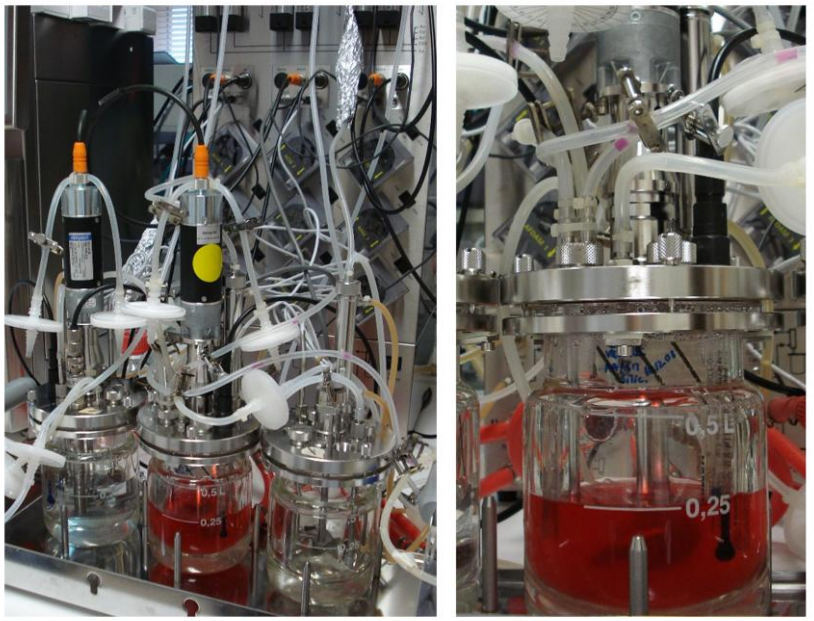

Figure 2.1 - 250 ml bioreactor used for cultivating rat cortical astrocytes and mimicking ischemia-like conditions.

The experimental setup is depicted in Figure 2.2. The ischemic insult was mimicked by allowing the cells to consume the glucose available until its concentration dropped below 0.2 mM. pO_2 level was decreased below 1% by injection of N_2. The duration of the insult was five hours. After this period, standard culture conditions regarding O_2 and glucose were re-established; a medium exchange was performed using fresh DMEM culture medium containing 5 mM [1-^{13}C] glucose and no glutamine, and supplemented with 1% FBS and 100 U/ml Pen-Strep. The culture was monitored during another 48-60 h after the end of the insult by collecting samples of cells and culture supernatant at several time-points. A membrane integrity assay was carried out to assess cell death (see details below). Cell suspensions were centrifuged at 200 g for 10

minutes to separate cells and microcarriers from the supernatant. Cell pellets were either treated to determine the concentration of viable cells throughout the experiments or immediately frozen in liquid nitrogen and stored at -80°C until later analysis of the ATP content. Cell supernatants were stored at -20°C until further analysis. Four independent experiments were conducted.

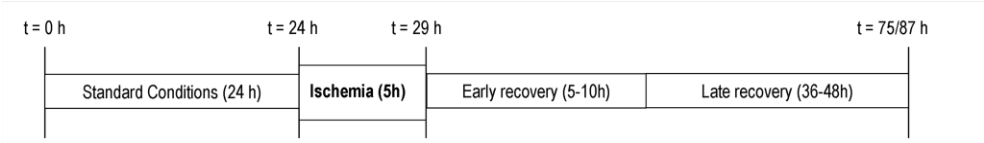

Figure 2.2 - Timeline of events in the experiments. The duration of each period is indicated inside square brackets. For details see the Materials and Methods section.

2.4 Protein determination

Protein was quantified in cell pellets collected at the time of inoculation of the spinner flasks in order to obtain a correlation between protein amount and the number of viable cells determined throughout the experiments. Cells were disrupted using 0.1 M NaOH and incubated overnight at 37°C to ensure complete protein extraction. The bicinchoninic acid (BCA) protein assay from Pierce (Rockford, IL, USA) was used to determine total protein amounts using bovine serum albumin as standard.

2.5 Determination of intracellular ATP concentration

Cellular ATP concentrations were determined with the ATPlite 1-step assay system (Perkin Elmer, Zaventem, Belgium), according to manufacturer's instructions. This assay is based on the emission of light as a result of the reaction of ATP with added luciferase and D-luciferin. The emitted light is proportional to the ATP concentration. A Modulus luminescence counter (Turner Biosystems, Sunnyvale, CA) was used to measure the luminescence signal of the samples in opaque 96-well plates. Cell samples were diluted in PBS in order to have 50 000 cells per well.

2.6 Cell viability assays

To assess cell lysis, the activity of lactate dehydrogenase (LDH; EC 1.1.1.27) released to the culture supernatant was measured by following the rate of pyruvate reduction to lactate. This reaction is coupled with the oxidation of NADH to NAD+, which can be measured spectrophotometrically at 340 nm (Racher et al. 1990). A cell membrane integrity test using the enzyme substrate fluorescein diacetate and the DNA-dye ethidium bromide as described in Dankberg and Persidsky (1976) was also performed. Cell samples were diluted 1:1 in the staining solution containing 8 μg/ml fluorescein diacetate and 10 μg/ml ethidium bromide and images were acquired under an inverted fluorescence microscope (Leica DM IRB). Fluorescein diacetate and ethidium bromide staining were observed with green and red fluorescence, respectively.

2.7 Analytical Methods

Total cell number on the microcarriers was determined by counting cell nuclei using a Fuchs-Rosenthal hemacytometer after treatment with 0.1 M citric acid/1% (v/v) Triton X-100 / 0.1% (w/v) crystal violet. Total glucose and lactate concentrations in the culture supernatant were determined with automated enzymatic assays (YSI 7100 Multiparameter Bioanalytical System; Dayton, Ohio, USA). Amino acids in cell supernatant samples were quantified by HPLC using a pre-column derivatisation method based on the Waters AccQ.Tag Amino Acid Analysis method as described previously (Carinhas et al. 2009). Briefly, both primary and secondary amino acid derivatives were generated by reaction with 6-aminoquinolyl N-hydroxysuccinimidyl-carbamate, allowing their separation in a reversed phase column (AccQ.Tag, Waters, Milford, MA). An internal standard (α-aminobutyric acid) was added to all the samples to ensure consistent measurements between runs. The separated amino acids were detected by fluorescence at 395 nm and quantified by comparison to a calibration curve of standard solutions of amino acids.

2.8 ^{13}C NMR Spectroscopy

Cell supernatant samples were lyophilized and re-dissolved in 99% D_2O. Dioxane 10% (v/v) in D_2O was then added as an internal standard to all samples after pH adjustment to values between 6.8 and 7. Proton decoupled ^{13}C NMR spectra of these samples were acquired in a Bruker Avance 500 Mhz spectrometer (Wissenbourg, France) operating at a frequency of 125.77 MHz, using the following parameters: 30º pulse angle, 30 kHz spectral width, 65-K data points, acquisition time of 1.048 s and a 0.76 s relaxation delay. The number of scans was typically 5120 and for data processing a line broadening of 2 Hz was used. Some spectra were also broad band decoupled only during acquisition and accompanied by a relaxation delay of 20 s, to achieve fully relaxed spectra without nuclear Overhauser effects. From several sets of spectra, correction factors were obtained and applied to the integrals of the individual peaks which were identified relatively to the chemical shift of the internal standard, dioxane, at 67.40 ppm.

2.9 Metabolic Flux Analysis (MFA) and ^{13}C NMR data

MFA is a well established technique for the determination of fluxes distribution in metabolic networks (Lee et al. 1999). This technique relies on the assumption of metabolic pseudo-steady-state for intracellular metabolite concentrations, which means that their accumulation inside the cells is negligible and, thus, the sum of the fluxes of synthesis and consumption of any metabolite must be equal to zero. This approximation is generally accepted as reasonable and valid in a wide range of scenarios. The intracellular fluxes distribution is estimated on the basis of this steady-state assumption, on the network stoichiometry, and using the information from transmembrane rates of metabolites measured in the culture supernatant (Varma and Palsson 1994).

The biochemical network considered in this work (Figure 2.3 and Appendix 1) is based on the network described before (Teixeira et al. 2008) with the addition of some extra reactions which are known to be more active under stress conditions such as the PPP (Bolanos et al. 2004).

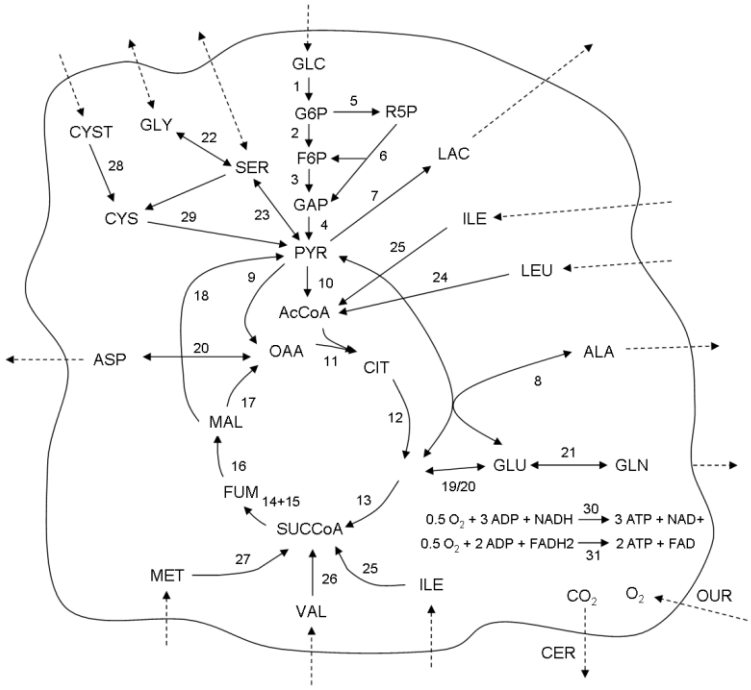

Figure 2.3 - Simplified network to calculate astrocytic metabolic fluxes using MFA. Briefly, the network accounts for glycolysis, pentose phosphate pathway, TCA cycle, amino acid catabolism and oxidative phosphorylation. The splitting pathway of pyruvate conversion through PC and PDH is represented by reactions 9 and 10, respectively. Pyruvate recycling is represented in reaction 18. Reaction 21 represents both glutamine synthetase and glutaminase activities. OUR refers to oxygen uptake rate; CER to carbon dioxide excretion rate. (Dashed arrows indicate the measured consumption/production fluxes of membrane-crossing compounds; full lined arrows refer to intracellular fluxes).

MFA cannot calculate the fluxes through parallel pathways, providing only the sum of their fluxes. Therefore, to overcome this problem, ^{13}C-labeled compounds can be used to determine the ratios between each of the pathways by analyzing the relative amounts of the produced labeled species. In this work, [1-^{13}C] glucose was used to estimate the ratio between the fluxes of two groups of parallel pathways: (i) the glycolytic and the pentose phosphate pathways, which both convert glucose-6-phosphate into pyruvate; (ii) the reactions catalyzed by the PDH (EC 1.2.4.1) and by PC (EC 6.4.1.1) enzymes, which use pyruvate as common substrate and end up producing citrate in TCA cycle. PC is an anaplerotic astroglial enzyme (Yu et al. 1983), whose function is supplying the TCA cycle with intermediates, when metabolites such as α-ketoglutarate leave the

cycle, in the form of glutamate. PC/PDH ratio was estimated from the rates of formation of the different glutamine isotopomers produced from [1-^{13}C] glucose in astrocytes (Shank et al. 1993), according to equation 1:

$$(1)\quad \frac{PC}{PDH} = \frac{C2 - C2_{(PDH)}}{C4} = \frac{Gln\ C2 - Gln\ C3}{Gln\ C4}$$

where C2 corresponds to glutamine labeled in position 2; $C2_{(PDH)}$ corresponds to glutamine labeled in position 2 (Gln C2) that comes from the second turn of the TCA cycle and consequently from the PDH pathway, which is theoretically equal to the synthesis of glutamine labeled in position 3 (Gln C3); C4 corresponds to glutamine labeled in position 4 (Gln C4). In order to estimate the fraction of glucose that was metabolized by the PPP, ^{13}C enrichment in lactate was used. Through this pathway, the labeled carbon from [1-^{13}C] glucose is lost and, thus, the metabolic products (fructose-6-phosphate or glyceraldehyde-3-phosphate) re-entering glycolysis will dilute the label in lactate. The rates of glycolysis and PPP were calculated using equation 2, which compares the rates of synthesis of [3-^{13}C] lactate (^{13}C *Lac*) with the rate of production of total lactate ($rLac_{total}$).

$$(2)\quad \frac{r^{13}CLac}{rLac_{total}} = \frac{rGlyc}{2 \cdot rGlyc + \left(\frac{5}{3}\right) \cdot rPPP + r_{aas}}$$

In this equation, $r\ ^{13}C\ Lac$ is equal to the rate of glucose conversion into fructose-6-phosphate through glycolysis (*rGlyc*), considering that only half of the lactate will be labeled from [1-^{13}C] glucose through this pathway. $rLac_{total}$ is equal to two times *rGlyc*, since two molecules of pyruvate are produced per glucose consumed, plus 5/3 of the rate of glucose metabolism through the PPP (*rPPP*) (5 pyruvate molecules are produced for each 3 molecules of glucose-6-phosphate entering the PPP, which gives a stoichiometry of 5/3 for lactate produced per glucose molecule). In addition, taking into account that serine and cysteine might also be converted to pyruvate, an additional factor corresponding to the sum of their uptake rates (r_{aas}) was included in equation 2.

In the model hereby considered, the total number of reactions was 44, with 36 internal (balanced) metabolites. 14 transmembrane rates - consumption or production rates - of different extracellular metabolites were experimentally determined based on their decrease or accumulation with time, in the culture supernatant. In order to determine specific rates (per milligram of protein) protein amounts were estimated by correlation with the average concentration of viable cells determined by counting in samples collected throughout the experiments. A value of 0.20 mg protein was found to correspond to $1x10^6$ cells, after quantification of the total protein amount in different cell pellets of astrocytes at the time of inoculation of spinner flasks (see above). The rank of the resulting stoichiometric matrix was 32, and the resulting number of degrees of freedom of the system is 12. Since the number of experimentally determined fluxes is higher than the number of degrees of freedom, the system of mathematical equations is redundant. The redundant system at hand was solved by the variances weighted least-squares method using the Penrose pseudo-inverse matrix. The balanceable rates, which arise from system redundancy, were used to calculate the consistency index, *h*, according to Wang and Stephanopoulos (1983). Comparison of *h* with the χ^2-test function was done in order to evaluate the consistency of the experimental values along with the assumed biochemistry and the pseudo-steady-state assumption within the error dictated by measurement uncertainties. Carbon balances closed with values of 99%, in average, thus indicating that the stoichiometry of the network is correct and fits well with experimental data. The above-mentioned calculations were performed using the CellNetAnalyzer software (Klamt et al. 2007).

2.10 Statistical Analysis

Differences between results obtained in the periods before and after ischemia were determined using single-factor analysis of variance (ANOVA) followed by the Dunnet's post hoc test. A level of $P < 0.05$ was considered statistically significant.

3 Results

3.1 Effect of ischemia on astrocytic viability

The effect of simulated ischemia on astrocytic metabolism and viability was studied in this work. To evaluate alterations in cell viability, cell death was assessed using different techniques. A five-hour period of oxygen and glucose deprivation resulted in an average of 30% cell death (Figure 2.4A). A decrease in the number of cells adherent to the microcarriers was observed during ischemia and until the first hours of the late recovery period. This pattern of loss of cell viability correlates with the observed increase in LDH activity measured in the culture supernatant during and after ischemia (Figure 2.4A). In addition, the membrane integrity test using fluoresceine diacetate and ethidium bromide (Figure 2.5), markers for cell viability and death, respectively, confirmed these results. Before the insult, the majority of cells attached to the microcarriers were stained bright green, indicating that most of the cells were viable (Figure 2.5A, 2.5B). However, after the end of the ischemic episode (early recovery), an increased number of cells with red nuclei was observed together with a decrease in the number of cells attached to the carriers (Figure 2.5C, 2.5D), comparing to the previous phase (Figure 2.5A, 2.5B). In the late recovery, the number of cells presenting red nuclei was reduced, suggesting a decreased cellular death rate for the remaining adherent cells (Figure 2.5E, 2.5F).

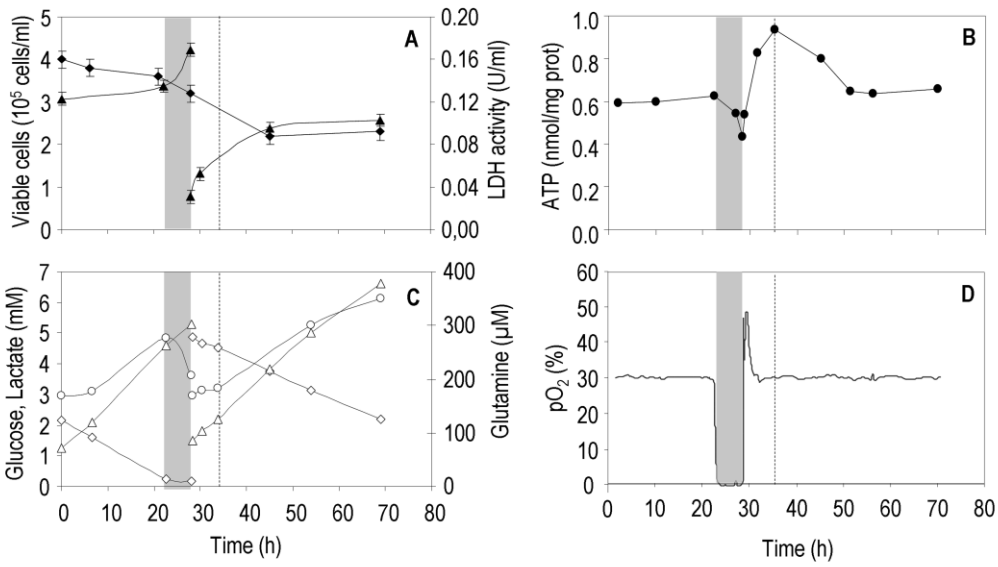

Figure 2.4 - Time-profiles of several culture parameters throughout the experiment: (A) concentration of viable cells (◇) ***and LDH activity*** (◆)***; (B) intracellular ATP concentration*** (●)***; (C) total glucose*** (×), lactate (°) ***and glutamine*** (▵) ***concentrations in the culture supernatants; (D) dissolved oxygen in the culture medium.*** The ischemic insult is represented with a grey rectangle. The dashed vertical line delimitates the transition from the early recovery to the late recovery phase, after the ischemic insult. Data presented are from a representative experiment of a total of four independent experiments.

3.2 Changes in intracellular ATP levels

The pool of intracellular ATP was quantified in samples of cells collected along the experiments; the results are shown in Figure 2.4B. During ischemia, a 30% reduction of the ATP levels was observed. Nevertheless, in the first hours after the end of the insult (early recovery), an overshoot in the ATP concentration occurred, leading to a 70% increase, comparing to the end of ischemia. In the late recovery, ATP levels stabilized back to the concentrations observed before the insult.

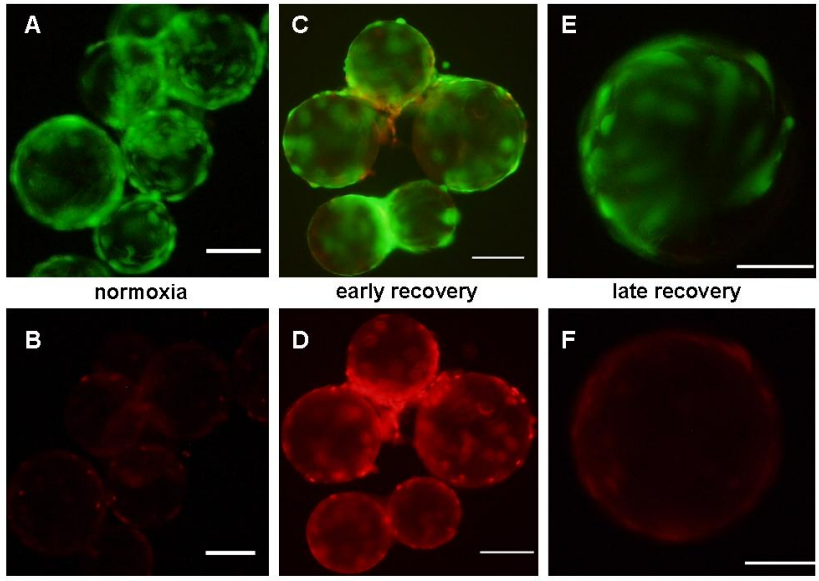

Figure 2.5 - Effect of ischemia on cell viability. Cell samples were collected throughout the experiments (before ischemia/normoxia – A, B; early recovery – C, D; late recovery – E, F) and immediately stained with fluoresceine diacetate (green = viable; A, C, E) and ethidium bromide (red = dead; B, D, F). Scale bar = 100 μm.

3.3 Glucose, lactate and amino acids metabolism

Glucose and lactate profiles are shown in Figure 2.4C and the corresponding specific consumption/production rates, in the different metabolic phases, are presented in Table 2.2. The results indicate that, before ischemia, glucose metabolism was mainly glycolytic, with a lactate production rate over glucose consumption rate (Lac/Glc) ratio of 1.78 (Table 2.2). A residual uptake of glucose was observed during ischemia together with a high lactate production rate, which consequently increased the Lac/Glc ratio to 7.14. In the early recovery, the significant enhancement of glucose uptake (~35%) together with a lower increment in lactate production (Lac/Glc = 1.57) suggests that oxidative glucose metabolism increased in this period. The use of [1-^{13}C] glucose in the culture medium enabled to determine the ^{13}C enrichment in extracellular lactate, alanine and glutamine (Table 2.2), which was calculated by comparing the rates of formation of the labeled pools, obtained from ^{13}C NMR analysis, with the production rates of the total pools.

Table 2.2 – Effect of 5 hours of ischemia on different metabolic parameters of astrocytes.

		Before Ischemia [24 h]	Ischemia [5 h]	Early Recovery [5/10 h]	Late Recovery [~36 h]
Glucose uptake[a] (µmol mg protein^{-1} h^{-1})		1.17 ± 0.04	0.28 ± 0.07*	1.59 ± 0.05	1.79 ± 0.07*
Lactate production[a] (µmol mg protein^{-1} h^{-1})		2.08 ± 0.08	2.0 ± 1.4	2.5 ± 0.2	3.0 ± 0.1*
Glycolysis flux[b] (Glucose → F6P) (µmol.mg protein^{-1} h^{-1})		1.06 ± 0.03	n.d.	1.03 ± 0.05	1.73 ± 0.07*
PPP flux[b] (µmol.mg protein^{-1} h^{-1})		0.12 ± 0.01	n.d.	0.56 ± 0.01*	0.053 ± 0.007
ratio Lac/Glc		1.78	7.14	1.57	1.68
PC/PDH[c]		0.1	n.d.	0	0
^{13}C % enrichment[d]	Lactate	45 ± 7	n.d.	34 ± 5	48 ± 7
	Alanine	45 ± 10	n.d.	35 ± 6	45 ± 9
	Glutamine	23 ± 4	n.d.	10 ± 7	11 ± 4

Results presented are from a representative experiment of a total of 4 independent experiments. Values are rate ± error derived from rate calculation. n.d., not determined. Asterisks indicate a significant difference from values obtained before ischemia (ANOVA followed by Dunnet's post-hoc test, $P < 0.05$).

[a] Specific rates for glucose uptake and lactate production were determined from total amounts measured in the culture supernatant using enzymatic methods.

[b] Glycolysis and PPP fluxes were determined using equation 2 described in the text.

[c] PC/PDH ratio was determined from the rates of production of the different labelled species of glutamine quantified by ^{13}C NMR spectroscopy in samples of cell supernatant, according to equation 1 described in the text.

[d] % ^{13}C enrichment in extracellular lactate, alanine and glutamine was calculated from the rates of accumulation of labelled metabolite quantified by ^{13}C-NMRS compared to the rate of accumulation of the total metabolite pool for each time-interval.

Based on the ^{13}C enrichment of lactate, the fraction of glucose metabolized through glycolysis could be distinguished from the fraction metabolized via PPP (see Materials and Methods for details), and the corresponding fluxes were calculated (Table 2.2). The results indicate that approximately one third of the glucose taken up during the early recovery entered the PPP and subsequently returned to the glycolytic pathway. In contrast, in the late recovery phase, the flux of the PPP was residual and similar to the values observed before ischemia (between 3 and 10% of the glucose uptake rate). Additionally, the increment in the Lac/Glc ratio in this phase suggests a return to a predominance of glucose glycolytic metabolism, even though with significantly elevated specific rates for glucose uptake and lactate production, 50% and 60%, respectively, comparing with the period before ischemia.

Amino acid concentrations in the culture supernatant were measured in samples collected throughout the experiments and their specific consumption or production

rates were determined, based on their decrease or accumulation in the medium, respectively (Table 2.3). The specific rate of glutamine synthesis more than doubled in the early recovery (from 19.8 ± 0.2 to 49.0 ± 2.0 nmol mg $prot^{-1}$ h^{-1}) and was further increased in the late recovery, comparing with the initial phase of the experiments (Table 2.3).

Table 2.3 – Effect of 5 hours of ischemia on astrocytic amino acids metabolic rates.

	Before ischemia [24 h]	Early recovery [5-10 h]	Late recovery [~36 h]
r_{Ser}	-10 ± 1	-13 ± 3	-18 ± 3
r_{Gly}	29 ± 6	30 ± 5	40 ± 6
r_{Gln}	19.8 ± 0.2	49 ± 2	70 ± 20
r_{Ala}	19 ± 5	45 ± 6	40 ± 10
r_{Cyst}	- 17 ± 1	- 14.3 ± 3	- 19.4 ± 3
r_{Val}	-11 ± 2	-70 ± 10*	-7.2 ± 0.8
r_{Met}	-3.2 ± 0.8	0	0
r_{Ile}	-21 ± 2	-61 ± 8*	-7.4 ± 0.8
r_{Leu}	-19.4 ± 0.9	-40 ± 1*	-4 ± 1

Specific consumption/production rates of amino acids were determined from total amounts measured in the culture supernatant using HPLC (negative values refer to consumption rates). The units of all listed rates are nmol mg $protein^{-1}$ h^{-1}. Results presented are from a representative experiment of a total of four independent experiments. Values are rate ± error derived from rate calculation. Asterisks indicate a significant difference from values obtained before ischemia (ANOVA followed by Dunnet's post hoc test, $p < 0.05$). Abbreviations: Ser (serine), Gly (glycine), Gln (glutamine), Ala (alanine), Cyst (cystine), Val (valine), Met (methionine), Ile (isoleucine), Leu (leucine).

By comparing the rates of production of the different glutamine isotopomers ([2-^{13}C], [3-^{13}C] and [4-^{13}C] glutamine) to determine the PC/PDH ratio in the different metabolic phases considered, it was found that the pathway catalyzed by PC was only active before ischemia (PC/PDH=0.1), the calculated value for the PC/PDH ratio being zero in the recovery period (Table 2.2). In addition, ^{13}C % enrichment in glutamine was low, comparing to that of lactate and alanine, and was even more decreased in the recovery period (Table 2.2).

Concerning the remaining amino acids analyzed, in general, the main alterations were observed in the early recovery. The specific consumption of branched-chain amino acids (BCAAs) valine, leucine and isoleucine increased between two to five-fold, the major increment being observed for valine (from 11 ± 2 to 70 ± 10 nmol mg $prot^{-1}$ h^{-1}), whereas alanine production duplicated in the recovery period (Table 2.3). Together with

the contribution of the PPP, the BCAAs consumption rates can be used to predict a theoretical dilution on the enrichment in glutamine, as leucine and isoleucine can be transformed into acetyl-CoA (see Table 2.1). These calculations were done by comparing the flux through PDH (Pyr → ACoA - reaction 10) with the sum of fluxes leading to the production of acetyl-CoA (reactions 10, 24 and 25), multiplied by the enrichment in pyruvate (assumed to be the same of that of lactate – Table 2.2). The results obtained for the theoretical enrichment in glutamine were markedly higher than the ones determined experimentally, in particular for the periods after ischemia: 35% before ischemia, 27% in the early recovery and of 47% in the late recovery phase.

Regarding glycine and serine, their respective production and consumption increased slightly along the recovery period, comparing to the period before ischemia. It is worth to note that the culture medium used in the experiments (DMEM) did not contain aspartate or glutamate in its composition and, therefore, no uptake rates are presented for these amino acids.

3.4 Metabolic fluxes distribution

The fluxes estimated using MFA for the three distinct metabolic phases (before ischemia, early recovery and late recovery) are shown in Figure 2.6. It should be mentioned that no fluxes were calculated for the period of simulated ischemia since it is expected that the pools of many metabolites are altered during this period and thus, pseudo steady-state hypothesis cannot be assumed. Regarding the consistency test, it gave positive results for all metabolic phases, meaning that the biochemical network's stoichiometry and the metabolic steady-state assumption are consistent with the experimental data. The modeling results are consistent with the enhancement of the flux of glucose metabolism through the pentose phosphate pathway (G6P → R5P and R5P → F6P + GAP - Figure 2.6A) in parallel with the increased glucose uptake rate observed in the early recovery. Additionally, the flux of reaction 2 (G6P → F6P) in glycolysis, after the branch point between glycolysis and the PPP (see Figure 2.3) did not change in the early recovery and only increased significantly in the subsequent phase (Figure 2.6A). Moreover, during the

early recovery, a significant 2-fold increase in the fluxes of TCA cycle reactions (from 0.38 ± 0.03 to 0.78 ± 0.03 µmol mg prot^{-1} h^{-1}, in average) was estimated (Figure 2.6B).

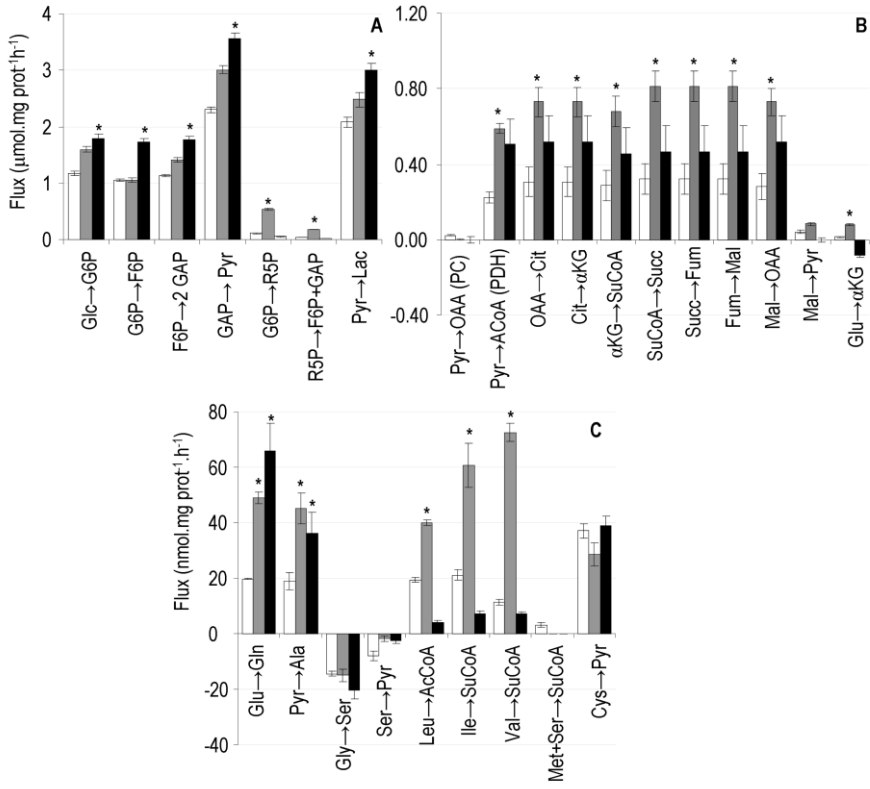

Figure 2.6 - Effect of ischemia in astrocytic metabolic fluxes. A – Glycolysis and pentose phosphate pathway reactions; B – Oxidative metabolism (TCA cycle); C – Amino acids metabolism. Fluxes were calculated by MFA for the periods before ischemia (normoxia) (white bars), and after ischemia - early recovery (grey bars) and late recovery (black bars), corresponding to average periods of 10 h and 48 h (as indicated in Figure 1), respectively. Asterisks indicate a significant difference from values obtained before ischemia (ANOVA followed by Dunnet's post hoc test, $p < 0.05$). Error bars indicate the errors associated with model estimations. Results shown are from a representative experiment of a total of four independent experiments.

By comparing the estimated fluxes for pyruvate production via glycolysis (GAP → Pyr) with the flux through PDH one can estimate the individual energy contributions of glycolysis and oxidative metabolism. Before ischemia, oxidative glucose metabolism was about 10% that of glycolysis, whereas in the early and late recovery this percentage

increased to 20% and 14%, respectively. The pyruvate recycling flux (reaction 18, Mal → Pyr) was active only before ischemia and in the early recovery, but the values obtained are very low when comparing to the estimated TCA cycle fluxes (Figure 2.6B).

Using only the metabolite balancing it is not possible to estimate the individual fluxes (forward and backwards) in bidirectional reactions as, for example, the case of the transamination between α-ketoglutarate (α-KG) and glutamate (reactions 19/20) Instead, the MFA results indicate only the net flux of reversible reactions. The conversion of glutamate into α-KG was favored before ischemia and significantly increased in the early recovery; on the other hand, glutamate synthesis from α-KG was predominant in the late recovery and, thus, the estimated flux is negative (Figure 2.6B). The same is applied for the reactions catalyzed by glutamine synthetase and glutaminase. In this case, the net flux favored glutamine synthesis, which is in agreement with the increased glutamine release along the experiments. In the early recovery, the fluxes of the BCAAs (valine, isoleucine, leucine) catabolism into acetyl-CoA and/or succinyl-CoA were also significantly increased by two to three-fold (Figure 2.6C), reflecting the measured consumption rates. In the late recovery, a decrease in the TCA cycle fluxes and the pronounced reduction in the utilization of BCAAs to values closer to the ones observed before ischemia were observed.

4 Discussion

In this work, the distribution of metabolic fluxes of the main pathways involved in astrocytic energy metabolism was estimated by MFA in combination with ^{13}C NMR data, allowing for the quantitative characterization of the consequences of ischemia in astrocytic metabolism. This approach is advantageous since it enables to estimate fluxes related with the main metabolic nodes. Furthermore, through the use of isotopic information, other important fluxes, such as pyruvate carboxylation and the PPP, can be additionally calculated thus improving the quality of model estimations.

The experimental setup used consisted in a stirred culture of rat cortical astrocytes adherent onto Cytodex3® microcarriers in a bioreactor (Figure 2.1), which allows for tightly controlled temperature, pO_2 and pH, and non-invasive sampling throughout experiment time, being suitable to mimic ischemia *in vitro*. In fact, our group has previously demonstrated the suitability of this system to cultivate brain cells and mimic brain insults, such as hypoxia (Sá Santos et al. 2005), due to the ability to readily alter the pO_2 in the culture medium. Figure 2.4F illustrates how this system allowed to rapidly (approximately 30 minutes) change the pO_2 without significant oscillations around the defined set-point. Furthermore, the use of this *in vitro* model is very advantageous compared to *in vivo* models since metabolic effects of ischemia in astrocytes can be studied in a "closed system", allowing for the study of specific effects in the astrocyte compartment and eliminating the possibility of glucose metabolism by other organs and the influence of blood. Even so, this model also has limitations. The strategy chosen to mimic ischemia (to allow first for glucose levels to decrease down to 0.2 mM and then decreasing pO_2 to below 1%) was conditioned by the technical complexity of the bioreactor system when comparing to monolayer cultures, where medium exchanges and washing steps are much easier to perform, and does not correspond exactly to the *in vivo* condition in which glucose levels are usually normal when blood supply is blocked. Therefore, it can not be excluded that in the last hour before the onset of the insult, an extracellular glucose concentration lower than 0.5 mM might have caused partial depletion of intracellular glucose and glycogen pools and possibly influenced the extent of glycogenolysis and lactate production during the ischemic period.

4.1 Cell death and ATP levels

Five hours of oxygen and glucose deprivation resulted in a substantial percentage of cell death (30%). Oxidative stress and impairment of mitochondrial activity are well described events contributing for astrocytic death under such conditions. Several lines of evidence suggest an increase in the generation of reactive oxygen species during ischemia

as well as during reperfusion, with the consequent oxidative stress being a major cause of cellular death (Juurlink 1997). Our results also confirm previous reports of the particular astrocytic vulnerability to ischemia, comparing with oxygen deprivation alone (Sochocka et al. 1994; Alves et al. 2000). Astrocytes present a higher glycolytic activity under anaerobic conditions, which is normally sufficient to maintain ATP stores (Hertz 2008); however, when the lack of oxygen is combined with substrate depletion, it has been observed that an adequate supply of ATP is no longer possible, thus contributing to astrocytic death (Sochocka et al. 1994). Actually, ischemic conditions induced a fast decline of 30% in cellular ATP levels (Figure 2.4B) that could nonetheless be rapidly restored in the recovery period. It has been reported that in severe or complete brain ischemia, ATP falls to 0-25% of that in normally perfused tissue whereas in the penumbra this fall reaches only 50–70% (Lipton 1999). Additionally, Yager et al (1994) demonstrated, in mouse astrocyte cultures, that cell death occurs only once a critically 'low' threshold of ATP has been reached (below 10% of control) (Yager et al. 1994). Considering that the measured values of ATP were relative to the viable cells present in the culture, the results indicate that a 30% decrease in ATP pools did not affect cell viability.

4.2 Glycolytic metabolism

Several metabolic alterations occurred after ischemia, reflecting a response of the surviving cells to the insult. A prominent increase in Lac/Glc ratio to 7.14 during ischemia (Table 2) was observed. This ratio provides information regarding glycolytic versus oxidative glucose metabolism, since a higher proportion of lactate production, comparing to glucose consumption, indicates that less glucose is oxidized. In non human primate brains, *in vivo*, this ratio was also increased by several fold during ischemia, returning to baseline levels with reperfusion in penumbral areas but remaining increased in severely affected regions (Frykholm et al. 2005). Our results suggest the use of alternative carbon sources as lactate precursors, since the maximum expected value for this ratio is 2, assuming that two molecules of lactate are originated from each glucose

consumed. The additional degradation of the cellular glucose and pyruvate pools and, particularly, the breakdown of astrocytic glycogen reservoirs (Dringen et al. 1993), which is not dependent on ATP availability, are likely explanations for this result. Although it has been suggested that astrocytes provide neurons glycogen-derived lactate to be oxidized in situations where glucose is limiting, mainly during hypoglycemia or during periods of increased energy demand (Tekkok et al. 2005; Brown and Ransom 2007), the role of glycogen in ischemia survival has not been yet elucidated. Nevertheless, the results support the classical concept that astrocytes up-regulate glycolysis to deal with the decline in ATP due to the inhibition of respiration caused by ischemia (Dienel and Hertz 2005).

The high glycolytic rates observed in this work and, particularly during ischemia, might be conditioned by the large extracellular culture volume in the bioreactor when comparing to the intracellular volume, favoring the diffusion of high amounts of lactate and other compounds to the large pool of medium, where they are constantly diluted. This contrasts markedly with the cellular environment of mature brain *in vivo*, as it has been discussed in the literature (Dienel and Hertz 2001). Even so, the lactate production rates obtained in this work, in the presence of glucose, are in the range of values previously obtained in other cell culture systems (Dienel and Hertz 2001). In addition, enhanced lactate release by astrocytes is favored by the existence, both *in vitro* and *in vivo*, of an extracellular concentration gradient which favors the rapid elimination of lactate from the brain (Dienel and Hertz 2005), and helps to prevent the disruption of the redox state of activated cells by high levels of lactate (Dienel and Hertz 2001), which indicates that these phenomena are not exclusive of *in vitro* cell preparations and have physiological significance. In fact, it has been proposed that increased lactate levels are good markers of severe ischemia *in vivo* (Frykholm et al. 2005). Interestingly, the neuroprotective effect of lactate administered right after ischemia has recently been proposed, using both *in vivo* and *in vitro* models (Berthet et al. 2009), thus supporting the

role of lactate as main astrocytic contributor for neuronal energy metabolism in ischemic brain (Phillis et al. 2001).

After the observed increase in oxidative metabolism in the early recovery period (to be discussed below) cell metabolism was characterized by an increased glycolytic activity during the late recovery (for, at least, 48h) suggesting a partial recovery from the insult, as cells remained in an activated metabolic status. These findings might be related with increased expression of hypoxia-inducible factor 1 (HIF-1) target genes as increased glucose transport and glycolysis have been observed as a result of HIF-1 activation by hypoxia in the peri-infarct penumbra of rats subjected to permanent middle cerebral artery occlusion (Bergeron et al. 1999).

4.3 Pentose phosphate pathway and dilution in lactate enrichment

Oxidative stress is typically increased in pathological situations such as ischemia, hypoxia or inflammation (Bolanos et al. 2004). In this context, it has been proposed that the up-regulation of the PPP provides protection through production of NADPH (Kussmaul et al. 1999) which is necessary for the regeneration of glutathione, an important antioxidant molecule (Dringen 2000). Moreover, increased glucose utilization by astrocytes has been reported to confer self-protection against nitric oxide-mediated glutathione oxidation (Garcia-Nogales et al. 1999). Thus, the observed reduction in ^{13}C enrichment in lactate in the early recovery phase comparing with the pre-ischemic period, was interpreted as a result of increased [1-^{13}C] glucose metabolism through the PPP, which products (unlabeled fructose-6-phosphate and unlabeled glyceraldehyde-3-phosphate) re-enter glycolysis, thus diluting the label in lactate C3. Even though it has been suggested that glycogenolysis plays an important role in astrocytic energy homeostasis under activation (Dienel et al. 2007; Walls et al. 2009), lactate derived from eventual glycogen degradation was not considered to contribute significantly to this label dilution, since (i) the glycogen pool was probably depleted during the ischemic period, which is supported by the large observed increased in the Lac/Glc ratio (Table 2.2) and, in fact, it was in the early recovery phase (immediately after ischemia) that a higher

dilution in lactate enrichment was observed; (ii) glycogen constitutes an insignificant proportion of the total lactate released in the presence of glucose (Dringen et al. 1993) and (iii) glycogenolysis is mainly thought to occur when the available glucose cannot meet the cellular energy requirements (Brown and Ransom 2007), which was not the case in the different phases in which MFA was applied. Furthermore, the estimated percentage of PPP flux for the periods before ischemia and late recovery (during which glycogen stores should be available and a higher contribution of glycogenolysis could be expected) were of 10% and 3%, respectively. These results correlate with values obtained for the rat brain *in vivo* (Ben-Yoseph et al. 1995) and therefore justify the assumption that dilution of lactate enrichment was mainly due to activation of the PPP. After ischemia, the PPP flux was increased to 35% of the glucose uptake rate, which is in accordance with previous observations of PPP flux up-regulation to ~67% in cultured astrocytes and up to ~36% in conscious rats, as a response to different oxidative stress conditions (Ben-Yoseph et al. 1994).

Interestingly, the important contribution of the PPP to the dilution of lactate enrichment in the brain was recently discussed in the literature in the context of *in vivo* brain activation studies and estimations of important metabolic fluxes, such as the glutamate-glutamine cycle. Dilution in glutamine C4 was found to significantly influence the estimation of the glutamate-glutamine cycle fluxes *in vivo* as it has been based on the measurement of glutamine turnover from ^{13}C-labeled glucose and acetate (Shen et al. 2009). Though this "glutamine dilution" has been attributed to lactate and glutamine exchange between brain and blood, further studies have shown that other pathways such as the PPP, oxidation of fatty acids and of BCAAs must contribute substantially to this observation (Cruz et al. 2007; Dienel and Cruz 2009). Hence, our results corroborate the importance of the PPP during brain activation and in response to pathologies such as ischemia.

4.4 TCA cycle and metabolism of BCAAs

Flux estimations provided by MFA (Figure 2.6) helped to explain the observed changes in glucose and lactate metabolic rates after ischemia and to understand its consequences. The reduction on the Lac/Glc ratio in the early recovery was indeed reflected into both an enhancement in the fluxes of the PPP and TCA cycle. In addition, the fraction of oxidative glucose metabolism was markedly increased in both recovery periods (from 10% before ischemia to 20% and 14% in early and late recovery, respectively), which can be interpreted as a cellular mechanism to replenish intracellular ATP pools that were depleted during the insult, as confirmed by experimental measurements (Figure 2.4B). Increased ATP production through oxidative phosphorylation after ischemia might also be related with altered ion homeostasis as the response of brain cells to energy deprivation has been reported as being a complex function of their capacity to produce ATP and of the activities of various pathways which are involved in ion homeostasis (Silver et al. 1997).

The catabolism of BCAAs was also increased in the early recovery phase. It is known that BCAAs are important brain energetic fuels in physiological conditions and also contribute to the maintenance of nitrogen homeostasis by providing amino groups to be used in glutamate and glutamine synthesis (Yudkoff 1997). For example, the catabolism of isoleucine results in the formation of both succinyl-CoA and acetyl-CoA, thus supplying both an anaplerotic substrate downstream of the α-ketoglutarate dehydrogenase step (if we consider that the pool of TCA cycle intermediates is approximately constant, the role of BCAAs generating succinyl-CoA should be related to anaplerosis, allowing to support the synthesis of biomass components and, especially, glutamine) as well as acetyl-CoA for synthesis of citrate. This has been shown to occur in cultures of astrocytes for isoleucine and valine (Johansen et al. 2007; Murin et al. 2009a, b). In addition, pyruvate recycling (reaction 18, Mal → Pyr), which might provide molecules to the glycolysis/gluconeogenesis, did not change appreciably during the experiments. This reinforces the idea that the BCAAs entering the TCA cycle were

either oxidized to CO_2 or were used for the synthesis of glutamate/glutamine, leaving the TCA cycle through reactions 8, 19, 20, 21. To our knowledge, a possible role of BCAAs in supporting brain metabolism during/after ischemia has not yet been explored, although some evidence exists that BCAAs derived from muscle proteolysis function as energy substrates for heart muscle (Li and Gao 1999), and provide protection in myocardial ischemia (Szpetnar et al. 2004). Hence, our results suggest that BCAAs might represent alternative fuels to support astrocytic and neuronal survival from ischemia, for which this subject should be further explored.

Still regarding MFA estimations, it is worth to mention that besides conversion into pyruvate (reaction 29) there are other known fates of cysteine in astrocytes, namely glutathione synthesis, for which cysteine is a limiting molecule (Kranich et al. 1996), and also taurine and hypotaurine synthesis, which was described to occur under physiological conditions (Brand et al. 1998). However, due to the difficulty in determining intracellular synthesis of these different compounds, this was not taken into account for the MFA calculations, and therefore the use of cysteine for pyruvate synthesis is certainly overestimated. Nevertheless, due to the low order of magnitude of the estimated flux for the reaction of conversion of cysteine to pyruvate (~20 nmol mg $prot^{-1}$ h^{-1}), comparing with the flux of pyruvate synthesis from glyceraldehyde-3-phosphate (2-3 μmol mg $prot^{-1}$ h^{-1}), it does not have a significant influence on the estimated fluxes.

4.5 Glutamine production and dilution in glutamine enrichment

Regarding the PC/PDH ratios determined (Table 2.2) and the observed rates of glutamine synthesis (Table 2.3), even though the anaplerotic reaction catalyzed by PC is important for the *de novo* synthesis of glutamine (Shank et al. 1985), PC activity was only detected before ischemia, when glutamine production rate was lower. Furthermore, the predominant conversion of glutamate into α-KG over glutamate release from the TCA cycle, and its significant enhancement in the early recovery, indicates that some glutamate was also oxidized in this phase instead of being used for glutamine synthesis. These results imply that other precursors, namely BCAAs (given its role as anaplerotic

molecules), likely contributed to the maintenance of glutamine production. The decrease in ^{13}C enrichment in extracellular glutamine, in the recovery period, also supports this hypothesis (Table 2.2). These results are particularly important since they suggest that PC was not a major contributor for de novo glutamine synthesis which might influence its estimation along with the astrocytic oxidation rate in other studies. Moreover, as discussed above regarding dilution in lactate enrichment, our results also indicate that utilization of unlabelled BCAAs as oxidative fuel significantly contributes to the "glutamine dilution" observed in many *in vivo* magnetic resonance studies. Nevertheless, a quantitative comparison of the PDH flux with metabolic rates of BCAAs catabolism, taking into account the contribution of the PPP to label dilution in pyruvate, shows that these pathways can not solely explain the observed dilution in glutamine enrichment in the present study. The distinct differences between theoretically estimated values and the ones determined experimentally suggest that activation of other pathways that were not taken into account in our metabolic network were likely to be active mainly after ischemia, such as fatty acids oxidation or even protein degradation, which have also been proposed to contribute to the "glutamine dilution" phenomenon observed *in vivo* (Shen et al. 2009). Even so, the increase in glutamine release after ischemia can be interpreted as an intrinsic glial mechanism aiming to support neuronal function under stress conditions. This finding is consistent with results obtained using rat models, indicating that astrocytes in the penumbra continue to produce glutamine even after 240 min of middle cerebral artery occlusion in rats, which demonstrated a good preservation of astrocytic metabolism in moderately ischemic tissue (Haberg et al. 2001).

4.6 Concluding remarks

In summary, this work reinforces the suitability and robustness of MFA not only to calculate metabolic fluxes in brain cell cultures but, more importantly, to characterize the main metabolic effects of a given insult, such as ischemia. Overall, our results show that changes in fluxes of key energy metabolism pathways, such as the PPP and the TCA

cycle, are implicated in the recovery from ischemia in astrocytes. Herein, BCAAs seem to play a crucial role as anaplerotic molecules and therefore their use as a therapeutic tool after ischemia should be investigated. In addition, the activation of the PPP underlines the importance of this pathway for cell protection under increased oxidative stress and highlights the relevance of this pathway regarding the estimation of metabolic fluxes based on the analysis of isotopic enrichment from ^{13}C-glucose metabolism. In general, this work provides valuable knowledge regarding ischemia-induced astrocytic metabolic alterations, which can help to understand findings obtained *in vivo*. In future studies we aim to address the significance of these alterations in the context of astrocytes-neurons interactions in more complex models of ischemia.

5 Acknowledgements

This research was supported by the Portuguese *Fundação para a Ciência e Tecnologia* (FCT) (project PTDC/BIO/69407/2006) and by Merck, Sharp & Dohme, Portugal. A.I. Amaral acknowledges FCT for her PhD grant (SFRH/BD/29666/2006) and V. Bernal acknowledges the *Fundación Séneca* (Murcia, Spain) for his post-doctoral fellowship. We acknowledge CERMAX at ITQB for access to NMR spectrometers, which are part of the National NMR Network and were bought in the framework of the National Program for Scientific Re-equipment (contract REDE/1517/RMN/2005) with funds from POCI 2010 (FEDER) and FCT. Dr. Ana Luisa Simplício is also gratefully acknowledged for the help in setting up the HPLC protocol for amino acids analysis. Nuno Carinhas is acknowledged for fruitful discussions and advice regarding statistical analysis.

6 References

Alves P. M., Fonseca L. L., Peixoto C. C., Almeida A. C., Carrondo M. J. and Santos H. (2000) NMR studies on energy metabolism of immobilized primary neurons and astrocytes during hypoxia, ischemia and hypoglycemia. *NMR Biomed* **13,** 438-448.

Bak L. K., Walls A. B., Schousboe A., Ring A., Sonnewald U. and Waagepetersen H. S. (2009) Neuronal glucose but not lactate utilization is positively correlated with NMDA-induced neurotransmission and fluctuations in cytosolic Ca2+ levels. *J Neurochem* **109 Suppl 1,** 87-93.

Ben-Yoseph O., Boxer P. A. and Ross B. D. (1994) Oxidative stress in the central nervous system: monitoring the metabolic response using the pentose phosphate pathway. *Dev Neurosci* **16,** 328-336.

Ben-Yoseph O., Camp D. M., Robinson T. E. and Ross B. D. (1995) Dynamic measurements of cerebral pentose phosphate pathway activity in vivo using [1,6-13C2,6,6-2H2]glucose and microdialysis. *J Neurochem* **64,** 1336-1342.

Bergeron M., Yu A. Y., Solway K. E., Semenza G. L. and Sharp F. R. (1999) Induction of hypoxia-inducible factor-1 (HIF-1) and its target genes following focal ischaemia in rat brain. *Eur J Neurosci* **11,** 4159-4170.

Berthet C., Lei H., Thevenet J., Gruetter R., Magistretti P. J. and Hirt L. (2009) Neuroprotective role of lactate after cerebral ischemia. *J Cereb Blood Flow Metab* **29,** 1780-1789.

Bluml S., Moreno-Torres A., Shic F., Nguy C. H. and Ross B. D. (2002) Tricarboxylic acid cycle of glia in the in vivo human brain. *NMR Biomed* **15,** 1-5.

Bolanos J. P., Cidad P., Garcia-Nogales P., Delgado-Esteban M., Fernandez E. and Almeida A. (2004) Regulation of glucose metabolism by nitrosative stress in neural cells. *Mol Aspects Med* **25,** 61-73.

Brand A., Leibfritz D., Hamprecht B. and Dringen R. (1998) Metabolism of cysteine in astroglial cells: synthesis of hypotaurine and taurine. *J Neurochem* **71,** 827-832.

Brown A. M. and Ransom B. R. (2007) Astrocyte glycogen and brain energy metabolism. *Glia* **55,** 1263-1271.

Carinhas N., Bernal V., Yokomizo A. Y., Carrondo M. J., Oliveira R. and Alves P. M. (2009) Baculovirus production for gene therapy: the role of cell density, multiplicity of infection and medium exchange. *Appl Microbiol Biotechnol* **81,** 1041-1049.

Contreras L. and Satrustegui J. (2009) Calcium signaling in brain mitochondria: interplay of malate aspartate NADH shuttle and calcium uniporter/mitochondrial dehydrogenase pathways. *J Biol Chem* **284,** 7091-7099.

Cruz N. F., Ball K. K. and Dienel G. A. (2007) Functional imaging of focal brain activation in conscious rats: impact of [(14)C]glucose metabolite spreading and release. *J Neurosci Res* **85,** 3254-3266.

Danbolt N. C. (2001) Glutamate uptake. *Prog Neurobiol* **65,** 1-105.

Dankberg F. and Persidsky M. D. (1976) A test of granulocyte membrane integrity and phagocytic function. *Cryobiology* **13,** 430-432.

Dienel G. A. and Hertz L. (2001) Glucose and lactate metabolism during brain activation. *J Neurosci Res* **66,** 824-838.

Dienel G. A. and Hertz L. (2005) Astrocytic contributions to bioenergetics of cerebral ischemia. *Glia* **50,** 362-388.

Dienel G. A. and Cruz N. F. (2009) Exchange-mediated dilution of brain lactate specific activity: implications for the origin of glutamate dilution and the contributions of glutamine dilution and other pathways. *J Neurochem* **109 Suppl 1,** 30-37.

Dienel G. A., Ball K. K. and Cruz N. F. (2007) A glycogen phosphorylase inhibitor selectively enhances local rates of glucose utilization in brain during sensory stimulation of conscious rats: implications for glycogen turnover. *J Neurochem* **102,** 466-478.

Dirnagl U., Iadecola C. and Moskowitz M. A. (1999) Pathobiology of ischaemic stroke: an integrated view. *Trends Neurosci* **22,** 391-397.

Dringen R. (2000) Glutathione metabolism and oxidative stress in neurodegeneration. *Eur J Biochem* **267,** 4903.

Dringen R., Gebhardt R. and Hamprecht B. (1993) Glycogen in astrocytes: possible function as lactate supply for neighboring cells. *Brain Res* **623,** 208-214.

Frykholm P., Hillered L., Langstrom B., Persson L., Valtysson J. and Enblad P. (2005) Relationship between cerebral blood flow and oxygen metabolism, and extracellular glucose and lactate concentrations during middle cerebral artery occlusion and reperfusion: a microdialysis and positron emission tomography study in nonhuman primates. *J Neurosurg* **102,** 1076-1084.

Garcia-Nogales P., Almeida A., Fernandez E., Medina J. M. and Bolanos J. P. (1999) Induction of glucose-6-phosphate dehydrogenase by lipopolysaccharide contributes to preventing nitric oxide-mediated glutathione depletion in cultured rat astrocytes. *J Neurochem* **72,** 1750-1758.

Haberg A., Qu H. and Sonnewald U. (2006) Glutamate and GABA metabolism in transient and permanent middle cerebral artery occlusion in rat: Importance of astrocytes for neuronal survival. *Neurochem Int*.

Haberg A., Qu H., Saether O., Unsgard G., Haraldseth O. and Sonnewald U. (2001) Differences in neurotransmitter synthesis and intermediary metabolism between glutamatergic and GABAergic neurons during 4 hours of middle cerebral artery occlusion in the rat: the role of astrocytes in neuronal survival. *J Cereb Blood Flow Metab* **21,** 1451-1463.

Hertz L. (2008) Bioenergetics of cerebral ischemia: a cellular perspective. *Neuropharmacology* **55,** 289-309.

Hertz L., Peng L. and Dienel G. A. (2007) Energy metabolism in astrocytes: high rate of oxidative metabolism and spatiotemporal dependence on glycolysis/glycogenolysis. *J Cereb Blood Flow Metab* **27,** 219-249.

Hyder F., Patel A. B., Gjedde A., Rothman D. L., Behar K. L. and Shulman R. G. (2006) Neuronal-glial glucose oxidation and glutamatergic-GABAergic function. *J Cereb Blood Flow Metab* **26,** 865-877.

Johansen M. L., Bak L. K., Schousboe A., Iversen P., Sorensen M., Keiding S., Vilstrup H., Gjedde A., Ott P. and Waagepetersen H. S. (2007) The metabolic role of isoleucine in detoxification of ammonia in cultured mouse neurons and astrocytes. *Neurochem Int* **50,** 1042-1051.

Juurlink B. H. (1997) Response of glial cells to ischemia: roles of reactive oxygen species and glutathione. *Neurosci Biobehav Rev* **21,** 151-166.

Klamt S., Saez-Rodriguez J. and Gilles E. D. (2007) Structural and functional analysis of cellular networks with CellNetAnalyzer. *BMC Syst Biol* **1,** 2.

Kranich O., Hamprecht B. and Dringen R. (1996) Different preferences in the utilization of amino acids for glutathione synthesis in cultured neurons and astroglial cells derived from rat brain. *Neurosci Lett* **219,** 211-214.

Kussmaul L., Hamprecht B. and Dringen R. (1999) The detoxification of cumene hydroperoxide by the glutathione system of cultured astroglial cells hinges on hexose availability for the regeneration of NADPH. *J Neurochem* **73,** 1246-1253.

Lebon V., Petersen K. F., Cline G. W., Shen J., Mason G. F., Dufour S., Behar K. L., Shulman G. I. and Rothman D. L. (2002) Astroglial contribution to brain energy metabolism in humans revealed by 13C nuclear magnetic resonance spectroscopy: elucidation of the dominant pathway for neurotransmitter glutamate repletion and measurement of astrocytic oxidative metabolism. *J Neurosci* **22,** 1523-1531.

Lee K., Berthiaume F., Stephanopoulos G. N. and Yarmush M. L. (1999) Metabolic flux analysis: a powerful tool for monitoring tissue function. *Tissue Eng* **5,** 347-368.

Li A. L. and Gao L. X. (1999) Protection of branched-chain amino acids against ischemic myocardial injury in rats. *Biomed Environ Sci* **12,** 62-65.

Lipton P. (1999) Ischemic cell death in brain neurons. *Physiol Rev* **79,** 1431-1568.

Mangia S., Simpson I. A., Vannucci S. J. and Carruthers A. (2009) The in vivo neuron-to-astrocyte lactate shuttle in human brain: evidence from modeling of measured lactate levels during visual stimulation. *J Neurochem* **109 Suppl 1,** 55-62.

Murin R., Mohammadi G., Leibfritz D. and Hamprecht B. (2009a) Glial metabolism of isoleucine. *Neurochem Res* **34,** 194-204.

Murin R., Mohammadi G., Leibfritz D. and Hamprecht B. (2009b) Glial metabolism of valine. *Neurochem Res* **34,** 1195-1203.

Pascual J. M., Carceller F., Roda J. M. and Cerdan S. (1998) Glutamate, glutamine, and GABA as substrates for the neuronal and glial compartments after focal cerebral ischemia in rats. *Stroke* **29,** 1048-1056; discussion 1056-1047.

Pellerin L. and Magistretti P. J. (1994) Glutamate uptake into astrocytes stimulates aerobic glycolysis: a mechanism coupling neuronal activity to glucose utilization. *Proc Natl Acad Sci U S A* **91,** 10625-10629.

Pellerin L., Bouzier-Sore A. K., Aubert A., Serres S., Merle M., Costalat R. and Magistretti P. J. (2007) Activity-dependent regulation of energy metabolism by astrocytes: an update. *Glia* **55,** 1251-1262.

Phillis J. W., Ren J. and O'Regan M. H. (2001) Studies on the effects of lactate transport inhibition, pyruvate, glucose and glutamine on amino acid, lactate and glucose release from the ischemic rat cerebral cortex. *J Neurochem* **76,** 247-257.

Racher A. J., Looby D. and Griffiths J. B. (1990) Use of lactate dehydrogenase release to assess changes in culture viability. *Cytotechnology* **3,** 301-307.

Richter-Landsberg C. and Besser A. (1994) Effects of organotins on rat brain astrocytes in culture. *J Neurochem* **63,** 2202-2209.

Riera J. J., Schousboe A., Waagepetersen H. S., Howarth C. and Hyder F. (2008) The micro-architecture of the cerebral cortex: functional neuroimaging models and metabolism. *Neuroimage* **40,** 1436-1459.

Rossi D. J., Brady J. D. and Mohr C. (2007) Astrocyte metabolism and signaling during brain ischemia. *Nat Neurosci* **10,** 1377-1386.

Sá Santos S., Fonseca L. L., Monteiro M. A., Carrondo M. J. and Alves P. M. (2005) Culturing primary brain astrocytes under a fully controlled environment in a novel bioreactor. *J Neurosci Res* **79,** 26-32.

Schurr A. (2002) Lactate, glucose and energy metabolism in the ischemic brain (Review). *Int J Mol Med* **10,** 131-136.

Shank R. P., Leo G. C. and Zielke H. R. (1993) Cerebral metabolic compartmentation as revealed by nuclear magnetic resonance analysis of D-[1-13C]glucose metabolism. *J Neurochem* **61,** 315-323.

Shank R. P., Bennett G. S., Freytag S. O. and Campbell G. L. (1985) Pyruvate carboxylase: an astrocyte-specific enzyme implicated in the replenishment of amino acid neurotransmitter pools. *Brain Res* **329,** 364-367.

Shen J., Rothman D. L., Behar K. L. and Xu S. (2009) Determination of the glutamate-glutamine cycling flux using two-compartment dynamic metabolic modeling is sensitive to astroglial dilution. *J Cereb Blood Flow Metab* **29,** 108-118.

Silver I. A., Deas J. and Erecinska M. (1997) Ion homeostasis in brain cells: differences in intracellular ion responses to energy limitation between cultured neurons and glial cells. *Neuroscience* **78,** 589-601.

Sochocka E., Juurlink B. H., Code W. E., Hertz V., Peng L. and Hertz L. (1994) Cell death in primary cultures of mouse neurons and astrocytes during exposure to and 'recovery' from hypoxia, substrate deprivation and simulated ischemia. *Brain Res* **638,** 21-28.

Swanson R. A., Farrell K. and Stein B. A. (1997) Astrocyte energetics, function, and death under conditions of incomplete ischemia: a mechanism of glial death in the penumbra. *Glia* **21,** 142-153.

Szpetnar M., Pasternak K. and Boguszewska A. (2004) Branched chain amino acids (BCAAs) in heart diseases (ischaemic heart disease and myocardial infarction). *Ann Univ Mariae Curie Sklodowska [Med]* **59,** 91-95.

Teixeira A. P., Santos S. S., Carinhas N., Oliveira R. and Alves P. M. (2008) Combining metabolic flux analysis tools and (13)C NMR to estimate intracellular fluxes of cultured astrocytes. *Neurochem Int* **52,** 478-486.

Tekkok S. B., Brown A. M., Westenbroek R., Pellerin L. and Ransom B. R. (2005) Transfer of glycogen-derived lactate from astrocytes to axons via specific monocarboxylate transporters supports mouse optic nerve activity. *J Neurosci Res* **81,** 644-652.

Thoren A. E., Helps S. C., Nilsson M. and Sims N. R. (2005) Astrocytic function assessed from 1-14C-acetate metabolism after temporary focal cerebral ischemia in rats. *J Cereb Blood Flow Metab* **25,** 440-450.

Varma A. and Palsson B. O. (1994) Stoichiometric flux balance models quantitatively predict growth and metabolic by-product secretion in wild-type Escherichia coli W3110. *Appl Environ Microbiol* **60,** 3724-3731.

Walls A. B., Heimburger C. M., Bouman S. D., Schousboe A. and Waagepetersen H. S. (2009) Robust glycogen shunt activity in astrocytes: Effects of glutamatergic and adrenergic agents. *Neuroscience* **158,** 284-292.

Wang N. S. and Stephanopoulos G. (1983) Application of macroscopic balances to the identification of gross measurement errors. *Biotechnol Bioeng* **25,** 2177-2208.

Yager J. Y., Kala G., Hertz L. and Juurlink B. H. (1994) Correlation between content of high-energy phosphates and hypoxic-ischemic damage in immature and mature astrocytes. *Brain Res Dev Brain Res* **82,** 62-68.

Yu A. C., Drejer J., Hertz L. and Schousboe A. (1983) Pyruvate carboxylase activity in primary cultures of astrocytes and neurons. *J Neurochem* **41,** 1484-1487.

Yudkoff M. (1997) Brain metabolism of branched-chain amino acids. *Glia* **21,** 92-98.

Chapter 3

Metabolic Flux Analysis of Cultured Cerebellar Neurons: Effects of Hypoglycaemia

Adapted from

Estimation of intracellular fluxes in cerebellar neurons after hypoglycaemia: importance of the pyruvate recycling pathway and glutamine oxidation

Ana I Amaral, Ana P Teixeira, Ursula Sonnewald, Paula M Alves (2011) J Neurosci Res 89:700-710

Abstract

Although glucose is the primary cerebral fuel, the brain is able to metabolize other substrates under hypoglycaemia. Nevertheless, the metabolic consequences of this pathology at the cellular level remain largely unknown. Taking advantage of the metabolic flux analysis (MFA) methodology, this work aimed at investigating and quantifying the effects of hypoglycaemia on cerebellar neurons. After 12 h without glucose, primary cultures were incubated with medium containing [1,6-^{13}C]glucose and unlabelled glutamine and metabolism was monitored for 30 h. Metabolic rates of glucose, lactate, and amino acids were determined based on cell supernatant analysis and used to estimate metabolic fluxes with MFA. Percent ^{13}C enrichment time-profiles of different keto and amino acids were measured by mass spectrometry in cell extracts and compared to the MFA results. Hypoglycaemia decreased the glucose uptake rate and glycolytic metabolism by 35% whereas glutamine uptake was increased by 4-fold. Flux estimations fit well with data from ^{13}C labelling dynamics, indicating a significant activation of the pyruvate recycling pathway, accounting for 43% of the total pyruvate synthesized in control conditions and up to 71% after hypoglycaemia. Increased pyruvate recycling appeared to be mainly due to increased glutamine oxidation given the higher label dilution observed in the hypoglycaemia group. In summary, this work provides new evidence for pyruvate recycling as an important pathway for glutamine oxidation in cerebellar neurons, particularly after glucose deprivation.

CONTENTS

1 Introduction

Hypoglycaemia is a condition characterized by decreased blood glucose levels and occurs frequently in diabetic patients undergoing insulin therapy (Suh et al. 2007). In addition to other symptoms, acute hypoglycaemia was shown to affect cognitive functions leading to impaired judgment and decreased memory function, which were suggested to be caused by alterations of brain energy metabolism (Warren and Frier 2005). Glucose is the major brain energy fuel and its concentration in blood (3.9 – 7.1 mM) and brain (0.8 – 2.3 mM) shows a linear correlation (Gruetter et al. 1998). Thus, in the case of a hypoglycemic episode, where blood glucose concentrations decrease below 2 mM, brain glucose levels might easily approach zero, as consumption exceeds transport capacity (Suh et al. 2007). However, studies in subjects with type 1 diabetes and hypoglycaemia unawareness suggested that cerebral metabolism is able to adapt to the use of other substrates after repeated deprivation of glucose (Criego et al. 2005). For instance, (Mason et al. 2006) reported an increase in cerebral metabolism of acetate in those patients and (Suh et al. 2005) showed that pyruvate improved cognitive function in rats after insulin-induced hypoglycaemia by circumventing a sustained impairment of neuronal glucose metabolism.

Brain metabolism depends on important neuronal-glial coupling mechanisms due to distinct enzymes and pathways occurring in each of these cell types (McKenna et al. 2006b) and controversy still exists regarding the cellular compartments where glucose or lactate are mainly metabolized under different conditions (Pellerin et al. 2007; Bak et al. 2009). Nevertheless, it has been proposed that neurons metabolize both substrates, depending on their relative concentrations under resting or activated conditions (Cerdan et al. 2006). Furthermore, the glutamate-glutamine cycle has been shown not to be stoichiometric, being able to provide glutamate or glutamine as energy substrates for neurons and astrocytes, depending on cellular requirements (McKenna 2007). These amino acids can only be oxidized in the tricarboxylic acid (TCA) cycle and for complete oxidation to occur a 4 carbon unit has to leave the cycle at the malate or oxaloacetate

nodes and re-enter afterwards as pyruvate (Cruz et al. 1998). This pathway, named "pyruvate recycling" was first reported in the brain by Cerdan and colleagues (Cerdan et al. 1990), who subsequently demonstrated that it should be mainly localized in neurons, contributing with 17% of the total pyruvate metabolized via pyruvate dehydrogenase (Kunnecke et al. 1993). However, contradicting data have been obtained regarding the cellular localization of this pathway. Later studies based on ^{13}C nuclear magnetic resonance (NMR) spectroscopy analysis, either in animals or cell cultures, suggested that pyruvate recycling took place predominantly in astrocytes, accounting for a significant amount of the lactate produced in this compartment (Bakken et al. 1997; Haberg et al. 1998; Alves et al. 2000; Waagepetersen et al. 2002). More recently, pyruvate recycling was shown to occur to a significant extent in cerebellar co-cultures (Bak et al. 2007) or monotypic cultures of cerebellar neurons (Olstad et al. 2007b). In principle, the presence of a pyruvate recycling pathway gives tissues the ability to continuously maintain sufficient energy metabolism when substrates such as glucose and ketone bodies are low. Thus, further investigation of the localization and importance of this pathway in the brain might provide important knowledge on the cellular responses to hypoglycaemia.

The use of ^{13}C-labelled compounds and mass spectrometry has enabled the investigation of different metabolic aspects using brain cell cultures in recent decades (Bak et al. 2007; Johansen et al. 2007; Olstad et al. 2007a). In this work, gas chromatography-mass spectrometry (GC-MS) was used to investigate the time-profiles of ^{13}C-glucose metabolism in astrocytes after a 12 h period of hypoglycaemia mimicked by glucose deprivation. Additionally, the Metabolic Flux Analysis (MFA) methodology (Teixeira et al. 2008; Amaral et al. 2010) was applied to estimate and quantify the effects of hypoglycaemia on intracellular metabolic fluxes of cerebellar neurons. The combination of data obtained using these different tools provided important knowledge regarding the role of glutamine and pyruvate recycling in neuronal metabolism both before and after hypoglycaemia.

2 Materials and Methods

2.1 Materials

Plastic tissue culture dishes (6-wells) were purchased from Nunc (Roskilde, Denmark); fetal calf serum from Seralab Ltd. (Sussex, UK); penicillin–streptomycin (Pen-Strep) solution was purchased from GIBCO, Invitrogen (Paisley, UK); Dulbecco's modified Eagle's Medium (DMEM), cat number D5030, was purchased from SIGMA-Aldrich (Steinheim, Germany), ^{13}C-labelled glucose was purchased from Cambridge Isotope Laboratories (Andover, MA, USA); N–Methyl-N-(t-Butyldimethylsilyl) trifluoroacetamide (MTBSTFA) + 1% t-butyldimethylchlorosilane (t-BDMS-Cl) was purchased from Regis Technologies (Morton Grove, IL, USA); toluene and acetonitrile were purchased from LabScan (Gliwice, Poland); all other chemicals were purchased from SIGMA-Aldrich (Steinheim, Germany). 7-day-old mice (NMRI) were purchased from Møllegaard Breeding Center (Ejby, Denmark).

2.2 Cerebellar neurons and culture conditions

All animal procedures were conducted according to national regulations. Cerebella were dissected from 7-day-old mice and cells were isolated following a previously described protocol (Olstad et al. 2007a). Briefly, the brain tissue was trypsinized followed by trituration in a DNase solution (100 µg/ml) containing a trypsin inhibitor from soybeans. Cells were suspended (2.5 x 10^6 cells/ml) in a slightly modified DMEM, containing 31 mM glucose; 0.45 mM glutamine, 7.3 µM *p*-aminobenzoic acid, 4 µg/l insulin; 100 U/ml Pen-Strep and 10% (v/v) fetal calf serum and seeded in 6-wells culture dishes coated with poly-D-lysine (50 mg/l). 2 ml of medium were used per well. Cytosine arabinoside (20 µM) was added after 24–48 h to prevent the proliferation of astrocytes. This protocol yields a culture 90% enriched in cerebellar granule neurons with a maximum of 5% glial cells (Drejer et al. 1985; Drejer and Schousboe 1989).

2.3 Hypoglycaemia in cerebellar neuronal cultures

After 7 days *in vitro*, the cultures were divided in two groups and incubated with 2 ml of medium containing 2.5 mM glutamine, 1% fetal calf serum, 100 (U/ml) Pen-Strep, 3 mM glucose (control group) or without glucose (hypoglycaemia group) after gently washing the cells with phosphate-buffered saline (PBS). After 12 h of incubation, the medium was again replaced by fresh medium with the composition described above, containing 3 mM [1,6-^{13}C] glucose and 2 mM unlabelled glutamine. The period of 12 h of glucose deprivation mimics a prolonged fasting period that can occur either in normal or diabetic subjects, for example, overnight. During approximately 30 h samples were collected at several time points (0, 4, 8, 13.5, 23.5, 29.5 h). The cell supernatant was removed and centrifuged at 3000 x g for 5 min. Cells were washed twice with cold PBS and extracted with 70% (v/v) ethanol. Cells were scraped off the dishes and centrifuged at 20000 x g for 15 min to separate metabolites from insoluble proteins and other macro molecules. The resulting supernatants (cell extracts) were stored at -80 ^{o}C until further analyses. The pellets (obtained after cell extraction) and supernatant samples were stored at -20^{o}C.

2.4 Quantification of total glucose, lactate, and amino acids

Glucose and lactate concentrations in cell supernatant samples were determined in a RAPIDLab 1265 blood gas analyzer (Siemens AG, Erlangen, Germany). Amino acids in cell supernatant samples and cell extracts were quantified by HPLC on a Hewlett Packard 1100 system (Agilent Technologies, Palo Alto, CA, USA). The amino acids were pre-column derivatized with *o*-phthaldialdehyde and subsequently separated on a ZORBAX SB-C18 (4.6 mm x 150 mm, 3.5 µm) column from Agilent using a phosphate buffer (50 mM, pH 5.9) and a solution of methanol (98.75%) and tetrahydrofurane (1.25%) as eluents as described before (Olstad et al. 2007a). Prior to derivatization, sample proteins were precipitated by adding an equal volume of acetonitrile and removed by centrifugation at 12,400×g for 15 min, at room temperature. An internal

standard (α-aminobutyric acid) was added to ensure consistent measurements between runs. The separated amino acids were detected by fluorescence and quantified by comparison to a standard curve of standard solutions of amino acids run after every twelve samples. The method's detection limit was 1 µM.

2.5 Determination of Protein Content

The pellets obtained after cell extraction were freeze-dried to remove any rest of ethanol, suspended in 1 M NaOH and incubated at 37°C to ensure complete dissolution of the protein. Since cells were carefully washed twice before extraction, protein content in the extracts corresponds only to viable cells, as possible dead cells in suspension were removed by the washing steps. The bicinchoninic acid (BCA) protein assay from Pierce (Rockford, IL, USA) was used to determine total protein amounts using bovine serum albumin as standard.

2.6 Gas Chromatography-Mass Spectrometry

The pH of the cell extracts in 70% ethanol was adjusted to pH < 2 with 6 M HCl and the samples were then dried under atmospheric air. The metabolites were extracted into an organic phase of ethanol and benzene and dried again under atmospheric air. N,N-Dimethylformamide (DMF) was added before derivatization with MTBSTFA in the presence of 1% t-BDMS-Cl as described before (Olstad et al. 2007a). The samples were analyzed on an Agilent 6890 gas chromatograph with a capillary column (WCOT fused silica 25x 0.25 mm ID, CP-SIL 5CB-MS, Varian), connected to an Agilent 5975B mass spectrometer with electron impact ionization. Atom percent excess (^{13}C) was determined after calibration using unlabelled standard solutions (Biemann 1962).

2.7 Metabolic fate of [1,6-^{13}C] glucose in cerebellar neurons

Interpretation of the results obtained from GC-MS is based on the metabolic fate of [1,6-^{13}C]glucose which enters neurons and is transformed via glycolysis to [3-^{13}C]pyruvate. The latter can be converted to [3-^{13}C]lactate or [3-^{13}C]alanine or be transported into

mitochondria to enter the TCA cycle as [2-^{13}C]acetyl-CoA. Condensation of [2-^{13}C]acetylCoA with unlabelled oxaloacetate will, after several steps, lead to the formation of [4-^{13}C]glutamate and to either [2-^{13}C]- or [3-^{13}C]aspartate after the scrambling of a 4-carbon unit via the action of fumarase and malate dehydrogenase, at the succinate step. These compounds have one ^{13}C atom and are thus detected as M+1 isotopomers in GC-MS. If labelled oxaloacetate condenses with labelled acetyl-CoA, double labelled metabolites are formed and they will be detected as M+2 by GC-MS.

2.8 Data Analysis

Consumption or production rates of glucose, lactate and amino acids whose concentrations changed with time in the culture supernatant were calculated by performing a linear regression analysis to the different time points corresponding to samples collected throughout the experiments, followed by correction for the average amount of cellular protein (average values of 0.07 ± 0.01 mg and 0.09 ± 0.01 mg were obtained for control and hypoglycaemia groups, respectively). These experimentally determined metabolic rates were then used to feed the MFA model in order to estimate intracellular metabolic fluxes (see next section). Peaks from mass spectra were integrated, and atom percent excess (^{13}C) of the selected metabolites was determined after calibration using unlabelled standard solutions (Biemann 1962). Alanine, glutamate, α-ketoglutarate, malate, aspartate, and citrate were analyzed in cell extracts and lactate and alanine were analyzed in cell supernatant samples collected at the end of the incubation with [1,6-^{13}C]glucose. Data from ^{13}C enrichment time-courses in intracellular metabolites were not used for metabolic modelling purposes but only to help interpreting MFA results and to evaluate their validity. Results are presented as means ± s.d. Differences between groups were analyzed using two-tailed Student's *t*-test, and $p < 0.05$ was considered statistically significant.

2.9 Metabolic Flux Analysis

MFA is a well established technique for the determination of flux distribution in metabolic networks (Lee et al. 1999). This technique relies on the assumption of metabolic pseudo-steady-state for intracellular metabolite concentrations, which means that their accumulation inside the cells is negligible and, thus, the sum of the fluxes of synthesis and consumption of any metabolite is equal to zero. The pseudo-steady-state approximation is generally accepted as reasonable and valid in a wide range of scenarios due to the very high turnover of the pools of most metabolites, especially those participating in central metabolism (Lee et al. 1999). Consequently, the concentrations of the different metabolite pools rapidly adjust to new levels even after large perturbations in the environment experienced by the cells (Lee et al. 1999). Examples of applications of the steady-state approximation to similar culture systems (primary cultures) to that used in the present work are studies from (Chan et al. 2003; Teixeira et al. 2008). The intracellular flux distribution is estimated on the basis of this steady-state assumption, on the network stoichiometry, and using the information from transmembrane rates of metabolites measured in the culture supernatant (Lee et al. 1999), which need to be linear, indicating that the fluxes are constant. The biochemical network considered to represent the metabolism of neurons is shown in Figure 3.1 and it includes the main reactions involved in central carbon metabolism, namely glycolysis, TCA cycle and amino acids metabolism. The complete list of reactions is presented in Appendix 2. The network considers 44 reactions, from which 13 are experimentally measured transmembrane rates (Table 3.1), and 34 internal (balanced) metabolites. The weighted least-squares method was used to calculate the unknown fluxes (Wang and Stephanopoulos 1983) (for further details in the calculation of metabolic fluxes see Lee et al, 1999 and Teixeira et al, 2008). The consistency index, *h*, was determined and compared with the χ^2-test function (degrees of freedom are equal to the number of redundant equations) to evaluate the consistency of the experimental values along with the assumed biochemistry and the pseudo-steady-state assumption (Wang and

Stephanopoulos 1983). The above-mentioned calculations were performed using the CellNetAnalyzer software (Klamt et al. 2007).

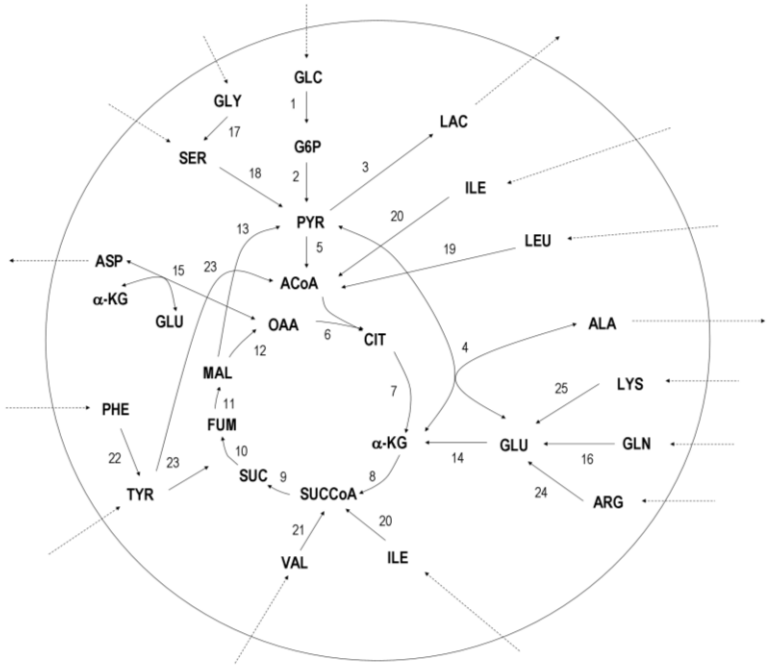

Figure 3.1 - Schematic representation of the metabolic network used to estimate metabolic fluxes of cerebellar granule neurons by MFA. The detailed stoichiometry of the reactions considered is given in Appendix 2 (supplementary material). Abbreviations: GLC, glucose; G6P, glucose-6-phosphate; PYR, pyruvate; LAC, lactate; GLU, glutamate; ALA, alanine; α-KG, α-ketoglutarate; OAA, oxaloacetate; CIT, Citrate; SUCCoA, succinyl-coenzyme A; SUC, succinate; FUM, fumarate; MAL, malate; ASP, aspartate; GLN, glutamine; GLY, glycine; SER, serine; LEU, leucine; ILE, isoleucine; VAL, valine; PHE, phenylalanine; TYR, Tyrosine; ARG, arginine; LYS, lysine.

3 Results

3.1 Glucose, lactate and amino acids metabolism

To study the effect of hypoglycaemia on neuronal metabolism, primary cultures of cerebellar granule neurons were subjected to 12 h of glucose deprivation and subsequently incubated in medium containing 3 mM [1,6-^{13}C]glucose and unlabelled glutamine for ~30 h. Protein content remained constant throughout the experiment. In

addition, cell inspection under an inverted microscope showed that cells remained attached to the culture dish surface, exhibiting a regular morphology, and no cells in suspension were observed, even at the end of the experiments (data not shown). Thus, it appears that no significant cell death occurred during the experiments.

Metabolic rates obtained for glucose, lactate and amino acids are presented in Table 3.1. Neurons subjected to hypoglycaemia presented both decreased glucose consumption and lactate production rates and a lower lactate to glucose (Lac/Glc) ratio, when compared to the control group (1.4 vs. 2, respectively), suggesting a higher degree of glucose oxidation. Concerning metabolic rates of amino acids, glutamine consumption was significantly increased after hypoglycaemia. Leucine and valine consumption rates presented a slight although not significant decrease after hypoglycaemia, whereas glycine and lysine were only consumed in the control group and alanine synthesis was also unaffected by hypoglycaemia.

Table 3.1 - Experimentally determined consumption/production rates (nmol.mg prot^{-1}.h^{-1}) of the main metabolites involved in neuronal metabolism.

	Control	Hypoglycaemia
rGlc	-296 ± 47	-190 ± 20*
rLac	595 ± 31	260 ± 20*
	Lac/Glc = 2	Lac/Glc = 1.4
rAla	17 ± 5	28 ± 4
rGln	-170 ± 130	-700 ± 100*
rArg	-40 ± 10	-30 ± 10
rSer	-50 ± 10	-30 ± 10
rGly	-117 ± 32	0*
rTyr	0	-30 ± 10*
rLys	-130 ± 60	0*
rVal	-150 ± 60	-80 ± 30
rIle	-140 ± 60	-110 ± 30
rLeu	-130 ± 50	-90 ± 30
rPhe	-40 ± 20	-40 ± 10

Cerebellar granule neurons were incubated for 12 h in DMEM with or without (hypoglycaemia) 3 mM glucose and subsequently medium was changed to DMEM containing 3 mM [1,6-^{13}C]glucose and unlabelled glutamine. Samples of culture supernatant were collected at different time points during ~30 h of incubation. Glucose, lactate and amino acid concentrations were later quantified and their specific consumption or production rates were determined (for details see Materials and Methods). Negative values refer to consumption rates. Results are presented as means ± standard error of regression analysis performed with all time-points (n=4). $p<0.05$ was considered statistically significant (Student's *t*-test).

*Different from control. Abbreviations: Glc (glucose), Lac (lactate), Ala (alanine), Gln (glutamine), Arg (arginine), Ser (serine), Gly (glycine), Tyr (Tyrosine), Lys (lysine), Val (valine), Ile (isoleucine), Leu (leucine), Phe (phenylalanine).

Intracellular content of some amino acids was quantified by HPLC in cell extracts at different incubation times (see Materials and Methods); average values are presented in Table 3.2. Alanine and glutamine pools were higher in the control group. The values obtained for glutamine pools are much larger than those reported by Olstad et al (2007a) (between 57 and 84 nmol/mg protein in the presence of 0.5 mM glutamine), probably due to the higher concentration of glutamine in the culture medium (2 mM). Glutamate pool sizes were much lower than those observed for glutamine but in the range of values previously reported for incubations in medium without glutamate (Olstad et al. 2007a; Peng et al. 2007).

Table 3.2- Cellular content (nmol/mg protein) of amino acids in cerebellar granule neurons.

	Control	Hypoglycaemia
Alanine	119 ± 22	85 ± 21*
Glutamate	126 ± 22	84 ± 47
Glutamine	1092 ± 276	571 ±185*

Cerebellar granule neurons were incubated for 12 h in DMEM with or without (hypoglycaemia) 3 mM glucose and subsequently medium was exchanged to DMEM containing 3 mM [1,6-^{13}C]glucose and unlabelled glutamine. During ~30 h of incubation, cell extracts were performed at different time-points and amino acids were later quantified as described in Materials and Methods. Results are presented as mean ± s. d of all time points as no significant changes were observed with time for each group (n=4). $p<0.05$ was considered statistically significant (Student's *t*-test). * Different from control.

3.2 ^{13}C enrichment in intracellular and extracellular metabolites

^{13}C enrichment (in atom percent excess) time-courses of some intracellular metabolites (citrate, glutamate, malate and aspartate) were followed by GC-MS and results are shown in Figure 3.2. Table 3.3 presents the values obtained for intra and extracellular metabolites at the end of the experiments. After 30 h of incubation with [1,6-^{13}C]glucose, only a maximum of 32% ^{13}C enrichment (sum of M+1 and M+2) was achieved (citrate), which shows a slow rate of incorporation of label in TCA cycle intermediates of cerebellar neurons and also suggests the significant contribution of other (unlabelled) metabolites. As expected, slightly lower labelling rates were observed in the hypoglycaemia group (Figure 3.2 - filled symbols), as the uptake of glucose was

35% less compared to the control group. In hypoglycaemia group, ^{13}C time-courses suggested that an intracellular labelling steady-state was reached, which was not observed for the control group. In both groups, percent ^{13}C enrichment in glutamate (Figure 3.2B) and α-ketoglutarate (data not shown) were comparable, although lower, than that observed for the other TCA cycle-related metabolites. Malate and aspartate labelling time-courses were also comparable (Figure 3.2C and 3.2D). In addition, intracellular alanine presented the highest enrichment in both groups (alanine M+1 ~65%; Table 3.3).

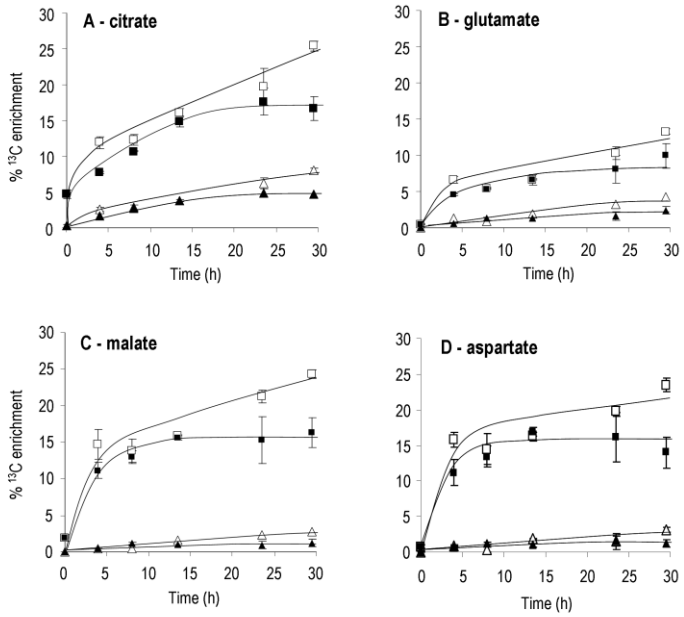

Figure 3.2- Effect of hypoglycaemia on percent ^{13}C enrichment in citrate (A), glutamate (B), malate (C) and aspartate (D) as detected by GC/MS. Cell extracts of cultured cerebellar neurons were performed at different time-points during incubation with [1,6-^{13}C]glucose, as described in Materials and Methods. Filled symbols – cells previously subjected to 12h of hypoglycaemia; white symbols - control conditions. Squares refer to molecules labelled in one carbon (M+1) and triangles refer to molecules labelled in two carbon positions (M+2). Note: black lines in the graphics were drawn in order to illustrate better the tendency of the data and do not represent any model fitting.

GC-MS analysis of the culture supernatant at the end of the experiments revealed significantly lower ^{13}C enrichment in secreted metabolites from the hypoglycaemia group (Table 3.3). Extracellular alanine was less enriched than its intracellular pool and also

compared to extracellular lactate, in both cases significantly lower in the hypoglycaemia group (Table 3.3).

Table 3.3- Percent ^{13}C enrichment in metabolites from cell extracts and supernatants of cerebellar neuronal cultures.

Cell Extracts	Control		Hypoglycaemia	
	M+1	M+2	M+1	M+2
Citrate	25.4 ± 0.7	8.0 ± 0.4	18.2 ± 1.5 *	5.3 ± 0.5 *
α-Ketoglutarate	10.7 ± 1.9	2.0 ± 1.5	7.0 ± 3.0	0.2 ± 0.3 *
Glutamate	13.3 ± 0.4	4.3 ± 0.2	7.4 ± 0.4 *	1.7 ± 0.1
Malate	24.3 ± 0.6	2.8 ± 0.4	16.3 ± 2.1 *	1.2 ± 0.3 *
Aspartate	23.5 ± 1.0	3.1 ± 0.3	12.7 ± 1.3 *	1.3 ± 0.5 *
Alanine	64.7 ± 2.5	0.39 ± 0.04	62 ± 8	0.8 ± 0.3 *
Supernatant	M+1	Concentration (mM)	M+1	Concentration (mM)
Alanine	47.9 ± 0.1	0.057 ± 0.002	43.6 ± 0.8 *	0.052 ± 0.007
Lactate	70.7 ± 0.8	0.85 ± 0.06	64.3 ± 0.3 *	0.55 ± 0.06

Cerebellar granule neurons were incubated for 12 h in DMEM with or without (hypoglycaemia) 3 mM glucose and subsequently medium was exchanged to DMEM containing 3 mM [1,6-^{13}C]glucose. After ~30 h of incubation, % ^{13}C enrichment in intra- and extracellular metabolites was analyzed by GC-MS. Extracellular concentration of lactate was measured using a blood gas analyzer and alanine was measured by HPLC, according to Materials and Methods. Results are presented as means ± s.d. in atom percent excess (n=4). $^{*}p<0.05$ vs. control (Student's *t*-test).

3.3 Metabolic flux distributions

To investigate in detail the main effects of 12 h of hypoglycaemia on the metabolism of cerebellar granule neurons, intracellular metabolic fluxes were estimated using MFA (Figure 3.3). A consistency test was performed (Wang and Stephanopoulos 1983) indicating that the biochemical network's stoichiometry and the metabolic steady-state assumption are consistent with the experimental data. MFA results reflect the measured metabolic rates for glucose and lactate, showing that the rate of anaerobic glycolysis was higher in control conditions and, conversely, the PDH flux was increased by hypoglycaemia (Figure 3.3A). In general, the fluxes of the TCA cycle reactions were similar between groups (Figure 3.3B), except for the reaction of conversion of α-ketoglutarate into succinyl-CoA, which was increased in the hypoglycaemia group. This can be explained by the higher flux of glutamine conversion into glutamate, meaning a higher carbon flux entering the TCA cycle at the α-ketoglutarate node. Additionally, the ratio between TCA cycle fluxes and glycolysis was higher in the hypoglycaemia group,

indicating that oxidative metabolism was augmented, when comparing to glycolysis (Figure 3.3). Pyruvate recycling flux (malate to pyruvate flux) was also increased by hypoglycaemia, probably also due to increased glutamine metabolism through the TCA cycle (Figure 3.3B). Concerning amino acids metabolism (Figure 3.3C), MFA results showed no significant differences between groups regarding most of the amino acids considered.

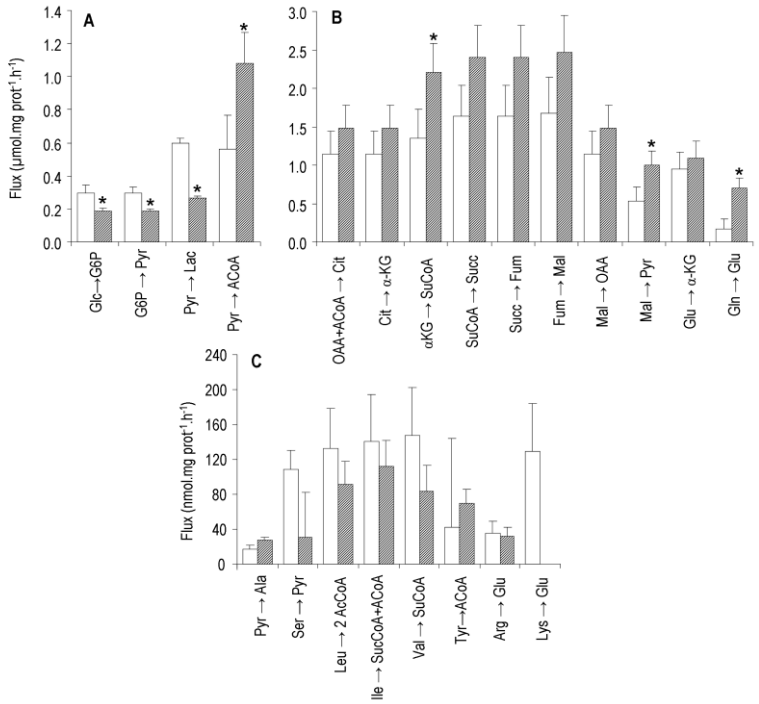

Figure 3.3 - Metabolic flux distributions estimated using MFA for the control group (white bars) and cells previously subjected to hypoglycaemia (grey bars). A – Reactions linked to glycolysis; B – TCA cycle-related reactions; C – Amino acids metabolism. Error bars correspond to standard deviations computed with the CellNetAnalyzer software by propagation of errors associated with rate estimations and experimental measurements. *$p<0.05$ vs. control (Student's *t*-test).

The careful analysis of key metabolic nodes of cellular metabolism offers valuable information on the fine-tuning of flux distributions in response to perturbations (Carinhas et al. 2010). Furthermore, the calculation of the partitioning coefficients

based on the MFA results allows to estimate values of ^{13}C enrichment for key intracellular metabolites, taking into account that all the glucose present in the culture medium ([1,6-^{13}C]glucose) was 99% enriched. Figure 3.4 schematizes the metabolic partitioning at the pyruvate (A), acetyl-CoA (B) and α-ketoglutarate (C) nodes in both scenarios analyzed by MFA, control and hypoglycaemia, as well as the calculated enrichments for the referred metabolites (see Appendix 3).

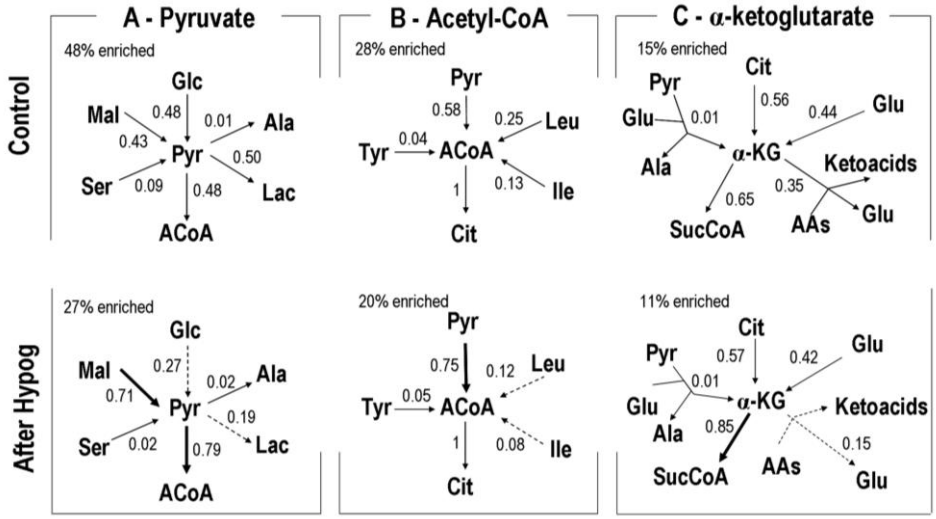

Figure 3.4 - Metabolic partitioning coefficients at the pyruvate (A), Acetyl-CoA (B) and α-ketoglutarate (C) nodes and respective values of ^{13}C enrichment estimated after metabolic node partitioning analysis based on MFA results. Coefficients were calculated based on all reaction rates leading to the formation or depletion of the metabolites in the centre of the node (see Appendix 3). Only the most representative pathways are included. Abbreviations: Glc, glucose, Ala, alanine; Lac, lactate; ACoA, acetyl-CoA; Ser, serine; Mal, malate; Pyr, pyruvate; Leu leucine; Ile, isoleucine; Cit, citrate; Tyr, tyrosine; Glu, glutamate; SucCoA, succinyl-CoA; α-KG, α-ketoglutarate; AAs, amino acids.

The estimations showed a marked reduction from 48% to 27% on pyruvate enrichment after hypoglycaemia, which was largely due to increased flux of pyruvate recycling through the malic enzyme (malate conversion into pyruvate) (Figure 3.4A); the fraction of pyruvate coming from malate was 43% in the control group, increasing to 71% after hypoglycaemia (Figure 3.4A). However, at the acetyl-CoA node (Figure 3.4B), the difference in enrichment between groups was not that pronounced due to the higher contribution of leucine and isoleucine catabolism to acetyl-CoA formation in the control

group, thus contributing to the dilution of the label from 48% to 28%, whereas the estimated enrichment in acetyl-CoA was 20% for the hypoglycaemia group. Regarding α-ketoglutarate, ^{13}C enrichment was further decreased in both groups, mainly due to glutamate (originated from unlabelled extracellular glutamine) conversion into α-ketoglutarate (Figure 3.4C). In addition, the results suggest that hypoglycaemia increased the fraction of α-ketoglutarate metabolized into succinyl-CoA (from 65% to 85%), compared to its conversion into glutamate, which is related to higher TCA cycle activity.

4 Discussion

4.1 General aspects of glucose, lactate and amino acids metabolism

In this work, neuronal metabolism of ^{13}C-labelled glucose was studied after a period of 12h hypoglycaemia in the presence of unlabelled glutamine, mimicking the presence of the astrocyte-derived glutamine, implicated in the glutamate-glutamine cycle (McKenna 2007). Our results suggest that after hypoglycaemia cerebellar neurons decrease their metabolic dependence on glucose, indicated by a 35% reduced glucose uptake rate, comparing to control conditions. In addition, the decreased Lac/Glc ratio and higher flux through PDH suggest a lower glycolytic activity and enhanced oxidative metabolism after hypoglycaemia. Although the rates obtained for glucose and lactate are within the ranges previously reported for cerebellar granule neurons (Schousboe et al. 1997; Waagepetersen et al. 2000; Dienel and Hertz 2001), the Lac/Glc ratio of 2 is not commonly observed in these cultures, being usually closer to 1 due to lower rates of lactate release (Schousboe et al. 1997). Eventually, in this case, the pyruvate recycling pathway (to be discussed below) might have contributed with additional lactate to be released.

Glutamine consumption rates were also in the range of values reported for cerebellar neurons (Olstad et al. 2007a), and increased significantly in cells subjected to hypoglycaemia. Similar findings have been observed in primary cultures of cerebellar neurons together with a 60% increase in [$^{14}CO_2$] production measured during 1 h of

glucose deprivation in the presence of 0.2 mM [U-^{14}C]glutamine (Peng et al. 2007). The same study also demonstrated that during hypoglycaemia, glutamine was able to maintain a significant rate of oxygen consumption, confirming that glutamine oxidation is an important energy source for cerebellar neurons. Hence, our results suggest that after hypoglycaemia, neuronal metabolism remained noticeably dependent on glutamine for at least 30 h. This will be further discussed below.

4.2 Metabolic fluxes in cerebellar neurons and effects of hypoglycaemia

The use of MFA allowed estimating intracellular fluxes of cerebellar neurons, providing also a detailed picture of the main metabolic alterations caused by 12 h of glucose deprivation. One can think that such a prolonged insult might have caused a transient change in the fluxes in the first hours after restoration of control conditions. In this context, flux estimation for the whole 30 h interval might lead to a loss of resolution regarding the metabolic changes caused by glucose deprivation. Nevertheless, the linearity exhibited by most of the extracellular metabolite time-courses during the 30 h period (data not shown) showed that there were no significant metabolic changes in those first hours. Thus, the adopted strategy seems to provide a reliable characterization of the metabolic response of cerebellar neurons to a prolonged period of hypoglycaemia. MFA results obtained in the recovery period (Figure 3.3) do not indicate major alterations in TCA cycle fluxes caused by hypoglycaemia; instead, the flux through glycolysis was significantly decreased in the group subjected to hypoglycaemia. The increase in the ratio between oxidative (TCA cycle) versus glycolytic fluxes after hypoglycaemia, compared to control, corroborates the importance of oxidative metabolism in neurons. In addition, it supports the concept that glutamine was the substrate responsible for the marked increase observed in the flux through PDH. On the other hand, higher brain glucose concentrations were observed in patients with type 1 diabetes and hypoglycaemia unawareness compared to controls under the same conditions (Criego et al. 2005). Moreover, the TCA cycle fluxes in the occipital cortex of diabetic patients were found unchanged, when comparing to healthy controls (Henry et

al. 2010). These observations can be correlated with the present results, namely regarding the observed decrease in glucose utilization after hypoglycaemia, which could contribute to higher glucose brain levels, and a preferential increase in glutamine metabolism, which was not assessed in the cited study.

In a recent work by our group, cultured cortical astrocytes were shown to increase their TCA cycle fluxes after a period of 5 hours of oxygen and glucose deprivation (Amaral et al. 2010) but still to values below those observed here for cerebellar neurons. On the other hand, the present results indicate that glucose utilization and lactate production rates are notably lower in cerebellar neurons than in astrocytes, which is in agreement with previously published data (Zwingmann and Leibfritz 2003; Bouzier-Sore et al. 2006). Evidently, these results should be carefully extrapolated to the *in vivo* situation due to the limitations underlying the cell culture environment, in particular due to the absence of contact with astrocytes, which occupy a large fraction of the brain volume and significantly contribute to the overall metabolic fluxes quantified in the intact brain *in vivo* (Lebon et al. 2002; Hyder et al. 2006). Nevertheless, the data actually support previous modeling results from *in vivo* measurements in rats, suggesting that neurons are responsible for the major fraction of energy generated through oxidative metabolism (Hyder et al. 2006). This is especially interesting taking into account the significant contribution of other substrates, such as glutamine, known to support neuronal metabolism (Schousboe et al. 1997). Noteworthy, ^{13}C magnetic resonance measurements in humans have shown that astroglial glutamine contributes significantly to support brain glutamatergic activity (Lebon et al. 2002).

4.3 Pyruvate recycling and hypoglycaemia

MFA allows investigating cellular metabolism at key metabolic nodes and to subsequently estimate the expected ^{13}C enrichment in those metabolites based on the calculated partitioning coefficients. Using this approach it was shown that MFA estimations fit well with experimental data obtained from GC-MS analyses. In fact, most

of the malate → pyruvate flux appears to be due to metabolism of unlabelled glutamine through the TCA cycle, which significantly dilutes the ^{13}C percent enrichment in the mitochondrial pyruvate pool and subsequently formed metabolites (see discussion below). The suggested pathway is the following: glutamine taken up by the neurons is oxidized after conversion to glutamate and subsequently enters the TCA cycle as α-ketoglutarate. It should be noted that the carbon skeleton of glutamate has to exit the TCA cycle in the step of malate and then re-enter as acetyl-CoA from pyruvate to be completely oxidized (McKenna et al. 2006b). This is part of the pyruvate recycling pathway for complete oxidation of glutamate. Eventually, incomplete recycling can occur through conversion of pyruvate to lactate or alanine.

The pyruvate recycling pathway was included in our model through the malic enzyme as this is thought to be the primary enzyme associated with pyruvate recycling in the brain, in particular its mitochondrial isozyme, highly present in synaptic terminals but also, to some extent, in cerebellar neurons (Cruz et al. 1998; Vogel et al. 1998; McKenna et al. 2000). Even so, many contradictory findings have been reported regarding the cellular localization of pyruvate recycling, since it was first described by Cerdan and colleagues (Cerdan et al. 1990; Kunnecke et al. 1993) (see introduction). The considerably higher pyruvate recycling flux estimated in the present work suggests that it might be more active in cerebellar neurons when a substantial amount of glutamine or glutamate is oxidized than when glucose or acetate are the main energy substrates. Pyruvate recycling also appears to be rather used for complete oxidation of glutamate and glutamine, thus leading to the release of labelled carbon atoms as CO_2. This would explain the difficulty in observing labelling in glutamate and aspartate after metabolism through this pathway (Haberg et al. 1998). Noteworthy, (Pascual et al. 1998) also observed increased flux due to augmented glutamine oxidation *in vivo* 24h after focal ischemia. Hence, our results bring new evidence supporting the potentially neuroprotective role of pyruvate recycling in conditions involving a lack of glucose supply as it has been shown that malic enzyme activity contributes to increased NADPH

production, which could consequently play an important role in detoxifying reactive oxygen species through the reduction of oxidized mitochondrial glutathione (Bukato et al. 1995; Vogel et al. 1999).

4.4 Metabolite enrichment, labelling dynamics and intracellular compartmentation

The analysis of ^{13}C enrichment of intracellular metabolites at several time-points provided detailed information on metabolite labelling dynamics from labelled glucose in cerebellar neurons. Apparently, labelling steady-state was achieved for most metabolites after 30 h in the hypoglycaemia group but not in the control. This could be related to lower pool sizes in the first group, observed at least for some metabolites (Table 3.2) which, together with higher PDH and TCA cycle fluxes and increased unlabelled glutamine metabolism, probably contributed to the faster achievement of this equilibrium.

Another relevant aspect concerns the discrepancies between enrichment of intra and extracellular alanine pools, extracellular lactate enrichment (Table 3.3) and estimated pyruvate enrichment (Figure 3.4). The existence of different pyruvate pools should be considered to interpret these observations. After [1,6-^{13}C]glucose metabolism through glycolysis, the cytosolic pool of pyruvate will be approximately 100% M+1 at labelling steady-state. This value can be slightly diluted due to some activity through the pentose phosphate pathway (PPP; not considered in our metabolic network), since the first carbon of glucose is lost as CO_2 in this pathway. PPP is thought to be very active in cortical neurons (Herrero-Mendez et al. 2009); however, the activity of the rate-limiting enzyme of this pathway, glucose-6-phosphate dehydrogenase, was barely detectable in cerebellar neurons (Biagiotti et al. 2003), suggesting that PPP activity should not be significant in these neurons. Then, pyruvate is transported into the mitochondria where the pyruvate recycling pathway will markedly dilute the labelling in its mitochondrial pool (down to 48% in control group and to 27% in the hypoglycaemia group – Figure 3.4). Some of this pyruvate might be transported back to the cytosol, where it will dilute the enrichment of the cytosolic pool and, subsequently, the intracellular lactate and

alanine pools and then, to some extent, their extracellular pools. In fact, studies on co-cultures of cerebellar neurons and astrocytes suggested that alanine and lactate might actually be produced form different neuronal pyruvate pools (Bak et al. 2007). Pyruvate compartmentation has also been reported in cortical neuronal cultures (Cruz et al. 2001; Bouzier-Sore et al. 2003). It should, however, be noted that the unlabelled fraction of lactate and alanine initially present in the medium (in part, due to the contribution of serum) reduces the maximum enrichment of the extracellular pools (alanine initially present in the medium represents 18% of its final value in both groups, whereas for lactate this percentage is 22% in control group vs. 40% in the hypoglycaemia group). In addition, a slower rate of alanine release into the medium could have contributed to a slower attainment of a labelling steady-state of this pool, which probably did not occur after 30h of incubation.

The estimated enrichments obtained after metabolic partitioning analysis on the acetyl-CoA and α-ketoglutarate nodes are also in good agreement with experimental values observed for citrate, malate and aspartate, supporting the assumption on the contribution of the pyruvate recycling flux (due to metabolism of unlabelled glutamine) to the dilution of pyruvate enrichment. The considerable label dilution estimated for glutamate and α-ketoglutarate, and confirmed by GC-MS, was observed in the same proportion in both groups, and therefore it does not seem to be related to hypoglycaemia. This can be explained taking into account the existence of mitochondrial and cytosolic glutamate pools and the fact that aspartate aminotransferase (AAT) catalyzes a transamination between α-ketoglutarate and glutamate in each of those compartments (see Hertz et al. 2000 for details). Hence, glutamate synthesized from glutamine in the mitochondria will be unlabelled and its contribution to the total glutamate pool will depend on the extent of the AAT activity (Hertz et al. 2000). The remaining fraction of α-ketoglutarate produced from glutamate will be metabolized in the TCA cycle and will be in equilibrium with α-ketoglutarate formed from isocitrate. It is important to note here that, since this methodology enables only the estimation of

net fluxes and not of fluxes through parallel or reversible reactions, the model provides only the net flux of glutamate production, including both the flux through AAT (reaction 15 in Figure 3.1 and Appendix 3) and that through glutamate dehydrogenase (GDH; reaction 14). The similar labelling dynamics observed for malate and aspartate (Figure 2C and 2D) show that AAT was active, supporting the existence of the malate-aspartate shuttle in these neurons (Ramos et al. 2003; McKenna et al. 2006a). Nevertheless, GDH should also be taken into account as it has been shown that cerebellar neurons have high GDH activity when compared to cortical neurons (Zaganas et al. 2001). Finally enrichment of TCA cycle metabolites downstream of α-ketoglutarate, such as malate, resembles that of citrate, appearing not to be so much affected by the metabolism of unlabelled glutamine, also suggesting the existence of distinct malate pools in cerebellar neurons.

4.5 Conclusion

In conclusion, the application of MFA allowed to estimate metabolic fluxes in primary cultures of cerebellar neurons and to predict quantitatively the effect of hypoglycaemia in the different metabolic pathways of these cells. Our results confirm that glutamine is an important energy substrate for cerebellar neurons in the recovery from hypoglycaemia. Furthermore, we provide new evidence on the crucial role of the pyruvate recycling pathway in this process, corroborating that pyruvate recycling is indeed an important metabolic pathway in cerebellar neurons, particularly after glucose deprivation.

5 Acknowledgements

This work was supported by the *Fundação para a Ciência e Tecnologia* (FCT), Portugal (project ref. PTDC/BIO/69407/2006 and PhD fellowship SFRH/BD/29666/2006 to A. Amaral) and the Norwegian Research Council. A.P. Teixeira acknowledges the MIT-Portugal Program. The technical assistance by Lars Evje, Bjørn Isak Håkonsen and

Sunniva Hoel from NTNU, Norway, is gratefully acknowledged. The authors also acknowledge Dr. Vicente Bernal and Nuno Carinhas from IBET, Portugal, for fruitful discussions and advice regarding metabolic flux analysis and statistical analysis.

6 References

Alves P. M., Nunes R., Zhang C., Maycock C. D., Sonnewald U., Carrondo M. J. and Santos H. (2000) Metabolism of 3-(13)C-malate in primary cultures of mouse astrocytes. *Dev Neurosci* **22,** 456-462.

Amaral A. I., Teixeira A. P., Martens S., Bernal V., Sousa M. F. and Alves P. M. (2010) Metabolic alterations induced by ischemia in primary cultures of astrocytes: merging (13)C NMR spectroscopy and metabolic flux analysis. *J Neurochem* **113**.

Bak L. K., Waagepetersen H. S., Melo T. M., Schousboe A. and Sonnewald U. (2007) Complex glutamate labeling from [U-13C]glucose or [U-13C]lactate in co-cultures of cerebellar neurons and astrocytes. *Neurochem Res* **32,** 671-680.

Bak L. K., Walls A. B., Schousboe A., Ring A., Sonnewald U. and Waagepetersen H. S. (2009) Neuronal glucose but not lactate utilization is positively correlated with NMDA-induced neurotransmission and fluctuations in cytosolic Ca2+ levels. *J Neurochem* **109 Suppl 1,** 87-93.

Bakken I. J., White L. R., Aasly J., Unsgard G. and Sonnewald U. (1997) Lactate formation from [U-13C]aspartate in cultured astrocytes: compartmentation of pyruvate metabolism. *Neurosci Lett* **237,** 117-120.

Biagiotti E., Guidi L., Del Grande P. and Ninfali P. (2003) Glucose-6-phosphate dehydrogenase expression associated with NADPH-dependent reactions in cerebellar neurons. *Cerebellum* **2,** 178-183.

Biemann K. (1962) *Mass spectrometry*, pp 223-227. McGraw-Hill, New York.

Bouzier-Sore A. K., Voisin P., Canioni P., Magistretti P. J. and Pellerin L. (2003) Lactate is a preferential oxidative energy substrate over glucose for neurons in culture. *J Cereb Blood Flow Metab* **23,** 1298-1306.

Bouzier-Sore A. K., Voisin P., Bouchaud V., Bezancon E., Franconi J. M. and Pellerin L. (2006) Competition between glucose and lactate as oxidative energy substrates in both neurons and astrocytes: a comparative NMR study. *Eur J Neurosci* **24,** 1687-1694.

Bukato G., Kochan Z. and Swierczynski J. (1995) Different regulatory properties of the cytosolic and mitochondrial forms of malic enzyme isolated from human brain. *Int J Biochem Cell Biol* **27,** 1003-1008.

Carinhas N., Bernal V., Monteiro F., Carrondo M. J., Oliveira R. and Alves P. M. (2010) Improving baculovirus production at high cell density through manipulation of energy metabolism. *Metab Eng* **12,** 39-52.

Cerdan S., Kunnecke B. and Seelig J. (1990) Cerebral metabolism of [1,2-13C2]acetate as detected by in vivo and in vitro 13C NMR. *J Biol Chem* **265,** 12916-12926.

Cerdan S., Rodrigues T. B., Sierra A., Benito M., Fonseca L. L., Fonseca C. P. and Garcia-Martin M. L. (2006) The redox switch/redox coupling hypothesis. *Neurochem Int* **48,** 523-530.

Chan C., Berthiaume F., Lee K. and Yarmush M. L. (2003) Metabolic flux analysis of cultured hepatocytes exposed to plasma. *Biotechnol Bioeng* **81,** 33-49.

Criego A. B., Tkac I., Kumar A., Thomas W., Gruetter R. and Seaquist E. R. (2005) Brain glucose concentrations in patients with type 1 diabetes and hypoglycemia unawareness. *J Neurosci Res* **79,** 42-47.

Cruz F., Scott S. R., Barroso I., Santisteban P. and Cerdan S. (1998) Ontogeny and cellular localization of the pyruvate recycling system in rat brain. *J Neurochem* **70,** 2613-2619.

Cruz F., Villalba M., Garcia-Espinosa M. A., Ballesteros P., Bogonez E., Satrustegui J. and Cerdan S. (2001) Intracellular compartmentation of pyruvate in primary cultures of cortical neurons as detected by (13)C NMR spectroscopy with multiple (13)C labels. *J Neurosci Res* **66,** 771-781.

Dienel G. A. and Hertz L. (2001) Glucose and lactate metabolism during brain activation. *J Neurosci Res* **66,** 824-838.

Drejer J. and Schousboe A. (1989) Selection of a pure cerebellar granule cell culture by kainate treatment. *Neurochem Res* **14,** 751-754.

Drejer J., Larsson O. M., Kvamme E., Svenneby G., Hertz L. and Schousboe A. (1985) Ontogenetic development of glutamate metabolizing enzymes in cultured cerebellar granule cells and in cerebellum in vivo. *Neurochem Res* **10,** 49-62.

Gruetter R., Ugurbil K. and Seaquist E. R. (1998) Steady-state cerebral glucose concentrations and transport in the human brain. *J Neurochem* **70,** 397-408.

Haberg A., Qu H., Bakken I. J., Sande L. M., White L. R., Haraldseth O., Unsgard G., Aasly J. and Sonnewald U. (1998) In vitro and ex vivo 13C-NMR spectroscopy studies of pyruvate recycling in brain. *Dev Neurosci* **20,** 389-398.

Henry P. G., Criego A. B., Kumar A. and Seaquist E. R. (2010) Measurement of cerebral oxidative glucose consumption in patients with type 1 diabetes mellitus and hypoglycemia unawareness using (13)C nuclear magnetic resonance spectroscopy. *Metabolism* **59,** 100-106.

Herrero-Mendez A., Almeida A., Fernandez E., Maestre C., Moncada S. and Bolanos J. P. (2009) The bioenergetic and antioxidant status of neurons is controlled by continuous degradation of a key glycolytic enzyme by APC/C-Cdh1. *Nat Cell Biol* **11,** 747-752.

Hertz L., Yu A. C., Kala G. and Schousboe A. (2000) Neuronal-astrocytic and cytosolic-mitochondrial metabolite trafficking during brain activation, hyperammonemia and energy deprivation. *Neurochem Int* **37,** 83-102.

Hyder F., Patel A. B., Gjedde A., Rothman D. L., Behar K. L. and Shulman R. G. (2006) Neuronal-glial glucose oxidation and glutamatergic-GABAergic function. *J Cereb Blood Flow Metab* **26,** 865-877.

Johansen M. L., Bak L. K., Schousboe A., Iversen P., Sorensen M., Keiding S., Vilstrup H., Gjedde A., Ott P. and Waagepetersen H. S. (2007) The metabolic role of isoleucine in detoxification of ammonia in cultured mouse neurons and astrocytes. *Neurochem Int* **50,** 1042-1051.

Klamt S., Saez-Rodriguez J. and Gilles E. D. (2007) Structural and functional analysis of cellular networks with CellNetAnalyzer. *BMC Syst Biol* **1,** 2.

Kunnecke B., Cerdan S. and Seelig J. (1993) Cerebral metabolism of [1,2-13C2]glucose and [U-13C4]3-hydroxybutyrate in rat brain as detected by 13C NMR spectroscopy. *NMR Biomed* **6,** 264-277.

Lebon V., Petersen K. F., Cline G. W., Shen J., Mason G. F., Dufour S., Behar K. L., Shulman G. I. and Rothman D. L. (2002) Astroglial contribution to brain energy metabolism in humans revealed by 13C nuclear magnetic resonance spectroscopy: elucidation of the dominant pathway for neurotransmitter glutamate repletion and measurement of astrocytic oxidative metabolism. *J Neurosci* **22,** 1523-1531.

Lee K., Berthiaume F., Stephanopoulos G. N. and Yarmush M. L. (1999) Metabolic flux analysis: a powerful tool for monitoring tissue function. *Tissue Eng* **5,** 347-368.

Mason G. F., Petersen K. F., Lebon V., Rothman D. L. and Shulman G. I. (2006) Increased brain monocarboxylic acid transport and utilization in type 1 diabetes. *Diabetes* **55,** 929-934.

McKenna M. C. (2007) The glutamate-glutamine cycle is not stoichiometric: fates of glutamate in brain. *J Neurosci Res* **85,** 3347-3358.

McKenna M. C., Waagepetersen H. S., Schousboe A. and Sonnewald U. (2006a) Neuronal and astrocytic shuttle mechanisms for cytosolic-mitochondrial transfer of reducing equivalents: current evidence and pharmacological tools. *Biochem Pharmacol* **71,** 399-407.

McKenna M. C., Gruetter R., Sonnewald U., Waagepetersen H. S. and Schousboe A. (2006b) Energy Metabolism of the Brain, in *Basic Neurochemistry: Molecular, Cellular and Medical Aspects,* Seventh Edition (Bazan N., ed.), pp 531-558. Elsevier Academic Press.

McKenna M. C., Stevenson J. H., Huang X., Tildon J. T., Zielke C. L. and Hopkins I. B. (2000) Mitochondrial malic enzyme activity is much higher in mitochondria from cortical synaptic terminals compared with mitochondria from primary cultures of cortical neurons or cerebellar granule cells. *Neurochem Int* **36,** 451-459.

Olstad E., Qu H. and Sonnewald U. (2007a) Glutamate is preferred over glutamine for intermediary metabolism in cultured cerebellar neurons. *J Cereb Blood Flow Metab* **27,** 811-820.

Olstad E., Olsen G. M., Qu H. and Sonnewald U. (2007b) Pyruvate recycling in cultured neurons from cerebellum. *J Neurosci Res* **85,** 3318-3325.

Pascual J. M., Carceller F., Roda J. M. and Cerdan S. (1998) Glutamate, glutamine, and GABA as substrates for the neuronal and glial compartments after focal cerebral ischemia in rats. *Stroke* **29,** 1048-1056; discussion 1056-1047.

Pellerin L., Bouzier-Sore A. K., Aubert A., Serres S., Merle M., Costalat R. and Magistretti P. J. (2007) Activity-dependent regulation of energy metabolism by astrocytes: an update. *Glia* **55,** 1251-1262.

Peng L., Gu L., Zhang H., Huang X., Hertz E. and Hertz L. (2007) Glutamine as an energy substrate in cultured neurons during glucose deprivation. *J Neurosci Res* **85,** 3480-3486.

Ramos M., del Arco A., Pardo B., Martinez-Serrano A., Martinez-Morales J. R., Kobayashi K., Yasuda T., Bogonez E., Bovolenta P., Saheki T. and Satrustegui J. (2003) Developmental changes in the Ca2+-regulated mitochondrial aspartate-glutamate carrier aralar1 in brain and prominent expression in the spinal cord. *Brain Res Dev Brain Res* **143,** 33-46.

Schousboe A., Westergaard N., Waagepetersen H. S., Larsson O. M., Bakken I. J. and Sonnewald U. (1997) Trafficking between glia and neurons of TCA cycle intermediates and related metabolites. *Glia* **21,** 99-105.

Suh S. W., Hamby A. M. and Swanson R. A. (2007) Hypoglycemia, brain energetics, and hypoglycemic neuronal death. *Glia* **55,** 1280-1286.

Suh S. W., Aoyama K., Matsumori Y., Liu J. and Swanson R. A. (2005) Pyruvate administered after severe hypoglycemia reduces neuronal death and cognitive impairment. *Diabetes* **54,** 1452-1458.

Teixeira A. P., Santos S. S., Carinhas N., Oliveira R. and Alves P. M. (2008) Combining metabolic flux analysis tools and (13)C NMR to estimate intracellular fluxes of cultured astrocytes. *Neurochem Int* **52,** 478-486.

Vogel R., Wiesinger H., Hamprecht B. and Dringen R. (1999) The regeneration of reduced glutathione in rat forebrain mitochondria identifies metabolic pathways providing the NADPH required. *Neurosci Lett* **275,** 97-100.

Vogel R., Jennemann G., Seitz J., Wiesinger H. and Hamprecht B. (1998) Mitochondrial malic enzyme: purification from bovine brain, generation of an antiserum, and immunocytochemical localization in neurons of rat brain. *J Neurochem* **71,** 844-852.

Waagepetersen H. S., Sonnewald U., Larsson O. M. and Schousboe A. (2000) A possible role of alanine for ammonia transfer between astrocytes and glutamatergic neurons. *J Neurochem* **75,** 471-479.

Waagepetersen H. S., Qu H., Hertz L., Sonnewald U. and Schousboe A. (2002) Demonstration of pyruvate recycling in primary cultures of neocortical astrocytes but not in neurons. *Neurochem Res* **27,** 1431-1437.

Wang N. S. and Stephanopoulos G. (1983) Application of macroscopic balances to the identification of gross measurement errors. *Biotechnol Bioeng* **25,** 2177-2208.

Warren R. E. and Frier B. M. (2005) Hypoglycaemia and cognitive function. *Diabetes Obes Metab* **7,** 493-503.

Zaganas I., Waagepetersen H. S., Georgopoulos P., Sonnewald U., Plaitakis A. and Schousboe A. (2001) Differential expression of glutamate dehydrogenase in cultured neurons and astrocytes from mouse cerebellum and cerebral cortex. *J Neurosci Res* **66,** 909-913.

Zwingmann C. and Leibfritz D. (2003) Regulation of glial metabolism studied by 13C-NMR. *NMR Biomed* **16,** 370-399.

Chapter 4

Improving metabolic flux estimation in astrocytes with ^{13}C isotopic transient MFA

Adapted from

A comprehensive metabolic profile of cultured astrocytes using isotopic transient metabolic flux analysis and ^{13}C-labelled glucose

Ana I Amaral, Ana P Teixeira Bjørn I Håkonsen, Ursula Sonnewald, Paula M Alves (2011) Front Neuroenerg 3:5 doi 10.3389/fnene.2011.00005

Abstract

Metabolic models have been used to elucidate important aspects of brain metabolism in recent years. This work applies for the first time the concept of isotopic transient ^{13}C metabolic flux analysis (MFA) to estimate intracellular fluxes in primary cultures of astrocytes. This methodology comprehensively explores the information provided by ^{13}C labelling time-courses of intracellular metabolites. Cells were incubated with medium containing [1-^{13}C]glucose for 24 h and samples of cell supernatant and extracts collected at different time-points were then analyzed by mass spectrometry and/or HPLC. Metabolic fluxes were estimated by fitting a carbon labelling network model to isotopomer profiles experimentally determined. Both the fast isotopic equilibrium of glycolytic metabolite pools and the slow labelling dynamics of TCA cycle intermediates are described well by the model. The large pools of glutamate and aspartate which are linked to the TCA cycle via reversible aminotransferase reactions are likely to be responsible for the observed delay in equilibration of TCA cycle intermediates. Furthermore, it was estimated that 11% of the glucose taken up by astrocytes was diverted to the pentose phosphate pathway. In addition, considerable fluxes through pyruvate carboxylase (PC) (PC/pyruvate dehydrogenase (PDH) ratio = 0.5), malic enzyme (5% of the total pyruvate production) and catabolism of branched-chained amino acids (contributing with ~40% to total acetyl-CoA produced) confirmed the significance of these pathways to astrocytic metabolism. Consistent with the need of maintaining cytosolic redox potential, the fluxes through the malate-aspartate shuttle and the PDH pathway were comparable. Finally, the estimated glutamate/α-ketoglutarate exchange rate (~0.7 μmol.mg prot^{-1}.h^{-1}) was similar to the TCA cycle flux. In conclusion, this work demonstrates the potential of isotopic transient MFA for a comprehensive analysis of energy metabolism.

CONTENTS

1 Introduction

Isotopic labelling experiments and ^{13}C NMR spectroscopy have been extensively applied to investigate particular aspects of cerebral metabolism both in cell cultures (Merle et al. 1996b; Waagepetersen et al. 2003; Sonnewald et al. 2004) and *in vivo* (Gruetter et al. 2001; Garcia-Espinosa et al. 2004; Hyder et al. 2006) due to the highly specific metabolic information generated. The metabolism of a ^{13}C labelled substrate through different pathways originates distinct labelling patterns and ^{13}C time-courses. These data can then be translated into quantitative metabolic fluxes using mathematical models. In fact, metabolic modelling was crucial to show the existence of metabolic compartmentation (Gruetter et al. 2001) and to determine the contributions from astrocytes (Lebon et al. 2002) and neurons (Hyder et al. 2006) to the overall oxidative metabolism of glucose in the brain.

Simple mathematical models have been used to estimate the PDH and PC fluxes based on steady-state ^{13}C fractional enrichment of glutamate or glutamine (Malloy et al. 1988; Martin et al. 1993; Merle et al. 1996b). On the other hand, more sophisticated models consisting of mass and isotope balances have been used to fit glutamine and glutamate ^{13}C time-courses from *in vivo* NMR experiments and estimate fluxes in relatively simple networks (Henry et al. 2006). These modelling studies have allowed estimating the main metabolic fluxes in the rodent and human brain: neuronal and glial TCA cycle, glial anaplerotic PC flux (V_{PC}), glutamate-glutamine cycle flux (V_{NT}) and glutamate/α-ketoglutarate exchange rate (V_x) (Henry et al. 2006 and references therein). In addition, Patel et al have developed a three compartment model (astrocytes, glutamatergic neurons and GABAergic neurons) to estimate the contribution of GABAergic activity to cerebral energetics (Patel et al. 2005). More recently, Jolivet et al reported a novel approach based on estimations of state-dependent brain energy budget for neurons and astrocytes using data sets of cerebral glucose and oxygen utilization during different brain activation states (Jolivet et al. 2009).

However, most current models do not consider flux routes that can contribute substantially to the observed isotopic labelling patterns. For instance, label dilution in glutamine and glutamate, usually attributed to metabolite exchange between brain and blood, could actually derive from the PPP or oxidation of fatty acids or of poorly labelled amino acids that might result from proteolysis (Dienel and Cruz 2009; Shen et al. 2009). These are usually not considered to avoid an increase in the complexity of the metabolic network. Consequently, a larger amount of data would be required to reliably identify all unknown fluxes, which is difficult when working *in vivo*. Therefore, many assumptions are generally used to determine metabolic fluxes *in vivo*. However, this issue has raised concern about the reliability of estimated fluxes based on isotopomers derived from ^{13}C glucose metabolism (Shestov et al. 2007).

In contrast to the metabolic modelling tools referred above, a more comprehensive metabolic picture can be provided by MFA, one of the first tools targeting systems level analysis of intracellular fluxes in microbial and animal cell cultures (Varma and Palsson 1994; Lee et al. 1999; Quek et al. 2010). This methodology requires the definition of material-balance equations for all metabolites included in the network. Then, by measuring a sufficient number of metabolite consumption/production rates in cell culture supernatants, intracellular fluxes can be estimated based on the network's stoichiometry and assuming intracellular steady-state (Lee et al. 1999). This implies that the sum of the fluxes leading to the synthesis and consumption of each metabolite is equal to zero and, consequently, intracellular metabolite pools will be constant. Using a simple network, we have recently characterized the effects of hypoglycaemia on metabolic fluxes of cultured cerebellar neurons using MFA (Amaral et al. 2011).

Still, MFA based on metabolite balancing alone does not allow well-resolved flux distributions, as the fluxes through parallel pathways or reversible reactions cannot be distinguished. To improve flux resolution, classical MFA has been complemented with ^{13}C labelling data collected at isotopic steady-state. This has been applied by our group to

characterize the metabolism of astrocytic cultures under normal conditions and after an ischemic episode (Teixeira et al. 2008; Amaral et al. 2010). In these studies, the steady-state label distribution in certain metabolites in the culture medium was analyzed and this information used to elucidate flux ratios in parallel routes that contribute differently to label distribution, such as the flux ratio of PC to PDH or the flux ratio of glycolysis to PPP.

Recently, Wiechert and Noh (2005) introduced the concept of non-stationary ^{13}C-MFA. In this methodology the metabolic steady-state is also assumed but the isotopic transient state (i.e., the time period during which the ^{13}C label is being distributed by the different metabolite isotopomers until isotopic steady state is reached) in intracellular metabolites is taken into consideration. In this case, mass isotopomers are analyzed at different time points, normally using sensitive MS techniques, to follow the label incorporation immediately after incubating cells with a labelled substrate (Hofmann et al. 2008). Current developments in MS enable a precise assessment of ^{13}C labelling in several metabolites of the main pathways of carbon metabolism in a relatively small sample volume (Noh et al. 2007). Subsequently, to translate the time-series labelling data into metabolic fluxes, such mathematical models combine balances of the total metabolite pools and of individual isotopomers, containing full information about the transition of the labelled carbons within metabolites (Wiechert and Noh 2005; Noh et al. 2007). Model inputs are isotopomer ^{13}C time-courses and some metabolite pools determined experimentally, in addition to the consumption or production rates of metabolites measured in cell supernatants. Isotopic transient MFA has been successfully applied to estimate fluxes in prokaryotic and mammalian cell systems (Schaub et al. 2008; Metallo et al. 2009). When comparing to the classical MFA, it has as main advantages not relying on uncertain cofactor balances and allowing the estimation of fluxes through both parallel and cyclic pathways as well as through bidirectional reactions (Wiechert and Noh 2005). It is, however, experimentally and computationally

more demanding, requiring the solution of a large number of differential equations (Noh et al. 2006; Noh and Wiechert 2006).

Hence, the main aim of this study was to apply for the first time the isotopic transient ^{13}C MFA methodology to the study of astrocytic metabolism in order to obtain an integrated picture of their metabolic fluxes. This was achieved by fully exploring the isotopic transient information collected after [1-^{13}C]glucose administration to primary cultures of astrocytes. Quantification of the labelling time-courses was accomplished by GC-MS and metabolites pool sizes were measured by HPLC. A comprehensive metabolic network including glycolysis, PPP, TCA cycle and amino acids metabolism was considered to fit metabolite ^{13}C time-courses and estimate metabolic fluxes. This approach allowed estimating important metabolic fluxes of astrocytes with high statistical quality and provided valuable information on the contribution of other sources than glucose to the main pathways of astrocytic energy metabolism. Thus, it represents a powerful and new tool to investigate still unclear aspects of brain metabolism or metabolic responses of cultured cells to pathological conditions, which can be further explored *in vivo*.

2 Materials and Methods

2.1 Materials

Plastic tissue culture dishes were purchased from Nunc (Roskilde, Denmark); FBS, Pen-Strep solution and DMEM were purchased from GIBCO, Invitrogen (Paisley, UK); ^{13}C-labelled glucose was purchased from Cambridge Isotope Laboratories (Andover, MA, USA); MTBSTFA + 1% t-BDMS-Cl was purchased from Regis Technologies (Morton Grove, IL, USA); toluene and acetonitrile were purchased from LabScan (Gliwice, Poland); all other chemicals were purchased from Sigma-Aldrich (Munich, Germany). Animals were purchased from Instituto de Higiene e Medicina Tropical (Lisbon, Portugal).

2.2 Cell culture and metabolite extraction

Primary cultures of cortical astrocytes were obtained from 1 to 2-day-old rats and prepared as described previously (Richter-Landsberg and Besser 1994). Cells were cultured in DMEM containing 5 mM glucose and supplemented with Pen-Strep (100 U/mL) and 20% (v/v) FBS, gradually reducing its concentration to 10%. Cultures were kept in a humidified atmosphere with 7% CO_2 in air and 37°C. After 3 weeks in culture cells were trypsinised and seeded into 6-well plates at a cell density of $5x10^4$ cells/cm^2. Experiments were performed when cells reached confluence: the culture medium was removed, cells were washed with PBS and subsequently incubated with DMEM with 1% FBS containing 4 mM [1-^{13}C]glucose (2 ml of culture medium per well). The transient period of label incorporation into intracellular metabolites was followed during 24h, using a shorter sampling time in the beginning. Samples of medium and cell content were collected at 0, 6, 12, 30 min, 1, 2, 4, 7, 10, 16 and 24 h after labelled glucose administration. Experiments were run in triplicate. The cell supernatant was collected, centrifuged at 200 x *g* for 10 minutes and stored at -20°C until further analysis. Cell monolayers were washed with cold PBS to eliminate tracer amounts of extracellular metabolites, frozen in liquid nitrogen to rapidly stop metabolism and extracted with 70% (v/v) ethanol, followed by centrifugation at 20 000 x *g* for 15 min. The resulting supernatants (cell extracts) were stored at -80 °C until GC-MS or HPLC analysis. The pellets were stored at -20 °C and were later used either for protein analysis.

2.3 Quantification of extra- and intracellular metabolite concentrations

Glucose and lactate concentrations in samples of cell supernatants were determined using an automated YSI 7100 Multiparameter Bioanalytical System (Dayton, Ohio, USA). Intra- and extracellular concentrations of amino acid were quantified by HPLC using a pre-column derivatisation method based on the Waters AccQ.Tag Amino Acid Analysis method as described elsewhere (Amaral et al. 2010).

2.4 Protein quantification

The total cellular protein content was determined by dissolving the cell pellets in 0.1 M NaOH followed by incubation overnight at 37°C, to ensure complete protein extraction. The BCA protein assay from Pierce (Rockford, IL, USA) was used to determine total protein amounts using bovine serum albumin as standard.

2.5 Quantification of mass isotopomers by GC-MS

For analysis of lactate, amino acids (alanine, aspartate, glutamate and glutamine) and TCA cycle intermediates (α-ketoglutarate, fumarate and malate), samples of cell extracts and cell supernatants were lyophilized and dissolved in 0.01 M HCl followed by pH adjustment to pH < 2 with 6 M HCl. The samples were then dried under atmospheric air (50°C). The metabolites were extracted into an organic phase of ethanol and benzene and dried again under atmospheric air (50°C). DMF was added before derivatisation with MTBSTFA in the presence of 1% t-BDMS-Cl (Mawhinney et al. 1986). It was not possible to obtain consistent values for the enrichment of intracellular lactate.

The protocol used for analysis of the glycolytic intermediates phosphoenolpyruvate (PEP) and 3-phosphoglycerate (3PG), was based on that described in Hofmann et al. (2008). Samples of cell extracts were lyophilized, dissolved in methanol and dried under atmospheric air (50°C). The metabolites were then extracted with toluene and dried again under atmospheric air (50°C). Derivatisation was performed using a mixture of N-Methyl-N-(trimethylsilyl)trifluoroacetamide (MSTFA) + 1 % trimethylchlorosilane and acetonitrile.

All samples were analyzed on an Agilent 6890 gas chromatograph with a capillary column (WCOT fused silica 25x 0.25 mm ID, 0.25 µm film thickness, VF-1ms, Varian), connected to an Agilent 5975B mass spectrometer with electron impact ionization. Atom percent excess (^{13}C) in the different metabolites was determined after calibration using unlabelled standard solutions (Biemann 1962). Mass isotopomers differ by the number of labelled carbons; *m* represents the fraction of unlabelled compound in

the total compound pool, *m+1* the fraction of compound labelled in one carbon and so on. All fractions of a metabolite sum up to 100%.

2.6 Isotopic transient ^{13}C Metabolic Flux Analysis

i) Metabolic Network and metabolite balancing

According to the main changes observed intracellularly and in the culture supernatant, a metabolic network was established to represent the metabolism of astrocytes (Figure 4.1). The network comprises the following metabolic pathways: glycolysis, PPP, TCA cycle, malate-aspartate shuttle (MAS), catabolism of some amino acids and synthesis of glutathione, glutamine, alanine and taurine/hypotaurine. It contains 32 balanced intracellular metabolites and a total of 47 fluxes, from which 3 were considered reversible.

Isotopic transient MFA relies in both metabolite and mass isotopomers balancing. If the metabolic network has m metabolites and q reactions, the following steady-state material balances can be formulated (Equation 1):

$$\mathbf{Nr} = \mathbf{0} \tag{1}$$

with **N** being a $m \times q$ stoichiometric matrix, and **r** the vector of q metabolic rates.

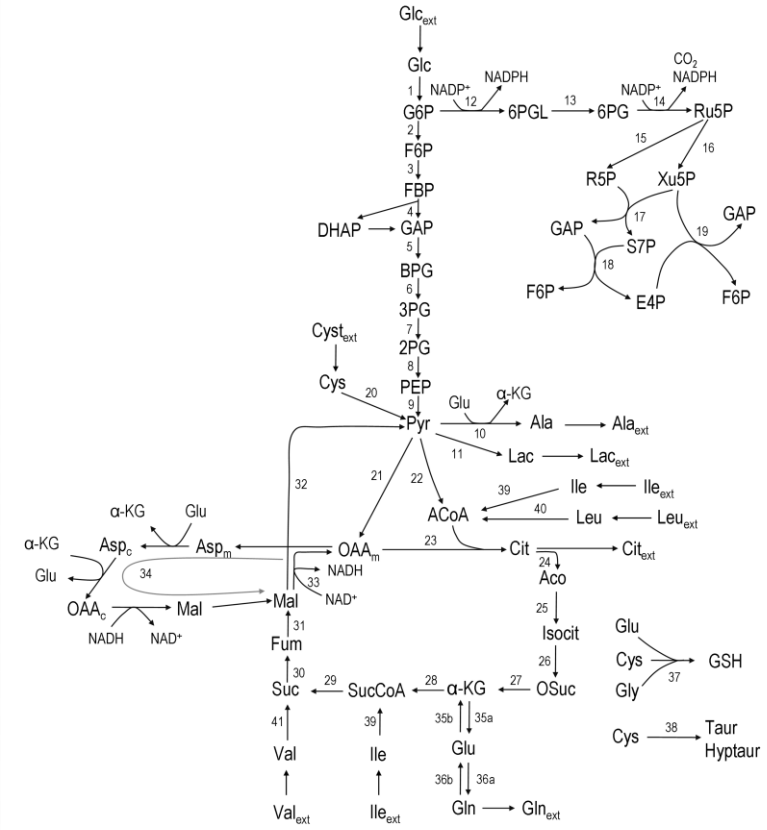

Figure 4.1 - Network representing astrocytic metabolism (the stoichiometry of the reactions can be found in Appendix 4). Abbreviations: Glc, glucose; G6P, glucose-6-phosphate; F6P, fructose-6-phosphate; DHAP, Dihydroxy-acetone phosphate; GAP, glyceraldehyde-3-phosphate; BPG, 1:3-bis-phosphoglycerate; 3PG, 3-phosphoglycerate, 2PG, 2-phosphoglycerate; PEP, phosphoenolpyruvate; PYR, pyruvate; 6PGL, 6-phospho-gluconolactone; 6PG, 6-phosphogluconate; Ru5P, ribulose-5-phosphate; R5P, ribose-5-phosphate; Xu5P, xylulose-5-phosphate; S7P, sedoheptulose-7-phosphate; E4P, erythrose-4-phosphate; Lac, lactate; Glu, glutamate; ACoA, Acetyl-Coenzyme A; Cyst, cystine; Cys, cysteine; Gly, glycine; GSH, glutathione; Ala, alanine; α-KG, α-ketoglutarate; OAA, oxaloacetate; Cit, Citrate; Aco, cis-aconitate; Isocit, isocitrate; OSuc, oxalosuccinate; SucCoA, succinyl-coenzyme A; Succ, succinate; Fum, fumarate; Mal, malate; Asp_m, aspartate – mitochondrial pool; Asp_c, aspartate – cytosolic pool; Gln, glutamine; Leu, leucine; Ile, isoleucine; Val, valine; Lys, lysine; ext refers to metabolites taken up from/released to the medium.

ii) Modelling of isotopomer ^{13}C time-courses

After administration of the labelled substrate, the mass isotopomer distribution of each metabolite changes over time depending on the flux distribution. To represent mathematically the system and estimate the unknown fluxes, a set of differential equations needs to be established for each isotopomer, fulfilling the stoichiometric

constraints of the metabolic network. Carbon transitions occurring in biochemical reactions are well established for the majority of metabolic pathways and documented in biochemical textbooks. Equations 2 and 3 represent the balances for the two mass isotopomers of glucose, when [1-^{13}C]glucose is the labelled substrate:

$$\frac{dGlc_m}{dt} = \frac{1}{Glc_{pool}} \cdot r_1 \cdot Glc_m \quad (2)$$

$$\frac{dGlc_{m+1}}{dt} = \frac{1}{Glc_{pool}} \cdot r_{Glc} - r_1 \cdot Glc_{m+1} \quad (3)$$

where Glc_m is the fraction of unlabelled glucose, Glc_{m+1} is the fraction of glucose labelled in one carbon, Glc_{pool} is the intracellular glucose pool, r_{Glc} is the uptake rate of glucose and r_1 is the flux through reaction 1. The equations for the remaining intracellular metabolites are listed in Appendix 5.

[1-^{13}C]glucose is taken up by astrocytes and subsequently metabolized either via PPP, where the labelled carbon is lost as CO_2, or via glycolysis, labelling 3PG, PEP and pyruvate in carbon number 3. [3-^{13}C]pyruvate can be converted to [3-^{13}C]lactate or [3-^{13}C]alanine, be transported into mitochondria to enter the TCA cycle as [2-^{13}C]acetyl-CoA via pyruvate dehydrogenase or as [3-^{13}C]oxaloacetate by anaplerosis through the pyruvate carboxylation pathway (Shank et al. 1985). Condensation of [2-^{13}C]acetyl-CoA with unlabelled oxaloacetate will, after several steps, lead to the formation of [4-^{13}C]glutamate and to either [2-^{13}C]- or [3-^{13}C]aspartate after the symmetrical succinate step. These compounds have one ^{13}C atom and are thus detected as m+1 isotopomers in GC-MS. If labelled oxaloacetate condenses with labelled acetyl-CoA, double labelled metabolites are formed and they will be detected as m+2 by GC-MS. Eventual cycling of the labelled compounds in the TCA cycle may lead to the synthesis of triple labelled metabolites (m+3) after condensation of double labelled oxaloacetate with [2-^{13}C]acetyl-

CoA. From the ^{13}C-labelling time-courses experimentally observed by GC-MS analysis, we have considered two isotopomers for glycolysis and PPP intermediates (*m* and *m+1*), three isotopomers for pyruvate, lactate, alanine and acetyl-CoA (*m*, *m+1* and *m+2*), and 4 isotopomers (*m*, *m+1, m+2* and *m+3*) for the TCA cycle intermediates and remaining amino acids. In total, the system is represented by 96 differential equations.

^{13}C-labelling time-courses are influenced by the pool sizes of the metabolites. If these pools are not measured then they must be considered as unknown parameters in the model. On the other hand, lumping reactions in linear pathways cannot be done if the involved metabolites have different pool sizes. As they take different times to reach isotopic steady-state, lumping such reactions can perturb the fitting to the experimental data and falsify flux estimations. It should be mentioned that no intracellular compartments were distinguished as it is still unfeasible to quantify separately metabolite concentrations in different compartments. Therefore, only one single pool was considered for each intracellular metabolite.

iii) Parameter estimation

For parameter identification, an optimization routine iteratively minimizes the function (F) represented in Equation 4, until an acceptable small value is achieved. F is a variance-weighted difference between mass isotopomer measurements (I_m) and model predictions (I_p). Mass isotopomer data, I_m, from the different metabolites collected at the time-points indicated above (0, 6, 12, 30 min, 1, 2, 4, 7, 10, 16 and 24 h) were used for model fittings. As the various isotopomer profiles are measured with different accuracies, the errors must be weighted by the corresponding standard deviations:

$$\min_{p}\left\{F=\frac{1}{T\times n}\sum_{t=1}^{T}\sum_{i=1}^{n}\left(\frac{I_{m,i}(t)-I_{p,i}(t)}{\sigma_i}\right)^2\right\} \qquad (4)$$

where p is the vector of parameters, T is the number of measured time points, n is the number of mass isotopomers and σ_i^2 the variances of the mass isotopomer measurements. The set of fluxes and unmeasured pools corresponding to the minimum value of Eq. 4 is the solution for the flux calculation problem. To solve this optimization problem a quasi-Newton optimizer was employed (fmincon function from MATLAB™). As gradient algorithms are prone to converge to local optima, the optimization was repeated systematically with different parameter starting values in order to increase the probability of reaching the global optimum. The initial parameter set was selected to be consistent with available primary literature on astrocytic metabolism. We then screened each initial parameter guess within a biologically relevant range, and chose the optimum parameter minimizing Eq. 4.

Computationally, it is more efficient to work with a set of independent fluxes, also called free fluxes, rather than with all metabolic fluxes (Wiechert and de Graaf 1997). From the 47 fluxes composing the metabolic network, 10 were experimentally measured (glucose, lactate, alanine, glutamine, leucine, isoleucine, valine, cystine production or consumption rates) or taken from literature (citrate and glutathione release rates) (see below – Tables 4.1 and 4.4). Since the rank of the stoichiometric matrix is 31, there are 6 free fluxes (37-31) that need to be estimated; the remaining fluxes are subsequently calculated through linear combinations of these independent fluxes. Several pool sizes could not be experimentally measured and it is not possible to estimate those for which experimental ^{13}C time-courses are also not available. Since published data on absolute pool concentrations is still limited, the pools of acetyl-CoA and all glycolytic and PPP intermediates were considered equivalent and the average pool size (Glycolysis/PPP pool) was included in the group of parameters to be estimated. Regarding the TCA cycle intermediates for which mass isotopomer data was not available, an average pool size was tuned by trial-and-error and set equal to 0.03 μmol/mg protein. In total, 11 parameters (6 free fluxes and 5 pool sizes) were estimated by fitting the model to the experimentally observed labelling dynamics.

iv) Parameter confidence limits

Since parameter estimation involves a variety of possible errors, including measurements, modelling, and numerical errors, uncertainty analysis of the optimized parameters constitutes an important part of this estimation. Parameter uncertainty is assessed by its covariance. Assuming that the solution converges to a global minimum, the Hessian matrix **H** can be approximated from the Jacobian matrix **J** as follows:

$$\mathbf{H} = \mathbf{J}^T\mathbf{J} \tag{5}$$

The Jacobian matrix includes the partial derivatives of the model output with respect to the model parameters evaluated at each data point. The covariance matrix (cov) can then be estimated as

$$\mathrm{cov} = RMSE \cdot H^{-1} \tag{6}$$

with RMSE being the root mean squared error.

The confidence interval for each parameter p_i is obtained from the estimate of the standard deviation $\sigma_i = \mathrm{cov}_{i,i}^{1/2}$ as follows:

$$CI_i = p_i \pm \sigma_i \cdot t_{0.975,T-p} \tag{7}$$

with $t_{0.975,T-p}$ being the t-student's distribution for *T-p* (the number of measured data points minus the number of parameters) degrees of freedom and probability 0.975.

v) Sensitivity analysis

To investigate the possibility of accurately identifying each model parameter on the basis of the available experimental data, a sensitivity analysis must be performed. The sensitivity coefficient, Sens_i, reveals how the objective function F (Equation 4) will be influenced by a differential change in the parameter p_i.

$$\mathrm{Sens}_i = \left| \frac{\partial F}{\partial p_i} \frac{p_i}{F} \right| \tag{8}$$

The goal is to determine how "sensitive" the mathematical model is to changes in the value of its parameters. Small sensitivities, i.e., large changes in the parameter value resulting in small changes in the minimized sum of squared residuals, indicate that the parameter cannot be estimated accurately. Large sensitivities, on the other hand, indicate that the parameter can be estimated with high confidence.

3 Results

Primary cultures of astrocytes were incubated with [1-^{13}C]glucose and, during 24 h, samples of culture supernatant and cell content were collected at different time points, in order to estimate astrocytic metabolic fluxes and characterize metabolite labelling dynamics. This time window was enough to ensure isotopic steady-state in almost all intracellular metabolites analyzed by GC-MS.

3.1 Specific rates of consumption/production of glucose, lactate and amino acids

Consumption or secretion rates of relevant compounds were determined based on the changes of their concentrations in the culture medium (Table 4.1). It is generally accepted that glucose is the main energy substrate for the brain and also for astrocytes under physiological conditions (Zwingmann and Leibfritz 2003). In agreement with previous studies, glucose was consumed at a constant rate of 1.06±0.05 μmol.mg prot^{-1}.h^{-1}, representing about 70% of the total carbon taken up by astrocytes. Amino acid analysis showed a decrease in the extracellular levels of the three BCAAs: isoleucine, leucine, and, to a lesser extent, valine. Consumption of these amino acids by astrocytes under physiological conditions has also been reported by other authors (Yudkoff et al. 1996; Johansen et al. 2007; Murin et al. 2009). Furthermore, cystine levels decreased in the supernatant, with an uptake rate larger than that of BCAA. Cystine is the precursor for cysteine, and both amino acids can be used for the biosynthesis of glutathione, taurine and hypotaurine in astrocytes (Brand et al. 1998; Kranich et al. 1998).

Table 4.1 – Experimentally measured values for intracellular pools of some amino acids and transmembrane rates of glucose, lactate and amino acids whose concentration changed significantly during incubation time (negative values refer to consumption rates).

Specific transmembrane rates ($\mu mol \cdot mg\ protein^{-1} \cdot h^{-1}$)	r_{Glc}	-1.06 ± 0.05
	r_{Lac}	2.11 ± 0.10
	r_{Gln}	0.049 ± 0.005
	r_{Ala}	0.042 ± 0.004
	r_{Val}	-0.053 ± 0.005
	r_{Ile}	-0.10 ± 0.05
	r_{Leu}	-0.11 ± 0.05
	r_{Cyst}	-0.36 ± 0.04
Intracellular pools ($\mu mol \cdot mg\ protein^{-1}$)	Ala	0.18 ± 0.04
	Glu	0.18 ± 0.04
	Gln	0.08 ± 0.02
	Asp	0.15 ± 0.03

Abbreviations: Ala, alanine; Asp, aspartate; Cyst, cystine; Glc, glucose; Gln, glutamine; Glu, glutamate; Ile, isoleucine; Lac, Lactate; Leu, leucine; Val, valine.

Lactate, alanine and glutamine were steadily released by astrocytes during incubation. GC-MS analysis of the supernatant at the end of the experiment confirmed the release of these compounds, providing the fractional enrichment of each isotopomer (Table 4.2) (see next sub-section). Citrate secretion was also evident from the GC data. However, its release rate could not determined because the GC-MS method used in this work only provides the relative abundance of isotopomers, not the total concentrations. Consequently, the release rate of 0.025 μmol.mg $prot^{-1}.h^{-1}$, reported by (Westergaard et al. 1994) was used for modelling purposes. Intracellular amino acid pools were measured by HPLC and are listed in Table 4.1.

Table 4.2 – Percent ^{13}C enrichment in extracellular metabolites.

Metabolite	**% ^{13}C enrichment (m+1)**
Lactate	33.5 ± 0.7
Alanine	24.1 ± 2.2
Glutamine	28.84 ± 0.04
Citrate	30.7 ± 0.3

Primary cultures of cortical astrocytes were incubated with medium containing 4 mM [1-^{13}C]glucose for 24 h. Percent ^{13}C enrichment in different extracellular metabolites was analyzed by mass spectrometry in samples of culture medium collected at the end of the incubation period. Results are presented as means ± s.d. in atom percent excess (n=3).

Cellular growth was negligible during the time frame considered as indicated by the amount of protein measured in different cell samples (0.126 ± 0.009 mg protein/well).

3.2 Experimental ^{13}C labelling time-courses

Samples of cell extracts were collected during the isotopic transient period in order to characterize labelling dynamics of intracellular metabolites of astrocytes using GC-MS. The metabolites analyzed include the glycolytic intermediates PEP and 3PG, the TCA cycle intermediates citrate, α-ketoglutarate, fumarate, and malate, and the amino acids alanine, glutamine, glutamate and aspartate. Glycolytic intermediates reached isotopic steady-state much faster than TCA cycle intermediates (Figure 4.2). After addition of labelled glucose, the fraction of the unlabelled pools of PEP and 3PG decreased very fast, reaching isotopic steady-state within less than 30 minutes with an enrichment of 45% in m+1. Regarding alanine, it seems that isotopic steady-state was not reached within the 24h of incubation. At this time, 31% of the pool was labelled in one carbon. Citrate, the first TCA cycle intermediate after acetyl-CoA condenses with oxaloacetate, reached 45% of isotopic enrichment (m+1 and m+2) whereas the enrichment in fumarate was about 15% less (Figure 4.2). In addition, the labelled pools of malate and aspartate were very similar and slightly more enriched than that of fumarate. Furthermore, labelling time-courses of α-ketoglutarate, glutamate and glutamine were comparable but slower than that of citrate. It is noteworthy that synthesis of m+2 and m+3 mass isotopomers was observed for most of the TCA cycle intermediates analyzed, representing up to 8% of the total pools, for citrate and glutamate. This suggests that some mass isotopomers are formed after condensation of ^{13}C labelled acetyl-CoA with ^{13}C labelled oxaloacetate.

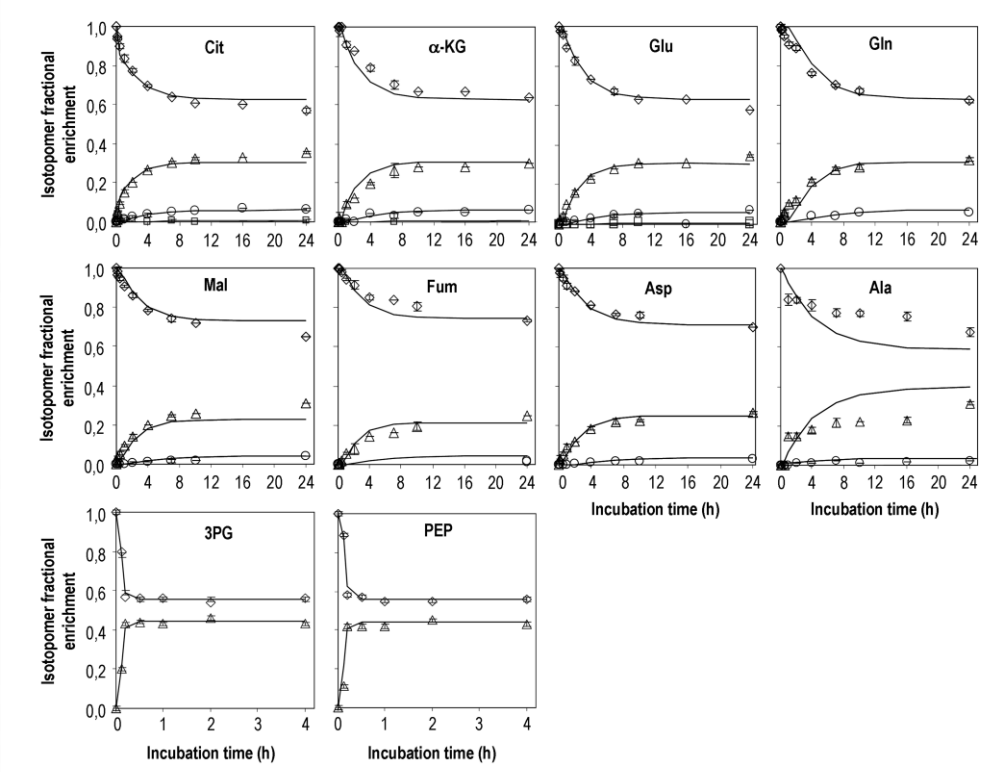

Figure 4.2 - Mass isotopomers distribution after incubation of primary cultures of astrocytes with DMEM containing [1-^{13}C]glucose. Diamonds – m; triangles – m+1; circles – m+2; squares m+3. Experimental data obtained for m+3 isotopomers of glutamine, fumarate, malate and aspartate were below 0.5% ^{13}C enrichment and therefore are not presented. Symbols are average values of GC-MS analysis of cell extracts from 3 parallel cultures of astrocytes; error bars correspond to standard deviations; lines are model predictions.

^{13}C enrichment of extracellular metabolites was also analyzed at the end of the incubation time (Table 4.2). The difference between % ^{13}C enrichment in lactate and alanine (34 vs. 24% m+1, respectively) can be surprising given their common origin – pyruvate, suggesting metabolic compartmentation (see discussion). Moreover, alanine enrichment in the culture medium differed significantly from its intracellular enrichment. Extracellular citrate was ~30% enriched in m+1, which is similar to the data obtained for its intracellular pool, the same being observed for glutamine.

3.3 Flux estimations by isotopic transient ^{13}C MFA

Intracellular flux estimations were obtained by minimizing the difference between model simulations and experimentally observed isotopomer profiles. The optimal fittings to the ^{13}C labelling time-courses of the 10 metabolites experimentally analyzed are shown in Figure 4.2. For some metabolites, the enrichment in heavy mass isotopomer fractions (m+2 and m+3) was detectable but with very low values (<1% above natural abundance) and with large associated standard deviations. Therefore, they were not considered in model fitting. Estimated parameters together with their 95% confidence intervals are presented on Table 4.3.

Table 4.3 – Parameter values (fluxes and metabolite pools) which allowed the best fit to the mass isotopomer data.

	Fluxes ($\mu mol.mg\ prot^{-1}.h^{-1}$)	**95% Confidence Limit**
r_2 (G6P → F6P)	0.940	0.001
r_{32} (Mal → Pyr)	0.12	0.03
r_{34} (Mal-Asp shuttle)	0.16	0.08
r_{35a} (α-ketoglutarate → glutamate)	0.32	0.06
r_{36a} (Glu → Gln)	0.052	0.002
r_{38} (Cys → Taur+Hyptaur)	0.17	0.02
	Pool size ($\mu mol.mg\ prot^{-1}$)	**95% Confidence Limit**
Citrate	0.05	0.02
α-Ketoglutarate	0.15	0.03
Malate	0.05	0.06
Fumarate	0.05	0.03
Glycolysis/PPP intermediates	0.027	0.001

The 6 free fluxes and 5 metabolite pools were estimated using an optimization routine (see Materials and Methods) that allowed finding the optimal values that better described the experimental data.

The remaining intracellular fluxes were calculated from the estimated free fluxes and are shown in Table 4.4. Both the fast labelling dynamics of PEP and 3PG and the slow dynamics of TCA cycle related metabolites were well described by the model (Figure 4.2).

Table 4.4 – Astrocytic metabolic fluxes estimated using the isotopic transient MFA methodology.

Reaction	Flux (μmol.mg prot^{-1}. h^{-1})
r_1 (Glc → G6P) (=rGlc)[1]	1.06 ± 0.02
r_3 - r_4 (F6P → 2GAP)	1.02 ± 0.03
r_5 – r_9 (GAP → Pyr)	2.08 ± 0.03
r_{10} (Pyr → Ala) (=rAla) [1]	0.042 ± 0.004
r_{11} (Pyr → Lac) (=rLac) [1]	2.11 ± 0.04
r_{12} - r_{14} (G6P → Ru5P)	0.12 ± 0.02
r_{15} (Ru5P → R5P)	0.04 ± 0.02
r_{16} (Ru5P → Xu5P)	0.08 ± 0.01
r_{17} - r_{19} (R5P + 2 Xu5P → GAP + 2 F6P)	0.04 ± 0.01
r_{20} (Cys → Pyr)	0.16 ± 0.01
r_{21} (Pyr → OAA) (pyruvate carboxylase flux)	0.07 ± 0.02
r_{22} (Pyr → AcoA) (pyruvate dehydrogenase flux)	0.14 ± 0.07
r_{23} (ACoA+Oxa → Cit)	0.45 ± 0.08
r_{24} - r_{27} (Cit → α-KG)	0.43 ± 0.08
r_{28} (α-ketoglutarate →SucCoa)	0.35 ± 0.08
r_{29} - r_{31} (SucCoa → Mal)	0.51 ± 0.08
r_{33} (Mal → OAA)	0.39 ± 0.08
r_{35b} (Glu → α-KG)	0.46 ± 0.07
r_{36b} (Gln → Glu)	0.003 ± 0.003
r_{37} (Cys → GSH) [2]	0.030
r_{39} (Ile → AcoA + SucCoA) (=r_{Ile})[1]	-0.10 ± 0.05
r_{40} (Leu → AcoA) (=r_{Leu})[1]	-0.11 ± 0.05
r_{41} (Val → Suc) (=r_{Val})[1]	-0.053 ± 0.005
Citrate release rate[2]	0.025

The fluxes that are missing (r_2, r_{32}, r_{34}, r_{35a}, r_{36a}, r_{38}) correspond to the 6 free fluxes estimated through an optimization routine (see Materials and Methods) and are presented on Table 3.

[1] These rates correspond to those experimentally measured - see Table 1.

[2] Taken from the literature (O'Connor et al 1995; Westergaard et al 1994).

However, the predicted labelling time-courses of alanine differed from experimental data to some extent. Different model structures were attempted to improve fittings for alanine; for instance, reaction r_{10} was turned reversible, but a null flux was identified for inverse reaction. These results suggest that labelling of the alanine pool is more complex than that described by our model and is probably related to the existence of different pyruvate pools (discussed below). The average error between measured and predicted mass isotopomer profiles of the remaining metabolites was below 3%. The reason for the small deviations between α-ketoglutarate time-courses and model predictions might be

worth to investigate further. According to the metabolic network adopted, α-ketoglutarate and glutamate are constantly being inter-converted, implying that the different isotopomers of both metabolites reach the same steady-state values. However, the unlabelled pool of α-ketoglutarate seems to be systematically ~4% higher than that of glutamate, also at isotopic steady-state. This is probably due to cellular compartmentalization not taken into account by the metabolic network adopted.

Concerning the estimated fluxes, astrocytes showed a high glycolytic flux, converting most of the glucose to lactate. In addition, the model estimated that 11% of the glucose flux was diverted to the PPP (r_{12}). Some activity through the PPP could be anticipated based on the 45% enrichment in m+1 of PEP and 3PG at isotopic steady-state, as further sources of label dilution in upper glycolytic metabolites (like glycogen degradation) were not considered in the model. In fact, [1-^{13}C]glucose metabolism through the PPP leads to the loss of ^{13}C as CO_2 (r_{14}). Subsequently formed metabolites might re-enter glycolysis at the 3-phosphate-glyceraldehyde node, consequently diluting the enrichment of downstream metabolites.

Furthermore, 14% ^{13}C enrichment for acetyl-CoA was predicted at isotopic steady-state (data not shown). Even though pyruvate was estimated to be 41% enriched, the synthesis of acetyl-CoA as a consequence of the metabolism of leucine and isoleucine (from incubation medium) dilutes the enrichment in this pool. Moreover, the model estimated the anaplerotic flux through PC as being 0.07 ± 0.02 μmol.mg prot^{-1}.h^{-1} (Table 4.4) and the flux through PDH as being 0.14 ± 0.07 μmol.mg prot^{-1}.h^{-1} (Table 4.4), which gives a PC/PDH ratio of 0.5. The model also estimated the flux through the MAS (0.16 μmol.mg prot^{-1}.h^{-1}). Regarding the flux for the conversion of malate into pyruvate (r_{32} - malic enzyme), it was estimated as being 0.12 ± 0.03 μmol.mg prot^{-1}.h^{-1} (Table 4.3). Furthermore, the experimentally measured uptake rate of cystine would significantly dilute the labelling dynamics of pyruvate and subsequently formed metabolites, if that would be its only metabolic fate. However, it is known that the major metabolic products of cystine/cysteine in astrocytes are taurine and hypotaurine (Brand et al.

1998), in addition to being a rate limiting substrate in the biosynthesis of glutathione (Dringen and Hirrlinger 2003). Thus, these different fates of cysteine were included in the model (reactions 37 and 38). Glutathione synthesis was set to 0.030 μmol.mg prot^{-1}.h^{-1}, as reported in the literature for physiological conditions (O'Connor et al. 1995), and the model estimated a net rate of taurine and hypotaurine synthesis (r_{38} - 0.17 ± 0.02 μmol.mg prot^{-1}.h^{-1} – Table 4.3) as well as the fraction which is converted into pyruvate (r_{20} - 0.16 ± 0.01 μmol.mg prot^{-1}.h^{-1} – Table 4.4) in order to have a cysteine to pyruvate rate that would fit better with the observed labelling dynamics.

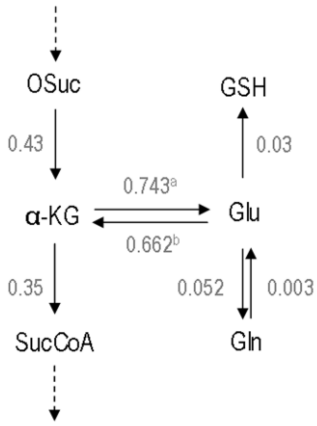

Figure 4.3 - Total metabolic fluxes at the glutamate/α-ketoglutarate node. The forward and reverse fluxes of α-ketoglutarate/glutamate exchange were calculated by summing up all fluxes of the reactions in which they are included. Values are μmol mg prot^{-1} h^{-1}. a – The total flux α-ketoglutarate → glutamate is the sum of the fluxes r_{34}, r_{35a}, r_{39}, r_{40} and r_{41}. b - The total flux glutamate → α-ketoglutarate is the sum of the fluxes r_{35b}, r_{34} and r_{10}. Abbreviations: α-KG, α-ketoglutarate; Gln, glutamine; Glu, glutamate; GSH, glutathione; OSuc, oxalosuccinate; SucCoA, succinyl-Coenzyme A.

This approach additionally enabled to estimate the fluxes of exchange between α-ketoglutarate and glutamate (Tables 4.2 and 4.3, Figure 4.3), which were similar to the TCA fluxes. Interestingly, a net flux favoring glutamate release from the TCA cycle was estimated. Regarding glutamine, the predicted isotopomer dynamics was a little slower than that experimentally observed. This might indicate a glutamine pool smaller than the measured value. The estimated flux through the reaction catalyzed by glutamine

synthetase (r_{36a}) (Table 4.3) was slightly higher than the observed glutamine secretion rate, resulting in some flux through the inverse reaction (r_{36b}) (Table 4.4).

3.4 Statistical significance of estimated fluxes and pool sizes

After estimation of the free fluxes, their statistical validity must be evaluated. Besides the confidence limits (Table 4.3), also the sensitivity coefficients were derived for each parameter. All free fluxes presented small confidence intervals showing low uncertainty. Moreover, sensitivity coefficients higher than 1 were obtained for all fluxes and pool sizes (data not shown). A sensitivity coefficient equal to 1 means that a variation of 10% in the corresponding parameter affects the function F (Eq. 4) in 10%. Thus, sensitivity coefficients higher than 1 mean that the model is sensitive to the parameter value, and indicate that the free fluxes were identified with good precision. Together with intracellular fluxes, intracellular pool sizes determine the isotopomer profiles of the various metabolites during incubation time; thus, the pool sizes which were not experimentally determined had to be estimated by model fitting to the experimental data (Table 4.3). The average pool for glycolytic and PPP intermediates was estimated as 0.027 ± 0.001 μmol mg prot^{-1}. The small confidence interval for this pool shows its statistical validity. The citrate and α-ketoglutarate pools could also be estimated with reasonable statistical confidence. The same is not true for fumarate and malate pools, presenting wide confidence intervals.

The fitting performance (defined by the objective function) is rather sensitive to the optimized parameters. Inversely, the proposed parameter set is quite robust to variations in the fitting performance, revealing that even if reaching only a sub-optimal solution within the biologically relevant parameter space, the optimal parameter set would be relatively closer to the sub-optimal one. This means that the deviations between model and experimental measurements have a small impact on flux estimations.

4 Discussion

4.1 ^{13}C isotopic transient MFA vs. other modelling methodologies

In this work, a state-of-the-art metabolic modelling tool, isotopic transient ^{13}C MFA (Wiechert and Noh 2005), was applied for the first time to estimate intracellular fluxes of brain cells. This methodology uses all the information contained in the isotopic transient data and, thus, the quality of flux estimations is strongly improved when compared to the classical MFA. The latter provides only the net fluxes (not the separate fluxes) through parallel metabolic pathways and reversible reactions. Isotopic transient ^{13}C MFA allows the resolution of important branches of the metabolic network. This is the case for the fluxes of parallel pathways (glycolysis vs. PPP and PC vs. PDH), bidirectional reactions (the reversible exchange between α-ketoglutarate and glutamate and between glutamate and glutamine – see Figure 4.3) and cyclic pathways (MAS).

Isotopic transient MFA constitutes an improved, although more complex, alternative to the model pioneered by Malloy, which was initially developed to investigate heart metabolism (Malloy et al. 1988) and later adapted to estimate fluxes based on isotopomer composition of glutamate in neurons or glutamine in astrocytes (Martin et al. 1993; Merle et al. 1996a). Nevertheless, both MFA/^{13}C MFA and the Malloy model have only been applied to estimate fluxes in a single cellular compartment. A network describing metabolic interactions between astrocytes and neurons would include a much larger number of reactions and, consequently, of unknown fluxes. This would require a larger set of experimental data and, in particular, the separate measurement of specific metabolic rates and pools for astrocytes and neurons, in order for the system to be determined. Still, this could be performed in a co-culture system, in which neurons and astrocytes could be physically separated (for example, using cell culture inserts).

The present methodology thus requires the use of sensitive techniques, such as MS, and considerable experimental work. ^{13}C NMR spectroscopy can also be used, particularly when the labelled substrates yield more complex labelling patterns. However,

its low sensitivity compared to MS becomes a disadvantage when the goal is to have labelling time-courses for as many metabolites as possible. In the present study, mass isotopomer data and metabolite pools were still limited to a relatively small number. Actually, quantification of metabolite pools has been one of the major drawbacks of isotopic transient MFA. GC-MS provided only the relative isotopic enrichment of intracellular pools. To have absolute pool concentrations, difficult-to-obtain labelled standards would be required. Nevertheless, the number of quantifiable mass isotopomers and absolute pool concentrations is expected to increase as MS techniques continue to improve. In addition, the high specificity of ^{1}H nuclear magnetic resonance spectroscopy widely used in the metabolomics field (Weljie et al. 2006) could also be a good tool to quantify metabolite pools.

To investigate brain metabolism in the scope of larger (underdetermined) networks, another metabolite balancing approach called flux balance analysis (FBA) has been applied (Cakir et al. 2007; Lewis et al. 2010). FBA relies on linear programming to obtain a solution for the intracellular fluxes in underdetermined systems (Kauffman et al. 2003). However, it requires the definition of a metabolic objective which is maximized or minimized during flux calculations (Kauffman et al. 2003). This metabolic objective might be hard to define, particularly concerning the complex interactions between brain cells. (Cakir et al. 2007) reported recently the application of FBA to investigate the metabolic interactions between neurons and astrocytes using diverse metabolic objective functions. Comparing to literature findings the best flux prediction was achieved when the maximization of the glutamate-glutamine-GABA cycle flux was the objective function (Cakir et al. 2007). Also based on linear programming, Lewis et al (2010) have recently reported a large-scale *in silico* model, including genomic and proteomic data, to recapitulate metabolic interactions between astrocytes and different types of neurons. This model correlates flux changes with altered expression or activity of particular enzymes (Lewis et al. 2010), representing a major breakthrough in this field, although it goes much beyond the scope of isotopic transient MFA.

4.2 Estimation of fluxes in parallel pathways: PPP/glycolysis and PC/PDH branch points

The PPP plays a key role in the maintenance of the cellular redox-balance by ensuring the recycling of the reducing cofactor NADPH, necessary for the regeneration of glutathione, the major antioxidant molecule in brain cells (Dringen 2000). In fact, the model takes some synthesis of glutathione from cysteine into account. Also based on the 45% enrichment in PEP and 3PG at isotopic steady-state, the model estimated an 89%:11% flux ratio between glycolysis and the PPP. Most of the available estimations of the PPP flux were carried out using data from *in vitro* studies. Fitting with the present results, using the classical MFA combined with ^{13}C labelling data collected at isotopic steady-state, we have recently estimated that ~10% of the total glucose consumed was metabolized through the PPP in astrocytes cultured in stirred bioreactors (Amaral et al. 2010). Previously, Ben-Yoseph et al. (1996) had reported a basal astrocytic PPP flux of ~7% of the total lactate produced from glucose in cultured astrocytes, determined by a GC-MS method based on the differential labelling of released lactate following metabolism of [1,6-C_2,6,6-$^2H_2$]glucose. This value increased to 67% during exposure to oxidative stress (Ben-Yoseph et al. 1996). A PPP flux of 7% has also been reported in healthy human subjects using [1,2-^{13}C]glucose and ^{13}C-NMR spectroscopy (Dusick et al. 2007). The importance of considering the PPP in modelling studies and of providing better tools to estimate its flux is justified by its significant influence on estimations of the glutamate-glutamine cycle *in vivo* (Shen et al. 2009). In addition, experimental data obtained in the context of brain activation studies in rats provided further evidence that the PPP might contribute more than previously estimated to the "glutamine dilution" phenomenon (Cruz et al. 2007; Dienel and Cruz 2009).

Still, we cannot exclude that minor glycogen degradation could also have influenced the observed enrichment in glycolytic intermediates. In fact, lactate released by astrocytes was shown to partially result from glycogen breakdown, even in the presence of glucose (Sickmann et al. 2005). Nevertheless, the role of glycogen as energy

fuel appears to be more significant in the context of brain activation (Dienel et al. 2007). Glycogenolysis was not included in the model due to the lack of experimental data enabling us to distinguish between the contribution from the glycogen shunt and the PPP to PEP and 3PG ^{13}C time-courses. More isotopomer time-courses would be required, for example, those from glucose or glucose-6-phosphate and intermediates of the PPP. It was decided to include the PPP instead of the glycogen shunt since it is more likely that this pathway accounts for the label dilution observed in glycolysis. The PPP is required for maintaining the basal cellular redox balance (Dringen 2000), even when significant oxidative stress is not present.

Pyruvate carboxylation is an important anaplerotic reaction in the brain and is thought to occur predominantly in astrocytes due to the specific glial localization of the PC enzyme (Shank et al. 1985). The PC/PDH ratio is usually estimated based on the different metabolite isotopomers, such as glutamate or glutamine, originating from [^{13}C]glucose metabolism through each of these pathways. In this work, the PC/PDH ratio (0.5) was calculated directly from the estimated PC and PDH fluxes, based on total carbon fluxes and not only on the ^{13}C fluxes coming from glucose. This PC/PDH ratio fits well with those determined *in vitro* (Hassel et al. 1995; Waagepetersen et al. 2001) and also *in vivo* (Gruetter et al. 2001; Merle et al. 2002; Oz et al. 2004) for the glial compartment. Interestingly, Merle et al. (1996b) estimated a PC/PDH ratio of 0.54 in cultured cerebellar astrocytes and a similar value was obtained by us (Teixeira et al. 2008) in cultured cortical astrocytes. Taking into account the measured rates of release of different metabolites, the present results confirm that PC significantly contributes to the release of citrate and glutamine from astrocytes (Waagepetersen et al. 2001). Moreover, the PC flux is known to be implicated in glutamine synthesis also in the resting human brain (Gruetter et al. 1998) and its contribution was estimated to be 35% by metabolic modelling (Gruetter et al. 2001). Also, Duarte et al very recently estimated a 25% contribution of PC to the glial TCA cycle rate in the rat brain and a PC/PDH ratio of 30% for the glial compartment (Duarte et al. 2011). Even though the absence of

neurons might reduce the need of glutamine synthesis by a monotypic culture of astrocytes, our results suggest that PC also significantly contributes to glutamine synthesis in this context.

4.3 TCA cycle Fluxes and BCAAs catabolism

The TCA cycle fluxes estimated in this work are in the range of values previously estimated by us using the classic MFA methodology (Teixeira et al. 2008; Amaral et al. 2010). The estimated reduction in ^{13}C enrichment from 41% in pyruvate to 14% in acetyl-CoA corroborates a study by Merle et al. (1996b) in cerebellar astrocytes. These authors justified the label dilution of acetyl-CoA with the consumption of extracellular amino acids and fatty acid degradation (Merle et al. 1996a). Our model considers also the metabolism of BCAA as an additional source of acetyl-CoA and elevated uptake rates (when comparing to the flux obtained for PDH) were measured for these amino acids. Actually, 14% enrichment in glutamate isotopomers produced after one turn of the TCA cycle was observed after incubation of astrocytes with [U-^{13}C]isoleucine (56% enriched in the medium) (Johansen et al. 2007) confirming that BCAAs are oxidized to a large extent.

The role of BCAAs as energy fuels is also relevant *in vivo*. It has been suggested that these substrates are oxidized by astrocytes in the rat brain to a significant extent (Dienel and Cruz 2009). Additional findings indicate that BCAAs also contribute to the "glutamine dilution" phenomenon observed in ^{13}C isotopomer studies (Cruz et al. 2007; Dienel and Cruz 2009). However, BCAAs taken up by astrocytes can also be metabolized into ketone bodies, which are subsequently released and can eventually be taken up by neurons (Bixel and Hamprecht 1995). Thus, we cannot exclude a slight overestimation of the TCA cycle fluxes as well as the fluxes through the reactions bridging glycolysis and TCA cycle. Experimental labelling time-courses of intracellular lactate and/or pyruvate (which were not possible to obtain in the present study) would enable more accurate estimations at this metabolic node.

Glycolytic metabolites reached isotopic steady-state much faster than TCA cycle-related metabolites, which can be due to the large pools of glutamate and aspartate (Table 4.1). These are linked to the TCA cycle through reversible aminotransferase reactions, delaying the labelling time-courses of TCA cycle metabolites. This is clearly observed in the labelling time-course of the citrate pool, which is faster during the first 30 min of incubation. Then, it becomes slower as it is more dependent on the labelling dynamics of the downstream metabolites and subsequent turns of the TCA cycle. The model could describe this phenomenon quite well. The lower enrichment observed for fumarate, when compared to citrate, can be explained by the funneling of BCAAs from the incubation medium into the TCA cycle at the succinyl-CoA node, which dilutes the labelled fraction of the downstream compounds. On the other hand, the higher enrichment in aspartate and malate compared to that of fumarate is explained by the flux through PC. PC converts pyruvate into oxaloacetate that, subsequently, might exchange ^{13}C label with malate to a significant extent through "back-cycling" in the TCA cycle (Sonnewald et al. 1993; Merle et al. 1996a). Actually, we have evidence that extensive malate to fumarate back-flux occurs in cultured astrocytes (unpublished data). In addition, the MAS activity further explains the isotopomer distribution similarity between malate and aspartate pools.

4.4 Malate-Aspartate Shuttle and Glutamate/α-Ketoglutarate exchange

The link between oxidative glucose metabolism and glutamate labelling is established by an active exchange rate between α-ketoglutarate and glutamate pools (a flux normally represented by Vx), which is, together with the oxaloacetate/aspartate exchange, mediated by the MAS (Gruetter et al. 2003). NADH is produced in glycolysis at the same rate of pyruvate synthesis. In order to maintain the cytosolic redox balance required for the continuous operation of glycolysis it needs to be recycled back to NAD^+ (McKenna et al. 2006). Thus, reducing equivalents from NADH are transported into the mitochondrion by the MAS and are oxidized at the same rate that pyruvate enters the TCA cycle (Gruetter et al. 2003). This justifies the role of the MAS in mediating the

exchange of label across the mitochondrial membrane (Gruetter et al. 2003). In fact, our results agree with this direct relationship between the pyruvate oxidation rate, i.e., the rate of pyruvate entry in the TCA cycle - PDH+PC (0.21 ± 0.08 μmol.mg $prot^{-1}$. h^{-1}) and the MAS (0.16 ± 0.08 μmol.mg $prot^{-1}$. h^{-1}) flux.

Still, a large debate exists concerning the relative magnitude of the Vx and PDH fluxes in the brain. Whereas some authors provided evidence that Vx and PDH fluxes are in the same range (Gruetter et al. 2001; Choi et al. 2002; Henry et al. 2002), others have proposed that Vx rate should be much higher than PDH (Mason et al. 1992; Mason et al. 1995). A scheme describing all reactions linked to glutamate and α-ketoglutarate pools and their corresponding estimated fluxes can be seen in Figure 4.3. Our approach allowed distinguishing between these reversible fluxes, taking into account all carbon sources involved in α-ketoglutarate and glutamate metabolism. The present work importantly provides new evidence that V_x is in the range of the TCA cycle fluxes and not several fold higher. It should be highlighted that most of the cited investigations refer to whole brain fluxes whereas this study is focused only on astrocytic metabolic fluxes, although obtained from primary cultures. Nevertheless, Duarte et al have recently reported new supporting evidence for this concept, using an improved model allowing to estimate Vx in both the neuronal and glial compartment in the rat brain *in vivo* (Duarte et al. 2011). Taken together, these findings support the importance of the present results as reflecting what could be happening in the astrocytic compartment *in vivo*.

4.5 Pyruvate compartmentation and malic enzyme

Different labelling time-courses between extracellular lactate and alanine can be interpreted based on the existence of distinct astrocytic pyruvate pools. Labelling of alanine from glucose was previously observed to be lower than that of lactate in astrocyte cultures (Brand et al. 1992; Brand et al. 1993), which corroborates our results. These observations can additionally explain the poor fitting of the model to alanine

experimental ^{13}C time-courses, since the model does not take into account distinct metabolite pools.

The decarboxylation reaction by malic enzyme was also included in the model and its flux represented about 5% of the fluxes leading to pyruvate synthesis. Pyruvate formed via malic enzyme must re-enter the TCA cycle to be completely oxidized. This pathway is called pyruvate recycling and has been described both *in vitro* (Sonnewald et al. 1996; Bakken et al. 1997; Waagepetersen et al. 2002) and *in vivo* (Cerdan et al. 1990; Haberg et al. 1998). As discussed by Waagepetersen et al. (2002), this pathway is likely to be more active when cells need to dispose of glutamate and glutamine by oxidative degradation. The preferential release α-ketoglutarate via glutamate from the TCA cycle and subsequent production of glutamine observed in this work thus explains the low contribution of this flux to the total pyruvate production.

Also related to pyruvate synthesis is the degradation of cysteine. There are not many published values for these rates. Beetsch and Olson (1998) reported a rate of [^{35}S]taurine synthesis from [^{35}S]cysteine in cultured rat astrocytes of 1.27 nmol.mg protein^{-1}.h^{-1}, which is much lower than that estimated in this work (0.17 µmol.mg protein^{-1}.h^{-1}). However, in the same study, the measured activity of the rate-limiting enzyme involved in cysteine degradation into taurine, cysteine dioxygenase, was 144 nmol·mg protein^{-1}·h^{-1}, which fits well with the taurine/hypotaurine synthesis rate estimated by our model. These results are also supported by findings from Brand et al (1998) showing that cultured astrocytes mainly use cysteine for the synthesis of taurine and hypotaurine as observed by ^{13}C NMR spectroscopy after incubation with [3-^{13}C]cysteine (Brand et al. 1998). Still, Beetsch and Olson (1998) observed that taurine synthesis from extracellular cysteine is also supported by a robust rate of cysteine accumulation, and thus we cannot exclude that this factor might have contributed to the overestimation of the rate, as some of the cysteine taken up could have been accumulated to later yield taurine/hypotaurine. Nevertheless, this would not have an impact on the remaining estimated fluxes.

4.6 Final remarks

This work clearly shows the potential of ^{13}C isotopic transient MFA to provide a reliable metabolic profile of cultured astrocytes in a variety of conditions. Important metabolic fluxes of astrocytes normally not easily accessible were estimated, namely the PPP, PC, PDH, TCA cycle, MAS and also the α-ketoglutarate/glutamate exchange fluxes. In addition to corroborating *in vivo* and *in vitro* findings reported in the literature, this work also sheds new light on the important contribution of non glucose carbon sources to the global carbon fluxes of astrocytic energy metabolism, even under resting conditions. In summary, ^{13}C isotopic transient MFA allows for the integration of the high amount of metabolomics data being generated and for an increased resolution of estimated fluxes. Due to its flexibility, the structure of the model is easy to adapt to a neuronal metabolic network or even to a co-culture system in which the different cellular compartments can be separated. Depending on the choice of the ^{13}C-labelled substrate(s), this tool will allow the *in vitro* investigation of relevant aspects of cerebral bioenergetics, including specific metabolic disease hallmarks, which can provide important clues to help understanding *in vivo* data.

5 Acknowledgements

This work was supported by the *Fundação para a Ciência e Tecnologia* (FCT), Portugal (project ref. PTDC/BIO/69407/2006). Ana Amaral acknowledges the FCT PhD grant (ref SFRH/BD/29666/2006) and Ana Teixeira acknowledges the MIT Portugal Program. Prof. Rui Oliveira (FCT-UNL, Portugal) is acknowledged for fruitful discussions regarding metabolic modelling issues and the critical reading of the manuscript. The technical assistance by Lars Evje (NTNU, Norway) on GC-MS analyses is gratefully acknowledged.

6 References

Amaral A. I., Teixeira A. P., Sonnewald U. and Alves P. M. (2011) Estimation of intracellular fluxes in cerebellar neurons after hypoglycemia: importance of the pyruvate recycling pathway and glutamine oxidation. *J Neurosci Res* **89,** 700-710.

Amaral A. I., Teixeira A. P., Martens S., Bernal V., Sousa M. F. and Alves P. M. (2010) Metabolic alterations induced by ischemia in primary cultures of astrocytes: merging (13)C NMR spectroscopy and metabolic flux analysis. *J Neurochem* **113,** 735-748.

Bakken I. J., White L. R., Aasly J., Unsgard G. and Sonnewald U. (1997) Lactate formation from [U-13C]aspartate in cultured astrocytes: compartmentation of pyruvate metabolism. *Neurosci Lett* **237,** 117-120.

Beetsch J. W. and Olson J. E. (1998) Taurine synthesis and cysteine metabolism in cultured rat astrocytes: effects of hyperosmotic exposure. *Am J Physiol* **274,** C866-874.

Ben-Yoseph O., Boxer P. A. and Ross B. D. (1996) Assessment of the role of the glutathione and pentose phosphate pathways in the protection of primary cerebrocortical cultures from oxidative stress. *J Neurochem* **66,** 2329-2337.

Biemann K. (1962) *Mass spectrometry*, pp 223-227. McGraw Hill, New York.

Bixel M. G. and Hamprecht B. (1995) Generation of ketone bodies from leucine by cultured astroglial cells. *J Neurochem* **65,** 2450-2461.

Brand A., Engelmann J. and Leibfritz D. (1992) A 13C NMR study on fluxes into the TCA cycle of neuronal and glial tumor cell lines and primary cells. *Biochimie* **74,** 941-948.

Brand A., Richter-Landsberg C. and Leibfritz D. (1993) Multinuclear NMR studies on the energy metabolism of glial and neuronal cells. *Dev Neurosci* **15,** 289-298.

Brand A., Leibfritz D., Hamprecht B. and Dringen R. (1998) Metabolism of cysteine in astroglial cells: synthesis of hypotaurine and taurine. *J Neurochem* **71,** 827-832.

Cakir T., Alsan S., Saybasili H., Akin A. and Ulgen K. O. (2007) Reconstruction and flux analysis of coupling between metabolic pathways of astrocytes and neurons: application to cerebral hypoxia. *Theor Biol Med Model* **4,** 48.

Cerdan S., Kunnecke B. and Seelig J. (1990) Cerebral metabolism of [1,2-13C2]acetate as detected by in vivo and in vitro 13C NMR. *J Biol Chem* **265,** 12916-12926.

Choi I. Y., Lei H. and Gruetter R. (2002) Effect of deep pentobarbital anesthesia on neurotransmitter metabolism in vivo: on the correlation of total glucose consumption with glutamatergic action. *J Cereb Blood Flow Metab* **22,** 1343-1351.

Cruz N. F., Ball K. K. and Dienel G. A. (2007) Functional imaging of focal brain activation in conscious rats: impact of [(14)C]glucose metabolite spreading and release. *J Neurosci Res* **85,** 3254-3266.

Dienel G. A. and Cruz N. F. (2009) Exchange-mediated dilution of brain lactate specific activity: implications for the origin of glutamate dilution and the contributions of glutamine dilution and other pathways. *J Neurochem* **109 Suppl 1,** 30-37.

Dienel G. A., Ball K. K. and Cruz N. F. (2007) A glycogen phosphorylase inhibitor selectively enhances local rates of glucose utilization in brain during sensory stimulation of conscious rats: implications for glycogen turnover. *J Neurochem* **102,** 466-478.

Dringen R. (2000) Metabolism and functions of glutathione in brain. *Prog Neurobiol* **62,** 649-671.

Dringen R. and Hirrlinger J. (2003) Glutathione pathways in the brain. *Biol Chem* **384,** 505-516.

Duarte J. M. N., Lanz B. and Gruetter R. (2011) Compartmentalized cerebral metabolism of [1,6-13C]glucose determined by in vivo 13C NMR spectroscopy at 14.1 T. *Frontiers in Neuroenergetics* **3**.

Dusick J. R., Glenn T. C., Lee W. N., Vespa P. M., Kelly D. F., Lee S. M., Hovda D. A. and Martin N. A. (2007) Increased pentose phosphate pathway flux after clinical traumatic brain injury: a [1,2-13C2]glucose labelling study in humans. *J Cereb Blood Flow Metab* **27,** 1593-1602.

Garcia-Espinosa M. A., Rodrigues T. B., Sierra A., Benito M., Fonseca C., Gray H. L., Bartnik B. L., Garcia-Martin M. L., Ballesteros P. and Cerdan S. (2004) Cerebral glucose metabolism and the glutamine cycle as detected by in vivo and in vitro 13C NMR spectroscopy. *Neurochem Int* **45,** 297-303.

Gruetter R., Seaquist E. R. and Ugurbil K. (2001) A mathematical model of compartmentalized neurotransmitter metabolism in the human brain. *Am J Physiol Endocrinol Metab* **281,** E100-112.

Gruetter R., Seaquist E. R., Kim S. and Ugurbil K. (1998) Localized in vivo 13C-NMR of glutamate metabolism in the human brain: initial results at 4 tesla. *Dev Neurosci* **20,** 380-388.

Gruetter R., Adriany G., Choi I. Y., Henry P. G., Lei H. and Oz G. (2003) Localized in vivo 13C NMR spectroscopy of the brain. *NMR Biomed* **16,** 313-338.

Haberg A., Qu H., Bakken I. J., Sande L. M., White L. R., Haraldseth O., Unsgard G., Aasly J. and Sonnewald U. (1998) In vitro and ex vivo 13C-NMR spectroscopy studies of pyruvate recycling in brain. *Dev Neurosci* **20,** 389-398.

Hassel B., Sonnewald U. and Fonnum F. (1995) Glial-neuronal interactions as studied by cerebral metabolism of [2-13C]acetate and [1-13C]glucose: an ex vivo 13C NMR spectroscopic study. *J Neurochem* **64,** 2773-2782.

Henry P. G., Lebon V., Vaufrey F., Brouillet E., Hantraye P. and Bloch G. (2002) Decreased TCA cycle rate in the rat brain after acute 3-NP treatment measured by in vivo 1H-[13C] NMR spectroscopy. *J Neurochem* **82,** 857-866.

Henry P. G., Adriany G., Deelchand D., Gruetter R., Marjanska M., Oz G., Seaquist E. R., Shestov A. and Ugurbil K. (2006) In vivo 13C NMR spectroscopy and metabolic modelling in the brain: a practical perspective. *Magn Reson Imaging* **24,** 527-539.

Hofmann U., Maier K., Niebel A., Vacun G., Reuss M. and Mauch K. (2008) Identification of metabolic fluxes in hepatic cells from transient 13C-labelling experiments: Part I. Experimental observations. *Biotechnol Bioeng* **100,** 344-354.

Hyder F., Patel A. B., Gjedde A., Rothman D. L., Behar K. L. and Shulman R. G. (2006) Neuronal-glial glucose oxidation and glutamatergic-GABAergic function. *J Cereb Blood Flow Metab* **26,** 865-877.

Johansen M. L., Bak L. K., Schousboe A., Iversen P., Sorensen M., Keiding S., Vilstrup H., Gjedde A., Ott P. and Waagepetersen H. S. (2007) The metabolic role of isoleucine in detoxification of ammonia in cultured mouse neurons and astrocytes. *Neurochem Int* **50,** 1042-1051.

Jolivet R., Magistretti P. J. and Weber B. (2009) Deciphering neuron-glia compartmentalization in cortical energy metabolism. *Front Neuroenergetics* **1,** 4.

Kauffman K. J., Prakash P. and Edwards J. S. (2003) Advances in flux balance analysis. *Current Opinion in Biotechnology* **14,** 491-496.

Kranich O., Dringen R., Sandberg M. and Hamprecht B. (1998) Utilization of cysteine and cysteine precursors for the synthesis of glutathione in astroglial cultures: preference for cystine. *Glia* **22,** 11-18.

Lebon V., Petersen K. F., Cline G. W., Shen J., Mason G. F., Dufour S., Behar K. L., Shulman G. I. and Rothman D. L. (2002) Astroglial contribution to brain energy metabolism in humans revealed by 13C nuclear magnetic resonance spectroscopy: elucidation of the dominant pathway for neurotransmitter glutamate repletion and measurement of astrocytic oxidative metabolism. *J Neurosci* **22,** 1523-1531.

Lee K., Berthiaume F., Stephanopoulos G. N. and Yarmush M. L. (1999) Metabolic flux analysis: a powerful tool for monitoring tissue function. *Tissue Eng* **5,** 347-368.

Lewis N. E., Schramm G., Bordbar A., Schellenberger J., Andersen M. P., Cheng J. K., Patel N., Yee A., Lewis R. A., Eils R., Konig R. and Palsson B. O. (2010) Large-scale in silico modelling of metabolic interactions between cell types in the human brain. *Nat Biotechnol* **28,** 1279-1285.

Malloy C. R., Sherry A. D. and Jeffrey F. M. (1988) Evaluation of carbon flux and substrate selection through alternate pathways involving the citric acid cycle of the heart by 13C NMR spectroscopy. *J Biol Chem* **263,** 6964-6971.

Martin M., Portais J. C., Labouesse J., Canioni P. and Merle M. (1993) [1-13C]glucose metabolism in rat cerebellar granule cells and astrocytes in primary culture. Evaluation of flux parameters by 13C- and 1H-NMR spectroscopy. *Eur J Biochem* **217,** 617-625.

Mason G. F., Rothman D. L., Behar K. L. and Shulman R. G. (1992) NMR determination of the TCA cycle rate and alpha-ketoglutarate/glutamate exchange rate in rat brain. *J Cereb Blood Flow Metab* **12,** 434-447.

Mason G. F., Gruetter R., Rothman D. L., Behar K. L., Shulman R. G. and Novotny E. J. (1995) Simultaneous determination of the rates of the TCA cycle, glucose utilization, alpha-ketoglutarate/glutamate exchange, and glutamine synthesis in human brain by NMR. *J Cereb Blood Flow Metab* **15,** 12-25.

Mawhinney T., Robinett R., Atalay A. and Madson M. (1986) Analysis of amino acids as their tert-butyldimethylsilyl derivatives by gas-liquid chromatography and mass spectrometry. *Journal of Chromatography* **358,** 231-242.

McKenna M. C., Waagepetersen H. S., Schousboe A. and Sonnewald U. (2006) Neuronal and astrocytic shuttle mechanisms for cytosolic-mitochondrial transfer of reducing equivalents: current evidence and pharmacological tools. *Biochem Pharmacol* **71,** 399-407.

Merle M., Bouzier-Sore A. K. and Canioni P. (2002) Time-dependence of the contribution of pyruvate carboxylase versus pyruvate dehydrogenase to rat brain glutamine labelling from [1-(13) C]glucose metabolism. *J Neurochem* **82,** 47-57.

Merle M., Martin M., Villegier A. and Canioni P. (1996a) Mathematical modelling of the citric acid cycle for the analysis of glutamine isotopomers from cerebellar astrocytes incubated with [1(-13)C]glucose. *Eur J Biochem* **239,** 742-751.

Merle M., Martin M., Villegier A. and Canioni P. (1996b) [1-13C]glucose metabolism in brain cells: isotopomer analysis of glutamine from cerebellar astrocytes and glutamate from granule cells. *Dev Neurosci* **18,** 460-468.

Metallo C. M., Walther J. L. and Stephanopoulos G. (2009) Evaluation of 13C isotopic tracers for metabolic flux analysis in mammalian cells. *J Biotechnol* **144,** 167-174.

Murin R., Mohammadi G., Leibfritz D. and Hamprecht B. (2009) Glial metabolism of valine. *Neurochem Res* **34,** 1195-1203.

Noh K. and Wiechert W. (2006) Experimental design principles for isotopically instationary 13C labelling experiments. *Biotechnol Bioeng* **94,** 234-251.

Noh K., Wahl A. and Wiechert W. (2006) Computational tools for isotopically instationary 13C labelling experiments under metabolic steady state conditions. *Metab Eng* **8,** 554-577.

Noh K., Gronke K., Luo B., Takors R., Oldiges M. and Wiechert W. (2007) Metabolic flux analysis at ultra short time scale: isotopically non-stationary 13C labelling experiments. *J Biotechnol* **129,** 249-267.

O'Connor E., Devesa A., Garcia C., Puertes I. R., Pellin A. and Vina J. R. (1995) Biosynthesis and maintenance of GSH in primary astrocyte cultures: role of L-cystine and ascorbate. *Brain Res* **680,** 157-163.

Oz G., Berkich D. A., Henry P. G., Xu Y., LaNoue K., Hutson S. M. and Gruetter R. (2004) Neuroglial metabolism in the awake rat brain: CO2 fixation increases with brain activity. *J Neurosci* **24,** 11273-11279.

Patel A. B., de Graaf R. A., Mason G. F., Rothman D. L., Shulman R. G. and Behar K. L. (2005) The contribution of GABA to glutamate/glutamine cycling and energy metabolism in the rat cortex in vivo. *Proc Natl Acad Sci U S A* **102,** 5588-5593.

Quek L. E., Dietmair S., Kromer J. O. and Nielsen L. K. (2010) Metabolic flux analysis in mammalian cell culture. *Metab Eng* **12,** 161-171.

Richter-Landsberg C. and Besser A. (1994) Effects of organotins on rat brain astrocytes in culture. *J Neurochem* **63,** 2202-2209.

Schaub J., Mauch K. and Reuss M. (2008) Metabolic flux analysis in Escherichia coli by integrating isotopic dynamic and isotopic stationary 13C labelling data. *Biotechnol Bioeng* **99,** 1170-1185.

Shank R. P., Bennett G. S., Freytag S. O. and Campbell G. L. (1985) Pyruvate carboxylase: an astrocyte-specific enzyme implicated in the replenishment of amino acid neurotransmitter pools. *Brain Res* **329,** 364-367.

Shen J., Rothman D. L., Behar K. L. and Xu S. (2009) Determination of the glutamate-glutamine cycling flux using two-compartment dynamic metabolic modelling is sensitive to astroglial dilution. *J Cereb Blood Flow Metab* **29,** 108-118.

Shestov A. A., Valette J., Ugurbil K. and Henry P. G. (2007) On the reliability of (13)C metabolic modelling with two-compartment neuronal-glial models. *J Neurosci Res* **85,** 3294-3303.

Sickmann H. M., Schousboe A., Fosgerau K. and Waagepetersen H. S. (2005) Compartmentation of lactate originating from glycogen and glucose in cultured astrocytes. *Neurochem Res* **30,** 1295-1304.

Sonnewald U., Schousboe A., Qu H. and Waagepetersen H. S. (2004) Intracellular metabolic compartmentation assessed by 13C magnetic resonance spectroscopy. *Neurochem Int* **45,** 305-310.

Sonnewald U., Westergaard N., Jones P., Taylor A., Bachelard H. S. and Schousboe A. (1996) Metabolism of [U-13C5] glutamine in cultured astrocytes studied by NMR spectroscopy: first evidence of astrocytic pyruvate recycling. *J Neurochem* **67,** 2566-2572.

Sonnewald U., Westergaard N., Hassel B., Muller T. B., Unsgard G., Fonnum F., Hertz L., Schousboe A. and Petersen S. B. (1993) NMR spectroscopic studies of 13C acetate and 13C glucose metabolism in neocortical astrocytes: evidence for mitochondrial heterogeneity. *Dev Neurosci* **15,** 351-358.

Teixeira A. P., Santos S. S., Carinhas N., Oliveira R. and Alves P. M. (2008) Combining metabolic flux analysis tools and (13)C NMR to estimate intracellular fluxes of cultured astrocytes. *Neurochem Int* **52,** 478-486.

Varma A. and Palsson B. O. (1994) Stoichiometric flux balance models quantitatively predict growth and metabolic by-product secretion in wild-type Escherichia coli W3110. *Appl Environ Microbiol* **60,** 3724-3731.

Waagepetersen H. S., Sonnewald U. and Schousboe A. (2003) Compartmentation of glutamine, glutamate, and GABA metabolism in neurons and astrocytes: functional implications. *Neuroscientist* **9,** 398-403.

Waagepetersen H. S., Sonnewald U., Larsson O. M. and Schousboe A. (2001) Multiple compartments with different metabolic characteristics are involved in biosynthesis of intracellular and released glutamine and citrate in astrocytes. *Glia* **35,** 246-252.

Waagepetersen H. S., Qu H., Hertz L., Sonnewald U. and Schousboe A. (2002) Demonstration of pyruvate recycling in primary cultures of neocortical astrocytes but not in neurons. *Neurochem Res* **27,** 1431-1437.

Weljie A. M., Newton J., Mercier P., Carlson E. and Slupsky C. M. (2006) Targeted profiling: quantitative analysis of 1H NMR metabolomics data. *Anal Chem* **78,** 4430-4442.

Westergaard N., Sonnewald U., Unsgard G., Peng L., Hertz L. and Schousboe A. (1994) Uptake, release, and metabolism of citrate in neurons and astrocytes in primary cultures. *J Neurochem* **62,** 1727-1733.

Wiechert W. and de Graaf A. A. (1997) Bidirectional reaction steps in metabolic networks: I. Modelling and simulation of carbon isotope labelling experiments. *Biotechnol Bioeng* **55,** 101-117.

Wiechert W. and Noh K. (2005) From stationary to instationary metabolic flux analysis. *Adv Biochem Eng Biotechnol* **92,** 145-172.

Yudkoff M., Daikhin Y., Grunstein L., Nissim I., Stern J. and Pleasure D. (1996) Astrocyte leucine metabolism: significance of branched-chain amino acid transamination. *J Neurochem* **66,** 378-385.

Zwingmann C. and Leibfritz D. (2003) Regulation of glial metabolism studied by 13C-NMR. *NMR Biomed* **16,** 370-399.

CHAPTER 5

Down-Regulation of Glial Glutamate Transporters by RNAi in Primary Cultures of Astrocytes

Ana I Amaral, Lydie Boussicault, Ana P Teixeira, Nicole Deglon, Gilles Bonvento and Paula M Alves

Part of this work was presented as a poster at the 9th European Meeting on Glial Cells in Health and Disease – Paris, France (2009)

Abstract

One of the main functions of astrocytes is to take up glutamate released during neurotransmission, due to the specific glial localization of glutamate transporters GLAST and GLT-1. This process plays a key role in the regulation of glucose metabolism in addition to preventing neuronal excitotoxicity. However, the distinct function of GLAST and GLT-1 is not known. Moreover, impaired glial glutamate uptake, due to decreased expression of these transporters, appears to be involved in the pathophysiology of neurodegenerative diseases, such as Huntington's disease (HD). Thus, the aim of this work was to investigate the role of GLAST and GLT-1 in astrocytic energy metabolism. The approach chosen was to down-regulate these transporters in cultured astrocytes using RNAi tools and subsequently quantify the changes in their metabolic fluxes using metabolic flux analysis. Different RNAi strategies were tested: transduction of cells with lentiviral vectors carrying shRNA sequences or cell transfections using plasmid DNA through lipofection or electroporation. Some results suggested that lentiviral vectors pseudo-typed with a mokola envelope were able to down-regulate glutamate transporters in cultured astrocytes, although to a low extent. This was indicated by the expression of the GFP-reporter gene measured by flow-cytometry and by the decrease in glutamate uptake rate and in protein expression levels, compared to non-infected cells. However, control vectors containing siRNA sequences targeting GFP or luciferase genes had similar or better effects than the vectors targeting glutamate transporters, thus proving not to be suitable control vectors and suggesting that results obtained with siGLAST and siGLT-1 vectors might not be specific. Further studies suggested that the inefficacy of the lentiviral vectors used could be due to the mokola envelope, as VSV-G pseudotyped vectors yielded better results concerning mRNA levels and protein expression of GFP in cultured astrocytes. Due to time constraints, it was not possible to test further the new viral constructs and clarify this issue. In summary, the down-regulation of glutamate transporters was not successful and, consequently, metabolic studies could not be performed. Future studies on viral vector constructs and infection protocols are required to allow the successful accomplishment of this project.

CONTENTS

1 Introduction

Astrocytes are the most numerous cells in the brain and participate in a large and diverse variety of functions (Ransom et al. 2003). Besides providing neurons with nutrients, growth factors, and structural support, they also protect against excitotoxicity by clearing excess excitatory neurotransmitters from the extracellular space. Indeed, the glial glutamate transporters, GLAST and GLT-1, are responsible for the bulk of extracellular glutamate clearance (Danbolt 2001), and provide glutamate for crucial metabolic pathways, such as the synthesis of the main brain antioxidant glutathione and the production of energetic substrates for neurons (Voutsinos-Porche et al. 2003).

Glucose consumption by astrocytes was shown to be directly linked to glutamatergic activity through glial glutamate uptake (Pellerin and Magistretti 1994; Sibson et al. 1998). According to the astrocyte-neuron lactate shuttle hypothesis this metabolic coupling implies the re-establishment of the Na^+ gradient (altered due to the Na^+ co-transport with glutamate via GLAST and GLT-1) by the Na^+/K^+ ATPase which consumes ATP provided by glycolysis. Glutamate transport stimulates glial glucose uptake (via the GLUT-1 transporter) and glycolytic activity, resulting in the production of lactate that is subsequently transferred to neurons, answering their energetic needs (Pellerin et al. 2007). In fact, it has been suggested that glial glutamate transporters mediate the metabolic cross-talk between neurons and astrocytes as this classical response to synaptic activation was decreased in either GLAST or GLT-1 knock-out mice (Voutsinos-Porche et al. 2003).

The differential expression of GLAST and GLT-1 with development has been described, with GLAST being predominant in the cortex during the first postnatal week, while GLT-1 expression increases during the second week to become the major transporter thereafter (Furuta et al. 1997). In addition, a predominant expression of GLAST has been described in primary cultures of cortical astrocytes from neonatal mice (Voutsinos-Porche et al. 2003). These observations suggest that GLAST and GLT-1

might play distinct roles in astrocytic physiology and therefore their individual roles should be further investigated.

Glial glutamate transporters are also thought to be involved in the pathologic processes underlying neurodegenerative diseases, including Huntington's disease (HD) (Maragakis and Rothstein 2006). HD is an autosomal dominant neurological disorder caused by a trinucleotide (coding for glutamine) repeat expansion in the Huntingtin (Htt) gene. This expansion produces an altered form of the Htt protein, mutant Htt (mHtt), resulting in the progressive loss of medium-sized spiny neurons (MSNs) in the striatum (Walker 2007). The expression of an N-terminal fragment of mHtt in cultured astrocytes has been recently shown to decrease both GLT-1 level and function, and to attenuate their protection of cultured neurons from glutamate toxicity (Shin et al. 2005). Moreover, it has been shown that expression of the N-terminal mHtt with a large poly-glutamine (poly-Q) repeat (160Q) in mouse brain astrocytes decreases the expression and function of GLT-1 and is sufficient to induce neurological symptoms in those mice (Bradford et al. 2009). These authors additionally observed that glial expression of mHtt exacerbates neurological symptoms in double transgenic mice expressing mHtt in both neuronal and glial cells, indicating that glial function might indeed be impaired in HD (Bradford et al. 2010).

Using a different approach, another rat model of HD has been developed in which different forms of mHtt are expressed selectively in striatal neurons via lentiviral-mediated delivery (de Almeida et al. 2002; Regulier et al. 2003). More recently, a gene transfer strategy that allows the selective expression of any transgene into astrocytes *in vivo* has been developed (Colin et al. 2009). This new approach relies on a lentiviral vector pseudotyped with mokola and includes a specific neuronal microRNA target sequence to eliminate residual expression of the transgene in neuronal cells. In addition, through RNA interference, these vectors can also be used to down-regulate specific proteins. Therefore, these experimental models provide the opportunity to selectively depict the functional consequences of mHtt expression in neurons and glia and also to

specifically study the role of GLAST and GLT-1 by manipulating their expression either *in vivo* or *in vitro*. Thanks to this new lentiviral vector, a mouse model expressing mHtt only in striatal astrocytes has also been developed and investigations in this model revealed a specific down-regulation of the expression and function of GLAST and GLT-1 (Faideau et al. 2010). Furthermore, co-localization of mHtt in astrocytes was also found in brain samples from HD patients together with a grade-dependent decrease in striatal GLT-1 expression (Faideau et al. 2010), suggesting that expression of mHtt in astrocytes alters glial glutamate transport capacity and may indeed contribute to HD pathogenesis.

Given all the findings described above, this work aimed to further investigate, at first, the physiological importance of the glial glutamate transporters GLAST and GLT-1 in neuronal-astrocytic metabolic interactions and, later on, to evaluate their possible role in the pathophysiology of HD and how this might be related with the expression of the mHtt protein. The main goal was to apply metabolic modelling tools, previously developed by our group and already applied to study astrocytic metabolism in physiological conditions, and to characterize astrocytic metabolic alterations after an ischemic insult (Teixeira et al. 2008; Amaral et al. 2010). The MFA methodology allows estimating intracellular metabolic fluxes requiring only the measurement of some transmembrane rates in samples of cell culture medium. If desired, information provided by the use of ^{13}C-labelled compounds can also be included in the model, extending the amount of information generated, since it allows distinguishing the fluxes through parallel pathways (Amaral et al. 2010). MFA is a powerful tool to investigate the metabolic role of glial glutamate transporters by depicting eventual alterations in the different metabolic fluxes after the down-regulation of those proteins.

This work resulted from a collaboration project between the Animal Cell Technology Unit at IBET (Portugal) and the groups of Dr. Gilles Bonvento and Dr. Nicole Deglon at MIRCen, CEA (France) in the context of the FP6-funded CliniGene NoE.

2 Materials and Methods

2.1 Experiments performed at IBET

2.1.1 Primary cultures of astrocytes

Primary cultures of astrocytes were prepared from 1-2 day-old rat pups as described in (Amaral et al. 2010). Briefly, prefrontal cortices were collected, the meninges were carefully removed and the tissue was mechanically disrupted with "up and down movements" using Pasteur pipettes. Cell suspensions were then centrifuged for 15 min at 200 g. The cell pellets were suspended in DMEM (Invitrogen) containing 6 mM glucose, 15% FBS and Pen-Strep (100 U/mL). Cells were plated in 175 cm^2 tissue-culture flasks (approximately 1.5 cortices per flask) and kept in a humidified atmosphere of 7% CO_2 in air at 37°C. Half of the culture medium was exchanged two days after the beginning of the culture and complete medium exchanges were performed twice a week thereafter, gradually reducing the percentage of FBS to 10%.

2.1.2 Preliminary infections with lentiviral vectors

After one week in culture, cells were trypsinized and plated into 24-well plates at a cell density of $1x10^5$ cells/cm^2. Some cells were plated on poly-D-lysine coated glass coverslips for immunostaining analysis. Two days later, astrocytes were infected with 50 or 100 ng p24/cm^2 of lentivirus carrying sequences to over-express green fluorescent protein (GFP), GLAST or GLT-1 or to down-regulate GLAST or GLT-1 (siGLAST or siGLT-1 vectors, respectively). Lentiviral vectors description is presented in Table 5.1. The viral infection protocol followed was always the same: viral suspensions were diluted in culture medium and a complete medium exchange was performed with this suspension. Another medium exchange was subsequently performed two days after infection. In the following experiments, cells were plated at a cell density of $5x10^4$ cells/cm^2 and infections were performed two days later using a viral inoculum of 50 ng p24/cm^2 of siGLAST or siLuc vectors (Table 5.1). The percentage of infected cells (GFP-positive, for cells infected with lentiviral vectors carrying the GFP reporter gene), was assessed 10 days after infection by

flow cytometry. Cells were trypsinised and suspended in culture medium followed by analysis in a Partec CyFlow® space equipment (Partec, Münster, Germany). Data were analyzed with the FloMax® software.

Table 5.1 - Lentiviral vectors used in the infections of primary cultures of astrocytes

Vector	Abbreviation
Mokola-SIN-cPPT-PGK-GFP-WHV-MIR7.8(2S)	GFP
Mokola-SIN-cPPT-PGK-mouseGLT1-HA-WHV-MIR7.8(2S)	GLAST
Mokola-SIN-cPPT-PGK-mouseGLAST-HA-WHV-MIR7.8(2S)	GLT-1
VSV-SIN-PGK-GFP	VSV-GFP
Mokola-SIN-cPPT-PGK-GFP-WHV-MIR7.8(2S)-LTR-(TRE-H1-siGLAST)	siGLAST
Mokola-SIN-cPPT-PGK-GFP-WHV-MIR7.8(2S)-LTR-(TRE-H1-siGLT-1)	siGLT-1
Mokola-SIN-cPPT-PGK-nls-LacZ-WHV-MIR7.8(2S)LTR(N)-(TRE-H1-siGFP)	siGFP
Mokola-SIN-cPPT-PGK-GFP-WHV-MIR7.8(2S)-LTR-(TRE-H1-siLuc)	siLuc

2.1.3 Transfection of astrocytes

2.1.3.1 Transfection with lipofectamine

Astrocytes were cultured for 3 weeks, as described above and then plated on 24-well plates at a cell density of 5 x 10^4 cells/cm^2. Before transfection, culture medium was changed completely (DMEM medium with 10% FBS, as used for culture maintenance) using 500 µl total volume per well. The plasmid used in these tests was the siUNIV plasmid (SIN-CWP-GFP-LTR(N)-TRE-siUNIV), a universal siRNA control vector containing a GFP reporter gene (provided by the CEA partners). Plasmid DNA dilutions were prepared in Opti-MEM (Invitrogen) serum-free medium and PLUS reagent (diluted 1/200), followed by incubation at room temperature for 10 minutes. Then, lipofectamine LTX (Invitrogen) was added to the DNA dilutions (two lipofectamine dilutions were tested: 0.15 µl /100 ng DNA and 0.6 µl /100 ng DNA) for a final volume of 100 µl, mixed gently and incubated for 30 min at room temperature. 100 µl of the DNA-lipid complex containing 500, 1000 or 2000 ng of DNA were added dropwise to the cells in 500 µl of growth medium followed by gentle mixing of the plates. Each

condition was performed in triplicate. GFP expression was quantified 48 hours after transfection by flow cytometry and/or fluorescence microscopy using a LEICA DMI6000 microscope. For flow cytometry analysis, cells were trypsinised and suspended in culture medium containing 1 µg/ml propidium iodide (red fluorophore which binds the DNA of dead cells), followed by analysis in a Partec CyFlow® space equipment (Partec, Münster, Germany). Data were analyzed with the FloMax® software.

2.1.3.2 Transfection by electroporation

Astrocytes were cultured for 3 weeks as described above, detached from the T-flasks using trypsin and cell suspensions were prepared in electroporation buffer (Invitrogen) at a cell density of $1x10^6$ cells/ml or $5x10^6$ cells/ml. 1 ml of astrocyte culture medium (see above) was distributed by the wells of 24-well plates prior to transfections and placed in the incubator. 10 µl of the cell suspensions were electroporated using the NEON® Transfection System (Invitrogen) under different conditions (Table 5.2) and pipetted into each well of the cell culture plates. Each condition was performed in triplicate. Gene expression was assessed 48 hours after transfection by flow cytometry and/or fluorescence microscopy, as described for cells transfected with lipofectamine.

Table 5.2 - Conditions tested in electroporation of astrocytes.

Condition	Cell inoculum (total cells/well)	Pulse Voltage (V)	Pulse Duration (ms)	Number of pulses
1	$1x10^5$	1600	20	1
2		1650	20	1
3		1300	20	2
4		1700	10	2
5	$5x10^5$	1300	20	2
6		1400	20	2
7		1400	30	1
8		1700	20	1
9		1700	10	2

2.1.4 Glutamate uptake determination

To assess the functional effect of the down-regulation of GLAST and GLT-1 proteins, glutamate uptake was determined by measuring the decrease of its concentration in the

culture supernatant with time. Cells were incubated with medium containing 300 μM glutamate (sodium salt) and samples of culture supernatant were collected at different time-points during 4h.

2.1.5 Metabolic studies

After one week in culture, cells were trypsinized and plated at a cell density of $5x10^4$ cells/cm^2 in 75 cm^2 flasks or 6-well plates and infection was performed two days later using a viral inoculum of 50 ng p24/cm^2 of siGLAST or siLuc vectors. 10 days after infection, cells were incubated with DMEM culture medium (D5030, Sigma) containing 3 mM glucose, 500 μm glutamate, 1% FBS, pen/strep (100 U/mL) and no glutamine. Cell supernatant samples were collected at several time points for later quantification of total glucose, lactate and glutamate. At the end of the incubations, cells were harvested by trypsinization and washed with PBS. Cell pellets were stored at -80ºC until further treatment for western blot analysis.

2.1.6 Other analytical methods

Glucose and lactate were analyzed by enzymatic methods (YSI 7100 Multiparameter Bioanalytical System; Dayton, Ohio, USA) in samples of cell supernatant. Glutamate was quantified by HPLC using a pre-column derivatisation method based on the AccQ.Tag method from Waters as described in (Amaral et al. 2010). Total protein amounts in cell pellets were determined using the BCA kit form Pierce using BSA as standard, after dissolution of the cell pellets with 0.1 M NaOH.

2.1.7 Western Blot

2.1.7.1 Sample preparation

Cells were collected from the plates by trypsinization and pellets washed with PBS. Then, extraction was performed by resuspending pellets in lysis buffer containing 50 mM Tris-HCl, 150 mM NaCl, 5 mM EDTA, 1% Triton X-100 and protease inhibitors (100 μl of lysis buffer/$1x10^6$ cells) followed by incubation at 4ºC for 30 min. Extracts

were centrifuged at 15 000 g for 15 min at 4°C and supernatants (extracts) were collected and stored at -80°C.

2.1.7.2 SDS-PAGE Electrophoresis and Immunoblots

Samples were suspended in sodium dodecyl sulphate-polyacrylamide gel electrophoresis (SDS-PAGE) sample buffer (Invitrogen) and heated for 10 min at 70°C. Then, samples were loaded in a NuPAGE Bis-Tris Mini Gel (Invitrogen) and an SDS-PAGE electrophoresis was performed according to the manufacturer's instructions. Proteins were then transferred to PVDF membranes which were subsequently blocked in tris-buffered saline (Sigma) + 0.1% Tween 20 (TBST) and 5% (w/v) non-fat milk for 1 hour at RT. Membranes were subsequently incubated overnight with different primary antibodies: anti-GLAST (Frontier Science) (1:2000), anti-α-tubulin (Sigma) (1:5000) as a loading control, followed by incubation with horseradish peroxidase-conjugated secondary antibodies (GE-Healthcare) (1:5000) and developed with the ECL Kit (Amersham). Band intensities were quantified using the ImageJ software. Results obtained for GLAST were normalized with the values obtained for the α-tubulin bands.

2.1.8 Immunostaining

Cells were fixed with 4% paraformaldehyde (PFA) + 4% sucrose in PBS for 20 min followed by permeabilization with 0.1% TX-100 in PBS for 15 min at RT. Blocking of unspecific epitopes was performed using 0.2% fish skin gelatine in PBS for 30 min. Cells were then incubated with the primary antibodies anti-glial fibrillary acidic protein (GFAP) from mouse (Chemicon) (1/200), anti-GLAST and anti-GLT-1 from rabbit (1/1000) (FrontierScience), anti-hemagglutinin (HA) from mouse (Covance) (1/1000) diluted in 0.125% fish skin gelatine in PBS for 2h followed by incubation with the secondary antibodies AlexaFluor 488 anti-mouse or 594 anti-rabbit (Molecular Probes) (1/500) for 1h at RT. Preparations were mounted with ProLong Gold anti-fade reagent (Invitrogen) containing DAPI and allowed to dry overnight. Cells were observed under

an inverted fluorescence microscope (Leica DM IRB, Wetzlar, Germany).

2.2 Experiments performed at MIRCen, CEA

2.2.1 Transfection of 293T cells

Human embryonic kidney (HEK) 293T cells were plated at a cell density of $8x10^5$ cells/well on 6-well plates and transfected 24 h later. Plasmids used in the transfections are listed in Table 5.3. The method used was the transient transfection method with calcium chloride ($CaCl_2$). Plasmids were diluted in H_2O and mixed with 50 µl of $CaCl_2$ 0.5 M and 100 µl Hepes Buffered Saline (HBS; Fluka) 2X to a total volume of 200 µl. The DNA precipitates were then carefully pipetted onto each well by ensuring a homogeneous distribution on the cell monolayers. Two experiments were performed. A total amount of 5 µg of plasmid was used per well (5 µg for single transfections and 2.5 + 2.5 µg for co-transfections) except in the second transfection, in which only 2.5 µg were used for single transfections (GLAST or GLT-1 plasmids alone). 5 h after transfection, the total volume was replaced by fresh culture medium [DMEM containing 10% FBS and 1% (v/v) Pen-Strep] and cells were kept at 37°C in a humidified incubator with 5% CO_2 in air for 48h until cell extraction.

Table 5.3 - Plasmids used for transfections of 293T cells.

Plasmids	Abbreviation
SIN-PGK-mouseGLAST-WHV	GLAST
SIN-PGK-mouseGLT-1-WHV	GLT-1
SIN-cPPT-PGK-nls-LacZ-WHV-mir78(2s)LTR(N)-(TRE-tight-siGLAST)	siGLAST
SIN-cPPT-PGK-nls-LacZ-WHV-mir78(2s)LTR(N)-(TRE-tight-siGLT-1)	siGLT-1
SIN-cPPT-PGK-nls-LacZ-WHV-mir78(2s)LTR(N)-(TRE-tight-siGFP)	siGFP
SIN-CWP-GFP-MIR7.8(2S)-LTR-TRE-siLuc	siLuc

2.2.2 Primary cultures of astrocytes and infection with siRNA lentiviral vectors

Primary cultures of cerebral cortical astrocytes were prepared from newborn rats or mice (1–2 days old) following a protocol adapted from (Sorg and Magistretti 1992). Briefly,

forebrains were removed aseptically from the skulls, the meninges were carefully excised under a dissecting microscope, and the neocortex was dissected free of brainstem, thalamus, striatum, and hippocampus. The cells were dissociated by several passages through a 5 ml syringe without needle and subsequently using needles of decreasing gauge size. After centrifugation for 10 min at 200 g, the cell pellets were re-suspended in DMEM (ref. 31885, Invitrogen, Paisley, UK) supplemented with 10% FBS and 1% Pen-Strep. Cells were seeded on 6-well plates (final volume of 2 ml/well) or on 24-well plates with poly-D-lysine-coated glass coverslips (final volume of 1 ml/well) and incubated at 37°C in an atmosphere containing 5% CO_2/95% air. Half of the culture medium was renewed 3–4 days after seeding and, subsequently, complete medium exchanges were performed twice a week with 2 ml. Before each complete medium exchange, plates were shaken by hand for some seconds to release oligodendrocytes and microglial cells.

At 10 days *in vitro* (DIV), cells were infected with the lentiviral vectors siGLAST, siGLT-1, siLuc or siGFP (Table 5.2). Vector production was carried out by Noëlle Dufour and Gwennaelle Auregan at CEA-MIRCen. The viral inocula used was based on the amount of protein p24 (a protein localized on the viral capsid) quantified by ELISA, which corresponds to the total number of particles in a viral batch. Astrocytes on 6-well plates were infected with 200 or 400 ng p24/well whereas cells on 24-well plates were infected with 40 or 80 ng p24. Viral suspensions were diluted in culture medium and a complete medium exchange was performed. Cells in 6-well plates were extracted at 22 DIV to analyze GLAST and GLT-1 mRNA and protein expression levels. Cells in 24-well plates were treated according with the immunostaining protocol described below.

Further tests were performed aiming to compare the efficiency of infection using different viral envelopes, due to low efficiencies obtained in previous experiments. Cells were infected with VSV-SIN-PGK-GFP or with Mokola-SIN-PGK-GFP at 9 days in culture. 3 viral inocula were tested for each vector in 6-well and 24-well plates (Table 5.4). Viral suspensions were first diluted in culture medium at 20 ng/µL (for infection in 6-well plates) and at 1 ng/µL (for infection in 24-well plates) and after completely

changing the medium, cells were infected. Nine days after infection cells were extracted for posterior mRNA analysis by Reverse Transcriptase - quantitative Polimerase Chain Reaction (RT-qPCR; see details below).

Table 5.4 - Viral inocula (ng of p24) of Mokola-GFP and VSV-GFP vectors used to compare the efficiency of infection using different envelopes.

Vector	Plate	Viral inoculum (ng p24)		
VSV-SIN-PGK-GFP	6 wells	100 ng	200 ng	400 ng
	24 wells	20 ng	40 ng	60 ng
Mokola-SIN-PGK-GFP	6 wells	200 ng	400 ng	600 ng
	24 wells	40 ng	60 ng	80 ng

2.2.3 Western Blot

2.2.3.1 Sample preparation

Medium was collected and discarded and cell monolayers carefully washed with PBS (only for astrocytes). Membrane proteins were extracted by quickly adding 300 µl of lysis buffer containing 50 mM Tris HCl, 100 mM NaCl and 1% (v/v) SDS) followed by scraping cells from the plates and harvesting the cell suspensions into microtubes. The viscous suspensions were sonicated for some seconds to help to dissolve precipitated DNA and samples were subsequently divided into two fractions. One was directly used to determine protein concentrations using the BCA kit from Pierce (Rockford, IL, USA) using bovine serum albumin as standard. The other fraction was diluted ¼ in loading buffer 4X (Tris base 0.25 M, 0.4 M DTT, 40% (w/v) glycerol, 8% (v/v) SDS, bromophenol blue) and stored at -20ºC until western blot analysis.

2.2.3.2 SDS-Page electrophoresis and immunoblots

Samples were diluted in loading buffer 1X in order to have the same protein concentration in all samples. Then, proteins were denatured by boiling for 5 min. 30 µg of protein were loaded per lane in a 12% acrylamide gel in Tris-SDS and allowed to migrate by electrophoresis. The proteins were subsequently transferred to a

nitrocellulose membrane using the iBlot® Gel Transfer System from Invitrogen. Membranes were blocked in TBST (Tris 25 mM pH 7.4, NaCl 150 mM and Tween 20 0.1%) and 5% (w/v) non-fat milk for 1 hour at RT. Membranes were subsequently incubated overnight with different primary antibodies: anti-GLAST and anti-GLT-1 (Frontier Science, Japan) (1/5000) or anti-actin (Sigma) as a loading control, followed by incubation with horseradish peroxidase-conjugated secondary antibodies (GE-Healthcare) (1:5000) and developed with the chemiluminescence ECL Kit (Amersham). Band intensities were quantified using the ImageJ software. Results obtained for GLAST and GLT-1 were normalized with the values obtained for the actin bands.

2.2.4 Reverse Transcriptase - quantitative Polimerase Chain Reaction (RT-qPCR)

2.2.4.1 Extraction of Total RNA

Medium was collected and discarded and cell monolayers carefully washed with PBS (only for astrocytes). RNA was extracted by adding 1 ml (6-well plates) or 250 µl (24-well plates) of TRIzol® reagent (Invitrogen). Cells were scraped from the plates and transferred into sterile microtubes. Chloroform was added to the samples and phase-separation was induced by centrifugation at 12 000 g for 15 at 4ºC. The aqueous phase containing RNA was collected and mixed with isopropanol to precipitate the RNA. After centrifugation, the RNA pellets were washed with 75% ethanol and allowed to dry for some minutes at RT. Finally, pellets were suspended in RNAse free water (30-50 µl).

2.2.4.2 RT reaction

2 µg of RNA per sample were treated with RQ1 DNase for 30 min at 37ºC and the reaction stopped by addition of EGTA 20 mM followed by incubation at 65ºC for 10 min. 200 ng of the final product was subjected to a reverse transcription reaction by treatment with the enzyme SuperScript® III (SuperScript III One-Step real-time PCR System with Platinum® *Taq* DNA Polymerase Kit, Invitrogen) followed by treatment

with RNase H. The cDNA obtained was diluted at 4 ng/µl in H_2O/BSA 1%.

2.2.4.3 Quantitative PCR

Quantitative PCR was performed using the Platinum® SYBR® Green qPCR SuperMix-UDG kit from Invitrogen. 3 ng of cDNA were amplified in triplicates by the polymerase *Taq* Platinum® and the PCR products quantified through the incorporated SYBR® green using the equipment of real-time PCR Mastercycler ep Realplex (Eppendorf). The oligonucleotides used are listed on Table 5.5. The values obtained for GLAST and GLT-1 were normalized using those obtained for the housekeeping genes ß-actin (for 293T cells) or cyclophilin A (for astrocytes).

Table 5.5 - Primer sequences used in the quantitative PCR reactions.

Name	Target	Sequence
mGLAST-F	Mouse GLAST	TCTCCAGTCTCGTCACAGGAATG
mGLAST-R	Mouse GLAST	TGCCAATCACCACAGCAATG
mGLT-1-F	Mouse GLT-1	GGCAATCCCAAACTCAAGAAGC
mGLT-1-R	Mouse GLT-1	GTCACTGTCTGAATCTGCTGGAAAC
rGLAST-F	Rat GLAST	GGATGGAAAGATTCCAGCAA
rGLAST-R	Rat GLAST	ACCTCCCGGTAGCTCATTTT
rGLT-1-F	Rat GLT-1	CTGGGAAGAAGAACGACGAG
rGLT-1-R	Rat GLT-1	ACTGCCTTGGTTGTATTGGC
GFP301F	GFP	GTGCAGTGCTTCAGCCGCTA
GFP614R	GFP	TCGATGTTGTGGCGGATC
ß-Actin-F	Mouse ß-actin	TGAAGGTGACAGCAGTCGGTTG
ß-Actin-R	Mouse ß-actin	GGCTTTTAGGATGGCAAGGGAC
CYCLO-F	Mouse, rat and human cyclophilin A	ATGGCAAATGCTGGACCAAA
CYCLO-R	Mouse, rat and human cyclophilin A	GCCTTCTTTCACCTTCCCAAA

2.2.5 Immunostaining

Cells were washed with PBS and fixed with 4% (w/v) PFA for 20 min at RT. After careful washing with PBS, coverslips were stored at 4°C in 600 µl of PBS + 0.05% sodium azide until the rest of the protocol was performed. Cell permeabilization and blocking was performed with PBS + 0.2% Triton and 5% normal goat serum (NGS) for 1h at RT. Cells were then incubated with the primary antibodies anti-GFAP-Cy3 from mouse (Sigma) (1/500), anti-Iba1 (Wako) (1/500) and anti-GFP (1/200) from rabbit (Invitrogen) diluted in PBS + 0.2% triton + 3% NGS + 0.1% sodium azide overnight at

4ºC followed by incubation with the secondary antibody Alexa A488 anti-rabbit (Invitrogen) (1/500) for 1h. Cells were then incubated for 5 min with DAPI (Invitrogen) (1/2000) in PBS and preparations were mounted with mounting medium Fluorsave™ reagent (Calbiochem) and allowed to dry overnight. Preparations were observed under an inverted fluorescence microscope (Carl Zeiss).

3 Results

3.1 Experiments performed at IBET

3.1.1 Endogenous expression of GLAST and GLT-1 in primary cultures of rat astrocytes

Primary cultures of astrocytes on glass coverslips were stained with anti-GLT-1 and anti-GLAST antibodies to assess the endogenous expression of these transporters in the cultures. Both GLAST (Figure 5.1A) and GLT-1 (Figure 5.1B) expression was observed. However, GLAST expression appeared to be higher than that of GLT-1. When using the anti-GFAP antibody, specific of astrocytes, it was confirmed that most of the cells present in the culture were GFAP-positive and co-localized with GLAST and GLT-1 staining, confirming the glial expression of these transporters. No neurons or undifferentiated cells were found in the cultures (data not shown). Only a few oligodendrocytes, stained with O4, were observed (data not shown).

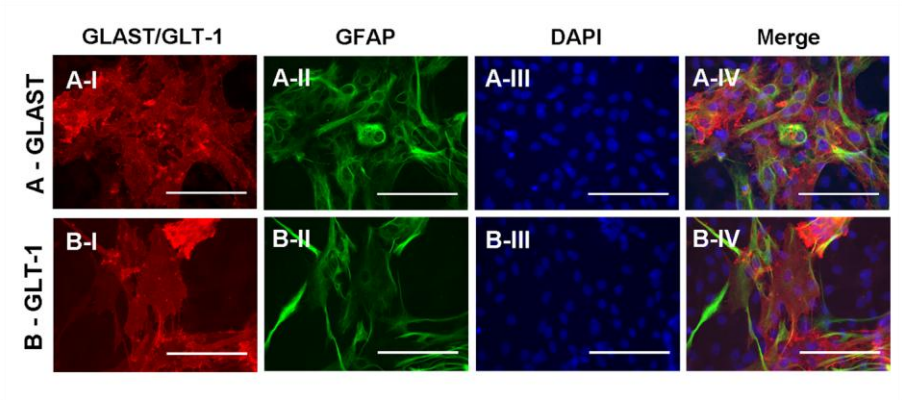

Figure 5.1 - Endogenous expression of GLAST and GLT-1 in primary cultures of astrocytes. A (I-IV): GLAST (red), GFAP (green), DAPI (blue); B (I-IV): GLT-1 (red), GFAP (green), nuclei (blue). Scale bar 50 μm.

3.1.2 Infection of astrocytes with lentiviral vectors

With the aim of establishing infection protocols and testing the efficiency of the lentiviral vectors in primary cultures of astrocytes, some preliminary tests were performed with the lentiviral vectors provided by Dr. Nicole Deglon (CEA, France).

3.1.2.1 Over-expression of GFP, GLAST and GLT-1 in astrocytes

Astrocytes were infected with lentiviral vectors carrying the GFP, GLAST, or GLT-1 genes (see Table 5.1) and the efficiency of infection in astrocytes was analyzed by flow-cytometry and immunofluorescence microscopy. A maximum average value of 50% GFP-positive cells was obtained by flow cytometry (Figure 5.2A) after infection with the GFP lentiviral vector. GFP expression in these cells was also observed by fluorescence microscopy (Figure 5.2B). The ability of the GLAST and GLT-1 lentiviral vectors to infect astrocytes was confirmed by immunostaining using an anti-HA antibody targeting a tag present in the transgene carried by the vector. As shown in Figure 5.2B, HA staining was observed by fluorescence microscopy after infection with both vectors, indicating the efficiency of infection.

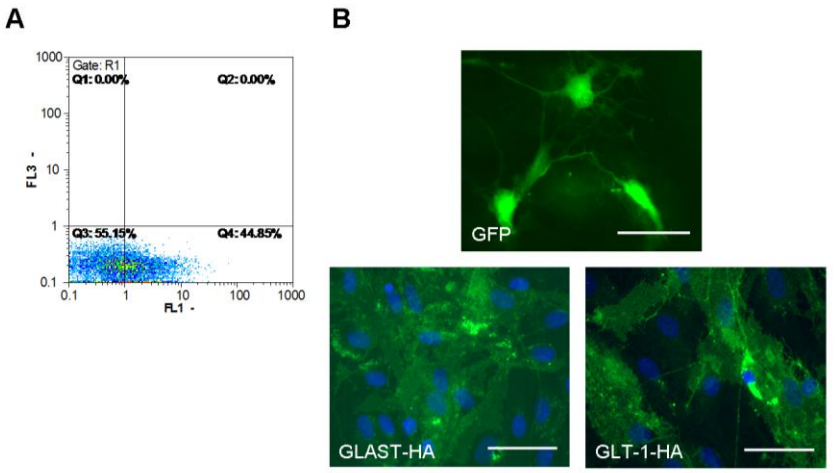

Figure 5.2 – Assessment of infected astrocytes by flow cytometry and fluorescence microscopy. A – Percentage of GFP-positive cells (Q4) determined by flow cytometry analysis; B – Fluorescence microscopy images of cells expressing GFP, GLAST or GLT-1 (green), as indicated. GLAST and GLT-1 were detected by immunostaining of the HA tag present in the gene carried by the vectors. Scale bar, 50 µm.

3.1.2.2 Down-regulation of GLAST and GLT-1 in astrocytes using lentiviral vectors

After testing lentiviral vectors to over-express GLAST or GLT-1, siRNA lentiviral vectors carrying a GFP reporter gene were also tested for their ability to down-regulate these genes in primary cultures of astrocytes. The percentage of infected cells was assessed by flow-cytometry and 24% GFP-positive cells were observed in siGLAST cultures whereas siGLT-1 cultures had 40% GFP-positive cells (Table 5.6).

Table 5.6 – GFP expression and glutamate uptake rate in astrocytes after infection with siRNA lentiviral vectors.

Vector	% GFP-positive cells	Glutamate uptake rate (nmol. mg prot^{-1}.min^{-1})	% Decrease in glutamate uptake rate[a]
(non-infected cells)	-	23	-
siGLAST	24	19	19
siGLT-1	40	16	30

[a] Relative to non-infected cells

This value was much lower than the ones obtained with the regular GFP lentiviral vectors used before (non siRNA). In addition to evaluating the percentage of infected

cells, a functional consequence of down-regulating GLAST and GLT-1 expression in astrocytes was also assessed. Since these proteins are glutamate transporters, the glutamate uptake rate was analyzed in the different cultures by measuring the rate of glutamate disappearance in the medium immediately after its addition. The results showed a decrease in the glutamate uptake rate of 19% and 30% in cells infected with siGLAST and siGLT-1 vectors, respectively, further confirming that the glutamate transporters were down-regulated. These results suggest that the percentage of infected cells and the effect at the glutamate uptake level were somewhat correlated, even though the effect at the level of glutamate uptake was not as pronounced as it would be expected from the GFP expression results. Consequently, new experiments were carried out to evaluate the extent of down-regulation of GLAST by using western blot instead of flow cytometry to directly check alterations in protein expression. At the same time, a siRNA control vector (siLuc) was also used for the first time. Western blot analysis showed that GLAST was successfully down-regulated in primary cultures of astrocytes by siGLAST (Figure 5.3). GLT-1 expression was also assessed but protein levels were very low, although they did not seem to be affected by siGLAST (data not shown), and consequently did not allow drawing any conclusions regarding cross-reactivity of siGLAST and GLT-1. Down-regulation of GLAST was also observed in cells infected with the siLuc control vector (Figure 5.3). The glutamate uptake rate was decreased in both cases, when compared to non-infected astrocytes, supporting the hypothesis that siLuc interfered with GLAST expression (Figure 5.4A). Again, it appears that the effect observed at the level of glutamate uptake is not as pronounced as the decrease in protein expression levels. Other metabolic consequences of decreased glutamate uptake were also observed in infected cells.

The increases of glucose uptake and lactate release, triggered by glutamate, that have been reported in the literature (Pellerin and Magistretti 1994) were reduced in cells infected with siGLAST but also with siLuc (Figure 5.4B and 5.4C).

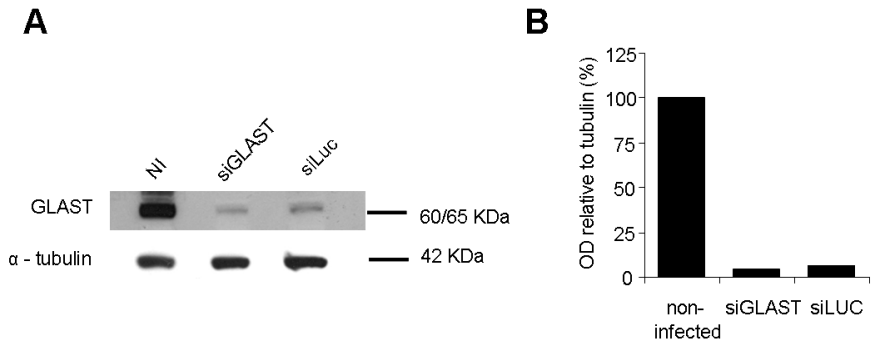

Figure 5.*3 – Down-regulation of GLAST in primary cultures of astrocytes using a siRNA lentiviral vector for GLAST.* A – Immunoblot of GLAST and α-tubulin (loading control); B – Densitometry analysis of GLAST expression normalized to α-tubulin levels.

These results from a preliminary experiment suggested that the siGLAST vector was able to down-regulate GLAST but a good control vector was still missing. Therefore, it was decided that future experiments would be performed at CEA (France) with the aims of defining a good siRNA control vector to be used in future studies and also validating the efficacy of the siRNA lentiviral vectors to down-regulate the GLAST and GLT-1 proteins in primary cultures of brain cells using well-established RT-qPCR and western blot protocols.

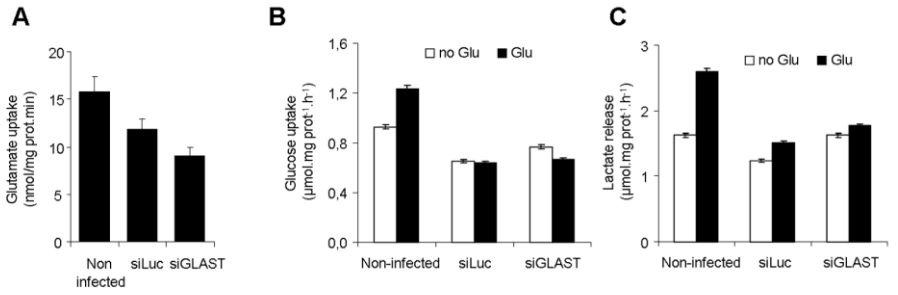

Figure 5.4 – Effect of the down-regulation of GLAST in glutamate uptake rate (A), glucose uptake (B) and lactate release (C) in primary cultures of astrocytes. Error bars correspond to the error associated to the linear regression function used to calculate the metabolic rates from metabolite concentration values measured along time in culture supernatants (n=1).

3.1.3 Transfection of astrocytes with plasmid DNA

Two different transfection methods (transfection with lipofectamine – lipofection - and electroporation) were additionally tested in alternative to the use of lentiviral vectors to perform RNA interference in primary cultures of astrocytes. These methods were chosen because they are described in the literature (Karra and Dahm 2010) as being suitable to transfect primary neuronal cells, which have similar characteristics to the cells used in this work. Lipofection is a conventional lipid-mediated gene delivery method based on cationic lipid molecules forming lipossomes that interact with negatively charged nucleic acids and facilitate the fusion of the lipid:DNA complexes with the negatively charged plasma membrane (Karra and Dahm 2010). Electroporation causes a temporary alteration of the plasma membrane properties by exposing cells to a voltage pulse and consequently allows charged extracellular material, e.g., plasmid DNA, to enter the cell, mainly to the cytoplasm (Karra and Dahm 2010). We have tested the NEON® electroporation system from Invitrogen, which is particularly indicated by the manufacturer to efficiently transfect sensitive cells, including primary cultures. A plasmid containing a universal siRNA control sequence and a GFP reporter gene was used to test these transfection methods.

3.1.3.1 Transfections with lipofectamine

Astrocytes were transfected with 500, 1000 and 2000 ng of DNA in 24 well plates using two lipofectamine/DNA dilutions per condition. Both non-transfected cells and controls to which only lipofectamine was added presented a regular morphology and were approximately 80% confluent 48h after transfection (approximately 50% confluent at transfection) (Figure 5.5). Cultures transfected with increasing amounts of DNA exhibited a very high percentage of dead cells and cell debris (>80% estimated by inspection under the microscope; Figure 5.5). In addition, attached cells presented a markedly altered morphology. These results were more evident in cultures transfected with 1000 and 2000 ng DNA/well and no differences were identified regarding the different lipofectamine/DNA ratios used. No green fluorescence was observed in the

cells that remained attached to the wells (data not shown) and, therefore, flow cytometry analysis was not performed. These results suggest that amounts higher than 500 ng of DNA are damaging the cells and that, above all, the conditions tested were not suitable to efficiently transfect these cells.

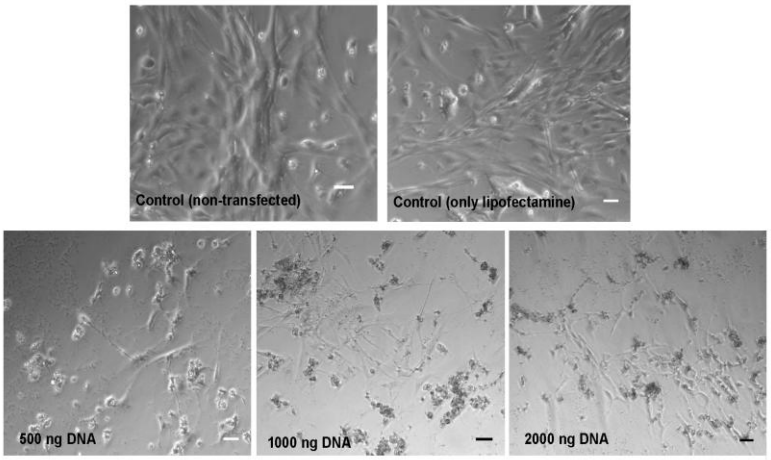

Figure 5.5 - Phase contrast microscopy images of astrocytes transfected with lipofectamine and increasing DNA amounts. Images presented correspond to the highest lipofectamine concentration used, as described in Materials and Methods. Scale bar, 50 µm.

3.1.3.2 Transfections by electroporation

We started by testing electroporation at a cell density of $1x10^6$ cells/ml. Very few cells were attached to the wells 48h after electroporation (data not shown). Furthermore, a very low percentage of GFP-positive cells was observed by fluorescence microscopy (data not shown). Flow cytometry results indicated low cell death (<15%) and only a maximum of 8.5% GFP-positive cells (data not shown). We concluded that such a low cell density would not be enough to evaluate transfection efficiency. Therefore, we decided to increase cell concentration to $5x10^6$ cells/ml and test similar electroporation conditions. In these experiments an increase in cell death was evident, as observed by phase contrast microscopy, when compared to controls, and very few GFP-positive cells were observed using fluorescence microscopy in the few cells that were attached to the

wells (Figure 5.6). Flow cytometry analysis showed a very high percentage of cell debris, indicated by a large population outside of the gated region in Figure 5.7A.

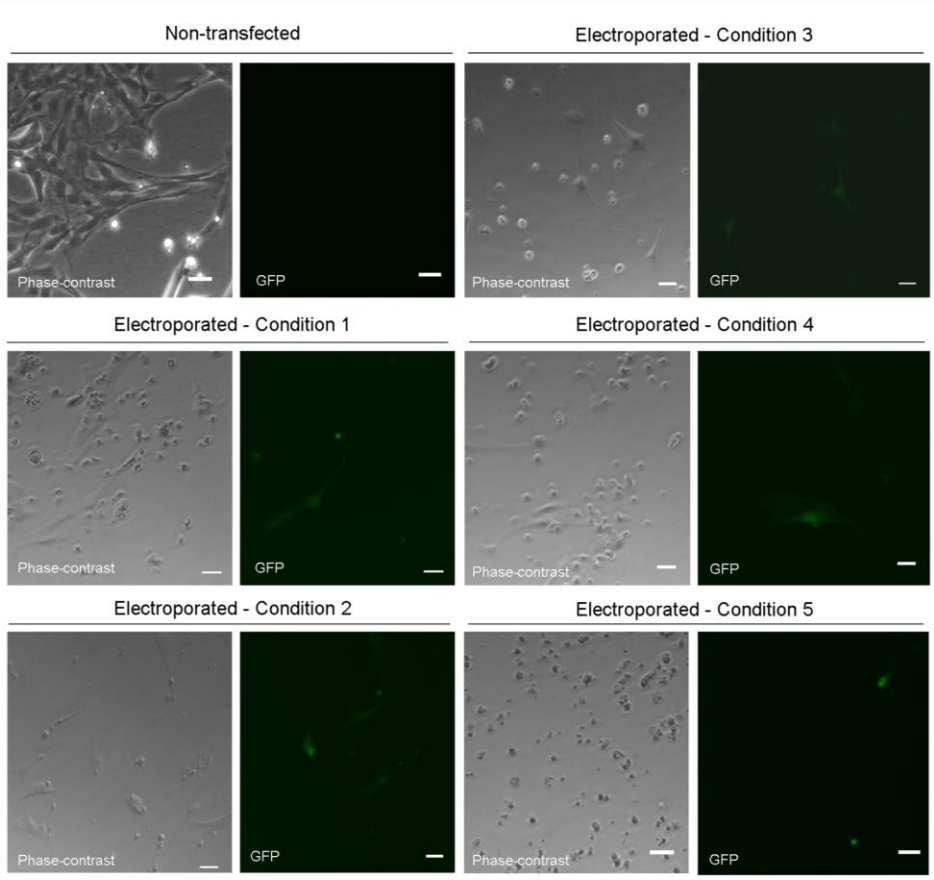

Figure 5.6 - Phase contrast and fluorescence microscopy images of astrocytes transfected by electroporation with a plasmid carrying a GFP-reporter gene. Cells were suspended in electroporation buffer at a cell concentration of $5x10^6$ cells/ml and 10 µl were electroporated in triplicate and plated in 24-well plates. 5 different conditions were tested, corresponding to different pulse voltages or pulse number, as described in the Materials and Methods. Transfection efficiency was evaluated 48 h after transfection. Scale bars, 50 µm.

Cells in the gated region R1 were about 50% for controls versus less than 20% for electroporated cells (Figure 5.7A), which clearly indicates the high percentage of cell death. Thus, since the calculations performed by the software are based on the gated

cells, there is an underestimation of the percentage of cell death, as the maximum observed was ~18% for PI-positive non-transfected (GFP-) cells (Figure 5.7B-I, condition 5). Furthermore, flow cytometry results indicated a very low efficiency of transfection with an average of only 2.5% of GFP-positive and viable cells (Figure 5.7B-II). In conclusion, electroporation conditions tested were too hard for the cells and appear not to be a good strategy to achieve a high efficiency of transfection in primary cultures of astrocytes.

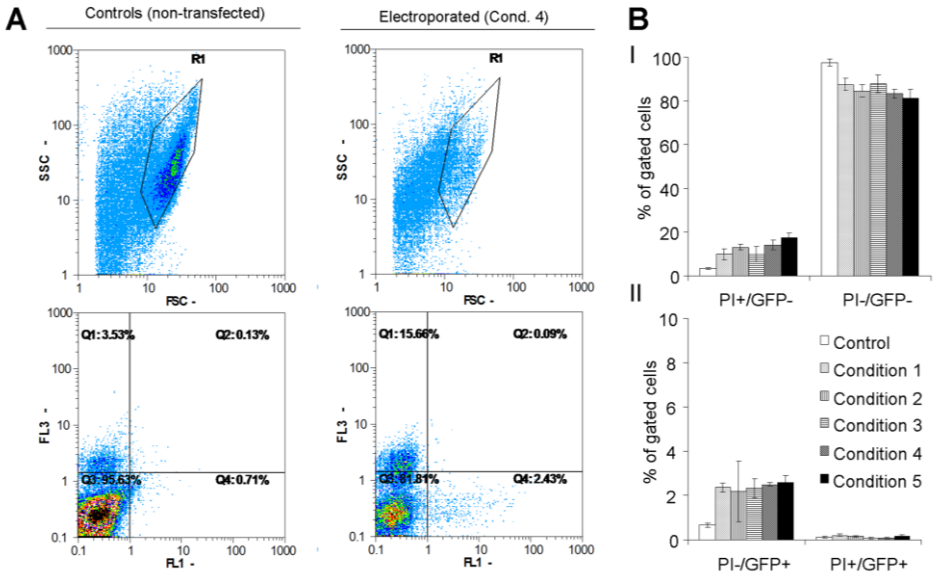

Figure 5.7 - Flow cytometry analysis of astrocytes transfected by electroporation with a plasmid containing a GFP-reporter gene. 48 h after transfection, cells were collected using trypsin, suspended in medium containing PI to label dead cells and analyzed by flow cytometry. A - Example of flow cytometry diagrams for control and transfected cells; R1 indicates the gated region based on which the calculations are performed; Q1 – PI+/GFP-; Q2 – PI+/GFP+; Q3 – PI-/GFP+; Q4 – PI-/GFP+. B – Relative percentage of the cell populations analyzed by flow cytometry for the different conditions tested. I – transfected cells (GFP+); II - non-transfected (GFP-) cells. Values are mean ± s.d. (n=3).

3.2 Experiments performed at MIRCen, CEA

3.2.1 Over-expression and down-regulation of GLAST and GLT-1 in 293T cells

In order to test the efficiency of the siRNA plasmids used in the construction of lentiviral vectors, 293T cells were transfected with GLAST or GLT-1 plasmids alone or

in combination with siGLAST and siGLT-1. In addition, two siRNA control plasmids, siGFP and siLuc were tested as siRNA control vectors. The results are presented in Figure 5.8.

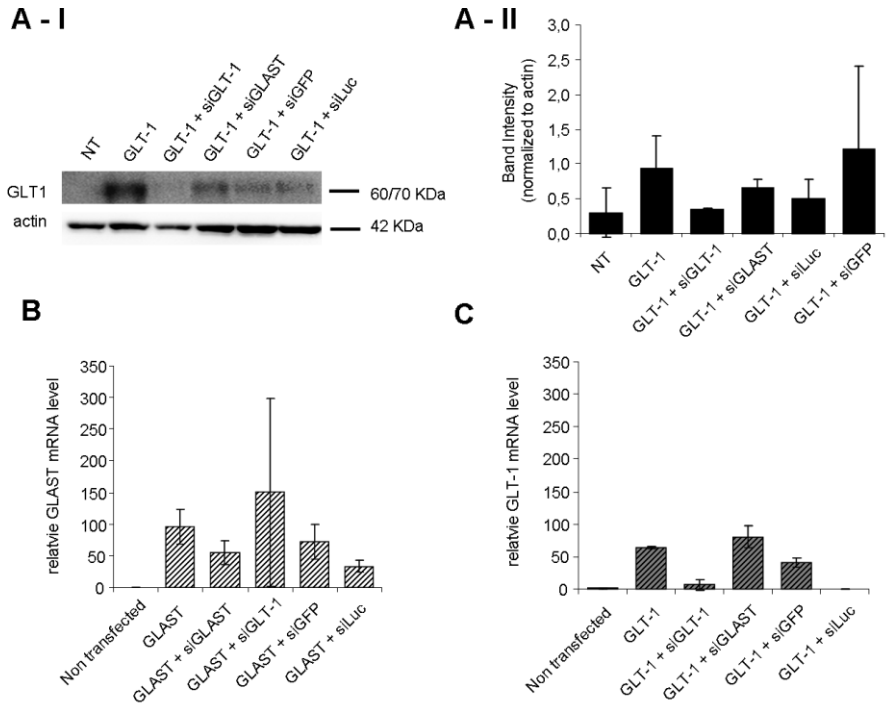

Figure 5.8 – Over-expression and down-regulation of GLAST and GLT-1 after transfection of 293T cells. A – Immunoblot for GLT-1 (I) and respective quantification of band intensities, relative to actin levels (II); B and C – Relative GLAST and GLT-1 mRNA level, respectively, as quantified by RT-qPCR. Values are mean ± s.d. (n=2).

By western blot, it was observed that GLT-1 proteins were efficiently over-expressed in 293T cells and subsequently down-regulated by siGLT-1, although not to 100%, whereas siGLAST had no effect on GLT-1 (Figure 5.8A). Regarding GLAST, only results for mRNA levels are presented (Figure 5.8B) as no GLAST bands could be detected by western blot in any of the samples of this experiment, possibly due to protein degradation during extraction. Nevertheless, analysis of mRNA levels confirmed that the siGLAST plasmid efficiently down-regulated GLAST, presenting low down-regulation of GLT-1. Results obtained for GLT-1 mRNA levels corroborated western blot results

(Figure 5.8C). The control vectors siGFP and siLuc also down-regulated GLAST and GLT-1 to some extent, in particular the siLuc vector, indicating that this is not a good siRNA control vector to be used in these experiments.

3.2.2 Down-regulation of GLAST and GLT-1 in astrocytes

After confirming the efficiency of the siRNA plasmids for their target genes in 293T cells, lentiviral vectors carrying the same siRNA sequences were used to infect primary cultures of rat astrocytes. siLuc and siGFP lentiviral vectors were also tested as siRNA controls. Two viral inocula were tested: 200 or 400 ng p24/well of 6-well plates. Using RT-qPCR, GLAST and GLT1 mRNA levels were quantified (Figure 5.9A and 5.9B). The results show that the GLAST mRNA levels are much higher than that of GLT-1, confirming previous reports indicating that GLT-1 starts being expressed in adulthood (Furuta et al. 1997). However, no differences were observed between controls and infected cells regarding GLAST and GLT-1 mRNA levels for all vectors and viral inocula tested, including the siRNA control vectors siLuc and siGFP (Figure 5.9A and 5.9B). In what concerns protein expression levels, the results were somewhat surprising as GLAST levels were more intense in infected cells, in some cases, when compared to non-infected cells suggesting an over-expression induced by infection rather than down-regulation (Figure 5.9C). Only the siLuc vector showed some silencing effect, a result previously observed by transfection of 293T cells. Regarding GLT-1, again, only siLuc was able to down-regulate this protein. The siGLT-1 vector had no apparent effect on GLT-1 whereas the remaining vectors tested slightly increased the expression of GLT-1 (Figure 5.9D).

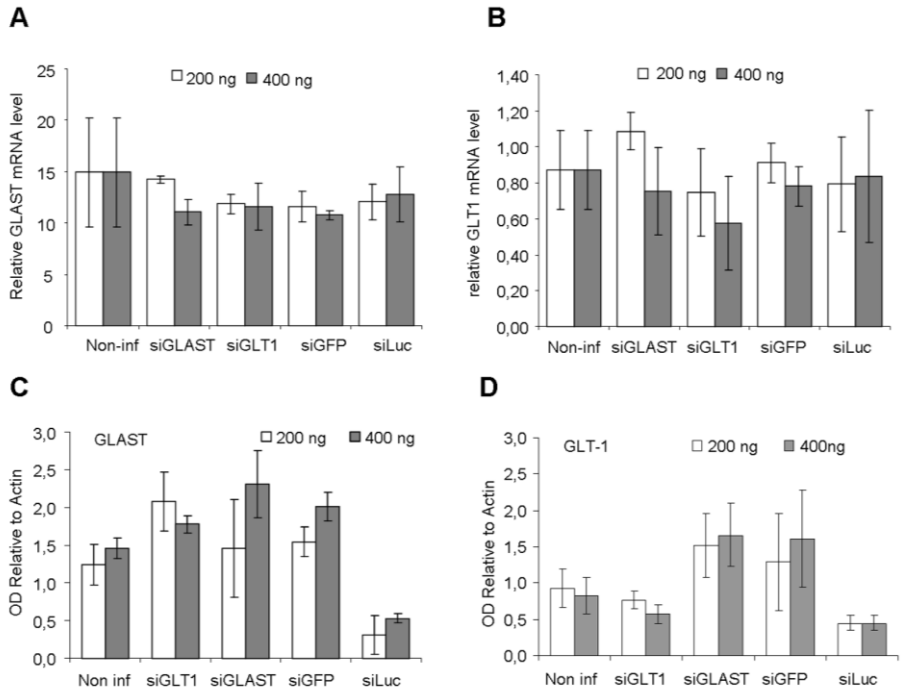

Figure 5.9 – Down-regulation of GLAST and GLT-1 in primary cultures of astrocytes using siRNA lentiviral vectors. A – Relative GLAST mRNA level; B – Relative GLT-1 mRNA level; C and D - Densitometry analysis of the immunoblots for GLAST and GLT-1 expression, respectively, normalized to actin levels. Values are mean ± s.d. (n=2).

Since the western blot and RT-qPCR analyses suggested that maybe cells were not efficiently infected due to the lack of protein down-regulation, it was decided to perform immunostaining to assess GFP expression in the infected cultures, as these lentiviral vectors carry a GFP reporter gene. It was necessary to use an anti-GFP antibody as GFP fluorescence was very difficult to observe directly under the fluorescence microscope. Additional antibodies against GFAP (astroglial marker) and Iba1 (microglial marker) were additionally used to characterize the cellular populations in the primary cultures. Results are shown in Figure 5.10. In non-infected cultures, a high percentage of cells expressing GFAP was observed and some Iba1 positive cells were also found, indicating the presence of microglia (Figure 5.10A and 5.10B). There were also some

areas where only cell nuclei were stained but no GFAP or Iba1 staining was observed. Concerning GFP expression in infected cultures, a very low number of GFP-positive cells was observed for batch 1 infected with either siGLAST (Figure 5.10C) or siGLT-1 (Figure 5.10D). Interestingly, GFP positive cells appeared not to co-localize with GFAP staining, which is more evident in Figure 5.10D and 5.10F. In cell batch 2, more GFP-positive cells were observed but mainly for the siGLAST cultures (Figure 5.10E).

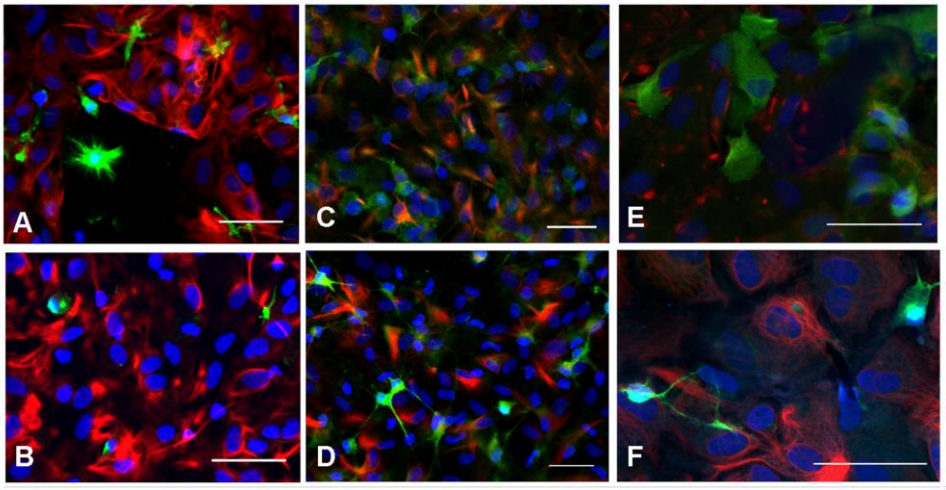

Figure 5.10 – Characterization of cell populations and assessment of infected cells in primary cultures of astrocytes by immunostaining and fluorescence microscopy. A, B – Non-infected astrocytes were stained with anti-GFAP (red), Iba1 (green) and DAPI (blue); Astrocytes infected with siGLAST (culture batch I – C; culture batch II – E) or siGLT-1 (culture batch II – D; culture batch II – F) were stained with anti-GFP (green), anti-GFAP (red) and DAPI (blue); Scale bar, 50 µm.

3.2.3 Effect of the viral envelope on the efficiency of infection by lentiviral vectors in primary cultures of astrocytes

Since very low infection efficiencies were obtained in previous experiments using the mokola-pseudotyped lentiviral vectors, further tests were performed at CEA using two lentiviral vectors carrying a GFP reporter gene with two different envelopes: mokola (the one used in previous experiments, which has a preferential glial tropism *in vivo*) and VSV (which has a strong neuronal tropism *in vivo*). Primary cultures of astrocytes were infected with different amounts of viruses in 6- and 24-well plates and GFP mRNA levels

were analyzed by RT-qPCR 9 days post-infection. Infection of astrocytes was efficient for both vectors, as doubling the dose doubled the number of GFP transcripts (Figure 5.11), particularly using 6-well plates. However, infection efficiency was markedly reduced when using the mokola envelope compared to VSV-G (approx. 20 times less GFP mRNA was obtained for mokola-vector infected cells). Among the different conditions tested, infection with 60 ng of p24 in 24-well plates or 400 ng of p24 in 6-well plates appear to be the best, considering the GFP mRNA levels obtained.

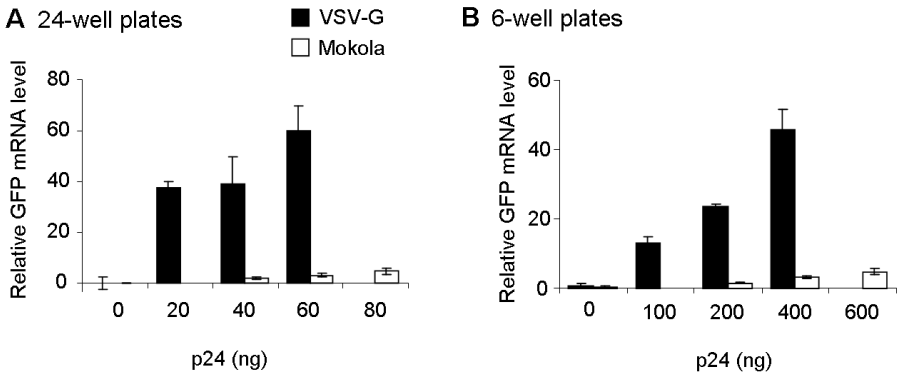

Figure 5.11 – GFP mRNA levels determined by RT-qPCR in primary cultures of astrocytes infected with VSV-G (black bars) or Mokola-pseudotyped (white bars) lentiviral vectors carrying a GFP-reporter gene. A) Infection was performed in 24 wells plates with 20, 40 or 60 ng of p24 for VSV-G vectors (n=2) and 40, 60 or 80 ng p24 for mokola vectors (n=2). 0 ng of p24 correspond to non-infected cultures and were used as control (n=1). B) Infection was performed in 6-wells plates with 100, 200 or 400 ng of p24 for VSV-G vectors (n=2) and 200, 400 or 600 ng p24 for mokola vectors (n=3). 0 ng of p24 correspond to non-infected cultures and were used as control (n=2). Values are mean ± s.d.

4 Discussion

Viral vectors are widely used tools for gene transfer and genetic manipulation in animal cells and therefore are useful to investigate phenomena related with gene alterations in brain cells. In the present work, different lentiviral vectors produced at MIRCen - CEA, were evaluated for their capacity of inducing an over-expression or down-regulation of some genes in primary cultures of astrocytes, namely GFP, GLAST and GLT-1. These

vectors were pseudotyped with a mokola envelope, which has been shown to direct viral tropism towards astrocytes *in vivo* (Colin et al. 2009). In addition, a neuronal detargeting sequence was incorporated in the vectors in order to reduce transgene expression in neurons. The efficiency of these strategies was confirmed *in vivo*, by showing an astrocyte selective over-expression of the transgene in different mouse brain areas as well as its down-regulation, the latter by inserting a shRNA sequence in the vector (Colin et al. 2009). These vectors were also able to over-express GLAST. Hence, in this work these vectors were used to manipulate the expression of glutamate transporters in primary cultures of astrocytes with the aim of investigating the metabolic consequences of these alterations at the level of astrocytic metabolic fluxes, in different conditions. The vectors (containing the mokola envelope and neuronal detargeting sequences) were used in experiments involving only monotypic cultures of astrocytes in order to utilize the same type of vectors in eventual later studies involving mixed primary cultures.

Infections with GFP, GLAST and GLT-1 lentiviral vectors showed that these vectors were able to efficiently over-express the referred genes in astrocytes. However, we could not get over 60% of infected cells which might be eventually related to the viral inoculum used. When the siRNA vectors were tested, a marked decrease in the maximum number of infected cells was observed by flow cytometry (below 40%). This led to the hypothesis that GFP fluorescence from the siRNA vectors was much weaker than the GFP intensity from GFP-lentiviral vectors. In fact, it was difficult to directly observe GFP fluorescence under the fluorescence microscope. A possible explanation for this might be some interference of the different regions of the viral vector that lead to the reduction of the GFP promoter in infected cells. Nevertheless, the efficacy to down-regulate GLAST in primary cultures of astrocytes was shown by western blot in experiments performed at IBET, in which cultures were infected at low cell density, resulting from a cell dilution step when cultures reached confluence. These results were also reflected at the metabolic level, as a decrease in the glutamate uptake rate was observed and glucose uptake and lactate release were not increased after stimulation with

glutamate.

Regarding the two transfection methods tested in alternative to the use of lentiviral vectors to transduce cells, both methods revealed not to be efficient to transfect primary cultures of astrocytes, at least in the conditions used. These cultures were shown to be very sensitive to both methods as cell death rates were very high and very low transfection efficiencies were obtained. The DNA amounts used in these transfections compared to those performed in 293T cells at MIRCen were very similar regarding DNA amount/area of culture (0.5 μg/cm^2 for 293T cells vs 0.2-1 μg/cm^2 for astrocytes), suggesting that this issue is unlikely to be the cause behind the unsuccessful results. Nevertheless, the high cell death rates could eventually be related with the type of plasmid since the one used in transfections of astrocytes was different from those used with 293T cells. Also, perhaps astrocytes are definitely more sensitive to this process and it could be the case that the cultures used were particularly more sensitive for any given reason. Only a few tests were performed using these methods since infection with lentiviral vectors is, in principle, much more efficient to transduce non-dividing cells and introduces the gene of interest directly into the genome (Karra and Dahm 2010).

Given the low transduction yields using siRNA lentiviral vectors plus the need for a good siRNA control vector, more experiments were carried out at MIRCen. In those experiments very low infection rates in astrocytes were again obtained. This was concluded from the following observations: no changes at the mRNA level or protein expression level were detected 10 days after infection and also a low number of GFP expressing cells was observed by fluorescence microscopy, although GFP fluorescence resulting from the reporter genes of siRNA lentiviral vectors appears not to be a good parameter to monitor infection. The unsuccessful down-regulation of GLAST or GLT-1 in primary cultures using lentiviral vectors appears not to be related with the siRNA sequences chosen since this was confirmed by performing transfections in 293T cells. The only difference between these experiments was that, in 293T cells, mouse genes were over-expressed and down-regulated, whereas, in primary cultures, the genes were

from rat origin. Nevertheless, it was confirmed that the siRNA sequences used in the construction of the vectors were also 100% homologous to GLAST and GLT-1 rat genes. Other factor possibly affecting the low infection yields obtained at MIRCen could be the elevated confluence of the astrocyte cultures at the time of infection, even though it is known that lentiviral vectors are able to infect non-dividing cells. Apparently, the fact that these vectors were shown to work *in vivo* might not be directly extrapolated for primary cultures possibly because, *in vivo*, the vectors are directly delivered inside the tissue, which is a compact cellular environment, whereas in a cell culture the amount of medium might impair the fast access of the viruses to the cells. These viruses have a very low stability at 37ºC (Carmo et al. 2009) and therefore it is important that the infection process occurs as fast as possible. Also, the ratio of non-infectious/infectious particles in the viral batches used might be elevated, as only the total amount of particles given by the quantification of the p24 protein is known and, therefore, a lot of non-infectious viral particles with a probable toxic effect are used, eventually prejudicing the infection process. Perhaps the mokola-pseudotyped vectors used in these experiments had a lower percentage of infectious particles which could have been damaged during the centrifugation process used for vector purification. New viral batches with a lower ratio of non-infected/infected particles should be tested and possibly using nlsLacZ instead of GFP as a reporter gene. The nlsLacZ reporter gene was considered to be better to identify infected cells by the CEA partners due to its localization and concentration in the cell nuclei.

After many inconclusive results regarding the efficiency of infection of these vectors in primary cultures of astrocytes, it was decided to test the effect of the viral envelope in this process. VSV-G-pseudotyped lentiviral vectors were tested in comparison with the mokola-pseudotyped vectors and actually showed a 20-fold increase in infection efficiency in cultured astrocytes. Even though these vectors were shown to successfully transduce astrocytes *in vivo* (Colin et al. 2009), the mokola envelope appears not to be a good option for *in vitro* studies, although the reasons for this remain unclear.

Despite the strong neuronal tropism of VSV-G enveloped vectors *in vivo*, this appears to be a better option for siRNA studies in monotypic cultures of astrocytes. Further studies are ongoing to evaluate if the use of the VSV-G envelope improves the efficacy of the siRNA vectors in cultured astrocytes.

Regarding the siLuc and siGFP controls tested, these were shown to interfere with GLAST and GLT-1 expression both by transfection and infection, although mainly siLuc. This suggests that the siLuc vector is probably having some toxic effect on the cells and therefore it should not be used as a control. The siGFP has also originated bad results in other experiments at MIRCen and it appears also to interfere with GLAST and GLT-1. Recently, a lentiviral vector carrying a universal siRNA control was produced at MIRCen and this is a potential candidate to be used in further experiments. The use of these controls in experiments involving RNAi technology is extremely important since it has to be shown that the observed changes are not due to the activation of the siRNA pathway.

Given all the results obtained until now, it was not possible to find the optimal vectors to perform the siRNA experiments required to achieve the aims of this project. Further studies regarding siRNA lentiviral vectors construction, batch variability and infection protocols for primary cultures of astrocytes will hopefully allow performing the metabolic studies aimed at addressing the role of glial glutamate transporters using MFA tools.

5 Acknowledgements

The research described in this chapter was supported by the European Consortium CliniGene NoE (LSHB-CT2006-010933). AI Amaral acknowledges Fundação para a Ciência e Tecnologia (Portugal) for her PhD fellowship (SFRH/BD/29666/2006). AP Teixeira acknowledges the MIT Portugal Program. Ivette Pacheco (IBET, Portugal) is acknowledged for the help on cell culture experiments and HPLC analysis. Lydie Boussicault (MIRCen – CEA) is acknowledged for performing the experiments

investigating the effect of the viral tropism in the transduction efficiency of primary cultures of astrocytes. Nöelle Dufour and Gwenaelle Auregan (MIRCen – CEA, France) are acknowledged for viral vector production and Marie-Claude Gaillard (MIRCen-CEA, France) for technical advice regarding RT-PCR analysis. Dr. Pedro Cruz (IBET, Portugal), Dr. Catarina Brito (IBET, Portugal) and Dr. Carole Escartin (MIRCen – CEA, France) are acknowledged for fruitful discussions.

6 References

Amaral A. I., Teixeira A. P., Martens S., Bernal V., Sousa M. F. and Alves P. M. (2010) Metabolic alterations induced by ischemia in primary cultures of astrocytes: merging 13C NMR spectroscopy and metabolic flux analysis. *J Neurochem* **113,** 735-748.

Bradford J., Shin J. Y., Roberts M., Wang C. E., Li X. J. and Li S. (2009) Expression of mutant huntingtin in mouse brain astrocytes causes age-dependent neurological symptoms. *Proc Natl Acad Sci U S A* **106,** 22480-22485.

Bradford J., Shin J. Y., Roberts M., Wang C. E., Sheng G., Li S. and Li X. J. (2010) Mutant huntingtin in glial cells exacerbates neurological symptoms of Huntington disease mice. *J Biol Chem* **285,** 10653-10661.

Carmo M., Alves A., Rodrigues A. F., Coroadinha A. S., Carrondo M. J., Alves P. M. and Cruz P. E. (2009) Stabilization of gammaretroviral and lentiviral vectors: from production to gene transfer. *J Gene Med* **11,** 670-678.

Colin A., Faideau M., Dufour N., Auregan G., Hassig R., Andrieu T., Brouillet E., Hantraye P., Bonvento G. and Deglon N. (2009) Engineered lentiviral vector targeting astrocytes in vivo. *Glia* **57,** 667-679.

Danbolt N. C. (2001) Glutamate uptake. *Prog Neurobiol* **65,** 1-105.

de Almeida L. P., Ross C. A., Zala D., Aebischer P. and Deglon N. (2002) Lentiviral-mediated delivery of mutant huntingtin in the striatum of rats induces a selective neuropathology modulated by polyglutamine repeat size, huntingtin expression levels, and protein length. *J Neurosci* **22,** 3473-3483.

Faideau M., Kim J., Cormier K., Gilmore R., Welch M., Auregan G., Dufour N., Guillermier M., Brouillet E., Hantraye P., Deglon N., Ferrante R. J. and Bonvento G. (2010) In vivo expression of polyglutamine-expanded huntingtin by mouse striatal astrocytes impairs glutamate transport: a correlation with Huntington's disease subjects. *Hum Mol Genet* **19,** 3053-3067.

Furuta A., Rothstein J. D. and Martin L. J. (1997) Glutamate transporter protein subtypes are expressed differentially during rat CNS development. *J Neurosci* **17,** 8363-8375.

Karra D. and Dahm R. (2010) Transfection techniques for neuronal cells. *J Neurosci* **30,** 6171-6177.

Maragakis N. J. and Rothstein J. D. (2006) Mechanisms of Disease: astrocytes in neurodegenerative disease. *Nat Clin Pract Neurol* **2,** 679-689.

Pellerin L. and Magistretti P. J. (1994) Glutamate uptake into astrocytes stimulates aerobic glycolysis: a mechanism coupling neuronal activity to glucose utilization. *Proc Natl Acad Sci U S A* **91,** 10625-10629.

Pellerin L., Bouzier-Sore A. K., Aubert A., Serres S., Merle M., Costalat R. and Magistretti P. J. (2007) Activity-dependent regulation of energy metabolism by astrocytes: an update. *Glia* **55,** 1251-1262.

Ransom B., Behar T. and Nedergaard M. (2003) New roles for astrocytes (stars at last). *Trends Neurosci* **26,** 520-522.

Regulier E., Trottier Y., Perrin V., Aebischer P. and Deglon N. (2003) Early and reversible neuropathology induced by tetracycline-regulated lentiviral overexpression of mutant huntingtin in rat striatum. *Hum Mol Genet* **12,** 2827-2836.

Shin J. Y., Fang Z. H., Yu Z. X., Wang C. E., Li S. H. and Li X. J. (2005) Expression of mutant huntingtin in glial cells contributes to neuronal excitotoxicity. *J Cell Biol* **171,** 1001-1012.

Sibson N. R., Dhankhar A., Mason G. F., Rothman D. L., Behar K. L. and Shulman R. G. (1998) Stoichiometric coupling of brain glucose metabolism and glutamatergic neuronal activity. *Proc Natl Acad Sci U S A* **95,** 316-321.

Sorg O. and Magistretti P. J. (1992) Vasoactive intestinal peptide and noradrenaline exert long-term control on glycogen levels in astrocytes: blockade by protein synthesis inhibition. *J Neurosci* **12,** 4923-4931.

Teixeira A. P., Santos S. S., Carinhas N., Oliveira R. and Alves P. M. (2008) Combining metabolic flux analysis tools and (13)C NMR to estimate intracellular fluxes of cultured astrocytes. *Neurochem Int* **52,** 478-486.

Voutsinos-Porche B., Bonvento G., Tanaka K., Steiner P., Welker E., Chatton J. Y., Magistretti P. J. and Pellerin L. (2003) Glial glutamate transporters mediate a functional metabolic crosstalk between neurons and astrocytes in the mouse developing cortex. *Neuron* **37,** 275-286.

Walker F. O. (2007) Huntington's disease. *Lancet* **369,** 218-228.

Chapter 6

General Discussion and Conclusions

CONTENTS

1 Discussion

The availability of better characterized animal models and more reliable cell culture systems together with groundbreaking techniques and tools strongly contributed to the current knowledge on brain energy metabolism. However, there are still numerous elusive issues, including the selective importance of certain pathways and substrates in the different cellular compartments and the exact features and role of metabolic disturbances that have been implicated in many neurological disorders. In this context, there is a growing need of improved approaches to investigate metabolic aspects of brain cells and consequently help to answer these numerous research questions. As mentioned in earlier chapters, *in vitro* studies are still extremely relevant and will certainly continue to provide important findings in this field.

The work developed in this thesis aimed at contributing with a novel *in vitro* model to investigate brain ischemia and also with original approaches based on metabolic flux analysis methodologies allowing for a detailed and quantitative investigation of neural metabolism using cultured cells.

1.1 Mimicking ischemia *in vitro* using bioreactors

Ischemic stroke is one of the most devastating disorders affecting the brain and for which no effective treatment is available. Taking into account the key role of astrocytes in metabolic trafficking with neurons, one of the aims of this thesis was to investigate in detail the metabolic alterations occurring in astrocytes under ischemic conditions (Chapter 2). For that we have taken advantage of the bioreactors technology available at the Animal Cell Technology Unit to implement a novel *in vitro* model to mimic ischemia using primary cultures of astrocytes.

Historically, research on ischemia has relied both on animal and *in vitro* models. *In vivo* models involve procedures such as the transient or permanent occlusion of a major cerebral artery (e.g. Haberg et al. 2006), the induction of reproducible infarcts in

selected brain areas by means of artificially induced thrombosis (e.g. Watson et al. 2002) or even cardiac arrest in dogs or primates (e.g. Richards et al. 2007), which cause a high degree of discomfort to the animal. Although animal models more closely reproduce the characteristics of grey matter ischemic injury in humans, the patterns of pathology in the body resulting from ischemia in a particular brain region can differ substantially from those seen in humans. Moreover, the technical requirements and the underlying complexity of *in vivo* models render them disadvantageous compared to *in vitro* models to investigate mechanistic aspects of cerebral ischemia and isolated cellular events.

In vitro models of ischemia overcome these disadvantages, where the contribution of blood components is eliminated and the temperature and extracellular environment can be standardized (Lipton 1999). In most of these models, ischemic conditions are mimicked by a combination of oxygen and glucose deprivation (OGD) using either an "artificial" (Liniger et al. 2001) or "ischemic" cerebrospinal fluid (Rytter et al. 2003) equilibrated in N_2/CO_2 followed by the placement of cultures in an anaerobic or hypoxic chamber. Whereas hippocampal brain slices (Liniger et al. 2001) and organotypic hippocampal slice cultures (Rytter et al. 2003) retain the tissue cell stoichiometry and regional connectivity, monotypic cultures of neurons (Goldberg and Choi 1993) or astrocytes (Hertz 2003) enable to investigate specific cellular events associated to ischemia. Depending on the intrinsic sensitivity of these models to ischemia, they require different exposure times to reproduce cell damage, including delayed cell death, the fall of ATP levels and the release of glutamate from neurons (Lipton 1999).

It is noteworthy that cultured astrocytes require several hours of OGD until cell death and other cellular responses can be observed, compared to neurons or slices (Almeida et al. 2002; Hertz 2003), and cultures derived from the cortex are also much more resistant than those derived from the hippocampus (Zhao and Flavin 2000). This resistance was observed in the model implemented in this thesis (Chapter 2). To mimic ischemia, astrocytes immobilized in Cytodex3® were cultured in bioreactors and

deprived of oxygen and glucose for 5h: cells were allowed to consume all glucose from the culture medium followed by the replacement of oxygen by nitrogen using the control unit of the bioreactors. 5h of OGD led only to approximately 30% cell death in cortical astrocytes and a similar percentage of intracellular ATP depletion, which was rapidly replenished through a fast metabolic response.

An important advantage of the present model is the rigorous control of dissolved oxygen in the culture medium and also its fast manipulation enabling to completely remove oxygen in approximately 30 min, while maintaining pH control. pH control is carried out through injection of a mixture of air, N_2 and CO_2 and it can efficiently operate simultaneously to the manual injection of N_2 that was used to force oxygen to be completely removed from the medium. Therefore, pO_2 is decreased to 0% while pH is continuously being monitored, ensuring that cellular damage will only be due to the absence of glucose and oxygen.

These bioreactors are advantageous to perform different types of neural cell suspension cultures, including embryonic brain cell aggregates. These aggregates have been successfully cultured in bioreactors in our laboratory and were useful to elucidate neuronal-astrocytic metabolic interactions in the context of anoxia (Sa Santos et al. 2011). Aggregating brain cell cultures in Erlenmeyer flasks have been validated as promising *in vitro* models of ischemia (Pardo and Honegger 1999; Honegger and Pardo 2007), which is induced through the transient arrest of agitation during 1-2h. Nevertheless, oxygen levels have not been monitored in these studies, indicating that there is still space for improvement, which could be accomplished by taking advantage of the numerous features of bioreactors.

Above all, bioreactors technology provides high culture homogeneity and reproducibility, due to all the parameters that are monitored and controlled. These aspects are very important considering the development of robust models to investigate, for example, mechanisms of disease and, even more, for drug screening purposes. In this context, efficient processes which allowed to improve hepatocyte functionality (Tostoes

et al. 2011) and expansion of human embryonic stem cells (Serra et al. 2010) under defined conditions are good examples of other bioreactor applications at our group.

1.2 Application of Metabolic Flux Analysis tools to investigate neural cell metabolism

Metabolic modelling studies of ^{13}C NMR spectroscopy data obtained *in vivo* have generated important findings in this field (reviewed by Henry et al. 2006) but similar methodologies have not been as extensively employed *in vitro*. A major goal of this thesis was thus to explore the potential of MFA tools to estimate metabolic fluxes of neural cells in culture and increase the amount of information that can be obtained in these studies.

MFA tools have been valuable in biotechnology and metabolic engineering to characterize the physiology of bacterial, yeast, and mammalian cells and consequently improve their productivities (reviewed by Lee et al. 1999; Quek et al. 2010) by estimating intracellular metabolic fluxes. Classical MFA models are relatively easy to implement and require a reduced number of experimental data (mostly analysis of cell culture supernatants) to estimate intracellular fluxes in a typical metabolic network including glycolysis, TCA cycle, and amino acid catabolism. MFA allows for a comprehensive investigation of cellular metabolism as it estimates metabolic fluxes based on the stoichiometry of the metabolic network and on metabolic steady-state and, therefore, all fluxes are estimated as part of a "global picture" which defines the metabolic phenotype of the cell at a given time-period. Three applications of MFA were accomplished in this thesis to estimate metabolic fluxes of neural cells and consequently help to elucidate important metabolic mechanisms in neurons and in astrocytes.

1.2.1 MFA of astrocytic metabolism before and after ischemia

This thesis started by expanding an MFA model previously developed in the group (Teixeira et al. 2008) to investigate and quantify the effects of an ischemic episode in the metabolic fluxes of cultured astrocytes (Chapter 2). The main improvements in the

model presented in Chapter 2 were the introduction of additional data provided by ^{13}C-NMR spectroscopy analysis of the cell culture supernatant. In particular, ^{13}C % enrichment in lactate allowed estimating the fraction of glucose that was likely metabolised via the PPP versus that of glycolysis, by assuming that label dilution in lactate was derived from the loss of [$^{13}CO_2$] via the PPP. Consequently, this model provides a more reliable representation of astrocytic metabolism, taking into account the proven importance of the PPP in astrocytes in a variety of conditions involving the generation of reactive oxygen species or nitrosative stress (Ben-Yoseph et al. 1996; Garcia-Nogales et al. 1999; Bolanos and Almeida 2006; Allaman et al. 2010).

Even so, there is still space for model improvement as it would still be important to include glycogen degradation in the model due to strong evidence supporting its significant role in astrocytic metabolism under activation (Cruz and Dienel 2002; Dienel et al. 2007) and for long-term memory formation (Suzuki et al. 2011) in rats. It is possible that glycogen degradation might have contributed to a partial label dilution in lactate, which was only likely to have happened before ischemia, since glycogen reserves should have been totally depleted during the insult and, therefore, were more likely to be replenished than degraded during recovery. A fixed rate of glycogen degradation could have been estimated in a separate experiment, by pre-enriching the glycogen pool using [U-$^{13}C_6$]glucose and comparing lactate enrichment in the presence or absence of isofagomine, a glycogen phosphorylase inhibitor (Sickmann et al. 2005), and later added to the model.

This study was also used as a proof-of-concept that MFA is a valuable tool to investigate and characterize the metabolic response of astrocytes to pathological insults. MFA allowed simultaneously identifying and quantifying alterations induced by ischemia in glycolysis, TCA cycle and pentose phosphate pathway as well as determining how their fluxes changed during the recovery period. The importance of BCAAs as energy fuels after ischemia was shown and the usefulness of MFA to quantify the contribution of these substrates to the TCA cycle flux was demonstrated. In the MFA

model, fluxes of different reactions that constitute the TCA cycle are separately estimated and, hence, it is possible to depict the fuelling of carbons into the cycle through the increase in some of those fluxes at particular metabolic nodes, namely at the acetyl-CoA and succinyl-CoA nodes.

Overall, the use of MFA provided an original method to characterize the metabolic responses of astrocytes to ischemia *in vitro*. This approach, associated with the use of a robust *in vitro* model of ischemia is valuable to investigate the effect of drugs targeting specific metabolic targets in astrocytes in the context of ischemia.

1.2.2 MFA of cultured cerebellar neurons after hypoglycaemia

After successfully applying MFA to estimate metabolic fluxes of astrocytes, the next step was its application to cultured cerebellar neurons (Chapter 3), which are also widely used models to investigate particular aspects of brain metabolism. A very simple metabolic network could be used to describe the metabolism of these neurons since they do not possess significant parallel pathways. This model could also be perfectly applied to a culture of cortical neurons, although it would require the use of ^{13}C NMR data to determine the fraction of glucose metabolised through the PPP, similarly to what has been performed for astrocytes in Chapter 2. Extensive glucose metabolism through the PPP is thought to occur in cortical neurons (Herrero-Mendez et al. 2009), which appears not to be the case in cerebellar granule cells (Biagiotti et al. 2003). Even so, the study by Herrero-Mendez et al (2009) was performed in neurons in suspension after tripsinization of cells grown in a culture dish, which might lead to some controversy on the relevance of the metabolic results. In this context, the application of MFA would be valuable to confirm and estimate the extent of the PPP flux in a primary culture of cortical neurons.

The value of MFA to investigate the effects of a pathologic insult in metabolic fluxes of neurons was also shown in this work. In particular, the role of astrocytic-derived substrates (glutamine) as alternative fuels for cerebellar neurons exposed to a hypoglycaemic period was assessed. The characterization of the labelling dynamics of

neuronal metabolites from [1,6-$^{13}C_2$]glucose was also an original aspect of this work and provided important findings suggesting the existence cytosolic-mitochondrial compartmentation of different metabolites (e.g. pyruvate, alanine, glutamate, α-ketoglutarate and malate). In addition, the calculation of the flux partitioning coefficients at the pyruvate, acetyl-CoA and α-ketoglutarate nodes provided an estimation of the label dilution caused by unlabelled glutamine metabolism. This approach was crucial to support the MFA results suggesting that glutamine was significantly oxidized through the pyruvate recycling pathway. This is one of the most important findings of this work since most *in vitro* studies have suggested a preferential operation of the pyruvate recycling pathway in astrocytes (e.g. Waagepetersen et al. 2002), in contrast to what was initially described *in vivo* by Cerdan and colleagues (Cerdan et al. 1990). Therefore, this study reinforces the need to clarify the significance of this pathway in neurons. The proof of operation of pyruvate recycling in neurons might confirm their use of glutamine and/or glutamate as metabolic substrates. In addition, it might represent an important neuroprotective mechanism against oxidative stress, since malic enzyme activity contributes to increased NADPH production (Bukato et al. 1995; Vogel et al. 1999).

1.2.3 Improving metabolic flux estimations in neural cells with isotopic transient MFA

The work presented in Chapter 4 constituted a further challenge in the application of MFA tools to investigate astrocytic metabolism. ^{13}C isotopic transient MFA is the most recent advance of MFA methodologies and had been employed in a few studies to estimate fluxes in microbial cultures and hepatocytes in short-time experiments (e.g. Noh et al. 2007; Maier et al. 2008; Noack et al. 2010). The main novelty of ^{13}C isotopic transient MFA compared to classical MFA is the inclusion of ^{13}C time-courses of different intracellular metabolites in the model, leading to the improved estimation of metabolic fluxes. This approach is also constrained by metabolic steady-state (i.e.

metabolite pools are assumed to be constant during the time-interval considered) and still requires the collection of data from cell culture supernatants. Again, all fluxes estimated provide a global picture of the metabolic status of the cell, with the additional advantage of distinguishing fluxes through parallel and reversible pathways (Noh et al. 2007). However, the inclusion of ^{13}C time-courses in the model requires that metabolite pool sizes are additionally measured since they determine the rate of metabolite enrichment. This is a crucial aspect of isotopic transient MFA. On the other hand, if sufficient experimental data is available, some metabolite pools difficult to measure can be estimated by the model. All these characteristics make isotopic transient MFA a very demanding approach regarding both experimental and computational effort. Nevertheless, it provides significant new information with respect to the fluxes identified, non-measurable pool sizes, data consistency, or large storage pools that can be derived from this novel kind of experimental data included in the model (Noh et al. 2007).

The application of isotopic transient MFA to estimate metabolic fluxes of cultured astrocytes has shown that very detailed metabolic flux information can be obtained in cell culture experiments by taking advantage of the use of ^{13}C-labelled compounds, different analytical techniques and careful experimental planning. However, a few steps can still be improved. Metabolite quenching techniques are very important, particularly for metabolites with very small pool sizes, which become enriched very fast. This was the case of glycolytic intermediates which attained isotopic steady state within less than 30 min after the beginning of [1-^{13}C]glucose supply. Therefore, the use of shorter sampling times and more efficient sampling and quenching methods (Noh and Wiechert 2006; Noh et al. 2007; Hofmann et al. 2008) should provide more detailed ^{13}C enrichment time-courses for these metabolites. In addition, in this work, only a reduced number of metabolite pools could be determined using HPLC. The access to state of the art LC-MS techniques could enable to quantify a larger number of metabolite pools, particularly intermediates of glycolysis and of the PPP (very little

information could be obtained in this work for these metabolites), as well as their ^{13}C enrichment time-courses. Progresses in these aspects would certainly lead to significant improvements of flux estimations.

The isotopic transient MFA model implemented in this thesis has the potential to be applied to any type of monotypic neural cell culture, requiring only the change of particular fluxes that might be specific of a given cell type. Also, different labelled substrates can be used, either alone or combined (e.g Hofmann et al. 2008) to further improve flux estimation. Metallo et al (2009) have recently evaluated the suitability of isotopic tracers to probe different metabolic pathways. For example, [1-^{13}C]glucose is a good choice to estimate glycolytic flux but [2-^{13}C] or [1,2-$^{13}C_2$]glucose are better if the aim is to estimate the PPP flux (Metallo et al. 2009). These combined approaches require, however, additional work concerning the writing of all differential equations describing the mass isotopomer balances derived from each substrate into all metabolites included in the network. This will also add additional computational effort due to the larger number of equations in the model.

Concerning the specific metabolic aspects of astrocytes that can be highlighted in this work, it was possible to estimate the glutamate/α-ketoglutarate exchange rate and the contribution of different pathways and substrates to astrocytic metabolism. The exchange between glutamate and α-ketoglutarate rate has been a source of controversy in this field (Mason et al. 1992; Mason et al. 1995; Gruetter et al. 2001; Henry et al. 2002) and this work supported the view that this rate appears to be similar to the TCA cycle flux (Gruetter et al. 2001; Henry et al. 2002). In this context, this model could be useful to further investigate this issue, aiming to evaluate how the glutamate/α-ketoglutarate exchange rate might change under different conditions. Moreover, it was shown that the labelling dynamics in astrocytic metabolites is very complex, indicating the existence of several sources of label dilution, particularly BCAAs and the pentose phosphate pathway. These findings support recent studies that have justified the need to take into

account astrocytic sources of label dilution in metabolic modelling studies *in vivo* (Shen et al. 2009; Boumezbeur et al. 2010; Duarte et al. 2011).

Finally, it is noteworthy that the findings provided by isotopic transient MFA corroborate the main metabolic aspects of astrocytes described in Chapter 2 using classical MFA, thus showing that more simple approaches also provide accurate flux estimations and can be employed if a very detailed metabolic picture is not required.

In summary, isotopic transient MFA is a very experimentally and computationally demanding technique that can, however, generate extremely detailed metabolic data. Consequently, it is promising to investigate metabolic responses of neural cells under pathological conditions and the effect of drugs targeting specific metabolic pathways in these cells. This type of studies can be very useful to test different hypothesis *in vitro* before being translated to pre-clinical animal models of disease.

2 Recent advances and future prospects

A major challenge in this field will continue to be the investigation of the cellular responses under pathological conditions. Recently, a significant number of human stem-cell-derived *in vitro* models has emerged as valuable models that faithfully recapitulate disease features (reviewed by Gibbons and Dragunow 2010; Han et al. 2011). These are likely to become more and more used compared to primary rodent brain cell cultures due to the easier translation of findings obtained in human cells concerning potential therapeutically relevant discoveries.

With regard to the investigation of energy metabolism, advances in NMR spectroscopy and the availability of higher magnetic fields will continue to contribute to increase temporal-resolution and sensitivity of *in vitro* and *in vivo* studies and to consequently improve the estimation of cerebral metabolic fluxes. *In vivo* metabolic modelling studies will continue to be crucial to confirm findings obtained *in vitro*. It is noteworthy the most recent breakthrough in ^{13}C NMR spectroscopy - the use of

hyperpolarized ^{13}C-labelled substrates which greatly enhance the sensitivity of the method through dynamic nuclear polarization (Witney and Brindle 2010). These substrates have a number of promising applications in magnetic resonance imaging of brain metabolism, including the measurement of pH *in vivo* (Gallagher et al. 2008) and the development of tools to improve the diagnosis and efficiently monitoring response to treatment in patients with brain tumours (Day et al. 2007). The Henry group published recently the first model estimating fluxes through PDH and LDH from ^{13}C-labelled lactate and bicarbonate time-courses after injection of different hyperpolarized ^{13}C-labelled pyruvate substrates (Marjanska et al. 2010). Although these authors could not detect glutamate or glutamine isotopomers with this technique, hyperpolarized ^{13}C NMR spectroscopy is a promising tool for improved cerebral flux estimations in future studies.

In a different perspective, the "omics" field is providing a large amount of data that can improve and extend the study of metabolism to new levels of understanding (Hellerstein 2004; Lovatt et al. 2007; Cahoy et al. 2008; Yanes et al. 2010). In this context it was recently shown that metabolism has indeed a crucial role in cell physiology as metabolic fluxes are thought to regulate cell signalling pathways in mammalian cells (Metallo and Vander Heiden 2010). Metabolomics is becoming too narrow with regard to the large amount of data being generated both by experimental and bioinformatics means at different cellular levels. Genomics, proteomics and transcriptomics data are being incorporated in large and complex models aiming to comprehensively investigate the causes behind metabolic disturbances and identify possible therapeutic targets (e.g. Moxley et al. 2009). A good example is a large scale *in silico* model recently reported by Lewis et al (2010) who have included genomic and proteomic data to recapitulate metabolic interactions between astrocytes and different types of neurons. This model correlates flux changes with altered expression or activity of particular enzymes and was used to identify key genes and pathways contributing to the pathology of Alzheimer's Disease (Lewis et al. 2010).

In a broader context, the tools developed in this thesis have a tremendous potential of application in the field of neural stem cells. Different studies have shown that stem cells possess metabolic characteristics that differ from differentiated cells (reviewed by Rafalski and Brunet 2011). In particular, the transition from a neural stem/progenitor cell to its differentiated counterpart is associated with numerous transcriptional changes, including in genes associated with metabolism and energy sensing, due to the higher metabolic demands of differentiated cells (Rafalski and Brunet 2011). It is known that hypoxia favours the maintenance of pluripotency in embryonic stem cells (Ezashi et al. 2005; Forristal et al. 2010) due to their mitochondrial immaturity and predominance of glycolytic metabolism, in opposition to the high degree of oxidative phosphorylation in differentiated cells (Cho et al. 2006). A recent study interestingly suggested that human pluripotent stem cells inactivate PDH to maintain high glycolytic rates (Varum et al. 2011). These findings reinforce the potential of MFA-based approaches to further elucidate the metabolic fingerprints of neural stem cells which might lead to the discovery of important targets to promote or inhibit stem cell differentiation, depending on the research purpose. Consequently, these approaches might represent a breakthrough in the development of novel neural stem cell models by better manipulating the pluripotent/differentiated state.

In summary, a variety of cutting edge tools is now available to investigate brain energy metabolism either *in vitro*, *in vivo*, or *in silico*. These will not only be important to continue to elucidate the complexity of cerebral metabolism in physiological conditions but, above all, to better characterize the metabolic alterations known to be implicated in most neurological disorders. Thus, the identification of therapeutic targets with a metabolic origin and the consequent development of efficient therapies will continue to be a major goal in this field in upcoming years.

3 Conclusions

In conclusion, this thesis shows that metabolic flux analysis-based models combined with the use of ^{13}C-labelled compounds and ^{13}C NMR spectroscopy or MS are valuable and powerful to investigate in detail neural cell metabolism. These methodologies have the potential to be employed in numerous *in vitro* brain cell culture models and even stem cells, and therefore have a tremendous range of applications in the field of neuroenergetics.

4 References

Allaman I., Gavillet M., Belanger M., Laroche T., Viertl D., Lashuel H. A. and Magistretti P. J. (2010) Amyloid-beta aggregates cause alterations of astrocytic metabolic phenotype: impact on neuronal viability. *J Neurosci* **30,** 3326-3338.

Almeida A., Delgado-Esteban M., Bolanos J. P. and Medina J. M. (2002) Oxygen and glucose deprivation induces mitochondrial dysfunction and oxidative stress in neurones but not in astrocytes in primary culture. *J Neurochem* **81,** 207-217.

Ben-Yoseph O., Boxer P. A. and Ross B. D. (1996) Assessment of the role of the glutathione and pentose phosphate pathways in the protection of primary cerebrocortical cultures from oxidative stress. *J Neurochem* **66,** 2329-2337.

Biagiotti E., Guidi L., Del Grande P. and Ninfali P. (2003) Glucose-6-phosphate dehydrogenase expression associated with NADPH-dependent reactions in cerebellar neurons. *Cerebellum (London, England)* **2,** 178-183.

Bolanos J. P. and Almeida A. (2006) Modulation of astroglial energy metabolism by nitric oxide. *Antioxid Redox Signal* **8,** 955-965.

Boumezbeur F., Petersen K. F., Cline G. W., Mason G. F., Behar K. L., Shulman G. I. and Rothman D. L. (2010) The contribution of blood lactate to brain energy metabolism in humans measured by dynamic 13C nuclear magnetic resonance spectroscopy. *J Neurosci* **30,** 13983-13991.

Bukato G., Kochan Z. and Swierczynski J. (1995) Different regulatory properties of the cytosolic and mitochondrial forms of malic enzyme isolated from human brain. *The international journal of biochemistry & cell biology* **27,** 1003-1008.

Cahoy J. D., Emery B., Kaushal A., Foo L. C., Zamanian J. L., Christopherson K. S., Xing Y., Lubischer J. L., Krieg P. A., Krupenko S. A., Thompson W. J. and Barres B. A. (2008) A transcriptome database for astrocytes, neurons, and oligodendrocytes: a new resource for understanding brain development and function. *J Neurosci* **28,** 264-278.

Cerdan S., Kunnecke B. and Seelig J. (1990) Cerebral metabolism of [1,2-13C2]acetate as detected by in vivo and in vitro 13C NMR. *J Biol Chem* **265,** 12916-12926.

Cho Y. M., Kwon S., Pak Y. K., Seol H. W., Choi Y. M., Park do J., Park K. S. and Lee H. K. (2006) Dynamic changes in mitochondrial biogenesis and antioxidant enzymes during the spontaneous differentiation of human embryonic stem cells. *Biochem Biophys Res Com* **348,** 1472-1478.

Cruz N. F. and Dienel G. A. (2002) High glycogen levels in brains of rats with minimal environmental stimuli: implications for metabolic contributions of working astrocytes. *J Cereb Blood Flow Metab* **22,** 1476-1489.

Day S. E., Kettunen M. I., Gallagher F. A., Hu D. E., Lerche M., Wolber J., Golman K., Ardenkjaer-Larsen J. H. and Brindle K. M. (2007) Detecting tumor response to treatment using hyperpolarized 13C magnetic resonance imaging and spectroscopy. *Nature Medicine* **13,** 1382-1387.

Dienel G. A., Ball K. K. and Cruz N. F. (2007) A glycogen phosphorylase inhibitor selectively enhances local rates of glucose utilization in brain during sensory stimulation of conscious rats: implications for glycogen turnover. *J Neurochem* **102,** 466-478.

Duarte J. M. N., Lanz B. and Gruetter R. (2011) Compartmentalized cerebral metabolism of [1,6-13C]glucose determined by in vivo 13C NMR spectroscopy at 14.1 T. *Frontiers in Neuroenergetics* **3**.

Ezashi T., Das P. and Roberts R. M. (2005) Low O2 tensions and the prevention of differentiation of hES cells. *Proc Nat Acad Sci* **102,** 4783-4788.

Forristal C. E., Wright K. L., Hanley N. A., Oreffo R. O. and Houghton F. D. (2010) Hypoxia inducible factors regulate pluripotency and proliferation in human embryonic stem cells cultured at reduced oxygen tensions. *Reproduction (Cambridge, England)* **139,** 85-97.

Gallagher F. A., Kettunen M. I., Day S. E., Hu D. E., Ardenkjaer-Larsen J. H., Zandt R., Jensen P. R., Karlsson M., Golman K., Lerche M. H. and Brindle K. M. (2008) Magnetic resonance imaging of pH in vivo using hyperpolarized 13C-labelled bicarbonate. *Nature* **453,** 940-943.

Garcia-Nogales P., Almeida A., Fernandez E., Medina J. M. and Bolanos J. P. (1999) Induction of glucose-6-phosphate dehydrogenase by lipopolysaccharide contributes to preventing nitric oxide-mediated glutathione depletion in cultured rat astrocytes. *J Neurochem* **72,** 1750-1758.

Gibbons H. M. and Dragunow M. (2010) Adult human brain cell culture for neuroscience research. *Int J Biochem Cell Biol* **42,** 844-856.

Goldberg M. P. and Choi D. W. (1993) Combined oxygen and glucose deprivation in cortical cell culture: calcium-dependent and calcium-independent mechanisms of neuronal injury. *J Neurosci* **13,** 3510-3524.

Gruetter R., Seaquist E. R. and Ugurbil K. (2001) A mathematical model of compartmentalized neurotransmitter metabolism in the human brain. *Am J Physiol Endocrinol Metab* **281,** E100-112.

Haberg A., Qu H. and Sonnewald U. (2006) Glutamate and GABA metabolism in transient and permanent middle cerebral artery occlusion in rat: Importance of astrocytes for neuronal survival. *Neurochem Int.* **48** (6-7):531-40.

Han S. S., Williams L. A. and Eggan K. C. (2011) Constructing and deconstructing stem cell models of neurological disease. *Neuron* **70,** 626-644.

Hellerstein M. K. (2004) New stable isotope-mass spectrometric techniques for measuring fluxes through intact metabolic pathways in mammalian systems: introduction of moving pictures into functional genomics and biochemical phenotyping. *Metab Eng* **6,** 85-100.

Henry P. G., Lebon V., Vaufrey F., Brouillet E., Hantraye P. and Bloch G. (2002) Decreased TCA cycle rate in the rat brain after acute 3-NP treatment measured by in vivo 1H-[13C] NMR spectroscopy. *J Neurochem* **82,** 857-866.

Henry P. G., Adriany G., Deelchand D., Gruetter R., Marjanska M., Oz G., Seaquist E. R., Shestov A. and Ugurbil K. (2006) In vivo 13C NMR spectroscopy and metabolic modeling in the brain: a practical perspective. *Magn Reson Imaging* **24,** 527-539.

Herrero-Mendez A., Almeida A., Fernandez E., Maestre C., Moncada S. and Bolanos J. P. (2009) The bioenergetic and antioxidant status of neurons is controlled by continuous degradation of a key glycolytic enzyme by APC/C-Cdh1. *Nat Cell Biol* **11,** 747-752.

Hertz L. (2003) Astrocytic amino acid metabolism under control conditions and during oxygen and/or glucose deprivation. *Neurochem Res* **28,** 243-258.

Hofmann U., Maier K., Niebel A., Vacun G., Reuss M. and Mauch K. (2008) Identification of metabolic fluxes in hepatic cells from transient 13C-labeling experiments: Part I. Experimental observations. *Biotechnol Bioeng* **100,** 344-354.

Honegger P. and Pardo B. (2007) Aggregating brain cell cultures: investigation of stroke related brain damage. *Altex* **24 Spec No,** 32-34.

Lee K., Berthiaume F., Stephanopoulos G. N. and Yarmush M. L. (1999) Metabolic flux analysis: a powerful tool for monitoring tissue function. *Tissue Eng* **5,** 347-368.

Lewis N. E., Schramm G., Bordbar A., Schellenberger J., Andersen M. P., Cheng J. K., Patel N., Yee A., Lewis R. A., Eils R., Konig R. and Palsson B. O. (2010) Large-scale in silico modeling of metabolic interactions between cell types in the human brain. *Nature Biotech* **28,** 1279-1285.

Liniger R., Popovic R., Sullivan B., Gregory G. and Bickler P. E. (2001) Effects of neuroprotective cocktails on hippocampal neuron death in an in vitro model of cerebral ischemia. *Journal of Neurosurgical Anesthesiology* **13,** 19-25.

Lipton P. (1999) Ischemic cell death in brain neurons. *Physiological reviews* **79,** 1431-1568.

Lovatt D., Sonnewald U., Waagepetersen H. S., Schousboe A., He W., Lin J. H., Han X., Takano T., Wang S., Sim F. J., Goldman S. A. and Nedergaard M. (2007) The transcriptome and metabolic gene signature of protoplasmic astrocytes in the adult murine cortex. *J Neurosci* **27,** 12255-12266.

Maier K., Hofmann U., Reuss M. and Mauch K. (2008) Identification of metabolic fluxes in hepatic cells from transient 13C-labeling experiments: Part II. Flux estimation. *Biotechnol Bioeng* **100,** 355-370.

Marjanska M., Iltis I., Shestov A. A., Deelchand D. K., Nelson C., Ugurbil K. and Henry P. G. (2010) In vivo 13C spectroscopy in the rat brain using hyperpolarized [1-(13)C]pyruvate and [2-(13)C]pyruvate. *J Magn Reson* **206,** 210-218.

Mason G. F., Rothman D. L., Behar K. L. and Shulman R. G. (1992) NMR determination of the TCA cycle rate and alpha-ketoglutarate/glutamate exchange rate in rat brain. *J Cereb Blood Flow Metab* **12,** 434-447.

Mason G. F., Gruetter R., Rothman D. L., Behar K. L., Shulman R. G. and Novotny E. J. (1995) Simultaneous determination of the rates of the TCA cycle, glucose utilization, alpha-ketoglutarate/glutamate exchange, and glutamine synthesis in human brain by NMR. *J Cereb Blood Flow Metab* **15,** 12-25.

Metallo C. M. and Vander Heiden M. G. (2010) Metabolism strikes back: metabolic flux regulates cell signaling. *Genes & development* **24,** 2717-2722.

Metallo C. M., Walther J. L. and Stephanopoulos G. (2009) Evaluation of 13C isotopic tracers for metabolic flux analysis in mammalian cells. *J Biotechnol* **144,** 167-174.

Moxley J. F., Jewett M. C., Antoniewicz M. R., Villas-Boas S. G., Alper H., Wheeler R. T., Tong L., Hinnebusch A. G., Ideker T., Nielsen J. and Stephanopoulos G. (2009) Linking high-resolution metabolic flux phenotypes and transcriptional regulation in yeast modulated by the global regulator Gcn4p. *Proc Nat Acad Sci USA* **106,** 6477-6482.

Noack S., Noh K., Moch M., Oldiges M. and Wiechert W. (2010) Stationary versus non-stationary (13)C-MFA: A comparison using a consistent dataset. *J Biotechnol*.

Noh K. and Wiechert W. (2006) Experimental design principles for isotopically instationary 13C labeling experiments. *Biotech Bioeng* **94,** 234-251.

Noh K., Gronke K., Luo B., Takors R., Oldiges M. and Wiechert W. (2007) Metabolic flux analysis at ultra short time scale: isotopically non-stationary 13C labeling experiments. *J Biotechnol* **129,** 249-267.

Pardo B. and Honegger P. (1999) Aggregating Brain Cell Cultures as a Model to Study Ischaemia-induced Neurodegeneration. *Toxicol In Vitro* **13,** 543-547.

Quek L. E., Dietmair S., Kromer J. O. and Nielsen L. K. (2010) Metabolic flux analysis in mammalian cell culture. *Metabolic Eng* **12,** 161-171.

Rafalski V. A. and Brunet A. (2011) Energy metabolism in adult neural stem cell fate. *Prog Neurobiol* **93,** 182-203.

Richards E. M., Fiskum G., Rosenthal R. E., Hopkins I. and McKenna M. C. (2007) Hyperoxic reperfusion after global ischemia decreases hippocampal energy metabolism. *Stroke* **38,** 1578-1584.

Rytter A., Cronberg T., Asztely F., Nemali S. and Wieloch T. (2003) Mouse hippocampal organotypic tissue cultures exposed to in vitro "ischemia" show selective and delayed CA1 damage that is aggravated by glucose. *J Cereb Blood Flow Metab* **23,** 23-33.

Sa Santos S., Sonnewald U., Carrondo M. J. and Alves P. M. (2011) The role of glia in neuronal recovery following anoxia: In vitro evidence of neuronal adaptation. *Neurochem Int* **58,** 665-675.

Serra M., Brito C., Sousa M. F., Jensen J., Tostoes R., Clemente J., Strehl R., Hyllner J., Carrondo M. J. and Alves P. M. (2010) Improving expansion of pluripotent human embryonic stem cells in perfused bioreactors through oxygen control. *Journal Biotechnol* **148,** 208-215.

Shen J., Rothman D. L., Behar K. L. and Xu S. (2009) Determination of the glutamate-glutamine cycling flux using two-compartment dynamic metabolic modeling is sensitive to astroglial dilution. *J Cereb Blood Flow Metab* **29,** 108-118.

Sickmann H. M., Schousboe A., Fosgerau K. and Waagepetersen H. S. (2005) Compartmentation of lactate originating from glycogen and glucose in cultured astrocytes. *Neurochemical research* **30,** 1295-1304.

Suzuki A., Stern S. A., Bozdagi O., Huntley G. W., Walker R. H., Magistretti P. J. and Alberini C. M. (2011) Astrocyte-neuron lactate transport is required for long-term memory formation. *Cell* **144,** 810-823.

Teixeira A. P., Santos S. S., Carinhas N., Oliveira R. and Alves P. M. (2008) Combining metabolic flux analysis tools and 13C NMR to estimate intracellular fluxes of cultured astrocytes. *Neurochem Int* **52,** 478-486.

Tostoes R. M., Leite S. B., Miranda J. P., Sousa M., Wang D. I., Carrondo M. J. and Alves P. M. (2011) Perfusion of 3D encapsulated hepatocytes--a synergistic effect enhancing long-term functionality in bioreactors. *Biotech Bioeng* **108,** 41-49.

Varum S., Rodrigues A. S., Moura M. B., Momcilovic O., Easley C. A. t., Ramalho-Santos J., Van Houten B. and Schatten G. (2011) Energy metabolism in human pluripotent stem cells and their differentiated counterparts. *PloS one* **6,** e20914.

Vogel R., Wiesinger H., Hamprecht B. and Dringen R. (1999) The regeneration of reduced glutathione in rat forebrain mitochondria identifies metabolic pathways providing the NADPH required. *Neuroscience letters* **275,** 97-100.

Waagepetersen H. S., Qu H., Hertz L., Sonnewald U. and Schousboe A. (2002) Demonstration of pyruvate recycling in primary cultures of neocortical astrocytes but not in neurons. *Neurochem Research* **27,** 1431-1437.

Watson B. D., Prado R., Veloso A., Brunschwig J. P. and Dietrich W. D. (2002) Cerebral blood flow restoration and reperfusion injury after ultraviolet laser-facilitated middle cerebral artery recanalization in rat thrombotic stroke. *Stroke* **33,** 428-434.

Witney T. H. and Brindle K. M. (2010) Imaging tumour cell metabolism using hyperpolarized 13C magnetic resonance spectroscopy. *Biochemical Society transactions* **38,** 1220-1224.

Yanes O., Clark J., Wong D. M., Patti G. J., Sanchez-Ruiz A., Benton H. P., Trauger S. A., Desponts C., Ding S. and Siuzdak G. (2010) Metabolic oxidation regulates embryonic stem cell differentiation. *Nature Chemical Biology* **6,** 411-417.

Zhao G. and Flavin M. P. (2000) Differential sensitivity of rat hippocampal and cortical astrocytes to oxygen-glucose deprivation injury. *Neuroscience letters* **285,** 177-180.

Appendices

CONTENTS

1 Detailed reactions included in the simplified biochemical network of astrocytes (Chapter 2).

Central Metabolism

01. Glc + ATP → ADP + G6P

02. G6P → F6P

03. F6P + ATP → 2 GAP + ADP

04. GAP + NAD^+ + 2 ADP → Pyr + 2 ATP + NADH

05. G6P + 2 $NADP^+$ → 2 NADPH + CO_2 + R5P

06. R5P → 2 F6P + GAP

07. Pyr + NADH → Lac + NAD^+

08. Pyr + Glu → Ala + α-KG

09. Pyr + CO_2 + ATP → OAA + ADP

10. Pyr + CoA + NAD^+ → ACoA + NADH + CO_2

11. OAA + ACoA → Cit + CoA

12. Cit + NAD^+ → α-KG + NADH + CO_2

13. α-KG + NAD^+ + CoA → SuCoA + NADH + CO_2

14. SuCoA + ADP → Succ + CoA + ATP

15. FAD + Succ → $FADH_2$ + Fum

16. Fum → Mal

17. Mal + NAD^+ → OAA + NADH

18. Mal + $NADP^+$ → Pyr + CO_2 + NADPH

19. Glu + NAD^+ → αKG + NADH + NH_4^+

20. OAA + Glu → Asp + αKG

21. Glu + NH_4^+ → Gln

Amino Acids Metabolism

21. 2 Gly + NAD+ → Ser + NH_4^+ + CO_2 + NADH

23. Ser → Pyr + NH_4^+

24. Leu + αKG + ATP + NAD+ + FAD + 2 CoA → 2 ACoA + Glu + CO_2 + NADH + $FADH_2$ + ADP

25. Ile + αKG + 2 NAD^+ + FAD + 2 CoA → SuCoA +ACoA + 2 NADH + $FADH_2$ + Glu

26. Val + αKG + 3 NAD^+ + FAD + CoA → SuCoA + Glu + 3 NADH + $FADH_2$ + CO_2

27. Met + Ser + ATP + NAD^+ + CoA → Cys + SuCoA + NADH + NH_4^+ + ADP + CO_2

28. Cyst + NADH → 2 Cys + NAD^+

29. Cys → Pyr + NH_4^+

Oxidative Phosphorylation

30. 0.5 O_2 + 3 ADP + NADH → 3 ATP + NAD^+

31. 0.5 O_2 + 2 ADP + $FADH_2$ → 2 ATP + FAD

32. NADH + $NADP^+$ → NAD^+ + NADPH

Abbreviations: Glc (glucose), G6P (glucose-6-phosphate), F6P (fructose-6-phosphate), GAP (glyceraldehyde-3- phosphate), Pyr (pyruvate), R5P (ribose5-phosphate), Lac (lactate), Glu (glutamate), Ala (alanine), αKG (α-ketoglutarate), OAA (oxaloacetate), Cit (Citrate), SuCoA (succinyl-coenzyme A), Succ (succinate), Fum (fumarate), Mal (malate), NH4+ (ammonium ion), Asp (aspartate), Gln (glutamine), Gly (glycine), Ser (serine), Leu (leucine), Ile (isoleucine), Val (valine), Met (methionine), Cyst (cystine), Cys (cysteine).

2 Biochemical reactions included in the metabolic network of cerebellar granule neurons (Chapter 3)

Central Metabolism

01. Glc + ATP → ADP + G6P

02. G6P + 2 NAD^+ + 3 ADP → 2 Pyr + 2 NADH + 3 ATP

03. Pyr + NADH → Lac + NAD^+

04. Pyr + Glu → Ala + α-KG

05. Pyr + CoA + NAD^+ → ACoA + NADH + CO_2

06. OAA + ACoA → Cit + CoA

07. Cit + NAD^+ → α-KG + NADH + CO_2

08. α-KG + NAD^+ + CoA → SucCoA + NADH + CO_2

09. SucCoA + ADP → Suc + CoA + ATP

10. FAD + Suc → $FADH_2$ + Fum

11. Fum → Mal

12. Mal + NAD^+ → OAA + NADH

13. Mal + $NADP^+$ → Pyr + CO_2 + NADPH

14. Glu + NAD^+ → α-KG + NADH + NH_4^+

15. OAA + Glu → Asp + α-KG

16. Gln → Glu + NH_4^+

Amino Acids Metabolism

17. 2 Gly + NAD+ → Ser + NH_4^+ + CO_2 + NADH

18. Ser → Pyr + NH_4^+

19. Leu + α-KG + ATP + NAD+ + FAD + 2 CoA → 2 ACoA + Glu + CO_2 + NADH + $FADH_2$ + ADP

20. Ile + α-KG + 2 NAD^+ + FAD + 2 CoA → SucCoA +ACoA + 2 NADH + $FADH_2$ + Glu

21. Val + α-KG + 3 NAD^+ + FAD + CoA → SucCoA + Glu + 3 NADH + $FADH_2$ + CO_2

22. Phe + O_2 + NADH → Tyr + NAD^+

23. Tyr + α-KG + 2 O_2 + CoA → Fum + ACoA + Glu + CO_2

24. Arg + α-KG + NAD^+ → 2 Glu + NADH

25. Lys + 2 α-KG + 4 NAD^+ + FAD + CoA + NADPH → 2 Glu + 2 CO_2 + 4 NADH + $FADH_2$ + $NADP^+$

Oxidative Phosphorylation

26. 0.5 O_2 + 3 ADP + NADH → 3 ATP + NAD^+

27. 0.5 O_2 + 2 ADP + $FADH_2$ → 2 ATP + FAD

28. NADH + $NADP^+$ → NAD^+ + NADPH

Abbreviations: Glc, glucose; G6P, glucose-6-phosphate; Pyr, pyruvate; Lac, lactate; Glu, glutamate; Ala alanine; α-KG, α-ketoglutarate; OAA, oxaloacetate; Cit, Citrate; SucCoA, succinyl-coenzyme A; Suc, succinate; Fum, fumarate; Mal, malate; NH_4^+, ammonium ion; Asp, aspartate; Gln, glutamine; Gly, glycine; Ser, serine; Leu, leucine; Ile, isoleucine; Val, valine; Phe, phenylalanine; Tyr, Tyrosine; Arg, arginine; Lys, lysine.

3 Calculation of metabolic partitioning coefficients at the pyruvate, acetyl-CoA and α-ketoglutarate nodes (Chapter 3)

To analyze flux partitioning at the different nodes, i.e., to estimate the relative contributions of each flux to the synthesis and degradation of each metabolite, all intracellular fluxes leading to the formation or utilization of the metabolite in the center of the node were considered, as estimated with CellNetAnalyzer (Klamt et al., 2007).

Pyruvate Node

Incoming fluxes		
PEP (glycolysis)	*Pyruvate kinase* (PK)	$\frac{v_{PK}}{v_{PK}+v_{ME}+v_{SPT}}$
Malate	*Malic enzyme* (ME)	$\frac{v_{ME}}{v_{PK}+v_{ME}+v_{SPT}}$
Serine	Serine-Pyruvate transaminase (SPT)	$\frac{v_{SPT}}{v_{PK}+v_{ME}+v_{SPT}}$

Outgoing fluxes		
Lactate	*Lactate dehydrogenase* (LDH)	$\frac{v_{LDH}}{v_{LDH}+v_{AlaAT}+v_{PDH}}$
Alanine	Alanine aminotransferase (AlaAT)	$\frac{v_{AlaAT}}{v_{LDH}+v_{AlaAT}+v_{PDH}}$
Acetyl-CoA	Pyruvate dehydrogenase (PDH)	$\frac{v_{PDH}}{v_{LDH}+v_{AlaAT}+v_{PDH}}$

Acetyl-CoA node

Incoming fluxes		
Pyruvate	*Pyruvate dehydrogenase* (PDH)	$\frac{v_{PDH}}{v_{PDH}+v_{AasT}}$
Amino acids (Leu, Ile, Tyr)	Amino acids transaminases (AasT)	$\frac{v_{AasT}}{v_{PDH}+v_{AasT}}$
Outgoing Fluxes		
Citrate	Citrate synthase (CS)	$\frac{v_{CS}}{v_{CS}}$

α-Ketoglutarate node

Incoming fluxes		
Isocitrate	Isocitrate dehydrogenase (ICDH)	$\frac{v_{ICDH}}{v_{ICDH}+v_{AlaAT}+v_{GDH+AAT}}$

Alanine	Alanine aminotransferase (AlaAT)	$\frac{v_{AlaAT}}{v_{ICDH}+v_{AlaAT}+v_{GDH+AAT}}$
Glutamate	Glutamate dehydrogenase (GDH) + aspartate aminotransferase (AAT)	$\frac{v_{GDH+AAT}}{v_{ICDH}+v_{AlaAT}+v_{GDH+AAT}}$
Outgoing fluxes		
Succinyl-CoA	α-Ketoglutarate dehydrogenase (α-KGDH)	$\frac{v_{\alpha KGDH}}{v_{BCAAsTA}+v_{\alpha KGDH}}$
Glutamate	BCAAs transaminases (BCAAs TA)	$\frac{v_{BCAAsTA}}{v_{BCAAsTA}+v_{\alpha KGDH}}$

4 Stoichiometric matrix (metabolic reactions) of the Isotopic Transient MFA model describing astrocytic metabolism[1] (Chapter 4).

Glycolysis

01. Glc → G6P
02. G6P → F6P
03. F6P → FBP
04. F6P → 2 GAP
05. GAP → BPG
06. BPG → 3PG
07. 3PG → 2PG
08. 2PG → PEP
09. PEP → Pyr
10. Pyr + Glu → Ala + α-KG
11. Pyr → Lac

Pentose Phosphate Pathway

12. G6P → 6PGL
13. 6PGL → 6PG
14. 6PG → Ru5P + CO_2
15. Ru5P → R5P
16. Ru5P → Xu5P
17. R5P + Xu5P → GAP + S7P
18. GAP + S7P → F6P + E4P
19. Xu5P + E4P → GAP + F6P

TCA cycle and related reactions

21. Pyr + CO_2 → OAA_m

22. Pyr + CoA → ACoA + CO_2
23. OAA_m + ACoA → Cit + CoA
24. Cit → Aco
25. Aco → Isocit
26. Isocit → OSuc
27. OSuc → α-KG + CO_2
28. α-KG + CoA → SuCoA + CO_2
29. SuCoA → Succ + CoA
30. Succ → Fum
31. Fum → Mal
32. Mal → Pyr + CO_2
33. Mal → OAA_m

34a. OAA_m → Asp_m
34b. Asp_m + Glu → Asp_c + α-KG
34c. ASp_c + α-KG → OAA_c + Glu
34d. OAA_c → Mal
35a α-KG → Glu
35b Glu → α-KG

Amino Acids Metabolism

36a. Glu → Gln
36b. Gln → Glu
37. Glu + Cys + Gly → GSH
38. Cys → Taur + Hyptaur
39. Ile + α-KG + 2 CoA → SuCoA +ACoA + Glu
40. Leu + α-KG + 2 CoA → 2 ACoA + Glu + CO_2
41. Val + α-KG + CoA → SuCoA + Glu + CO_2
20. Cys → Pyr

Transport reactions from cell supernatant

Glc_{ext} → Glc
Ala → Ala_{ext}
Lac → Lac_{ext}
Cit → Cit_{ext}
$Cyst_{ext}$ → 2 Cys
Gln → Gln_{ext}
Ile_{ext} → Ile
Leu_{ext} → Leu
Val_{ext} → Val

[1]Only carbon stoichiometry is considered since ^{13}C isotopic transient MFA does not require balancing of cofactors or ATP to estimate metabolic fluxes. Abbreviations: Glc, glucose; G6P, glucose-6-phosphate; F6P, fructose-6-phosphate; DHAP, Dihydroxy-acetone phosphate; GAP, glyceraldehyde-3-phosphate; BPG, 1:3-bis-phosphoglycerate; 3PG, 3-phosphoglycerate, 2PG, 2-phosphoglycerate; PEP, phosphoenolpyruvate; PYR, pyruvate; 6PGL, 6-phospho-gluconolactone; 6PG, 6-phosphogluconate; Ru5P, ribulose-5-phosphate; R5P, ribose-5-phosphate; Xu5P, xylulose-5-phosphate; S7P, sedoheptulose-7-phosphate; E4P, erythrose-4-phosphate; Lac, lactate; Glu, glutamate; ACoA, Acetyl-Coenzyme A; Cyst, cystine; Cys, cysteine; Gly, glycine; GSH, glutathione; Ala, alanine; α-KG, α-ketoglutarate; OAA_m, oxaloacetate – mitochondrial pool; OAA_c, oxaloacetate – cytosolic pool; Cit, Citrate; Aco, cis-aconitate; Isocit, isocitrate; OSuc, oxalosuccinate; SucCoA, succinyl-coenzyme A; Succ, succinate; Fum, fumarate; Mal, malate; Asp_m, aspartate –

mitochondrial pool; Asp_c, aspartate – cytosolic pool; Gln, glutamine; Leu, leucine; Ile, isoleucine; Val, valine; Lys, lysine; ext refers to metabolites taken up from/released to the culture supernatant.

5 Mass isotopomer balances of metabolites represented in the network describing astrocytic metabolism (Chapter 4).

(1-2) $$\frac{d}{dt}\begin{bmatrix} G6P_0 \\ G6P_1 \end{bmatrix} = \frac{1}{G6P_{pool}}\left(r_1\begin{bmatrix} Glc_0 \\ Glc_1 \end{bmatrix} - (r_2 + r_{12})\begin{bmatrix} G6P_0 \\ G6P_1 \end{bmatrix}\right)$$

(3-4) $$\frac{d}{dt}\begin{bmatrix} F6P_0 \\ F6P_1 \end{bmatrix} = \frac{1}{F6P_{pool}}\left(r_1\begin{bmatrix} G6P_0 \\ G6P_1 \end{bmatrix} + r_{18}\begin{bmatrix} GAP_0 \\ GAP_1 \end{bmatrix} + r_{19}\begin{bmatrix} E4P_0 \\ E4P_1 \end{bmatrix} - r_3\begin{bmatrix} F6P_0 \\ F6P_1 \end{bmatrix}\right)$$

(5-6) $$\frac{d}{dt}\begin{bmatrix} FBP_0 \\ FBP_1 \end{bmatrix} = \frac{1}{FBP_{pool}}\left(r_3\begin{bmatrix} F6P_0 \\ F6P_1 \end{bmatrix} - r_4\begin{bmatrix} FBP_0 \\ FBP_1 \end{bmatrix}\right)$$

(7-8) $$\frac{d}{dt}\begin{bmatrix} GAP_0 \\ GAP_1 \end{bmatrix} = \frac{1}{GAP_{pool}}\left(r_4\begin{bmatrix} 2\cdot FBP_0 + FBP_1 \\ FBP_1 \end{bmatrix} + (r_{17} + r_{19})\begin{bmatrix} Xu5P_0 \\ Xu5P_1 \end{bmatrix} - (r_5 + r_{18})\begin{bmatrix} GAP_0 \\ GAP_1 \end{bmatrix}\right)$$

(9-10) $$\frac{d}{dt}\begin{bmatrix} BPG_0 \\ BPG_1 \end{bmatrix} = \frac{1}{BPG_{pool}}\left(r_5\begin{bmatrix} GAP_0 \\ GAP_1 \end{bmatrix} - r_6\begin{bmatrix} BPG_0 \\ BPG_1 \end{bmatrix}\right)$$

(11-12) $$\frac{d}{dt}\begin{bmatrix} 3PG_0 \\ 3PG_1 \end{bmatrix} = \frac{1}{3PG_{pool}}\left(r_6\begin{bmatrix} BPG_0 \\ BPG_1 \end{bmatrix} - r_7\begin{bmatrix} 3PG_0 \\ 3PG_1 \end{bmatrix}\right)$$

(13-14) $$\frac{d}{dt}\begin{bmatrix} 2PG_0 \\ 2PG_1 \end{bmatrix} = \frac{1}{2PG_{pool}}\left(r_7\begin{bmatrix} 3PG_0 \\ 3PG_1 \end{bmatrix} - r_8\begin{bmatrix} 2PG_0 \\ 2PG_1 \end{bmatrix}\right)$$

(15-16) $$\frac{d}{dt}\begin{bmatrix} PEP_0 \\ PEP_1 \end{bmatrix} = \frac{1}{PEP_{pool}}\left(r_8\begin{bmatrix} 2PG_0 \\ 2PG_1 \end{bmatrix} - r_9\begin{bmatrix} PEP_0 \\ PEP_1 \end{bmatrix}\right)$$

(17-18) $$\frac{d}{dt}\begin{bmatrix} 6PGL_0 \\ 6PGL_1 \end{bmatrix} = \frac{1}{6PGL_{pool}}\left(r_{12}\begin{bmatrix} G6P_0 \\ G6P_1 \end{bmatrix} - r_{13}\begin{bmatrix} 6PGL_0 \\ 6PGL_1 \end{bmatrix}\right)$$

(19-20) $$\frac{d}{dt}\begin{bmatrix} 6PG_0 \\ 6PG_1 \end{bmatrix} = \frac{1}{6PG_{pool}}\left(r_{13}\begin{bmatrix} 6PGL_0 \\ 6PGL_1 \end{bmatrix} - r_{14}\begin{bmatrix} 6PG_0 \\ 6PG_1 \end{bmatrix}\right)$$

(21-22) $$\frac{d}{dt}\begin{bmatrix} Ru5P_0 \\ Ru5P_1 \end{bmatrix} = \frac{1}{Ru5P_{pool}}\left(r_{14}\begin{bmatrix} 6PG_0 + 6PG_1 \\ 0 \end{bmatrix} - (r_{15} + r_{16})\begin{bmatrix} Ru5P_0 \\ Ru5P_1 \end{bmatrix}\right)$$

(23-24) $$\frac{d}{dt}\begin{bmatrix} R5P_0 \\ R5P_1 \end{bmatrix} = \frac{1}{R5P_{pool}}\left(r_{15}\begin{bmatrix} Ru5P_0 \\ Ru5P_1 \end{bmatrix} - r_{17}\begin{bmatrix} R5P_0 \\ R5P_1 \end{bmatrix}\right)$$

(25-26) $$\frac{d}{dt}\begin{bmatrix} Xu5P_0 \\ Xu5P_1 \end{bmatrix} = \frac{1}{Xu5P_{pool}}\left(r_{16}\begin{bmatrix} Ru5P_0 \\ Ru5P_1 \end{bmatrix} - (r_{17} + r_{19})\begin{bmatrix} Xu5P_0 \\ Xu5P_1 \end{bmatrix}\right)$$

(27-28) $$\frac{d}{dt}\begin{bmatrix} E4P_0 \\ E4P_1 \end{bmatrix} = \frac{1}{E4P_{pool}}\left(r_{18}\begin{bmatrix} S7P_0 \\ S7P_1 \end{bmatrix} - r_{19}\begin{bmatrix} E4P_0 \\ E4P_1 \end{bmatrix}\right)$$

(29-30) $$\frac{d}{dt}\begin{bmatrix} S7P_0 \\ S7P_1 \end{bmatrix} = \frac{1}{S7P_{pool}}\left(r_{18}\begin{bmatrix} Xu5P_0 \\ Xu5P_1 \end{bmatrix} - r_{19}\begin{bmatrix} S7P_0 \\ S7P_1 \end{bmatrix}\right)$$

(31-33) $$\frac{d}{dt}\begin{bmatrix} Pyr_0 \\ Pyr_1 \\ Pyr_2 \end{bmatrix} = \frac{1}{Pyr_{pool}}\left(r_{20}\begin{bmatrix} 1 \\ 0 \\ 0 \end{bmatrix} + r_9\begin{bmatrix} PEP_0 \\ PEP_1 \\ 0 \end{bmatrix} + r_{32}\begin{bmatrix} MAL_0 \\ MAL_1 \\ MAL_2 \end{bmatrix} - (r_{10} + r_{11} + r_{21} + r_{22})\begin{bmatrix} Pyr_0 \\ Pyr_1 \\ Pyr_2 \end{bmatrix}\right)$$

(34-36) $$\frac{d}{dt}\begin{bmatrix} AcoA_0 \\ AcoA_1 \\ AcoA_2 \end{bmatrix} = \frac{1}{AcoA_{pool}}\left((r_{Ile} + 3 \cdot r_{Leu})\begin{bmatrix} 1 \\ 0 \\ 0 \end{bmatrix} + r_{22}\begin{bmatrix} Pyr_0 \\ Pyr_1 \\ Pyr_2 \end{bmatrix} - r_{23}\begin{bmatrix} AcoA_0 \\ AcoA_1 \\ AcoA_2 \end{bmatrix}\right)$$

(37-39) $$\frac{d}{dt}\begin{bmatrix} Ala_0 \\ Ala_1 \\ Ala_2 \end{bmatrix} = \frac{1}{Ala_{pool}}\left(r_{10}\begin{bmatrix} Pyr_0 \\ Pyr_1 \\ Pyr_2 \end{bmatrix} - r_{Ala}\begin{bmatrix} Ala_0 \\ Ala_1 \\ Ala_2 \end{bmatrix}\right)$$

(40-42) $$\frac{d}{dt}\begin{bmatrix} Lac_0 \\ Lac_1 \\ Lac_2 \end{bmatrix} = \frac{1}{Lac_{pool}}\left(r_{11}\begin{bmatrix} Pyr_0 \\ Pyr_1 \\ Pyr_2 \end{bmatrix} - r_{Lac}\begin{bmatrix} Lac_0 \\ Lac_1 \\ Lac_2 \end{bmatrix}\right)$$

(43-46)

$$\frac{d}{dt}\begin{bmatrix} Glu_0 \\ Glu_1 \\ Glu_2 \\ Glu_3 \end{bmatrix} = \frac{1}{Glu_{pool}}\left((r_{Ile} + r_{Leu} + r_{Val} + r_{35a} + r_{34}) \begin{bmatrix} \alpha KG_0 \\ \alpha KG_1 \\ \alpha KG_2 \\ \alpha KG_3 \end{bmatrix} + r_{36b} \begin{bmatrix} G\ln_0 \\ G\ln_1 \\ G\ln_2 \\ G\ln_3 \end{bmatrix} - (r_{10} + r_{34} + r_{35b} + r_{36b} + r_{37}) \begin{bmatrix} Glu_0 \\ Glu_1 \\ Glu_2 \\ Glu_3 \end{bmatrix} \right)$$

(47-50) $$\frac{d}{dt}\begin{bmatrix} G\ln_0 \\ G\ln_1 \\ G\ln_2 \\ G\ln_3 \end{bmatrix} = \frac{1}{G\ln_{pool}}\left(r_{36b} \begin{bmatrix} Glu_0 \\ Glu_1 \\ Glu_2 \\ Glu_3 \end{bmatrix} - (r_{36a} + r_{G\ln}) \begin{bmatrix} G\ln_0 \\ G\ln_1 \\ G\ln_2 \\ G\ln_3 \end{bmatrix} \right)$$

(51-54)

$$\frac{d}{dt}\begin{bmatrix} \alpha KG_0 \\ \alpha KG_1 \\ \alpha KG_2 \\ \alpha KG_3 \end{bmatrix} = \frac{1}{\alpha KG_{pool}}\left((r_{10} + r_{34} + r_{35b} + r_{37}) \begin{bmatrix} Glu_0 \\ Glu_1 \\ Glu_2 \\ Glu_3 \end{bmatrix} + r_{27} \begin{bmatrix} Osu_0 \\ Osu_1 \\ Osu_2 \\ Osu_3 \end{bmatrix} - (r_{Ile} + r_{Leu} + r_{Val} + r_{28} + r_{35a} + r_{34}) \begin{bmatrix} \alpha KG_0 \\ \alpha KG_1 \\ \alpha KG_2 \\ \alpha KG_3 \end{bmatrix} \right)$$

(55-58) $$\frac{d}{dt}\begin{bmatrix} Cit_0 \\ Cit_1 \\ Cit_2 \\ Cit_3 \end{bmatrix} = \frac{1}{Cit_{pool}}\left(r_{23} \begin{bmatrix} OAA_0 \cdot AcoA_0 \\ OAA_0 \cdot AcoA_1 + OAA_1 \cdot AcoA_0 \\ OAA_0 \cdot AcoA_2 + OAA_1 \cdot AcoA_1 + OAA_2 \cdot AcoA_0 \\ OAA_1 \cdot AcoA_2 + OAA_2 \cdot AcoA_1 + OAA_3 \cdot AcoA_0 \end{bmatrix} - (r_{24} + r_{Cit}) \begin{bmatrix} Cit_0 \\ Cit_1 \\ Cit_2 \\ Cit_3 \end{bmatrix} \right)$$

(59-62) $$\frac{d}{dt}\begin{bmatrix} Aco_0 \\ Aco_1 \\ Aco_2 \\ Aco_3 \end{bmatrix} = \frac{1}{Aco_{pool}}\left(r_{24} \begin{bmatrix} Cit_0 \\ Cit_1 \\ Cit_2 \\ Cit_3 \end{bmatrix} - r_{25} \begin{bmatrix} Aco_0 \\ Aco_1 \\ Aco_2 \\ Aco_3 \end{bmatrix} \right)$$

(63-66) $$\frac{d}{dt}\begin{bmatrix} Iso_0 \\ Iso_1 \\ Iso_2 \\ Iso_3 \end{bmatrix} = \frac{1}{Iso_{pool}}\left(r_{25} \begin{bmatrix} Aco_0 \\ Aco_1 \\ Aco_2 \\ Aco_3 \end{bmatrix} - r_{26} \begin{bmatrix} Iso_0 \\ Iso_1 \\ Iso_2 \\ Iso_3 \end{bmatrix} \right)$$

$$(67\text{-}70)\quad \frac{d}{dt}\begin{bmatrix} Osu_0 \\ Osu_1 \\ Osu_2 \\ Osu_3 \end{bmatrix} = \frac{1}{Osu_{pool}}\left(r_{26}\begin{bmatrix} Iso_0 \\ Iso_1 \\ Iso_2 \\ Iso_3 \end{bmatrix} - r_{27}\begin{bmatrix} Osu_0 \\ Osu_1 \\ Osu_2 \\ Osu_3 \end{bmatrix}\right)$$

$$(71\text{-}74)\quad \frac{d}{dt}\begin{bmatrix} SuCoA_0 \\ SuCoA_1 \\ SuCoA_2 \\ SuCoA_3 \end{bmatrix} = \frac{1}{SuCoA_{pool}}\left(r_{Ile}\begin{bmatrix} 1 \\ 0 \\ 0 \\ 0 \end{bmatrix} + r_{28}\begin{bmatrix} \alpha KG_0 \\ \alpha KG_1 \\ \alpha KG_2 \\ \alpha KG_3 \end{bmatrix} - r_{29}\begin{bmatrix} SuCoA_0 \\ SuCoA_1 \\ SuCoA_2 \\ SuCoA_3 \end{bmatrix}\right)$$

$$(75\text{-}78)\quad \frac{d}{dt}\begin{bmatrix} Succ_0 \\ Succ_1 \\ Succ_2 \\ Succ_3 \end{bmatrix} = \frac{1}{Succ_{pool}}\left(r_{Val}\begin{bmatrix} 1 \\ 0 \\ 0 \\ 0 \end{bmatrix} + r_{29}\begin{bmatrix} SuCoA_0 \\ SuCoA_1 \\ SuCoA_2 \\ SuCoA_3 \end{bmatrix} - r_{30}\begin{bmatrix} Succ_0 \\ Succ_1 \\ Succ_2 \\ Succ_3 \end{bmatrix}\right)$$

$$(79\text{-}82)\quad \frac{d}{dt}\begin{bmatrix} Fum_0 \\ Fum_1 \\ Fum_2 \\ Fum_3 \end{bmatrix} = \frac{1}{Fum_{pool}}\left(r_{30}\begin{bmatrix} Succ_0 \\ Succ_1 \\ Succ_2 \\ Succ_3 \end{bmatrix} - r_{27}\begin{bmatrix} Fum_0 \\ Fum_1 \\ Fum_2 \\ Fum_3 \end{bmatrix}\right)$$

$$(83\text{-}86)\quad \frac{d}{dt}\begin{bmatrix} Mal_0 \\ Mal_1 \\ Mal_2 \\ Mal_3 \end{bmatrix} = \frac{1}{Mal_{pool}}\left(r_{31}\begin{bmatrix} Fum_0 \\ Fum_1 \\ Fum_2 \\ Fum_3 \end{bmatrix} + r_{34}\begin{bmatrix} OAA_0 \\ OAA_1 \\ OAA_2 \\ OAA_3 \end{bmatrix} - (r_{32} + r_{33})\begin{bmatrix} Mal_0 \\ Mal_1 \\ Mal_2 \\ Mal_3 \end{bmatrix}\right)$$

$$(87\text{-}90)\quad \frac{d}{dt}\begin{bmatrix} OAA_0 \\ OAA_1 \\ OAA_2 \\ OAA_3 \end{bmatrix} = \frac{1}{OAA_{pool}}\left(r_{33}\begin{bmatrix} Mal_0 \\ Mal_1 \\ Mal_2 \\ Mal_3 \end{bmatrix} + r_{21}\begin{bmatrix} Pyr_0 \\ Pyr_1 \\ Pyr_2 \\ Pyr_3 \end{bmatrix} - (r_{23} + r_{34})\begin{bmatrix} OAA_0 \\ OAA_1 \\ OAA_2 \\ OAA_3 \end{bmatrix}\right)$$

$$(91\text{-}94)\quad \frac{d}{dt}\begin{bmatrix} Asp_0 \\ Asp_1 \\ Asp_2 \\ Asp_3 \end{bmatrix} = \frac{1}{Osu_{pool}}\left(r_{34}\begin{bmatrix} OAA_0 \\ OAA_1 \\ OAA_2 \\ OAA_3 \end{bmatrix} - r_{34}\begin{bmatrix} Asp_0 \\ Asp_1 \\ Asp_2 \\ Asp_3 \end{bmatrix}\right)$$

ITQB-UNL | Av. da República, 2780-157 Oeiras, Portugal
Tel (+351) 214 469 100 | Fax (+351) 214 411 277

www.itqb.unl.pt

Thesis Cover: Composite image of a general metabolic network and a fluorescence microscopy image of rat cortical astrocytes immobilized in Cytodex 3® microcarriers stained with fluoresceine diacetate (green).